

Microwave Electronics

**PRINTED MONOPOLE ANTENNA FOR ULTRA
WIDE BAND (UWB) APPLICATIONS**

A thesis submitted by

K. FRANCIS JACOB

in partial fulfillment of the requirements for the degree of

DOCTOR OF PHILOSOPHY

Under the guidance of

Prof. P. MOHANAN



DEPARTMENT OF ELECTRONICS

FACULTY OF TECHNOLOGY

COCHIN UNIVERSITY OF SCIENCE AND TECHNOLOGY

COCHIN-22, INDIA

June 2008



Department of Electronics
Cochin University of Science and Technology,
Kochi – 682 022

Date: 25-06-2008

Dr. P. Mohanan
(Supervising Teacher)
Professor
Department of Electronics
Cochin University of Science and Technology

Certificate

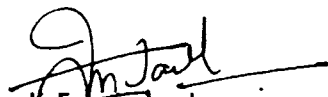
This is to certify that this thesis entitled "PRINTED MONOPOLE ANTENNA FOR ULTRA WIDE BAND (UWB) APPLICATIONS" is a bonafide record of the research work carried out by Mr. K. Francis Jacob under my supervision in the Department of Electronics, Cochin University of Science and Technology. The results embodied in this thesis or parts of it have not been presented for any other degree.


Dr. P. Mohanan

DECLARATION

I hereby declare that the work presented in this thesis entitled “PRINTED MONOPOLE ANTENNA FOR ULTRA WIDE BAND (UWB) APPLICATIONS” is a bonafide record of the research work done by me under the supervision of Dr. P. Mohanan, Professor, Department of Electronics, Cochin University of Science and Technology, India and that no part thereof has been presented for the award of any other degree.

Cochin-22
Date: 25-06-2008



K. Francis Jacob
Research Scholar
Department of Electronics
Cochin University of Science and Technology

ACKNOWLEDGEMENTS

My greatest appreciation, sincere gratitude and thanks to Dr. P. Mohanan, Professor, Department of Electronics, Cochin University of Science and Technology for his valuable guidance and constant encouragement, throughout my research work. I certainly could not have asked for a better adviser. He has been an outstanding teacher and mentor throughout the research work and I have learned a lot from him. I have been extremely fortunate to get a chance to work under him in CREMA Laboratory, Department of Electronics, Cochin University of Science and Technology, Kochi.

I would like to express my sincere thanks to Dr. K. Vasudevan, Professor, Department of Electronics, Cochin University of Science and Technology for his valuable support and suggestions during my research work.

I would like to express my sincere thanks to Dr. C. K. Aanandan, Reader, Department of Electronics, Cochin University of Science and Technology for his valuable suggestions .

I would like to thank Dr. P.R.S. Pillai, Professor and former Head, Department of Electronics, for his help during my research work.

I have enjoyed the friendship of research colleagues in the department Dr. Rohith K. Raj, Mr. Gijo Augustine, Mrs. Bybi P.C, Ms Jitha. B, Mr. Deepu V, Mr. Manoj Joseph, Ms. Suma M.N., Dr. Sreedevi. K. Menon, Dr. Mridula. S, Dr. Binu Paul, Dr. Anupam. R. Chandran, Dr.S.V. Shynu, , Mr. Gopikrishnan .M, Mr. Sujith .R, Mr. Praveen Kumar and Mrs. Deepthi Das Krishna . I would like to thank all of my good friends at the CUSAT, especially those at the CREMA Laboratory. I am also thankful to other teaching and non teaching , office as well as technical staff of the department and specially I would like to thank Mr. Ibrahim Kutty and Librarian Mr. Suresh , who always been very much willing to help me in need.

My sincere thanks to the General Managers of BSNL Trichur and Coimbatore for helping me pursue the research work for Ph.D amidst the important assignments bestowed on me during this period.

This list will be incomplete if I fail to acknowledge the support extended by my wife Binie and my son Jiztom during the research work. Their great interest, supreme sacrifices and deep love made this venture a success. I would like to thank my parents for their love and constant prayers. I remember all my well wishers and friends for their suggestions, support and prayers.

The last but not the least, I am deeply indebted to all graces received from above. But for His wishes this would never been a reality, It is for all of this that I dedicate this dissertation to God Almighty.

K. Francis Jacob

Contents

Chapter 1

INTRODUCTION----- 01 - 34

1.1 Compact Antennas	03
1.2 Feed for Compact antennas	07
1.3 Theoretical Analysis for Antenna Modeling	11
1.4 Compact Antenna applications	20
1.5 Printed Antenna for UWB Applications	22
1.6 Outline of the present work	25
1.7 Chapter Organization	26
1.8 References	27

Chapter 2

REVIEW OF LITERATURE----- 35 - 84

2.1 Compact Antennas	36
2.2 Band Widening Techniques	50
2.3 Ultra Wide Band Antennas	54
2.4 FDTD for Printed Antenna analysis	58
2.5 References	63

Chapter 3

EXPERIMENTAL AND NUMERICAL METHODOLOGY ----- 85 - 106

3.1 Printed Antenna fabrication and characterisation	85
3.2 Measurement techniques	86
3.3 Simulation studies	96
3.4 The FDTD Method	97
3.5 FDTD implementation	100
3.6 References	104

Chapter 4

INVESTIGATION ON PRINTED ULTRA WIDE BAND (UWB) MONOPOLES ----- 107 -212

4.1 Characteristics of the Printed strip monopoles.	108
4.1.1 Printed Antenna design parameters	108
4.1.2 Return Loss Characteristics	110
4.1.3 Effect of Truncated ground plane configuration	114

4.1.4	Radiation Pattern	120
4.1.5	Inferences	123
4.2	Wide Rectangular strip monopole	126
4.2.1	Printed Antenna design parameters	126
4.2.2	Return Loss Characteristics	127
4.2.3	Parametric analysis	128
4.2.4	Optimised Antenna characteristics	132
4.3	Wide Elliptical strip monopole	135
4.3.1	Printed Antenna design parameters	135
4.3.2	Optimised Antenna characteristics	136
4.4	Wide Circular strip monopole	138
4.4.1	Printed Antenna design parameters	138
4.4.2	Optimised Antenna characteristics	139
4.5	Wide Octagonal strip monopole	142
4.5.1	Printed Antenna design parameters	142
4.5.2	Optimised Antenna characteristics	143
4.6	Wide Hexagonal strip monopole	145
4.6.1	Printed Antenna design parameters	145
4.6.2	Optimised Antenna characteristics	146
4.7	Comparison of different antennas	148
4.8	Rectangular monopole loaded with strips	149
4.8.1	Printed Antenna design parameters	150
4.8.2	Return Loss Characteristics of the optimized antenna	159
4.8.3	Radiation Pattern	165
4.8.4	Gain	167
4.8.5	Compactness	168
4.8.6	Effect of Truncated ground plane configuration	169
4.9	Rectangular monopole loaded with slotted grounds	170
4.9.1	Printed Antenna design parameters	171
4.9.2	Return Loss Characteristics	175
4.9.3	Radiation Pattern	180
4.9.4	Gain	182
4.9.5	Compactness	183
4.10	Combo model with strips and ground slots	184
4.10.1	Printed Antenna design parameters	184
4.10.2	Parametric Analysis	185
4.10.3	Optimised Printed UWB Combo Antenna	197
4.10.4	Radiation pattern	201

4.10.5	Gain	204
4.10.6	Compactness	205
4.10.7	Efficiency	205
4.10.8	Phase response and group delay.	206
4.11	Conclusion	207
4.12	References	209

Chapter 5

CONCLUSIONS AND SUGGESTED FUTURE WORKS ----- 213 - 216

5.1	Thesis Highlights	213
5.2	Inferences on experimental and theoretical observations	213
5.3	Salient features of the antenna and applications	214
5.4	Suggestions for future work	215

Appendix - A

FDTD METHOD ----- 217 - 258

Appendix - B

CONFORMAL FDTD MODELING OF CIRCULAR MICROSTRIP ANTENNA ----- 259 - 264

LIST OF PUBLICATIONS OF THE AUTHOR

RESUME OF THE AUTHOR

INDEX

INTRODUCTION

Antenna “The eyes and ears in space” is undergoing a versatile change from earlier long wire type for radio broadcast, communication links to the military applications, aircraft, radars, missiles, space applications in the second half of last century. This scenario is fast changing with the evolution of Cellular mobile personal communication in the form of Global System for Mobile communications (GSM), Code Division Multiple Accessing (CDMA), Digital Communication System (DCS) 1800 systems, North American dual-mode cellular system Interim Standard (IS)-54, North American IS-95 system, and Japanese Personal Digital Cellular (PDC) system etc.. The era of plain voice service based on circuit switched communication service has gone. The broadband mobile personal communication with mobile high quality video is the buzz word today. 3rd Generation GSM (3G), Wide band-CDMA, Wireless Fidelity (WiFi), 4th Generation WiMax, Wi Bro, Wireless-LAN, are all towards this direction .

The wireless communication industry is growing rapidly and wireless communication products, Personal Digital Assistants (PDAs), Laptops and cell phones are becoming a necessity of life. Communication systems need a wide frequency bandwidth to transmit and receive multimedia information at high data rates. Mobile wireless communication products must be easily portable and cheap to make them attractive to modern people. Because Microstrip fed slot antennas have a wide impedance bandwidth and simple structure that is easily

manufactured at a low cost, are highly suitable for communication products such as WLAN or blue-tooth applications. Suddenly it seems everything from mobile phone to MP3 players, printers to GPS receivers, instruments in hospitals, pathology laboratories, even the chemistry and physics labs has the 'Blue-tooth' built-in for wireless operation 'cutting the usual wired cords'. There is precisely a need for compact antennas in these gadgets especially driven by fast changing mobile communication technology, that too in large volume of demand at affordable cost. This has kindled a vigorous research and development activity in compact Microstrip antennas which can straight way go into mobile handsets or as an antenna array in Base Transceiver Stations (BTS) for any of the prevailing mature Mobile communication and GPS Technologies and much more to come in immediate future. World over there is a frantic search for optimal use of scarce wireless spectrum resources. This needs thinking twice or more before allocating a spectrum for a specific service as this amount to huge investments in research, development, technology implementation and service operation.

Antenna does not become obsolete since they are based on unvarying physical principles. Only technology changes just like transition from tubes to transistor and then to ICs. Early large antennas 3- D antennas has reduced to 2D-planar type by way of printed antennas. Thanks to Microstrip revolution in antenna technology in 1970s. Antenna - the vital part of wireless gadgets has endured renovation from a simple metallic rod to ceramic chip, reconfigurable, active and complicated Smart Antenna. The day is not far when this is likely to reduce to physically sub miniature wavelength antennas with the advent of Meta materials and Nano Technology. In this scenario development of extremely compact antenna are highly relevant. Different types of compact antennas like Microstrip, Planar Inverted- F Antenna (PIFA), Planar

Inverted Cone Antenna (PICA), Dielectric Resonator Antenna (DRA) and Printed Monopole Antenna [1-10] are described in the next section.

1.1 Compact Antennas

Wireless gadgets are constantly getting smaller. The latest trend in terminal design is therefore ultra-thin phones, leading to very small heights above ground plane available to the antenna elements. This has a huge impact on patch type of antennas (such as the popular Planar Inverted F Antenna (PIFA)) as the achievable bandwidth and radiation efficiency is proportional to its height [11]. The recent trend in miniaturization of wireless gadgets triggered the evolution of planar antenna technology. It is worth noting that many of the planar antennas can be viewed as the modifications of conventional antennas. Broad band planar metal plate monopoles are fabricated by transforming a conventional monopole. Further miniaturization can be achieved by printing the monopole on a dielectric substrate

1.1.1 Microstrip Antenna Configurations

The concept of microstrip radiators was first proposed by Deschamps [12] in 1953. However, it took 20 years to realize the first practical antenna of this type. These classes of antennas has received much attention and research only in 1970's. These antennas are lightweight, easy to manufacture using printed-circuit techniques, and compatible with MMICs (Monolithic Microwave Integrated Circuits). An additional attractive property of these antennas is that they are low-profile and can be mounted on surfaces and referred to as conformal antennas. However, the inherent narrow bandwidth of these antennas limits their usage in many applications.

Microstrip Antenna consists of thin metallic radiating patch having a fraction of a wavelength above a conducting ground-plane on a low loss

substrate. The patch and ground-plane are separated by a low loss dielectric. The patch conductor is normally copper and can assume any shape, but simple geometries are used generally, and this simplifies the analysis and performance prediction. The patches are usually photo-etched on the dielectric substrate. The substrate is usually non-magnetic. The relative permittivity of the substrate is normally in between 1 and 10, which enhances the fringing fields that account for radiation, but higher values may be used in special circumstances.

Microstrip antenna can be divided into three basic categories: microstrip patch antennas, microstrip traveling wave antennas and microstrip slot antennas. Since Microstrip antenna is a mature technology their characteristics are briefly discussed below.

Microstrip Patch Antennas

A microstrip patch antenna consists of a conducting patch of any planar geometry on one side of a dielectric substrate backed by a conducting ground plane. Various microstrip patch configurations like circular disc, rectangular, square, triangle, ellipse, pentagon etc. are generally used.

Microstrip Traveling Wave Antennas

Microstrip Traveling Wave Antennas consists of chain shaped periodic conductors or an ordinary long TEM line which also supports a TE mode, on a substrate backed by a ground plane. The open end of the TEM line is terminated in a matched resistive load. As antenna supports traveling waves, their structures may be designed so that the main beam lies in any direction from broadside to end-fire.

Microstrip Slot Antennas

Microstrip slot antenna comprises of a slot in the ground plane fed by a microstrip line. The slot may have the shape of a rectangle or a circle or any other as required to radiate in a desired manner

1.1.2 Dielectric Resonator Antenna (DRA)

A high dielectric constant low loss material can also be used as emanating electromagnetic energy and is termed as Dielectric Resonator Antenna (DRA). The radiating mechanism in a DRA is due to displacement current circulating in the dielectric medium, usually a ceramic pellet. The stored energy inside the dielectric is extremely high and it is difficult for external objects to detune the device [5-6]. Unlike patch antennas they can radiate from all surfaces, rendering high radiation efficiency and low Q factor. Since its birth in the early 1980's, there has been a steady progress of research in this area over the years.

1.1.3 Planar Inverted - F Antenna (PIFA)

The inverted-F antenna printed on a dielectric substrate and the printed metallic strip of the antenna is shorted to the ground plane on the other side of the dielectric substrate for applications in wireless communication has been demonstrated [13-14]. PIFA can resonate at a smaller antenna size as compared to conventional antenna. For both designs, an integrated inverted-F antenna for Blue-tooth applications and a coplanar waveguide-fed folded inverted-F antenna for application to the UMTS band is available. To achieve dual-band operations for the WLAN and HIPERLAN systems, printed monopoles in the form of an F-shaped structure have also been tried [7-8].

The PIFA designs usually occupy a compact volume and can be integrated within the mobile housing, leading to internal mobile phone antenna.

These internal antennas can avoid the damages such as breaking compared with the conventional protruded whip or monopole antennas used for handheld applications. Compared to the whip antennas, these PIFA's have the advantage of relatively smaller backward radiation towards the mobile phone user. This suggests that electromagnetic energy absorption by the user's head can be reduced. These advantages led to many novel PIFA designs, most of them capable of dual or multiband operation to be applied in the mobile phones in the market. A variety of designs for dual-band PIFA's used in mobile handsets can be found in the literature [15- 20].

1.1.4 Planar Inverted Cone Antenna (PICA)

The new wideband, omni-directional, flat antenna called the planar inverted cone antenna (PICA) [6-11] can be thought of as an evolution of the volcano antenna and the circular disk antenna. The PICA is composed of a single flat element vertically mounted above a ground plane. The antenna geometry is very simple, yet provides outstanding impedance and radiation pattern performance. The impedance bandwidth is more than 10:1 and the pattern bandwidth is about 4:1. The antenna characteristics of the PICA element are similar to typical monopole disk antennas [9-10].

1.1.5 Printed Monopole Antenna.

Another versatile antenna which has large attention recently is Printed monopole antenna. They offer large bandwidth and are more attractive for wireless communication applications. The large ground plane used for the conventional Printed monopole is the main limitation. However, the move towards the truncated ground plane has made the antenna low profile and suitable for integration into circuit board as terminal antennas [10-11]. Recently printed antennas have received much attention due their low profile and omni-

directional radiation characteristics. The rapid growth of Ultra Wide Band communication [14] demands ultra wide band antennas to accommodate the large frequency spectrum of ultra short pulse used for this communication. There is a growing demand for small and low cost UWB antennas that can provide satisfactory performances in both frequency domain and time domain.

A circular planar monopole was presented for the design of an 8:1 impedance bandwidth [22]. Recently, monopoles with elliptical, square (rectangular), bow-tie, diamond, and trapezoidal sheets, have been designed and investigated [23-29].

Compared with traditional wire antennas, printed dipole antennas have extra advantages including planar structure, small volume, light weight and low cost, which are significantly suitable for applications sensitive to the receiver sizes. Recently, various types of printed dipole antennas have been studied [30–32] to comply with the compact high performance broad band/multiband requirements.

1.2 Feed for Compact Antennas

Patch antennas are commonly excited by one of the five methods: (a) coaxial probe, (b) microstrip line feed connected to the edge of the patch, (c) microstrip line coupled to the patch through electromagnetic method, and (d) microstrip line coupled to the patch through aperture (e) Co-planar feed. [33-36]. The selection of appropriate feed depends on the application.

(a) Coaxial feed

One of the common methods of feeding the microstrip antenna employs coaxial probe. The basic configuration is shown in Figure (1-1). Here the central conductor of the coaxial cable is connected to the radiating patch

whereas the outer conductor is attached to the ground plane. This type of feeding has the flexibility of impedance matching with low spurious radiation. Coaxially fed antenna has low impedance bandwidth. For increased bandwidth, thick substrates are to be used and which requires a longer probe. But, this gives rise to an increase in spurious radiation from the probe, increased surface wave power and increased feed inductance.

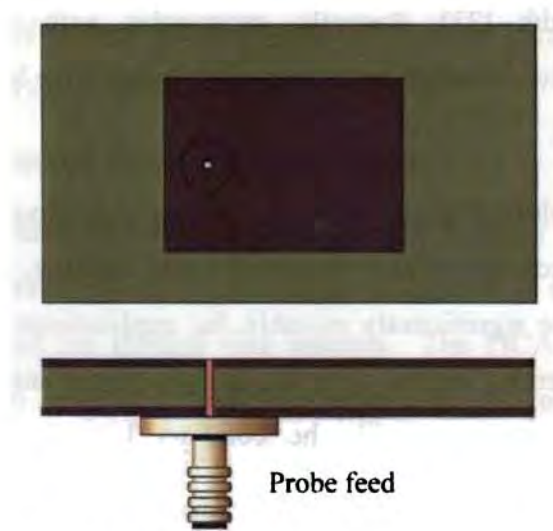


Fig.1.1 Co-axial fed Rectangular microstrip patch.

(b) Microstrip Line Feed

Microstrip line feed is the simplest of the excitation techniques and has the advantage of feed lying in the same plane of the radiating monopole. Figure (1-2) shows the microstrip line feeding arrangement. This method of directly connecting a strip to the edge of a patch is highly convenient when integrating the feeding network for large arrays. However, the spurious radiation from the feed often creates problems. This can be reduced by choosing a high dielectric constant substrate. In this type of excitation the prior knowledge of the feed point location is absolutely required for impedance matching.

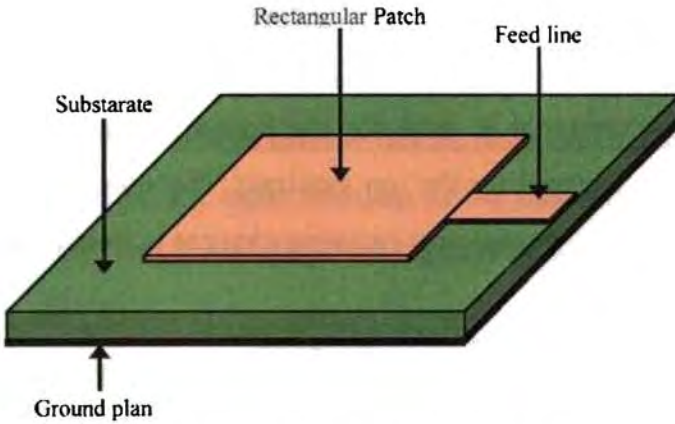


Fig.1.2 Microstrip line fed rectangular patch

(c) Electromagnetic (Proximity) Coupling

In this type of feeding system, the radiating patch is etched on another substrate and placed above the open-ended feed line. Thus the radiating element is parasitically coupled to the feed. Figure (1-3) depicts such a feeding mechanism. It has large bandwidth, low spurious radiation and easy to fabricate.

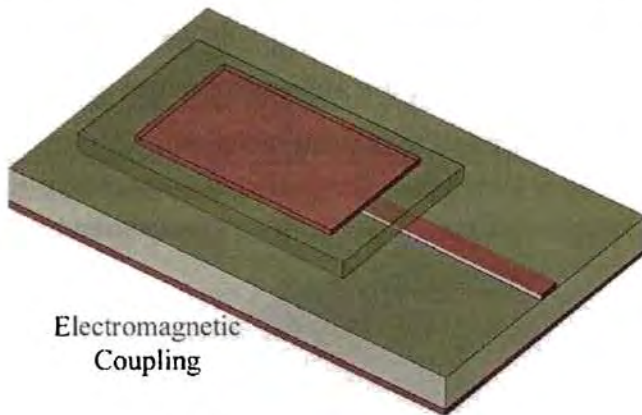


Fig.1.3 Proximity Coupling

(d) Aperture Coupling

A feeding method, which has become very popular, involves coupling of energy from a microstrip line through an aperture (slot) in the ground plane.

This method is known as the aperture coupling and is shown in Figure (1-4). The slot couples energy from the strip line to the patch. Typically high dielectric constant material is used for the bottom substrate and thick low dielectric constant material for the top substrate. The spurious radiation from the feed network is low because the radiating element is isolated from the feed by the ground plane.

Another method is also used for aperture coupling. The ground-plane is placed between the patch and the feed-line, and coupling between the two is provided by an aperture or slot in the ground plane.

A microstrip patch can be electromagnetically- coupled using a coplanar feed-line or a buried feed-line. The buried feed-line technique employs a two-layer substrate as shown in Figure (1-4), one for the radiator and one for the feed-line. The substrate parameters can be chosen separately. The upper substrate on which the antenna is printed requires a relatively thick substrate with a low relative dielectric constant to enhance radiation and increase bandwidth, whereas the lower feed-line substrate requires a thin substrate with a higher relative dielectric constant to prevent radiation.

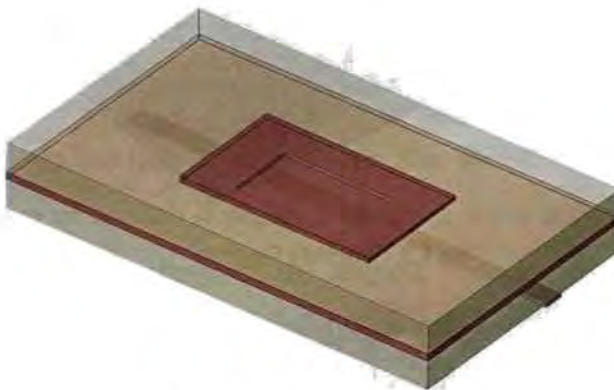


Fig.1.4 Aperture Coupling

(e) Coplanar feed

A microstrip patch can be electromagnetically- coupled using a coplanar feed-line. The coplanar feed-line tends to radiate more than the buried feed-line, because it is printed on the same substrate as the radiator, which has a high radiation efficiency. This is useful feed for coplanar printed antennas.



Fig.1.5 Coplanar feed coupling

1.3 Theoretical Analysis for Antenna modeling

Antenna engineers rely heavily on computer techniques to analyze and optimize the design. They have revolutionized the way in which electromagnetic problems are analyzed. Computer methods for analyzing problems in electromagnetics generally fall into one of the three categories:

1.3.1 Analytical techniques

Analytical techniques make simple assumptions about the geometry of a problem in order to apply a closed-form (or table look-up) solution. These techniques can be a useful tool when important electromagnetic (EM) interactions of the configuration can be anticipated. However, most electromagnetic compatibility (EMC) problems of interest are simply too unpredictable to be modeled by this approach. Cavity model is classical example and is detailed below here.

Cavity Model

Microstrip patch antennas are narrow band resonant antennas. In this model, the interior region of the patch is modeled as a cavity bounded by electric walls on the top and bottom, and magnetic walls along the periphery. The bases for these assumptions are the following:

For thin substrates,

- The fields in the interior region do not vary with substrate height because the substrate is very thin.
- Electric field is z directed along the height of the substrate only, and the magnetic field has only the transverse components in the region bounded by the patch metallization and the ground plane.
- The electric current in the patch has no component normal to the edges of the patch metallization, which implies that the tangential component of H along the edge is negligible, and the magnetic wall can be placed along the periphery.

The variation along the width of the patch is included in this model. The mutual coupling between the radiating edges are included implicitly in the form of radiated power, which accounts for the effect of mutual conductance. Its main limitation is that the variation of fields along the substrate thickness is not included.

Expert systems approach a problem in much the same way as a quick-thinking, experienced EM engineer with a calculator would. They do not actually calculate the fields directly, but instead estimate values for the parameters of interest based on a rules database. However, they are no better

than their rules database and are seldom used to model the complex EM interactions that cause EMI sources to radiate.

1.3.2 Numerical techniques

Numerical techniques attempt to solve fundamental field equations directly, subject to the boundary constraints posed by the geometry. They are the most powerful EM analysis tools, requiring more computation than the other techniques. They calculate the solution to a problem based on full-wave analysis. A variety of numerical techniques are available. The method used by a particular EM analysis program plays a significant role in determining the nature of problems it can handle and accuracy of results so obtained.

The main objective of any numerical method for Microwave circuit analysis is to develop an algorithm with minimum effort (in terms of CPU time & memory space), maximum accuracy and flexibility (to model a large variety of structures). Thus the choice of a numerical method is determined by its efficiency, accuracy and flexibility. The choice, however, is also strictly dependent on the problem at hand. No method can be thought of as the best one, but depending on the application, each can have advantages over the others. The EM modeling of Microwave circuits has to be viewed from the angles of radiating geometry, excitation techniques, boundary conditions etc..

The most important stage in EM modeling is the computation of EM fields in the structure by the solution of Maxwell's equations [37]. These equations are linear. But the boundary and interface conditions make it difficult to solve the Maxwell's equations analytically. The most commonly used methods in each category are briefly described below.

Method of Moments (MoM)

In the mid-1960's, Professor Harrington worked out a systematic, functional-space description of electromagnetic interactions, which he called the '*Method of Moments*'. The MoM is a general method for solving linear operator equations [38]. Here, an integral or integro-differential equation derived from Maxwell's equations for the structure of interest is interpreted as the infinite-dimensional functional equation, $Lf = g$, where L is a linear operator, g is a known function related to the excitation and f is an unknown function such as an induced current distribution that is to be determined.

The MoM approach is to set up a numerical solution by representing the unknown function f as a linear combination of a finite set of basis functions f_i in the domain of L . Then, a finite set of weighting functions w_i is defined in the range of L . After taking the inner product (usually integration) of the functional expansion with each weighting function, the linearity of the inner product is used to obtain a finite set of equations for the coefficients of the basis functions. This set of equations is then solved to obtain the approximate or exact solution of f , depending on the choice of the basis and weighting functions. The set of basis functions should have the ability to accurately represent and resemble the anticipated unknown function, while minimizing the computational effort required [39].

In principle, the MoM can be applied to the numerical modeling of arbitrary linear structures. However, this method has limitations primarily governed by the speed and storage capabilities of available digital computers [40]. Using more powerful computers increases the capability of MoM. Another option is to refine the method by choosing proper starting equations, developing flexible basis and weighting functions and using more sophisticated algorithms for the numerical evaluation of integrals encountered in the solution. However,

Moment Method techniques based on integral equations are not very effective when applied to arbitrary configurations with complex geometries or inhomogeneous dielectrics. Nevertheless, they do an excellent job of analysing a wide variety of three 3 dimensional electromagnetic radiation problem. Historically, the use of basis and testing functions to discretize integral equations of electromagnetics is most often named the “*Method of Moments*”, the same process applied to differential equations is usually known as the “*finite element method*”. However, the term finite element method is reserved for variational methods, explicitly minimizing a quadratic functional [49] as explained in the following section.

Finite Element Method (FEM)

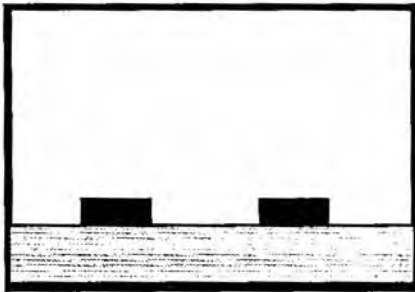
The Finite element method is one of the classic tools of numerical analysis, suitable for the solution of a wide class of partial differential or integral equations. In the mid-1970’s Mei, Morgan and Chang introduced the finite-element approach for the Helmholtz equation [38]. Later, in the early 1980’s, they shifted their finite element research to direct solutions of Maxwell’s curl equations. Finite element techniques require the entire volume of the configuration to be meshed as opposed to surface integral techniques, which require only the surfaces to be meshed. Each mesh element has completely different properties from those of neighbouring elements. In general, finite element techniques excel at modeling complex inhomogeneous configurations. However they do not model unbounded radiation problems as effectively as moment method techniques.

In general, finite element techniques excel at modeling complex inhomogeneous configurations. However, they do not model unbounded radiation problems as effectively as moment method techniques.

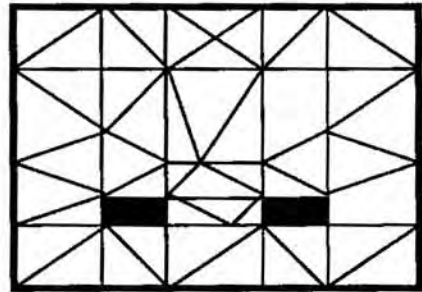
The finite element analysis of any problem involves basically four steps :

- discretizing the solution region into a finite number of sub regions or elements,
- deriving governing equations for a typical element,
- assembling of all elements in the solution region, and
- Solving the system of equations.

An example of a discretised finite–element model is shown in Figure 1.6. The model contains information about the device geometry, material constants, excitations and boundary constraints. In each finite element, a simple (often linear) variation of the field quantity is assumed. The corners of the elements are called *nodes*. The goal of the finite-element analysis is to determine the field quantities at the nodes.



Structure Geometry



Finite-element Model

Fig. 1.6 Finite-element modeling example

Generally, finite element analysis techniques solve for the unknown field quantities by minimising energy functional. The energy functional is an expression describing all the energy associated with the configuration being analysed.

The first step in finite element analysis is to divide the configuration into a number of small homogeneous pieces or *elements*. The model contains information about the device geometry, material constants, excitations and boundary constraints. In each finite element, a simple (often linear) variation of the field quantity is assumed. The corners of the elements are called *nodes*. The goal of the finite-element analysis is to determine the field quantities at the nodes. Generally, finite element analysis techniques solve for the unknown field quantities by minimizing an energy functional. The energy functional is an expression describing all the energy associated with the configuration being analysed. For 3-dimensional time-harmonic problems this functional may be represented as

$$F = \int_v \left(\frac{\mu |H|^2}{2} + \frac{\epsilon |E|^2}{2} - \frac{J \cdot E}{2j\omega} \right) dv \quad \dots\dots\dots (1.1)$$

The first two terms represent the energy stored in the magnetic and electric fields, and the third term is the energy dissipated by the conduction current. Expressing H in terms of E and setting the derivative of this functional with respect to E equal to zero, an equation of the form $f(J,E) = 0$ is obtained. A k^{th} order approximation of the function f is then applied at each node and boundary conditions enforced, resulting in the system of equations,

$$[J] = [Y][E] \quad \dots\dots\dots (1.2)$$

The elements of J are referred to as the source terms, representing the known excitations. The elements of the Y-matrix are functions of the problem geometry and boundary constraints. The elements of the E-matrix represent the unknown electric field at each node, obtained by solving the system of equations. In order to obtain a unique solution, it is necessary to constrain the values of the field at all boundary nodes. For example, the metal box of the

model in Figure 1.3 constrains the tangential electric field at all boundary nodes to be zero. Therefore, a major weakness of FEM is that it is relatively difficult to model open configurations. However, in finite element methods, the electrical and geometric properties of each element can be defined independently. This permits the problem to be set up with a large number of small elements in regions of complex geometry and fewer, larger elements in relatively open regions. Thus it is possible to model complicated geometries with many arbitrarily shaped dielectric regions in a relatively efficient manner.

Transmission Line Matrix (TLM) method

It is based on the equivalence between Maxwell's equations and the equations for voltages and currents on a mesh of continuous two-wire transmission lines. The main feature of this method is the simplicity of formulation and programming for a wide range of applications. In the TLM method, the entire region of the analysis is gridded. A single grid is established and the nodes of this grid are interconnected by virtual transmission lines. Excitations at the source nodes propagate to adjacent nodes through those transmission lines at each time step. Generally, dielectric loading is accomplished by loading nodes with reactive stubs, whose characteristic impedance is appropriate for the amount of loading desired. Lossy media can be modeled by introducing loss into the transmission line equations or by loading the nodes with lossy stubs. Absorbing boundaries are constructed in TLM meshes by terminating each boundary node transmission line with its characteristic impedance. Analysis is performed in the time domain.

TLM method shares the advantages and disadvantages of the FDTD method. Complex, nonlinear materials are readily modeled, impulse responses and time-domain behaviour of the systems are determined explicitly, and the technique is

suitable for implementation on massively parallel machines. Another advantage of using the TLM method is that certain stability properties can be deduced by inspection of the circuit. There are no problems with convergence, stability or spurious solutions. The method is limited only by the amount of memory storage required, which depends on the complexity of the TLM mesh. Also, being an explicit numerical solution, the TLM method is suitable for nonlinear or inhomogeneous problems since any variation of material properties may be updated at each time step. Thus voluminous problems using fine grids require excessive amounts of computation. Nevertheless, both TLM and FDTD techniques are very powerful and widely used. For many types of EM problems, they represent the only practical methods of analysis. Deciding whether to utilize a TLM or FDTD technique is a largely personal decision. Though the TLM method requires significantly more computer memory per node, it generally does a better job of modeling complex boundary geometries. On the other hand, the FDTD method is attractive because of its simple, direct approach to the solution of Maxwell's equations.

Finite Difference Time Domain (FDTD) Method

The Finite Difference Time Domain (FDTD) method introduced by K. S. Yee in 1966 [42] and later developed by Taflove [43] in the 1970's permits in principle, the modeling of electromagnetic wave interactions with a level of detail as high as that of the Method of Moments. Unlike MoM, however, the FDTD does not lead to a system of linear equations defined over the entire problem space. Updating each field component requires knowledge of only the immediately adjacent field components calculated one-half time step earlier. Therefore, overall computer storage and running time requirements for FDTD are linearly proportional to N , the number of field unknowns in the finite volume of space being modeled. The FDTD method has thus emerged as a viable alternative to the conventional Frequency Domain methods because of its dimensionally reduced

computational burdens and ability to directly simulate the dynamics of wave propagation [44-49]. The survey paper by Shlager and Schneider illustrates the rapid growth of FDTD [14]. Appendix-A describes in detail the FDTD method employed for the numerical computation of the radiation characteristics of the Rectangular Printed monopole UWB Antenna in the present work.

1.4 Compact Antenna Applications

The diversity of applications and operational environments has led, through the accompanying high production volumes, to tremendous advances in cost-efficient manufacturing capabilities of microwave and RF products. This, in turn, has lowered the implementation cost of a host of new wireless as well as wired RF and microwave services. Inexpensive handheld GPS navigational aids, automotive collision-avoidance radar, and widely available broadband digital service access are among these. Microwave technology is naturally suited for these emerging applications in communications and sensing, since the high operational frequencies permit both large numbers of independent channels for the wide variety of uses envisioned as well as significant available bandwidth per channel for high speed communication [53]. One of the envisaged applications concerns the field of medical imaging. The reason is their fully planar format, which makes them a more suitable at UWB microwave applications.[50-54]. Compact broad band antenna is essentially required for the following applications.

- DTV band 470 to 860 MHz
- Cellular band 800 to 970 MHz
- PCS(Personal communication band) 1.8 to2 GHz
- UMTS band 2 to 2.3 GHz
- WiMax , WiFi , Wibro and other OFDM bands 2.3 to 3.7 GHz

- Bluetooth 2.4 to 2.4835 GHz
- WLAN 2.4 to 2.4835 GHz, 5.15 to 5.35 GHz and 5.725 to 5.850 GHz
- Low band UWB 3.1 to 5.15 GHz

The frequency bands allotted for the popular wireless communication services are listed in Table 1.4.

Table 1.4 Frequency bands allotted for various wireless communication services

Wireless communication service		Allotted frequency band	Antenna type
GPS 1575 GPS 1400	Global Positioning System	1565-1585 MHz 1227-1575 MHz	Microstrip or Helix
GSM 900	Global system for mobile communication	890-960 MHz	Dipoles or patch array in BTS. Monopoles, sleeve dipoles and patch in hand held sets.
DCS 1800	Digital communication system	1710-1880 MHz	
PCS 1900	Personal Communication System	1850-1990 MHz	
UMTS 2000	Universal Mobile Telecommunications Systems	1920-2170 MHz	
3G IMT-2000	International Mobile Telecommunications-2000	1885-2200 MHz	
ISM 2.4 ISM 5.2 ISM 5.8	Industrial, scientific, medical	2400-2484 MHz 5150-5350 MHz 5725-5825 MHz	
RFID	Radio Frequency Identification system	30MHz-2.4GHz	Loops, folded F patch and monopole
DVB-H	Digital Video Broadcasting on hand held devices	470-890MHz	Compact printed Antennas
UWB	Ultra Wide Band	3.1 -10.6GHz	Printed dipoles or Monopoles

Very recently, the addition of more and more features in each new generation communication systems demands universal antennas. A universal antenna should support five cellular bands (GSM850/900/1800/1900 + 3G), Wireless LAN, Bluetooth, Digital TV (DVB-H), FM radio and GPS. In the next few years to come , several new wireless systems such as RF-ID, UWB, WiMAX etc. will probably also be integrated to the terminal.

1.5 Printed Antenna for UWB Applications

Ultra-wideband (UWB) antennas are of great interest for a variety of applications such as transient radars, mine detection, and unexploded ordnance (UXO) location and identification, especially, in military fields. Recently, in early 2002, the Federal Communication Commission (FCC)'s released of the UWB for commercial communication applications and sparked renewed interest in the subject of UWB antennas. Ultra wide-Band (UWB) technology is one of the most promising solutions for future communication systems due to its high-speed data rate and excellent immunity to multipath interference.

Since the approval of UWB spectrum for unlicensed use by the Federal Communications Commission (FCC) in 2002 [21], UWB technology and its potential applications in wireless communications systems have been attracting increasing interests from both academia and industry. According to the Federal Communications Commission (FCC), the frequency band of the UWB should be between 3.1 and 10.6 GHz. To achieve the high data rate UWB antenna should radiate short pulse with duration of 0.3ns without time ranging. In wireless communications, UWB will see its application in high data rates (> 100 Mb/s) transmission over very short distance (< 10 m) and low data rates (< 1 Mb/s) with very low power consumption for medium indoor

communications. UWB wireless communications systems have many expected attractive features and advantages. There are, however, also many technical issues needed to be resolved. UWB antenna should cover the allocated 7500 MHz of spectrum so to fully utilize the spectrum. The UWB antennas proposed in [54-57], have wide impedance bandwidth and good radiation patterns. However, these are not planar structure. Recently, a microstrip planar circular disc monopole antenna has been reported [58] , which presents a CPW fed circular UWB antenna, with better flexibility for circuit integration.

The inherent drawback of microstrip antenna is its narrow impedance bandwidth. Different approaches for increasing the bandwidth are available in the literature. They include thick substrate with low dielectric constant, using multiple patches stacked vertically, using multiple patches in one plane, and using broadband impedance matching networks [58]. By using thick substrate the enhancement of bandwidth is limited because of the large inductance and radiation associated with the feed, and increased excitation of surface waves. Use of parasitic patches increases the overall volume of the antenna.

For the commercial applications, the UWB antennas should be low profile, light weight, low cost, and fabricated easily. The traditional microstrip antennas can meet most of these needs only with the narrow bandwidth. Many designers have tried various ways to improve the above handicap and many valuable results have been obtained.

Today the state of the art of UWB antennas focuses on the microstrip, slot and planar and printed monopole antennas. In the design of a printed UWB antenna, the radiator and ground plane shapes as well as the feeding structure can be optimized to achieve a broad impedance bandwidth [59-63].

Many techniques were reported in recent years to broaden the impedance bandwidths of planar antennas and to reduce their electrical dimensions, including RC-loading [62], resistor-loading [63], gap loading [64], the folding [65], the multi-feed [66], the beveling [67], and adding the shorting pin [68], [69], etc. In addition, a coupled sectorial loop antenna is presented by connecting two sectorial loop antennas in parallel [70], square planar monopole [71]. Asymmetrical feed arrangement [72], adjusting the gap between radiating element and ground plane [73], a double feed [74] is reported for extending bandwidth to UWB.

Use of multiple resonators in the same plane is another method to increase the bandwidth. Stagger tuned resonators leads to wider bandwidth. But the two associated problems are large area requirement and deterioration of radiation pattern over bandwidth. A method to overcome these two problems is by the use of multiple resonators gap-coupled along the non-radiating edges. Techniques like U-shaped slot and L-probe are also used for the enhancement of bandwidth. These methods also increase the volume of the antenna substantially. A novel technique to enhance the bandwidth of microstrip antenna without much increase in volume is presented in this thesis. The strips in patch and slots in truncated ground is proposed here to increase the current path for compactness and multiple current path to merge suitable resonance to enhance the bandwidth.

The printed UWB antenna consisting of a planar radiator and a ground plane which is essentially an unbalanced design, where the electric currents are distributed on both the radiator and the ground plane so that the radiation from the ground plane is inevitable. Therefore, the performance of the printed UWB antenna is significantly affected by the shape and size of the ground plane in

terms of the operating frequency, impedance bandwidth, and radiation patterns [44-45]. Such a ground-plane effect causes severe practical engineering problems such as design complexity and deployment difficulty. Therefore, this work presents a technique to reduce the ground-plane effect on the performance of a small printed UWB antenna. The printed antenna is designed to cover the UWB band of 3.1-10.6 GHz, in particular, the lower band of 3.1-5 GHz. By adding a rectangular strip horizontally from the printed radiator and asymmetrically attaching a conducting strip to the radiator, Band width can be extended to higher frequencies. The overall size of this antenna is printed onto a 1.6mm thick FR4 substrate is only $20 \times 30 \text{ mm}^2$.

1.6 Outline of the Present Work

In this thesis, the theoretical and experimental investigations towards the development of a Ultra-Wideband printed Monopole Antenna with various patch geometries are presented. The performance of the antenna to various parameters are discussed in detail.

Ground plane is a crucial factor for these printed monopoles. The antenna performance significantly varies for infinite to finite ground plane transition. When the ground plane is truncated, the current distribution on the ground plane at the radiating frequency becomes more significant. This influences the radiation characteristics of the antenna to a great extent. Unfortunately antenna designers often choose the ground plane dimension in an adhoc manner driven by the convenience rather than through examination of electrical limitations. Even though the printed technology is fully matured, the dependence of ground plane on the antenna characteristics is often least considered by the researchers and designers. This state of affairs inspired for detailed investigations on the ground plane effects of simple

strip monopole. The procedure is successfully applied to reduce the dimensions of Rectangular patch antenna using the discontinuities such as Defected Ground Structure (DGS) and Defected Microstrip Structure (DMS) [75-77]. Since it has more discontinuities providing larger targets for EM wave, the net result in area reduction. The DGS is realized by etching slots in the truncated ground plane of the printed monopole. This property of DGS is effective for miniaturization of printed planar antennas.

The bandwidth enhancement is achieved by preserving the omnidirectional radiation characteristics of the antenna. The experimental and theoretical studies revealed that the optimized top loaded strip monopole antenna is suitable for UWB operation and compact type [78]. These desirable characteristics make the present antenna suitable for Ultra wide band applications. The Rectangular or square geometry is found to be most suitable for Ultra wide band applications even though all the optimized geometries for top loading results in wide band compact antennas as proved experimentally and reported here. This thesis gives the systematic evolution of the simple printed strip monopole to UWB antenna.

For the theoretical analysis, Finite Difference Time Domain method (FDTD) is employed. Radiation and reflection characteristics of the optimized Antenna for each optimized geometry are studied using FDTD.

1.7 Chapter Organization

Following the introductory Chapter 1, a brief review of the past work in the field of patch antennas mainly wide band monopoles with due emphasis on impedance matching for UWB applications are presented in Chapter 2.

Chapter 3 deals with the methodology of design, simulation, optimization, fabrication and the experimental measurements carried out on different antenna configurations. Selection of the best geometry for structural modification for Ultra wide band applications is also presented in this chapter. This chapter also describes the analysis of the proposed antenna by FDTD method using the in house developed code.

Chapter 4 gives the systematic evolution of the simple printed strip monopole towards UWB antenna by top loading patch geometries. The comparisons between the theoretical and experimental results on various antenna configurations are also presented. Excellent agreement between theory and experiment is observed.

Ultra wide Bandwidth antenna configuration and its radiation properties like pattern, polarization, Gain, efficiency, etc.. are presented. This observations lead to the development of a compact printed UWB antenna in chapter -4.

The conclusions derived from the theoretical and experimental studies are described in Chapter 5. Salient features of proposed monopole loaded antennas for UWB applications and the scope of further work is also outlined.

Appendix A deals with the theoretical analysis by FDTD method.

Appendix B deals with the experimental and theoretical results of the studies conducted on Circular microstrip patch with conformal FDTD.

1.8 References.

- [1] Planar Monopole Antennas for 2.4/5.2 GHz Dual-Band Application” Jen-Yea Jan and Liang-Chih Tseng, Department of Electronic Engineering National Kaohsiung University of Applied Sciences, **Kaohsiung 807, Taiwan**

- [2] M. Ali and G. J. Hayes, "Analysis of integrated inverted-F antennas for Bluetooth applications." 2000 *IEEE AP-S Conf Antenna Propagation for Wireless Communication*, Waltham, MA, pp. 21-24.
- [3] R.B.Waterhouse, "Printed antenna suitable for mobile communication handsets," *Electron. Lett.*, vol.33, no.22 pp.1831-1832, 23 October 1997.
- [4] R.B.Waterhouse, "Small printed antenna easily integrated into a mobile handset terminal," *Electron. Lett.*, vol.34, no.17, pp.1629-1631, 20 August 1998
- [5] E. Lee, P. S. Hall, and P. Gardner, "Compact wideband planar monopole antenna," *Electron. Lett.*, vol. 35, no. 25, pp. 2157–2158, Dec. 1999
- [6] M.T.Lee, K.M.Luk, K.W.Leung and M.K.Leung, "A small Dielectric Resonator Antenna," *IEEE Trans. Antennas Propagat.*, vol.50, no.10, pp.1485-1487, October 2002.
- [7] Corbett R.Rowell, R.D.Murch, "A capacitively loaded PIFA for compact mobile telephone handsets," *IEEE Trans. Antennas Propagat.*, vol.45, no.5, pp.837-841, May 1997.
- [8] Kathleen.L.Virga, Yahya Rahmat- Samii, "Low Profile Enhanced Bandwidth PIFA Antennas for Wireless Communications Packaging," *IEEE Trans. Microwave Theory Tech.*, vol.45, no.10, pp.1879-1889, October 1997.
- [9] A Planar Inverted Cone Antenna, S.-Y. Suh and W. L. Stutzman. (2000, Sept. 8). [Online]. Available: <http://www.vtip.org/Licensing/disclosures/00-130.htm>
- [10] S.-Y. Suh, "A comprehensive investigation of new planar wideband antennas," Ph.D. dissertation, Virginia Polytech. Inst. State Univ., Blacksburg, VA, July 2002.
- [11] K.-L. Wong, "Planar Antennas for Wireless Communications",. Wiley, 2003.
- [12] Deschamps G. A, "Microstrip Microwave Antennas", 3rd USAF symposium on Antennas, 1953.
- [13] Hassan M. Elkamchouchi and Hossam El-dien M.Hafez, "Multi-band smart patch antenna for GPS/PCS hand held units," Proc., *IEEE 3rd International Conference on Microwave and Millimeter wave Technology*, 2002.

- [14] X. H. Wu and Z. N. Chen, "Comparison of planar dipoles in UWB applications," *IEEE Trans. Antennas Propag.*, vol. 53, no. 6, pp. 1973–1983, Jun. 2005
- [15] Z.D. Liu, P.S. Hall, and D. Wake, "Dual-frequency planar inverted-F antenna". *IEEE Trans Antennas Propagat* AP-45 (1997), 1451–1458.
- [16] C.R. Rowell and R.D. Murch, "A compact PIFA suitable for dual-frequency 900/1800-MHz operation", *IEEE Trans Antennas Propagat.* AP-46 (1998), 596–598.
- [17] P. Salonen, M. Keskilammi, and M. Kivikoski, "New slot configurations for dual-band planar inverted-F antenna", *Microwave Opt Technol Lett* 28 (2001), 293–298.
- [18] M. Martı́nez-Va’zquez, M. Geissier, D. Heberling, A. Martı́nez-Gonza’-lez, and D. Sa’ńchez-Herna’ndez, "Compact dual-band antenna for mobile handsets" , *Microwave Opt Technol Lett* 32 (2002), 87–88.
- [19] F.R. Hsiao, H.T. Chen, T.W. Chiou, G.Y. Lee, and K.L. Wong, "A dual-band planar inverted-F patch antenna with a branch-line slit", *Microwave Opt Technol Lett* 32 (2002), 310–312.
- [20] C.W. Chiu and F.L. Lin,"Compact dual-band PIFA with multi resonators", *Electron Lett* 38 (2002), 538–540.
- [21] FCC, First Report and Order 02-48. February 2002.
- [22] S. Honda, M. Ito, H. Seki, and Y. Jinbo, "A disk monopole antenna with 1:8 impedance bandwidth and omnidirectional radiation pattern", *ISAP ’92*, Sapporo, Japan, (1992), 1145–1148.
- [23] N.P. Agrawall, G. Kumar, and K.P. Ray, "Wide-band planar monopole antenna", *IEEE Trans Antennas Propagat* AP-46 (1998), 294–295.
- [24] M.J. Ammann, "Square planar monopole antenna", *National Conf Antennas Propagat*, York, England (1999), 37–40.
- [25] Z.N. Chen, "Impedance characteristics of planar bow-tie-like monopole antennas", *Electron Lett* 36 (2000), 1100–1101.
- [26] Z.N. Chen, "Experimental on input impedance of tilted planar monopole antennas", *Microwave Opt Technol Lett* 26 (2000), 202–204.

-
- [27] Z.N. Chen and M.Y.W. Chia, "Impedance characteristics of trapezoidal planar monopole antenna", *Microwave Opt Technol Lett* 27 (2000), 120–122.
- [28] J.A. Evans and M.J. Ammann, "Planar trapezoidal and pentagonal monopoles with impedance bandwidths in excess of 10:1", *IEEE Int Symposium on Antennas and Propagat*, Orlando, USA, (1999), 1558–1561.
- [29] M. J. Ammann, "Impedance bandwidth of the square planar monopole", *Microwave and Opt Technol Lett* 24 (2000), 185–187.
- [30] G.Y. Chen and J.S. Sun, "A printed dipole antenna with microstrip tapered balun", *Microwave Opt Technol Lett* 40 (2004), 344–346.
- [31] T. Vasiliadis, E. Vaitopoulos, and G. Sergiadis, "A wideband printed dipole antenna with optimized tapered feeding balun for ISM, and FW bands", *Microwave Opt Technol Lett* 43 (2004), 437–441.
- [32] K. Chang, H. Kim, and Y. Yoon, "A triple-band printed dipole antenna using parasitic elements", *Microwave Opt Technol Lett* 47 (2005), 221–223
- [33] C. L. Mak, K.M.Luk and K.F.Lee, "Proximity-coupled U-slot patch antenna," *Electron. Lett.*, vol.34, no.8, pp.715-716, 16 April 1998.
- [34] Korada Umashankar and Allen Taflove, "Computational Electromagnetics," Artech House; Norwood, MA, 1993.
- [35] Constantine A. Balanis, "Advanced Engineering Electromagnetics," John Wiley and Sons, USA, 1989.
- [36] Branko M. Kolundzija and Antonije R. Djordjevic, "Electromagnetic modelling of composite metallic and dielectric structures," Artech House, Inc., Norwood, MA, 2002.
- [37] Allen Taflove, "Numerical issues regarding finite-difference time-domain modelling of Microwave structures," *Time-Domain Methods for Microwave structures – Analysis and Design*, Ed. Tatsuo Itoh and Bijan Houshmand, *IEEE Press*.
- [38] Allen Taflove and Morris E. Brodwin, "Numerical solution of steady – state electromagnetic scattering problems using the time-dependent Maxwell's equations," *IEEE Trans. Microwave Theory Tech.*, vol.23, pp.623-630, August 1975.

- [39] Ying Shen, Zhiqiang Bi, Keli Wu and John Litva, "FD-TD analysis of open cylindrical dielectric resonators," *Microwave Opt. Technol Lett.*, vol.5, no.6, pp.261-265, 5 June 1992.
- [40] S.M.Shum and K.M.Luk, "Characteristics of dielectric ring resonator antenna with an air gap" *Electron. Lett.*, vol.30, no.4, pp. 277-278, 17 February 1994.
- [41] A.V. Nogueira, M. F. Bataller, and M. Cabedo-Fabres, "A wideband arrowhead planar monopole antenna for multi-service mobile systems," *Microw. Opt. Technol. Lett.*, vol. 37, no. 3, pp. 188–190, May 2003.
- [42] Jaakko Juntunen, Outi Kivekas, Jani Ollikainen and Pertti Vainikainen, "FDTD Simulation of a wide-band half volume DRA," *IEEE Antennas Propagat. Soc. Int. Symp.*, Salt lake city, Ohio pp.223-226, June 2000.
- [43] Elena Semouchkina, Wenwu Cao, Michael Lanagan, Raj Mittra and Wenhua Yu, "Combining FDTD simulations with measurements of Microstrip ring resonators for characterization of low and high K dielectrics at microwaves," *Microwave Opt. Technol Lett.*, vol.29, no.1, pp.21-24, 5 April 2001.
- [44] Elena Semouchkina, George Semouchkin, Raj Mittra and Wenwu Cao, "Finite-Difference Time-Domain simulation of resonant modes of rectangular dielectric resonators," *Microwave Opt. Technol.Lett.*, vol.36, no.3, pp.160-164, 5 February 2003.
- [45] Takashi Ando, Junji Yamauchi and Hisamatsu Nakano, "Numerical analysis of a dielectric rod antenna-demonstration of the discontinuity-radiation concept," *IEEE Trans. Antennas Propagat.*, vol.51, no.8, pp. 2007-2013, August 2003.
- [46] Kurt L.Shlager and John B.Schneider, "A selective survey of the Finite-Difference Time-Domain literature," *IEEE Antennas Propagat. Mag.*, vol.37, no.4, pp.39-57, August 1995.
- [47] A. Cai, T. S. P. See, and Z. N. Chen, "Study of human head effects on UWB antenna," in *IEEE Int.Workshop on Antenna Technology (iWAT)*, Singapore, Mar. 7–9, 2005, vol. 1, pp. 310–313.
- [48] Ya Jun Wang, Ching Kwang Lee, Wee Jin Koh and Yeow Beng Gan, "Design of Small and Broad-band Internal Antennas for IMT-2000 Mobile Handsets," *IEEE Trans. Microwave Theory Tech.*, vol.49, no.8, pp.1398 – 1403, August 2001.

-
- [49] Marta Martinez-Vazquez, Matthias Geissier, Dirk Heberling, Antonio Martinez-Gonzalez and David Sanchez-Hernandez, "Compact Dual-band antenna for mobile handsets", *Microwave Opt. Technol. Lett.*, vol.32, no.2, pp. 87-88, 20 January 2002
- [50] T.Yang and W. A. Davis, "Planar half-disk antenna structures for ultrawideband communications," in *Proc. IEEE Int. Symp. Antennas Propagation*, Jun. 2004, vol. 3, pp. 2508–2511.
- [51] D. H. Kwon and Y. Kim, "CPW-fed planar ultrawideband antenna with hexagonal radiating elements," in *Proc. IEEE Int. Symp. Antennas Propagation*, Jun. 2004, vol. 3, pp. 2947–2950.
- [52] J. Liang, C. C. Chiau, X. Chen, and C. G. Parini, "Printed circular ring monopole antennas," *Microw. Opt. Technol. Lett.*, vol. 45, no. 5, pp. 372–375, Jun. 5, 2005.
- [53] H. S. Choi, J. K. Park, S. K. Kim, and J. Y. Park, "A new ultrawideband antenna for UWB applications," *Microw. Opt. Technol. Lett.*, vol. 40, no. 5, pp. 399–401, Mar. 5, 2004.
- [54] K. Chung, H. Park, and J. Choi, "Wideband microstrip-fed monopole antenna with a narrow slit," *Microw. Opt. Technol. Lett.*, vol. 47, no. 4, pp. 400–402, Nov. 20, 2005.
- [55] Z. N. Chen, "Impedance characteristics of planar bow-tie-like monopole antennas," *Electron. Lett.*, vol. 36, no. 13, pp. 1100–1101, 2000.
- [56] T.Yang and W. A. Davis, "Planar half-disk antenna structures for ultrawideband communications," in *Proc. IEEE Int. Symp. Antennas Propagation*, Jun. 2004, vol. 3, pp. 2508–2511.
- [57] D. H. Kwon and Y. Kim, "CPW-fed planar ultrawideband antenna with hexagonal radiating elements," in *Proc. IEEE Int. Symp. Antennas Propagation*, Jun. 2004, vol. 3, pp. 2947–2950.
- [58] J. Liang, C. C. Chiau, X. Chen, and C. G. Parini, "Printed circular ring monopole antennas," *Microw. Opt. Technol. Lett.*, vol. 45, no. 5, pp. 372–375, Jun. 5, 2005.
- [59] H. S. Choi, J. K. Park, S. K. Kim, and J. Y. Park, "A new ultrawideband antenna for UWB applications," *Microw. Opt. Technol. Lett.*, vol. 40, no. 5, pp. 399–401, Mar. 5, 2004.

- [60] K. Chung, H. Park, and J. Choi, "Wideband microstrip-fed monopole antenna with a narrow slit," *Microw. Opt. Technol. Lett.*, vol. 47, no. 4, pp. 400–402, Nov. 20, 2005.
- [61] Y. Zhang, Z. N. Chen, and M. Y. W. Chia, "Effects of finite ground plane and dielectric substrate on planar dipoles for UWB applications," in *Proc. IEEE Int. Symp. Antennas Propagation*, Jun. 2004, pp. 2512–2515.
- [62] C. Waldschmidt and K. D. Palmer, "Loaded wedge bow-tie antenna using linear profile," *Electron. Lett.*, vol. 37, no. 4, pp. 208–209, Feb. 2001.
- [63] D. Uduwawala, M. Norgren, P. Fuks, and A. W. Gunawardena, "A deep parametric study of resistor-loaded bow-tie antennas for ground-penetrating radar applications using FDTD," *IEEE Trans. Geosci. Remote Sensing*, vol. 48, no. 4, pp. 732–742, Apr. 2004.
- [64] R. L. Li and V. F. Fusco, "Broadband semiloop antenna," *Microw. Opt. Technol. Lett.*, vol. 34, no. 4, pp. 233–234, Aug. 2002.
- [65] F.-R. Hsiao and K.-L. Wong, "Omnidirectional planar folded dipole antenna," *IEEE Trans. Antennas Propag.*, vol. 52, no. 7, pp. 1898–1902, Jul. 2004.
- [66] K.-L. Wong, C.-H. Wu, and S.-W. Su, "Ultrawide-band square planar metal-plate monopole antenna with a trident-shaped feeding strip," *IEEE Trans. Antennas Propag.*, vol. 53, no. 4, pp. 1262–1268, Apr. 2005.
- [67] J. Qiu, Z. Du, J. Lu, and K. Gong, "A case study to improve the impedance bandwidth of a planar monopole," *Microw. Opt. Technol. Lett.*, vol. 45, no. 2, pp. 124–126, Apr. 2005.
- [68] M. J. Ammann and Z. N. Chen, "A wide-band shorted planar monopole with bevel," *IEEE Trans. Antennas Propag.*, vol. 51, no. 4, pp. 901–903, Apr. 2003.
- [69] A. V. Nogueira, M. F. Bataller, and M. Cabedo-Fabres, "A wideband arrow head planar monopole antenna for multi-service mobile systems," *Microw. Opt. Technol. Lett.*, vol. 37, no. 3, pp. 188–190, May 2003.
- [70] N. Behdad and K. Sarabandi, "A compact antenna for ultrawide-band applications," *IEEE Trans. Antennas Propag.*, vol. 53, no. 7, pp. 2185–2192, Jul. 2005.

- [71] S. W. Su, K.-L. Wong, and C.-L. Tang, "Ultra-wideband square planar monopole antenna for IEEE 802.16a operation in the 2–11-GHz band," *Microw. Opt. Technol. Lett.*, vol. 42, no. 6, pp. 463–466, Sep. 2004.
- [72] Ammann, M.J., and Chen, Z.N.: 'An asymmetrical feed arrangement for improved impedance bandwidth of planar monopole antennas', *Microw. Opt. Technol. Lett.*, 2004, 40, pp. 156–158.
- [73] Floch, J.M., and Desclos, L.: "Surface-mounted monopole antenna", *Microw. Opt. Technol. Lett.*, 1997, 16, pp. 349–352.
- [74] Antonino-Daviu, E., Cabedo-Fabres, M., Ferrando-Bataller, M., and Valero-Nogueira, A.: "Wideband double-fed planar monopole antennas", *Electron Lett.*, 2003, 39, pp. 1635–1636.
- [75] J.S. Lim, Y.T. Lee, C.S. Kim, D. Ahn and S. Nam, "A vertically Periodic Defected Ground Structure and its applications in reducing the size of microwave circuits" *IEEE microwave and Wireless Components Letters*, Vol.12, No.12, December 2002, pp.479-481.
- [76] J.A. Tirando-Mendez, H. Jardon-Aguilar, F. Iturbide-Sanchez, I Gracia – Ruiz, V. Molina-Lopez and R. Acevo-Herrera, "A Proposed Defected Microstrip Structure (DMS) Behavior for reducing Rectangular patch antenna size", *Microwave and optical Technology Letters*, Vol.43, No.6, December 2004, pp. 481-484.
- [77] J.A. Tirando-mendez, H. Jardon –Aguiliar and F. Iturbide-Sanchez, "Application of the Defected Microstrip Structure as a Tuning Technique for Rectangular Printed Antenna," *Microwave and optical Technology Letters*, Vol.48, No.2, February 2006, pp. 370-373.
- [78] K. F. Jacob, M. N. Suma, R. K. Raj, M. Joseph and P. Mohanan, "Planar Branched Monopole Antenna for UWB Applications," *Microw. Opt. Technol. Letts.*, vol.49, no.1, pp45-47, Jan. 2007

REVIEW OF LITERATURE

Introduction

Microstrip Antenna have developed a long way ever since it was first fabricated by Byron [13] in early 1970's as a long strip of various patch geometries like rectangular, circular etc.. These developments are well documented in books [1-12] and the technology is now mature enough for the specialized Microstrip antennas for the specific civil and military applications. The literature survey is carried out to assess the past work done on the subject to steer the research work towards the goal of developing a Printed Monopole antenna for Ultra Wide Band (UWB) Applications. This survey has covered Compact antennas, Band widening techniques, Ultra Wide Band (UWB) antennas, Numerical Techniques and finally the specific technique of FDTD analysis.

A major trend in Mobile Communication technology is the dramatic reduction in the size and weight of handsets. Common requirements on the antenna design regardless of the frequency include low cost, low profile, and in most applications, a large operating bandwidth. Antenna designers are therefore encountered with the difficulty of designing compact, multi-band, highly efficient antennas. Some of the typical antenna elements used for small mobile terminals are monopole, dipole, normal mode helix, planar inverted-F, Microstrip, meander line, ceramic and chip antenna. Although whip antennas are inexpensive and mechanically simple, they are easily prone to damage.

Helical antennas are relatively inexpensive and exhibit wide bandwidth performance, but are not low profile. Mechanical resistance, aesthetic criteria and the need for high performance antennas are the key points that have brought internal antennas into the spot light. In the existing built-in antenna schemes, much attention has been paid to Microstrip antennas. However, they suffer from inherent bandwidth limitations and their physical size becomes large at low frequencies. Printed Monopole Antennas present a better alternative because of their relatively large bandwidth and compact size. A chronological review of the work done in the field of Compact antennas is presented in the beginning of the chapter. The progress of research in the Band widening technique, Ultra wide band (UWB), FDTD in Printed Antenna analysis is outlined in the next sections.

The recent, unprecedented increase in wireless mobile telephone usage and the subsequent explosive proliferation of related wireless mobile telecommunication systems has necessarily created a strong interest in compact, easily manufactured antennas to support these systems. The standard monopole is probably the most widely used antenna on existing mobile telecommunication applications, with the axial - mode helix coming in a close second. These two antenna types are simple to manufacture but they are not particularly easy to integrate into handset or mobile terminal cases, and they have relatively narrow operational bandwidths. Therefore, planar antennas, particularly printed circuit antennas are of considerable interest for modern applications.

2.1 Compact Antennas

In all wireless communications especially the recent interest in the technique of wireless connection between PC and other equipment such as mouse, keyboard, printer, etc. In all these cases one of the main concerns is the

size reduction of each module, especially for antennas. By decreasing the size of an antenna, the module volume can be reduced for a competitive price. Here comes the compactness of antenna to play a major role in gadget miniaturisation.

Antenna size can be reduced by using very high dielectric materials, but at a cost in antenna gain is reported by Y. Dakeya [14]. This paper gives the details of chip multilayer antenna for 2.45GHz application using LTCC technology.

To minimize the size of an antenna while retaining high gain, mainly four kinds of techniques like shorted wall, meander line, adding skirts and offset slit are applied to an antenna. M. Chair, K.M. Luk, and K.F. Lee [15] has reported one of the technique to reduce the size by a quarter wave by using shorted walls.

M. Ali and S.S. Stuchly [16] have reported use of meander line between the coaxial probe feeder on the ground plane and a patch to reduce the size. In the third method, both skirts are added to both edges of the patch downward. Lastly, the patch has an offset slit at the connection part (between meander line and patch) but maintains the same meander- line width. This resulted a compact planar antenna.

Monopole antennas have found widespread applications in wireless mobile communication systems. The increasing use of mobile communication systems has stimulated the interest in the dual-frequency monopole antennas for dual band operation. Numerous designs of dual-frequency compact monopole antennas have been reported, including the use of a center-fed monopole surrounded by multiple parasitic monopoles D. Liu [17], R. Schlub et al [18].

A multi-branch monopole is reported in D. Liu [19] for dual band cellular applications. C. T. P. Song et al [20] has reported multi-circular loop monopole antenna, a dual band folded monopole for terrestrial communication is reported in E. Lee et al [21].

Dual frequency wire antenna described in P. Eratuuli et al [22] and A combination of the inverted F antenna and normal- mode helix is reported H. Nakano et al [23].

It is noted that the above mentioned monopole antennas are commonly mounted above a large ground plane and excited by a probe feed. Recently, the microstrip-line-fed technique has also been applied for designing dual-frequency printed monopole compact antenna and reported in H. M. Chen [24] and F. S. Chang, S. H. Yeh, and K. L. Wong [25].

A monopole antenna fed by a coplanar waveguide (CPW) have been reported in Horng-Dean Chen et al [26]. CPW-fed antennas have many attractive features, such as no soldering points, easy fabrication and integration with monolithic microwave integrated circuits, and a simplified configuration with a single metallic layer. Thus, the designs of the CPW-fed antennas have recently received much attention.

Use the electromagnetic coupling technique for planar monopole antenna as reported in C. Y. Pan et al [27] is capable of broadband operation. This dual-band printed planar monopole antenna consists of crisscross monopole element, conductor-backed parasitic plane and microstrip feed line. Simply by loading a crisscross conducting strip and parasitic plane, dual-band operation can be easily obtained for WLAN operations in the 2.4 and 5.2 GHz bands.

The inverted-F antenna printed on a dielectric substrate for applications for Blue-tooth and UMTS applications has been demonstrated by M. Ali and G. J. Hayes [28], Y. L. Kuo and K. L. Wong [29]. The printed metallic strip of the antenna is shorted to the ground plane on the other side of the dielectric substrate. This methodology has tremendously reduced the size of the antenna by two fold.

To achieve dual-band operations for the WLAN and HIPERLAN systems, printed monopoles in the form of an F-shaped structure have also been proposed by S. H. Yeh and K. L. Wong [30]. The paper, Jen-Yea Jan and Liang-Chih Tseng [31] gives two new designs of planar monopole antennas with a shorted parasitic inverted-L wire for achieving dual-band operations: one is a rotated-F planar monopole driven patch coupled with a shorted inverted-L wire and the other is a T-shaped planar monopole driven patch coupled with a shorted inverted-L wire.

New slot configuration for dual band planar inverted F antenna as reported by P. Solomen *et al* [32]. A shorted microstrip antenna for 2.4/ 5.2GHz dual band operation H. C. Tung [33] is an interesting paper. A low cost microstrip fed dual frequency printed dipole antenna for wireless communications is reported by Y. W. Suh *et al* [34]

M. C. Pan and K. L. Wong [35] demonstrates a simple design of a printed triangular monopole for improving the operating bandwidth and reducing the length of a printed strip monopole. By choosing a suitable flare angle of the triangular monopole, it is expected that the impedance matching of the monopole to the feeding stripline can be significantly improved. Furthermore, due to the increased effective current path in the triangular monopole, as compared with a simple strip monopole of the same length, the required

monopole length at a fixed operating frequency can be reduced. The design and characteristics of the printed triangular monopole are also presented and discussed.

Fuhl.J *et al.* [36] analysed the performance of a radiation coupled Dual L antenna, placed on the back side of the metallic housing of the handset, resulting in a improved radiation pattern pointing away from the user's head. The antenna was designed for operation in the GSM 900 frequency band.

Z.D.Liu and P.S.Hall [37] proposed a dual-band Planar Inverted F Antenna (PIFA) for hand held portable telephones to operate at 0.9 GHz and 1.8 GHz. The compact antenna displayed omni-directional radiation patterns and 7% and 6.25% impedance bandwidths respectively in the two bands. J.C.Batchelor and R.J.Langley [38] carried out an investigation on narrow annular Microstrip slot antennas excited in a higher order mode, so as to give circularly polarized, conical radiation pattern at 7.1 GHz.

G.T.Pedersen *et al.* [39] discussed the development of a single integrated PIFA and diversity antenna configurations with low absorption. FDTD analysis of the antenna with the presence of the head is also carried out. The measurements of angular information in the environment were also provided in this paper. Their study highlighted the fact that a significant amount of shielding could be achieved by the case of the handset.

Y.J. Guo *et al.* [40] reported a TM_{02} circular patch antenna operating at 5.2 GHz. The antenna exhibited 3.3% bandwidth, 4.2 dB gain and a circularly symmetrical pattern with a notch in the zenith direction, suitable for radio LAN's. K.Takei *et al.* [41] proposed a 3 layered TEM slot antenna for personal handy - phone terminal. The antenna exhibited uniform radiation pattern,

resulting in high antenna gain and low electromagnetic hazard to the user and possessing a conventional surface mounting technology, resulting in reduced fabrication cost.

Corbett R.Rowell *et al.* [42] investigated the feasibility of utilizing a PIFA with a capacitive load to reduce the overall length from $\lambda/4$ to less than $\lambda/8$ for a mobile telephone handset suitable for DCS 1800. They also proposed a design methodology for capacitively loaded PIFA's.

Hiroyuki Arai *et al.* [43] measured the variation in antenna gain of handheld terminals for different terminal boxes and different human carriers. A $\lambda/4$ whip antenna mounted on a conducting box was used for the study at 900MHz. A compact printed antenna consisting of an annular ring coupled to a shorted circular patch suitable for mobile communication handset was proposed by R.B.Waterhouse [44]. The antenna provided 10% bandwidth.

Kathleen.L.Virga and Yahya Rahmat - Samii [45] discussed the development of low profile integrated antennas with enhanced bandwidth performance. The Planar Inverted F Antenna (PIFA), Radiation coupled dual L antenna and the diode tunable PIFA were considered for use in the 900 MHz band. Up to 9.6%, 16% and 50% bandwidth respectively was obtained for the three antennas.

A.Serrano-Vaello and D.Sanchez-Hernandez [46] demonstrated a dual band bow-tie antenna with impressive size reduction compared to conventional patch antennas. The radiation characteristics of this antenna for dual-band GSM/DCS 1800 mobile handsets were similar to conventional Microstrip patches. C.L.Mak *et al.* [47] presented the design and experimental results of a proximity-coupled U-slot patch antenna excited by a π shaped feed line

connected at the end of the usual Microstrip line. The antenna displayed 20% bandwidth at 4.3 GHz, 7.5 dBi average gain and -20 dB cross-polarisation.

Ch.Dalaveaud *et al.* [48] proposed a monopolar wire-patch antenna for portable telephones. The antenna operating at 1.8 GHz was characterized by a monopole type radiation with wide bandwidth. Corbett R. Rowell and R. D. Murch [49] described the design of a compact Planar Inverted-F Antenna (PIFA) suitable for cellular and PCS operation. The frequency of the conventional PIFA designed at 2.2 GHz was brought down to 900 MHz by the introduction of a shorting post, capacitor load and a slot cut on the top plate. By removing part of the top plate and inserting another PIFA, a dual fed, dual band antenna resonating at 900 and 1800 MHz was also constructed.

Reflectively coupled dipole configuration with strongly improved radiation efficiency was proposed by Roger Yew-Siow Tay *et al.* [50]. They demonstrated that reduction of the magnetic field strength at the surface of the user's head was the key parameter to improve the efficiency of the hand set. H.Iwasaki [51] proposed a Microstrip antenna with back-to-back configuration relative to a slot on a ground plane, for use in base station / portable telephones. The input impedance and radiation pattern were measured as parameters of the slot length. It was observed that an omni-directional or bi-directional radiation pattern could be obtained by feeding the antenna in phase or out of phase respectively.

O. Leisten *et al.* [52] described a dielectric loaded twisted loop antenna, which projected a magnetic field minimum and a radiated far field minimum towards the head to reduce user exposure. SAR measurements of the proposed antenna were performed using the DASY3 - the enhanced version of the dosimetric system. R.B.Waterhouse [53] presented a loaded cavity backed

patch antenna for PCS Network operating at 1.9 GHz, which could be easily integrated within a handset terminal. The observed radiation patterns were similar to a conventional shorted patch mounted on a large ground plane.

K.Hettak *et al.* [54] presented the design and experimental results of a coplanar waveguide (CPW) aperture coupled patch antenna for EHF band around 37 GHz. The antenna structure combined the advantages of CPW with those of aperture coupled Microstrip Antennas and also reduced the number of metallization levels. N.Chiba *et al.* [55] proposed a compact dual band internal antenna fed by a single feed, designed for the 900/1800 MHz band. The antenna comprised of an outer $\lambda/4$ annular ring antenna with a short circuited plane and an inner $\lambda/4$ rectangular patch antenna, designed for the lower and higher resonant frequency respectively. The radiation patterns of the antenna were shown to be almost similar to that of a conventional $\lambda/4$ Microstrip antenna with a short-circuited plane.

J. Ollikainen *et al.* [56] demonstrated a stacked, shorted patch antenna resonating at 900/1800 MHz. This small size, low profile antenna with 9% impedance bandwidth was found to be suitable for directive, internal cellular handset antenna applications. Jack. T. Rowley and Rod.B.Waterhouse [57] compared the performance of a single shorted patch and a stacked shorted patch antenna at 1800 MHz with that of a $\lambda/4$ monopole. Experimental and simulation results were presented for each of the antennas, in 3 different cases: on a handset in isolation, a handset near the realistic head model and with the inclusion of a block model of the hand.

C.T.P.Song *et al.* [58] presented a novel method for improving the design of a circular disc monopole by introducing a discontinuity effect resulting in

multiple loop monopole. Better control of the radiation pattern beyond a frequency ratio of 1:5.33 was demonstrated.

A compact circularly polarised printed antenna was proposed by H.Kan and R.B.Waterhouse [59]. The antenna consisted of a synchronous sub-array of shorted patches with the required feed network etched on a high dielectric constant substrate located below the ground plane of the antenna. The antenna displayed 10 dB return loss bandwidth of 8.5% and 3 dB axial ratio bandwidth of 11.3%. An antenna configuration incorporating one shorted driven patch and another shorted and coupled coplanar patch using a single probe feed to achieve broadband characteristics (up to 25% bandwidth) was proposed by Ya Jun Wang *et al.* [60] for use in IMT 2000 handsets. The patches were either rectangular or semicircular and 8 different combinations were used.

Marta Martinez - Vazquez, and her team of researchers [61] reported a compact dual-band antenna consisting of a shorted rectangular patch designed for 1.8 GHz. A spur-line filter embedded in its perimeter introduced a new resonance at 925 MHz. Hassan M. Elkamchouchi and Hossam El-dien M.Hafez [62] presented the detailed investigations using the Moment Method on a single layer multi-probe fed patch antenna. The antenna consisted of a hexagonal plate with unequal arms, suspended parallel to the ground plane. Up to 35% impedance bandwidth and stable radiation patterns throughout the band was observed.

Tsung-Wen Chiu *et al.* [63] proposed a Microstrip line fed circularly polarized ceramic chip antenna for GPS operation at 1575 MHz. The antenna comprised of a square radiating patch printed on the top surface of a grounded square disk ceramic chip having two side feeds printed at the centres of the two adjacent side surfaces of the ceramic chip ($\epsilon_r = 45$) to excite the antenna through

capacitive coupling. A connection metal line printed between the two side feeds served to provide the 90° phase difference. 12 MHz impedance bandwidth, 3.5 MHz 3 dB axial ratio bandwidth and 3.4 dBi gain was obtained.

Zhizhang Chen *et al.* [64] described a novel tuning technique that allows independent tuning of the two frequency bands of an integrated antenna for GPS/PCS dual-band application. Will Mckinzie *et al.* [65] presented a miniature Bluetooth antenna known as a DC inductive shorted patch antenna (DSPA), fabricated as a single layer flex circuit wrapped around a high temperature foam substrate. A novel packaging concept in which the antenna contains an embedded Bluetooth radio MCM (multi chip module) was also introduced. Peak antenna efficiency of 47% was observed.

A compact Planar Inverted F Patch Antenna with two shorted branch strips, sharing a common shorting pin and fed by the same feed for triple-frequency operation at 900, 1800 and 2450 MHz was presented by Fu-Ren Hsiao and Kin-Lu Wong [66]. Ansoft HFSS (High Frequency Structure Simulator) was used to obtain the design parameters. The three operating bands exhibited an impedance bandwidth of 1.9%, 4.8% and 2.9% respectively. The antenna possessed radiation characteristics acceptable for practical wireless communication applications.

C.W.Chiu and F.L.Lin [67] presented a design for a compact dual band PIFA with multi-resonators for GSM/DCS band. The nearly omni-directional patterns and the impedance bandwidth obtained indicated the usefulness in mobile phone devices. Gwo-yun Lee and Kin-Lu Wong [68] proposed a very low profile antenna for GSM / DCS dual-band mobile phone applications, by inserting several slits into a rectangular planar monopole and further bending it

into two equal and perpendicular sections. The obtained radiation patterns were stable across the operating bands (837-994 MHz) and (1705-1936 MHz).

Yongjin Kim and Sangseol Lee [69] designed and fabricated a Planar Inverted F Antenna with the rectangular planar element replaced by an L shaped element to increase the spatial efficiency. IE3D software was employed to obtain the various optimal design parameters. The antenna exhibited an impedance bandwidth of 580 MHz and good radiation characteristics for wireless LAN applications centered at 5.25 GHz. Hisashi Morishita, Yongho Kim and Kyohei Fujimoto [70] described in detail the design concept of antennas for small mobile terminals. The future perspective for the antenna structure was also discussed.

Hyun Jun Kim *et al.* [71] presented a small-chip Meander antenna for dual frequency operation. The frequency ratio of the proposed antenna was 1.35 and offered more than 50% size reduction compared to the rectangular patch. Han-Cheol Ryu *et al.* [72] described the design, fabrication and testing of a triple-stacked Microstrip patch antenna consisting of three patches for use in cellular phone/GPS/PCS centred at 0.83, 1.575 and 1.7 GHz.

Marc. C. Greenberg *et al.* [73] presented the far field radiation pattern characteristics of the dual exponentially tapered slot antenna (DE TSA) for wireless communications applications. The low profile antenna had slot line conductors tapered along the outer edge. The obtained radiation patterns remained fairly constant over a broad range of frequencies, indicating the suitability for multifunction applications.

Gwo-Yun Lee *et al.* [74] presented a low cost surface-mount monopole antenna for GSM / DCS dual band operation by folding a metallic strip onto a

foam base. The antenna was mounted on a FR4 substrate and fed by a 50Ω Microstrip line. The broad impedance bandwidths and radiation patterns confirmed the suitability of the antenna for Mobile Communications applications. Kin-Lu Wong *et al.* [75] proposed a diversity antenna comprising of two back-to-back PIFA's, with their shorting pins facing each other. The antenna showed 186 MHz bandwidth, less than -22.5 dB isolation and good gain at 2.4 GHz.

Yong-Xin Guo *et al.* [76] proposed a compact internal antenna for quad band operation at the GSM 900, DCS 1800, PCS 1900 and ISM 2450 band. The antenna comprised of a main plate in the top layer, a ground plane in the bottom layer, two folded arms in-between, a short circuited strip and a feed strip, supported by foam. The measured -6 dB return loss was 68 MHz, 260 MHz and 130 MHz respectively in the three bands and the patterns were all omnidirectional. The experimental results were compared with the simulation results performed using XFDTD 5.3.

A ceramic chip antenna for 2.4 /5.8 GHz dual ISM band applications was proposed by Jung-Ick Moon and Seong-Ook Park [77]. The antenna comprised of a small ceramic dielectric alumina ($\epsilon_r=7.7$) placed at the corner of the substrate through surface mount process and two metal layers forming meander lines, printed on the top and bottom faces of the substrate. The antenna exhibited 12% bandwidth and radiation patterns similar to that of a monopole antenna.

Shih-Huang Yeh *et al.* [78] presented a compact, dual band, internal antenna suitable for GSM/DCS applications. The antenna had 3 resonant elements; 2 meandered metallic strips and a nearly rectangular patch leading to 2 resonant modes in the lower band (890-960 MHz) and 3 resonant modes in

the upper band (1710-1880 MHz), covering the entire GSM and DCS bands. Triple-frequency annular-ring slot antennas operating at 1.74, 2.38 and 3.12 GHz for CPW-fed and 1.8, 2.38 and 2.91 GHz for Microstrip line-fed were proposed by Jin-Sen Chen [79]. It was observed that by controlling the circumference of the annular-ring slot of the proposed antenna, proper operating frequency could be obtained.

A compact antenna design for 900/1800-MHz Cellular Systems was proposed by Tzung-Wern Chiou and Kin-Lu Wong [80]. The antenna comprised of a rectangular ring patch (900 MHz) and a notched rectangular patch (1800 MHz) printed on the same layer and aperture coupled by a properly designed feed network. The antenna exhibited 10% impedance bandwidth in both bands and high isolation between the two feeding ports.

Christian Sabatier [81] described the use of T-Dipole arrays for mobile base stations in the different frequency bands for GSM, UMTS, HIPERLAN, etc. Low side lobes and low coupling between two orthogonal polarizations were the characteristic features. Qwo-Yun Lee *et al.* [82] proposed a planar folded-dipole antenna for spatial diversity in 5 GHz WLAN operations. The antenna comprised of two back-to-back folded dipoles separated by a central ground plane. Wide impedance bandwidth of about 1 GHz covering the 5.2 and 5.8 GHz bands, and good directional radiation pattern covering the two complementary half spaces was observed.

Chien-Jen Wang and Wen-Tsai Tsai [83] demonstrated a triple band Microstrip-fed stair-shaped slot antenna operating at 2.4, 5.2 and 5.8 GHz. 9.45% and 15.5% impedance bandwidths were obtained in the 2.4 GHz and 5 GHz bands respectively. Yeh-Chian Lin *et al.* [84] proposed a 50 Ω grounded coplanar waveguide excited circularly polarized antenna for GPS application at

1575 MHz, mainly consisting of a cross-slot loaded square patch printed on the top surface of a grounded square-disk ceramic chip [$\epsilon_r = 90$], and a single side-feed printed on the side surface of the ceramic chip.

D.S.Yim *et al.* [85] proposed a broadband, small, chip antenna with a branch structure meander line, suitable for Korean PCS (1750-1870 MHz) and IMT-2000 (1930-2170 MHz) dual bands. The conductor strip-line patterns were printed on the top and bottom layers of the substrate chip, and connected with each other through via holes. The antenna configuration was characterized by 21.4% bandwidth, 2.6 dBi gain and omni-directional radiation pattern similar to a monopole antenna.

Hong-Dean Chen and Hong-Two Chen [86] experimentally studied CPW-fed dual frequency monopole antennas. A frequency tunable ratio of 1.3 to 1.6 was obtained by varying the length of one of the two monopoles of the proposed antenna. H.C.Go and Y.W.Jang [87] proposed a multi-band modified fork-shaped Microstrip monopole antenna with a probe feed line. The antenna exhibited wideband characteristics of 29.8% for the lower band (cellular and GSM) at 860 MHz and 90.2% for the higher band (DCS, PCS, IMT-2000 and ISM) at 2.28 GHz.

Y.S.Shin and S.O.Park [88] performed experiments and numerical simulation on a compact, planar monopole type internal antenna suitable for DCS (1710-1880 MHz), PCS (1750-1870 MHz) and IMT-2000 (1885-2200 MHz) bands. The antenna resonated at 1810 MHz with a bandwidth of 41%, displaying omni directional radiation patterns and 2.9 dBi gain. B.S.Collins *et al.* [89] described an unconventional antenna comprising of a dual band radiator coupled to a Microstrip line by means of a shaped ceramic pellet, for use in the 2.4-2.5 GHz and 4.9-5.9 GHz band for laptop computers.

A multiple U-shaped slot Microstrip patch antenna for 5 GHz Band WLANs was described by Jeong-Min Ju *et al.* [90]. The U slot width, the position of U-slot sections, the thickness of the foam layer, and the position of the feed point were the optimized for bandwidth and gain. The antenna exhibited 17.04% bandwidth and 3.88-9.28 dBi gain in the 5.02-5.955 GHz band. H.K.Kan *et al.* [91] presented a compact dual-interleaved printed antenna consisting of two interleaved L shaped shorted patches with the required feed network etched on a high-dielectric constant substrate located below the ground plane of the antenna. The antenna displayed 16.9% impedance bandwidth and 2.3 dBi gain at 2.95 GHz.

Jeong-Min Ju *et al.* [92] designed, fabricated and measured a coaxial probe fed, arrow-shaped Microstrip patch antenna for the 5 GHz band WLAN applications. To achieve sufficient bandwidth a foam layer was inserted between the ground plane and the substrate. The antenna exhibited a gain of 5.02-7.25 dBi and broad radiation pattern. Saou-Wen Su *et al.* [93] experimentally studied the effects of a finite ground plane on the impedance and radiation characteristics of an ultra-wideband planar monopole antenna with a circular ground plane.

2.2 Band Widening Techniques

Hall *et al.* [94] reported the concept of multilayer substrate antennas to achieve broader bandwidth. These antennas constructed on alumina substrates which gave a bandwidth of 16 times that of a standard patch antenna with increased overall height. C.Wood [95] suggested a method for doubling the bandwidth of microstrip patch antennas by locating capacitively excited short circuit parasitic elements at their radiating edges.

Derneryd and Karlsson [96] have made a broadband microstrip antenna by using thicker substrates of low dielectric constant. This is used as antenna element in an array effectively for broadband operation. N. Das and Chaterjee [97] reported a conical microstrip antenna with much larger bandwidth than that of an identical circular patch antenna. The conical patch antenna is obtained by modifying the circular patch antenna by slightly depressing the patch configuration conically into the substrate.

Sabban [98] reported a stacked two layer microstrip antenna with an increase in bandwidth of 15%. This antenna has been used as an element for 64 element Ku band array. Bhatnagar *et al.* [99] proposed a stacked configuration of triangular microstrip antennas to obtain larger bandwidth

M.Deepu Kumar *et al.* [100] developed dual port microstrip antenna geometry for dual frequency operation. This antenna has wide impedance bandwidth and excellent isolation between ports.

K.M.Luk *et al.* [101] designed a proximity fed stacked circular disc antenna with an impedance bandwidth of 26% and gain of 8dBi. The essential feature of this design is the presence of four linear slots in the bottom patch of the stacked arrangement. K.M. Luk *et al.* [102] investigated an L-shaped probe fed broadband rectangular microstrip. It consists of a foam layer with a thickness of around 10% of the wave length is used as the supporting substrate. The proposed antenna has an impedance bandwidth of 35% and an average gain of 7.5 dBi.

Y.X Guo *et al.* [103] presented a broad band U-slot circular patch antenna with L-probe feeding with a foam layer supported substrate. An impedance bandwidth of 38% and gain of 6.8dBi have been achieved. Kin-Lu

Wong et al [104] reported Broadband Omni-directional Metal-Plate Monopole Antenna, where the problem of poor omni-directional radiation characteristics for higher operating frequencies is overcome by a novel broadband omni-directional metal-plate monopole antenna which has a simple step-shaped structure and is easy to implement.

The bandwidth can be widened using a flat metal structure rather than a thin wire structure was proposed by W. L. Stutzman and G. A. Thiele [105]. Many flat plate radiator geometries have been explored over several decades. However, these antennas suffer from pattern degradation at the high end of their impedance bandwidth. A new wideband, omni-directional, flat antenna called the planar inverted cone antenna (PICA) is given by S.-Y. Suh and W. L. Stutzman [106] and S.-Y. Suh [107].

Owing to such attractive merits as simple structure, pure polarisation and omni-directional radiation, monopoles and their variations have long been applied to a variety of systems. Much effort has been devoted to boost the bandwidth of simple thin-wire monopoles by thickening, loading or folding the wire elements. Conical or skeletal conical, cage, and various loaded monopoles, disc loaded and inverted F antennas have been proposed by Kawakami, H., and Sato, G.[108] Nakano et al,[109] Rogers, S.D., and Butler, C.M. N[110] and Cho, W et al [111].

However, the major drawback of conical or rotationally symmetric monopoles is their bulky structure. Recently, planar monopoles have been proposed for broadband designs which replace the wire elements with planar elements by researchers like Brown, G.H., and Woodward, O.M [112] Ammann, M.J et al,[113,115] Agrawal et al, [114] Chen, Z.N [116]. However, because of the asymmetrical structure, horizontal radiation patterns are not

omni-directional at higher frequencies. This degradation more or less mitigates the advantage of the volume reduction. Moreover, for broadband monopoles, beam squinting is observed along the E-plane.

Attempts to produce antennas that are more compact than the standard microstrip patch have produced antennas such as the planar inverted F antenna (PIFA) and patch antennas utilizing high-dielectric constant substrates. While smaller than the traditional patch antennas, these antennas generally offer no more bandwidth and can be difficult to manufacture. In paper J. Michael Johnson and Yahya Rahmat-Samii [117] reports on a newly developed planar antenna called the *tab monopole* featuring broadband operation that can be readily manufactured in a printed-circuit configuration.

S. Honda *et al* [118], presented a disc monopole antenna with 1:8 impedance bandwidth and omni-directional radiation pattern as Planar metal-plate monopole antenna having attractive feature of very wide impedance bandwidth. M. Hammoud *et al* [119] presented a work on Matching the input impedance of a broadband disc monopole in 1993.

N. P. Agrawal *et al* [120] proposed Wide-band planar monopole antennas, in 1998. P. V. Anob *et al* [121] reported a wideband orthogonal square monopole antenna with semi-circular base at an international Symposium in 2001. M. J. Ammann [122] presented control of the impedance bandwidth of wideband planar monopole antennas using a beveling technique. M. J. Ammann and Z. N. Chen [123], has reported wideband monopole antenna for multi-band wireless systems. S.-Y. Suh *et al* [124] has reported multi-broadband monopole disc antenna. E. Antonino-Daviu *et al* [125], proposed Wideband double-fed planar monopole antennas.

2.3 Ultra-Wide Band Antennas

Ultra wide Band (UWB) technology is one of the most promising solutions for future communication systems due to its high-speed data rate and excellent immunity to multi-path interference. In this context, the UWB antenna design plays a unique role because it behaves like a band pass filter and reshapes the spectra of the pulses, so it should be designed to avoid undesired distortions. Some of the critical requirements in UWB antenna design are: ultra wide bandwidth, directional or omni-directional radiation patterns, constant gain and constant group delay over the entire band, high radiation efficiency and low profile. The paper by M. A. Peyrot-Solis et al [126] reviews the state of the art in UWB antennas, where planar monopole antennas show a special interest because they exhibit excellent performance in matching impedance bandwidth as well as pattern.

Since the approval of UWB spectrum for unlicensed use by the Federal Communications Commission (FCC) in 2002, UWB technology and its potential applications in wireless communications systems have been attracting increasing interests from both academia and industry. In wireless communications, UWB will see its application in high data rates (> 100 Mb/s) transmission over very short distance (< 10 m) and low data rates (< 1 Mb/s) with very low power consumption for medium indoor communications [127].

UWB wireless communications systems have many expected attractive features and advantages. There are, however many technical issues needed to be resolved. UWB antenna should cover the allocated 7500 MHz of spectrum so as to fully utilize the spectrum. Some antennas have been proposed for ultra-wideband applications by K.L.Wong[128], H. Schantz [129], K.Siwiak et al

[130] and Federal Communication Report [131]. They all have wide impedance bandwidth and good radiation patterns. However, these are not planar structure.

Recently, a microstrip planar circular disc monopole antenna has been reported by Xuan Hu Wu et al [132]. They present a CPW fed circular UWB antenna, which not only offers even wider impedance bandwidth, but also a better flexibility for circuit integration via holes.

Shun-Yun Lin and Kuang-Chih Huang [133] propose a design to obtain band-notching characteristics in printed planar monopoles. An ultra-wide band was achieved by means of the beveled upper edge of the rectangular patch with dimension as small as 55 mm^2 . On the other hand, it is necessary to notch certain bands to avoid interference from existing wireless local area network (WLAN), such as the 5.2 GHz band (5150–5350 MHz) and 5.8 GHz band (5725–5875 MHz), in spite of the adoption of the FCC for UWB communication systems operating between 3.1 and 10.6 GHz. This feature can be easily achieved by embedding an inverted-V-shaped slot with length about one-half of the guided wavelength of the expected notched frequencies along the boundary of the beveled radiating patch. This article presents the design of the proposed slotted monopole antenna, demonstrates the UWB operation with a notched frequency band, and analyzes the effects of the dimensions of the inverted-V-shape slot on the notched frequency band

High performance antennas are being developed to satisfy emerging wireless applications with broad bandwidth or multi-band to support multiple services is reported in D. Porcino and W. Hirt [134]. Generally speaking, high performance means low voltage standing wave ratio (VSWR) and good radiation pattern throughout interested frequency band. Band-notched characteristics are also required in some cases, e.g., in ultra wide-band (UWB)

communication systems. The frequency range for UWB systems approved by the FCC is between 3.1 and 10.6 GHz, which will cause interference to existing wireless communication systems, e.g., IEEE 802.11a, GPS, etc. Although many technologies have been proposed to deal with the electromagnetic compatibility of UWB with existing systems, they will either increase the noise level or require a high complexity in the receiver.

Likewise, many antennas, such as conical antennas as reported in H. M. Shen et al [135], K. Y. A. Lai et al [136], planar monopole antennas as reported in N. P. Agrawal et al [137], M. J. Ammann [138], M. J. Ammann and Z. N. Chen [139], TEM horn antennas L.-C. T. Chang and W. D. Burnside [140] and other new antennas in T. Taniguchi and T. Kobayashi [141], have been shown to provide very low VSWR in extremely wide frequency ranges. However, they likely yield interference against existing systems.

Alternatively, UWB antennas with band-notched characteristics were proposed to deal with the interference issue in reports of Xuan Hui Wu et al [142], Y. Kim and D. H. Kwon [143], J. Qiu et al [144], S.-W. Su et al [145], K.-L. Wong et al [146]. A new type of band-notched antenna is proposed. Simulation results shows good performance in both impedance bandwidth and in the radiation pattern. More importantly, the bandwidth and the central frequency of the notched band may be adjusted by proper selection of the antenna parameters.

A more specific definition for an Ultra Wide Band (UWB) antenna is a non-resonant low-Q radiator whose input impedance remains constant over a wide-band operating frequency is reported by G. R. Aiello and G. D. Rogerson [147], this type of antenna requires a well matched transition to space to avoid energy reflection.

A remarkable characteristic of an UWB antenna is that it has a non-dispersive capability to avoid further pulse compensation. As regards the spark gap transmitter, reported in the open literature, which was a primitive form of impulse radio transmission, it is considered as the first ultra-wideband communication system by T. Ogawa et al [148] and M. Hamalainen et al [149], but unfortunately, some important UWB antenna designs were forgotten and re-discovered recently for modern applications. Current research works have been focused in omni-directional UWB antennas (because all the efforts are directed to improve the wireless communication industry, mainly in mobile devices that require omni-directional radiation patterns)

Conventional UWB antennas like log periodic or spiral tend to be dispersive. They usually radiate different frequency components from different parts of the antenna, which distorts and stretches out the radiated waveform as reported by H. G. Schantz [150].

Recently, several broadband monopole configurations, such as circular, square, elliptical, half disc, pentagonal and hexagonal, have been proposed for UWB applications by M. J. Ammann and Z. N. Chen [151], N. P. Agrawal et al [152], J. E. Antonino-Daviu et al [153] and J. Z. N. Chen et al [154]. These broadband monopoles feature wide operating bandwidths, satisfactory radiation properties, simple structures and ease of fabrication. However, they are not planar because their ground planes are perpendicular to the radiators. As a result, they are not suitable for integration with a printed circuit board.

A novel design of printed circular disc monopole fed by microstrip line is proposed and investigated by Jianxin Liang et al [155]. The parameters which affect the operation of the antenna in terms of its frequency domain characteristics are analyzed both numerically and experimentally in order to

understand the operation of the antenna. It has been demonstrated that the optimal design of this type of antenna can achieve an ultra wide bandwidth with satisfactory radiation properties. Furthermore, the simulations have also shown that the proposed monopole antenna is non dispersive, which is very important for UWB systems.

2.4 FDTD for Printed Antenna Analysis

The Finite-Difference Time-Domain (FDTD) method is arguably the most popular numerical method for the solution of problems in electromagnetics. Although the FDTD method has existed for nearly 30 years, its popularity continues to grow as computing costs continue to decline. Furthermore, extensions and enhancements to the method are continually being published, which further broaden its appeal. Because of the tremendous amount of FDTD-related research activity, the Finite-Difference Time-Domain (FDTD) method, as first proposed by Yee in 1966 [156], is a simple and elegant way to discretize the differential form of Maxwell's equations. Yee used an electric-field (E) grid, which was offset both spatially and temporally from a magnetic-field (H) grid, to obtain update equations that yield the present fields throughout the computational domain, in terms of the past fields. The update equations are used in a leapfrog scheme, to incrementally march the E and H fields forward in time. Despite the simplicity and elegance of Yee's algorithm, it did not receive much interest immediately after its publication. One could attribute the lack of attention to the high computational cost of the day, as well as to some of the limitations inherent in the original publication (such as the inability to model an "open" problem for any significant period of time). However, as the shortcomings of the original FDTD implementation were alleviated and the cost of computing fell, the interest in the FDTD method began to soar.

The original Yee FDTD algorithm is second-order accurate in both space and time. Numerical-dispersion and grid-anisotropy errors can be kept small by having a sufficient number of grid spaces per wavelength. Taflove was among the first to rigorously analyze these errors [157]. Taflove was also the first to present the correct stability criteria for the original orthogonal-grid Yee algorithm [158].

The FDTD method can be used to calculate either scattered fields or total fields. When calculating only the scattered fields, the source of the fields is a function of the known incident field, and the difference in material parameters from those of the background medium [159],[160]. When using total fields, the total fields are often calculated only over an interior subsection of the computational domain [161-163], while scattered fields are calculated in the remaining (exterior) portion of the grid. By using scattered fields in this way, the field incident on the absorbing boundary condition is more readily absorbed.

To obtain this division of the computational domain, into scattered-field and total-field regions, the incident field must be specified over the boundary between these two regions. Holland and Williams presented a comparison of scattered field formulations (i.e., only the scattered fields were computed throughout the computational domain) and total-field formulations (i.e., the total fields were computed in a sub-domain that contained the object under study) [163]. They determined, due to numerical dispersion, the total-field FDTD approach is superior to the scattered-field approach. Furthermore, the scattered-field approach has the disadvantage that it does not easily accommodate nonlinear media.

However, for certain problems, such as those that contain only linear media and do not contain shielded cavities, the scattered- field formulation may

be the more-desired approach [164]. The relative merits of the total-field and scattered-field formulations were also explored by Fang [165].

In order to model open-region problems, an absorbing boundary condition (ABC) is often used to truncate the computational domain, since the tangential components of the electric field along the outer boundary of the computational domain cannot be updated using the basic Yee algorithm. The quest for an ABC that produces negligible reflections has been, and continues to be, an active area of FDTD research. Most of the popular ABCs can be grouped into those that are derived from differential equations, or those that employ a material absorber. Differential-based ABCs are generally obtained by factoring the wave equation, and by allowing a solution which permits only outgoing waves. Material-based ABCs, on the other hand, are constructed so that fields are dampened as they propagate into an absorbing medium. Other techniques sometimes used are exact formulations and super absorption. ABCs tailored for specific applications have also been developed and used with the FDTD method.

Early techniques, used to truncate the FDTD computational domain, have included differential-based ABCs, such as those proposed by Merewether [166], Engquist and Madja [167], Lindman [168], and Mur [169]. These early techniques were vastly improved in the mid-1980s by formulations proposed by Higdon [170,171], Liao *et al.* [172]: and Keys [173]. Many other extensions of these differential- based ABCs have since been proposed. Exact ABCs have the advantage of giving accurate results, but since they are non-local, they are computationally expensive. Such approaches have been investigated by Ziolkowski *et al.* [174], Olivier [175], De Moerloose and De Zutter [176], and Tromp and Olivier [177].

In 1992, Mei and Fang [178] proposed a technique, “super absorption,” which can be applied to many absorbing boundary conditions to improve their performance. In certain applications, such as the termination of a waveguide or a microstrip, dispersive boundary conditions have been used [179-184]. Lastly, many researchers, including Fang [166], Blaschak and Kriegsman [185], Moore et al. [186], Railton and Daniel [187], and, most recently, Andrew et al. [188], have compared the accuracy of various ABCs. Comparative studies of the accuracy of ABCs have also been performed for dispersive media [189], [190].

As originally formulated, the Cartesian grids used in the FDTD method dictate that a smoothly varying surface must be approximated by one that is “stair cased.” This approximation may lead to significant errors in certain problems [191], [192]. Furthermore, if an object under consideration has small-scale structure, such as a narrow slot, the original method would have to use an excessively fine grid to accurately model the associated fields. To address these shortcomings, several solutions have been proposed.

If the object under consideration is more naturally described in an orthogonal coordinate system other than Cartesian, it is rather simple to develop update equations appropriate for that coordinate system, as was done by Merewether in 1971 [167] and by Holland in 1983 [193]. Alternatively, a grid that uses varying spatial increments along the different coordinate directions can be used.

In general, for a Cartesian grid, this results in rectangular cells, and permits finer discretization in areas of rapid field fluctuation. Kunz and Lee [194], [195] used this approach to calculate the external response of an aircraft to EMP. Monk and Suli have shown that this scheme preserves the second-order accuracy of the original algorithm [196], [197]. Furthermore, sub-

domains can be gridded more finely than the rest of the problem space. This type of “sub-gridding,” where information is passed between the coarse and fine grids, was put forward by a number of researchers.

An alternative sub-gridding scheme was proposed by Kunz and Simpson [198]. Their formulation requires two runs. The first is done for a coarse grid that spans the entire computational domain, while the second is done for the finely-gridded sub-domain, and takes its boundary values from the stored values calculated during the coarse simulation.

Following the work of Yee [199], Umashankar et al. [200] and Taflove et al. [201] derived update equations that were suitable for modeling sub-cellular structures, such as wires, narrow slots, and lapped joints in conducting screens. These equations were obtained from the integral form of Faraday’s law, rather than from the differential form, and they resulted in modified equations only for cells where the sub-cellular structure was present. Several other researchers, including Holland and Simpson [202,203], Gilbert and Holland [204], Demarest [205], Turner and Bacon [206], Riley and Turner [207,208], Oates and Shin [209], and Wang [210,211], have developed techniques to handle sub-cellular structures.

Reineix and Jecko [212] were the first to apply the FDTD method to the analysis of microstrip antennas. In 1992, Leveque et al. [213] modeled frequency-dispersive microstrip antennas, while Wu et al. [214] used the FDTD method to accurately measure the reflection coefficient of various microstrip-patch configurations.

Uehara and Kagoshima [215] presented an analysis of the mutual coupling between two microstrip antennas, while Oonishi et al. [216] and

Kashiwa et al. [217] used one of the conformal FDTD approaches to analyze microstrip antennas on a curved surface.

In 1994, Qian et al. [218] used the FDTD method to design twin-slot antennas. Recently, Reineix and co-workers [219-221] have expanded their FDTD analysis to include the input impedance of microstrips with slots, to obtain the radar cross section of microstrip patch antennas, and to model the radiation from microstrip patches with a ferrite substrate.

In 1992, Luebbers et al. [222] and Chen et al. [223] analyzed hand-held antennas, using an FDTD model of a monopole antenna on a conducting or dielectric box. Toftgird et al. [224] calculated the effect the presence of a person has on the radiation from such an antenna.

In 1994, Jensen and Rahmat-Samii [225] presented results for the input impedance and gain of monopole, PIFA, and loop antennas on hand-held transceivers. The interaction of a handheld antenna and a human were also studied by Jensen and Rahmat-Samii [226]. Also in 1994, Chen and Wang [227] calculated the currents induced in the human head with a dipole-antenna model for a cellular phone. Recently, Martens et al. [228] have used a dipole model and a full model for a hand-held.

2.5 References

- [1] I.J Bahl and Bhartia, "Microstrip Antennas", Artech House, Dedham, MA, 1980
- [2] J.R James, P.S Hall and C.Wood, "Microstrip antenna-theory and design", London, UK, Peter Peregrinus Ltd., IEE, 1981.
- [3] C.A Balanis, "Antenna Theory: Analysis and design", Harper and Row Publishers, New York, 1982.
- [4] L.V.Blake, "Antennas, artech House Dedham, MA, 1984.

- [5] John D.Kraus, "Antenna", Me Graw -Hill International Editions, 2 edition, 1988.
- [6] K.C. Gupta and Abdelaziz Benalla, "Microstrip antenna design", Artech House, Inc.Norwood MA, 1988.
- [7] J.R.James and P.S Hall, "Hand book of microstrip antennas", Peter Peregrinus Ltd., IEE Engieners IV series, 1989.
- [8] Allen Taflove, "Computational electrodynamics, The finite - difference time -domain method", Artech House, Norwood MA 1995.
- [9] Kai Fong Lee and Wei Chen, "Advances in microstrip and printed antennas", John Wiley & Sons, Inc. New York 1997.
- [10] IE3D User's manual, Release 7, Zeland Software, Inc.December 1999.
- [11] Fidelity User's manual, Release 3, Zeland Software, April 2000.
- [12] Rames Garg, Prakash Bhartia, Inder Bahl and Apisak Ittipiboon, "Microstrip antenna design handbook", Artech House, London, 2001.
- [13] E.V.Byron, "A new Flush Mounted Antenna Element for Phased Array application", Proc.Phased Array Antenna Symp., pp. 187-192, 1970
- [14] Y. Dakeya, T. Suesada, K. Asakura, N. Nakajima, and H. Mandai, Chip multilayer antenna for 2.45 GHz-Band Application using LTCC technology, IEEE MTT-S Int 3 (2000), 1693-1696.
- [15] M. Chair, K.M. Luk, and K.F. Lee, Miniature multilayer shorted patch antenna, Electron Lett 36 (2000), pp 3 and 4.
- [16] M. Ali, S.S. Stuchly, and K. Caputa, A wideband dual meander sleeve antenna, Antennas Propagat Soc Int Symp 3 (1996), 1598-1601.
- [17] D. Liu, "A dual-band antenna for cellular applications," in *Proc. IEEE Antennas Propagat. Soc. Int. Symp.* , vol. 2, June 21-26, 1998, pp. 786-789.
- [18] R. Schlub, D. V. Thiel, J.W. Lu, and S. G. O'Keefe, "Dual-band six-element switched parasitic array for smart antenna cellular communications systems," *Electron. Lett.*, vol. 36, pp. 1342-1343, 2000.
- [19] D. Liu, "A multi branch monopole antenna for dual-band cellular applications," in *Proc. IEEE Antennas Propagation Soc. Int. Symp.* , vol. 3, July 11-16, 1999, pp. 1578-1581.

- [20] C. T. P. Song, P. S. Hall, H. Ghafouri-Shiraz, and D. Wake, "Multi-circular loop monopole antenna," *Electron. Lett.*, vol. 36, pp. 391–393, 2000.
- [21] E. Lee, P. S. Hall, and P. Gardner, "Dual band folded monopole/loop antenna for terrestrial communication system," *Electron. Lett.*, vol. 36, pp. 1990–1991, 2000.
- [22] P. Eratuuli, P. Haapala, and P. Vainikainen, "Dual frequency wire antenna," *Electron. Lett.*, vol. 32, pp. 1051–1052, 1996.
- [23] H. Nakano, N. Ikeda, Y. Y. Wu, R. Suzuki, H. Mimaki, and J. Yamauchi, "Realization of dual-frequency and wide-band VSWR performances using normal-mode helical and inverted-F antennas," *IEEE Trans. Antennas Propagat.*, vol. 46, pp. 788–793, June 1998.
- [24] H. M. Chen, "Microstrip-fed dual-frequency printed triangular monopole," *Electron. Lett.*, vol. 38, pp. 619–620, 2002.
- [25] F. S. Chang, S. H. Yeh, and K. L. Wong, "Planar monopole in wrapped structure for low-profile GSM/DCS mobile phone antenna," *Electron. Lett.*, vol. 38, pp. 499–500, 2002.
- [26] A CPW-Fed Dual-Frequency Monopole Antenna Horng-Dean Chen, *Member, IEEE*, and Hong-Twu Chen, *Member, IEEE*
- [27] A Novel Printed Monopole Antenna with a Square Conductor-Backed Parasitic Plane for Dual-Band WLAN Applications 'C. Y. Pan, C. H Huang and T. S. Homg Department of Electrical Engineering, National Sun Yat-Sen University Kaohsiung 804, Taiwan.
- [28] M. Ali and G. J. Hayes, "Analysis of integrated inverted-F antennas for Buletooth applications." 2000 *IEEE AP-S Conf Antenna Propagation for Wireless Communication*, Waltham, MA, pp. 21-24.
- [29] Y. L. Kuo and K. L. Wong, "Coplanar waveguide-fed folded inverted-F antennas for UMTS application." *Microwave Opt. Technol. Lett.* vol. 32 pp.
- [30] S. H. Yeh and K. L. Wong, "Integrated F-shaped monopole antenna for "2.4/5.2 GHz dual-band operation." *Microwave Opt. Technol. Lett.* vol. 34 pp. 24-26, 2002.
- [31] Planar Monopole Antennas for 2.4/5.2 GHz Dual-Band Application 'Jen-Yea Jan and Liang-Chih Tseng, Department of Electronic Engineering National Kaohsiung University of Applied Sciences Kaohsiung 807, Taiwan

- [32] P. Salonen, M. Keskilammi, and M. Kivikoski, "New slot configurations for dual-band planar inverted-F antenna," *Microwave Opt. Technol. Lett.*, vol. 28, pp. 293-298, 2001.
- [33] H. C. Tung and K. L. Wong, "A shorted microstrip antenna for 2.4/5.2 GHz dual-band operation," *Microwave Opt. Technol. Lett.*, vol. 30, pp. 401-402, 2001
- [34] Y. W. Suh and K. Chang, "Low cost microstrip-fed dual frequency printed dipole antenna for wireless communications," *Electron. Lett.*, vol. 36, pp. 1177-1179, 2000.
- [35] M. C. Pan and K. L. Wong, "A broadband active equilateral-triangular microstrip antenna," *Microwave Opt. Technol. Lett.* 22, 387-389, Sept. 20, 1999.
- [36] Fuhl, P. Nowak and E. Bonek, "Improved internal antenna for hand-held terminals," *Electron. Lett.*, vol. 30, no. 22, pp. 1816-1818, 27 October 1994.
- [37] Z. D. Liu and P. S. Hall, "Dual-band antenna for hand held portable telephones," *Electron. Lett.*, vol. 32, no. 7, pp. 609-610, 28 March 1996.
- [38] J. C. Batchelor and R. J. Langley, "Microstrip annular ring slot antennas for mobile applications," *Electron. Lett.*, vol. 32 no. 18, pp. 1635-1636, 29 August 1996.
- [39] G. T. Pedersen, J. B. Andersen and S. Skjaeris, "Integrated Handset Antenna with Low absorption and handset antenna diversity," *IEE Colloquium*, Ref. 1997/022.
- [40] Y. J. Guo, A. Paez, R. A. Sadeghzadeh and S. K. Barton, "A circular patch antenna for radio LAN's," *IEEE Trans. Antennas Propagat.*, vol. 45, no. 1, pp. 177-178, January 1997.
- [41] K. Takei, H. Okabe, Y. Imakado, "TEM slot antenna for personal handy - phone terminal," *Electron. Lett.*, vol. 33, no. 9, pp. 732-733, 24 April 1997.
- [42] Corbett R. Rowell, R. D. Murch, "A capacitively loaded PIFA for compact mobile telephone handsets," *IEEE Trans. Antennas Propagat.*, vol. 45, no. 5, pp. 837-841, May 1997.
- [43] Hiroyuki Arai, Nobuhiro Igi and Hirokazu Hanaoka, "Antenna-gain measurement of handheld terminals at 900 MHz," *IEEE Trans. Veh. Technol.*, vol. 46, no. 3, pp. 537-543, August 1997.

- [44] R.B.Waterhouse, "Printed antenna suitable for mobile communication handsets," *Electron. Lett.*, vol.33, no.22 pp.1831-1832, 23 October 1997.
- [45] Kathleen.L.Virga, Yahya Rahmat- Samii, "Low Profile Enhanced Bandwidth PIFA Antennas for Wireless Communications Packaging," *IEEE Trans. Microwave Theory Tech.*, vol.45, no.10, pp.1879-1889, October 1997.
- [46] A.Serrano-Vaello and D.Sanchez-Hernandez, "Printed antennas for dual-band GSM/DCS 1800 mobile handsets," *Electron. Lett.*, vol.34, no.2, pp.140-141, 22 January 1998.
- [47] C.L.Mak, K.M.Luk and K.F.Lee, "Proximity-coupled U-slot patch antenna," *Electron. Lett.*, vol.34, no.8, pp.715-716, 16 April 1998.
- [48] Ch.Delaveaud, Ph.Leveque and B.Jecko, 'Small-sized low-profile antenna to replace monopole antennas', *Electron. Lett.*, vol.34, no.8, pp.716-717, 16 April 1998.
- [49] Corbett R. Rowell and R. D. Murch, "A compact PIFA suitable for Dual-Frequency 900/1800-MHz operation," *IEEE Trans. Antennas Propagat.*, vol.46, no.4, pp.596-598, April 1998.
- [50] Roger Yew-Siow Tay, Quirino Balzano and Niels Kuster, "Dipole Configurations with strongly improved radiation efficiency for hand-held transceivers," *IEEE Trans. Antennas Propagat.*, vol.46, no.6, pp.798-806, June 1998.
- [51] H.Iwasaki, "Microstrip antenna with back-to-back configuration relative to a slot on a ground plane," *Electron. Lett.*, vol.34, no.14, pp.1373-1374, 9 July 1998.
- [52] O. Leisten, Y. Vardaxglou, T. Schmid, B. Rosenberger, E. Agboraw, N. Kuster and G. Nicolaidis, "Miniature dielectric-loaded personal telephone antennas with low user exposure," *Electron. Lett.*, vol.34, no.17, pp.1628 -1629, 20 August 1998.
- [53] R.B.Waterhouse, "Small printed antenna easily integrated into a mobile handset terminal," *Electron. Lett.*, vol.34, no.17, pp.1629-1631, 20 August 1998.
- [54] K.Hettak, G.Delisle and M.Boulmalf, "A novel integrated antenna for millimeter-wave personal communications systems," *IEEE Trans. Antennas Propagat.*, vol.46, no.11, pp.1757-1759, November 1998.

- [55] N.Chiba, T.Amano and H. Iwasaki, "Dual-frequency planar antenna for handsets," *Electron. Lett.*, vol.34, no.25, pp.2362-2363, 10 December 1998.
- [56] J.Ollikainen, M.Fischer and P.Vainikainen, "Thin dual-resonant stacked shorted patch antenna for mobile communications," *Electron. Lett.*, vol.35, no.6, pp.437-438, 18 March 1999.
- [57] Jack.T.Rowley and Rod.B.Waterhouse, "Performance of shorted Microstrip Patch Antennas for Mobile Communications Handsets at 1800 MHz," *IEEE Trans. Antennas Propagat.*, vol.47, no.5, pp.815 – 822, May 1999.
- [58] C.T.P.Song, P.S.Hall, H.Ghafouri-Shiraz and D.Wake, "Multi-circular loop monopole antenna," *Electron. Lett.*, vol.36, no.5, pp. 391-393, 2 March 2000.
- [59] H.Kan and R.B.Waterhouse, "Small circularly polarised printed antenna," *Electron. Lett.*, vol.36, no.5, pp. 393-394, 2 March 2000.
- [60] Ya Jun Wang, Ching Kwang Lee, Wee Jin Koh and Yeow Beng Gan, "Design of Small and Broad-band Internal Antennas for IMT-2000 Mobile Handsets," *IEEE Trans. Microwave Theory Tech.*, vol.49, no.8, pp.1398 – 1403, August 2001.
- [61] Marta Martinez-Vazquez, Matthias Geissier, Dirk Heberling, Antonio Martinez-Gonzalez and David Sanchez-Hernandez, "Compact Dual-band antenna for mobile handsets", *Microwave Opt. Technol. Lett.*, vol.32, no.2, pp. 87-88, 20 January 2002.
- [62] Hassan M.Elkamchouchi and Hossam El-dien M.Hafez, "Multi-band smart patch antenna for GPS/PCS hand held units," Proc., *IEEE 3rd International Conference on Microwave and Millimeter wave Technology, 2002*.
- [63] Tsung –Wen Chiu, Cliff Wang, Chih-Ming Su and Kin-Lu Wong, "Surface mountable dual side-feed circularly polarized ceramic chip antenna," Proc. *IEEE International symposium on Electronic Materials and packaging*, pp. 434- 437, 2002.
- [64] Zhizhang Chen, Acep D. Ganjara and Xiaomin Chen, "Dual-L antenna with a novel tuning technique for dual frequency applications," *IEEE Trans. Antennas Propagat.*, vol.50, no.3, pp.402-404, March 2002.

- [65] Will Mckinzie, Greg Mendolia and John Dutton, "Novel packaging approaches for miniature antennas", *Proc. IMAPS/SMTA Conference on Telecom Hardware solutions*, Plano, TX, pp. 1-7, May 15-16 2002.
- [66] Fu-Ren Hsiao and Kin-Lu Wong, "Compact Planar Inverted – F Patch Antenna for triple frequency operation," *Microwave Opt. Technol. Lett.*, vol. 33, no.6, pp.459-462, 20 June 2002.
- [67] C.W.Chiu and F.L.Lin, "Compact dual-band PIFA with multi-resonators," *Electron. Lett.*, vol.38, no.12, pp.538-540, 6 June 2002.
- [68] Gwo-yun Lee and Kin-Lu Wong, "Very-low-profile bent planar monopole antenna for GSM/DCS dual-band mobile phone," *Microwave Opt. Technol. Lett.*, vol.34, no.6, pp.406-409, 20 September 2002.
- [69] Yongjin Kim and Sangseol Lee, "Design and fabrication of a planar inverted-F antenna for the wireless LAN in the 5 GHz band," *Microwave Opt. Technol Lett.*, vol.34, no.6, pp.469-475, 20 September 2002.
- [70] Hisashi Morishita, Yongho Kim and Kyohei Fujimoto, "Design concept of antennas for small mobile terminals and the future perspective," *IEEE Antennas Propagat. Mag.*, vol.44, no.5, pp.30-43, October 2002.
- [71] Hyun Jun Kim, Sewoong Kwon, Sung Hun Sim, Young Joong Yoon, Huyn Jai Kim, Seok Ji Yoon and Chong-Yun Kang, "Dual-frequency small-chip Meander Antenna," *Microwave Opt. Technol. Lett.*, vol.35, no.4, pp. 274-277, 20 November 2002.
- [72] Han-Cheol Ryu, Hee-Ran Ahn, Sang-Hwa Lee and Wee Sang Park, "Triple-stacked microstrip patch antenna for multi-band system," *Electron. Lett.*, vol.38, no.24, pp.1496-1497, 21 November 2002.
- [73] Marc. C. Greenberg, Kathleen L. Virga and Cynthia. L. Hammond, "Performance characteristics of the dual exponentially tapered slot antenna (DE TSA) for wireless communications applications," *IEEE Trans. Veh. Technol.*, vol.52, no.2, pp.305-312, March 2003.
- [74] Gwo-Yun Lee, Hong-Twu Chen and Kin-Lu Wong, "A Low cost surface-mount monopole antenna for GSM / DCS operation," *Microwave Opt. Technol. Lett.*, vol.37, no.1, pp.2-4, 5 April 2003.
- [75] Kin-Lu Wong, An-Chia Chen and Yen-Liang Kuo, "Diversity metal-plate planar inverted F antenna for WLAN operation," *Electron. Lett.*, vol.39, no.7, pp.590-591, 3 April 2003.

- [76] Yong-Xin Guo, Irene Ang and M.Y.W.Chia, "Compact Internal Multiband Antennas for Mobile Handsets," *IEEE Antennas and wireless Propagation Lett.*, vol.2, pp.143-146, 2003.
- [77] Jung-Ick Moon and Seong-Ook Park, "Small Chip Antenna for 2.4/5.8-GHz Dual ISM Band Applications," *IEEE Antennas and wireless Propagation Lett.*, vol.2, pp.313-315, 2003.
- [78] Shih-Huang Yeh, Kin-Lu Wong, Tzung-Wern Chiou and Shyh-Tirng Fang, "Dual-Band Planar Inverted F Antenna for GSM/DCS Mobile Phones," *IEEE Trans. Antennas Propagat.*, vol.51, no.5, pp.1124 – 1129, May 2003.
- [79] Jin-Sen Chen, "Triple-frequency annular-ring slot antennas fed by CPW and Microstrip line," *IEEE Antennas Propagat. Soc. Int. Symp.*, Michigan, pp. 557-560, June 2003.
- [80] Tzung-Wern Chiou, Kin-Lu Wong, "A Compact Dual-Band Dual-Polarized Patch Antenna for 900/1800-MHz Cellular Systems," *IEEE Trans. Antennas Propagat.*, vol.51, no.8, pp.1936-1940, August 2003.
- [81] Christian Sabatier, "T-Dipole arrays for Mobile applications," *IEEE Antennas Propagat., Mag.*, vol.45, no.6, pp.9-26, December 2003.
- [82] Qwo-Yun Lee, Wen-Shyang Chen and Kin-Lu Wong, "Planar diversity folded-dipole antenna for 5 GHz WLAN operation," *Microwave Opt. Technol. Lett.*, vol.39, no.5, pp.158-161, 5 December 2003.
- [83] Chien-Jen Wang and Wen-Tsai Tsai, "A stair-shaped slot antenna for the triple band WLAN applications," *Microwave Opt. Technol. Lett.*, vol.39, no.5, pp.370-373, 5 December 2003.
- [84] Yeh-Chian Lin, Tsung-Wen Chiu and Kin-Lu Wong. "Small-size surface-mountable circularly polarized ceramic-chip antenna for GPS application," *Microwave Opt. Technol. Lett.*, vol.40, no.4, pp.300-302, 20 February 2004.
- [85] D.S.Yim. J.Kim and S.O.Park, "Novel wideband internal chip antenna for PCS / IMT-2000 Dual-band applications," *Microwave Opt. Technol Lett.*, vol.40, no.4, pp.324-326, 20 February 2004.
- [86] Horng-Dean Chen and Hong-Two Chen, "A CPW-fed dual frequency monopole antenna," *IEEE Trans. Antennas Propagat.*, vol.52, no.4, pp.978-982, April 2004.

- [87] H.C.Go and Y.W.Jang, "Multi-band modified fork-shaped microstrip monopole antenna with ground plane including dual-triangle portion," *Electron. Lett.*, vol.40, no.10, 13 May 2004.
- [88] Y.S.Shin and S.O.Park, "Broadband internal antenna of planar monopole type for mobile handsets," *IEEE Antennas Propagat. Soc. Int. Symp.*, Monterrey, CA, June 2004.
- [89] B.S.Collins, V.Nahar, S.P.Kingsley, S.Q.Zhang and S.Krupa, "A dual-band hybrid dielectric antenna for laptop computers," *IEEE Antennas Propagat. Soc. Int. Symp.*, Monterrey, CA, June 2004.
- [90] Jeong-Min Ju, Gyey-Teak Jeong, Joong-Han Yoon, Sung-Won Ko and Kyung-Sup Kwak "Design of multiple U-shaped slot microstrip patch antenna for 5 GHz Band WLANs," *Microwave Opt. Technol. Lett.*, vol.43, no.6, pp. 486-488, 20 December 2004.
- [91] H.K.Kan, D.Pavlickovski and R.B.Waterhouse, "A compact dual-interleaved printed antenna," *Microwave Opt. Technol. Lett.*, vol.43, no.6, pp. 501-503, 20 December 2004.
- [92] Jeong-Min Ju, Joong-Han Yoon, Sung-Won Ko, Moon-Gyu Kang and Kyung-Sup Kwak, "Fabrication and measurement of an arrow-shaped Microstrip patch antenna in the 5 GHz band," *Microwave Opt. Technol. Lett.*, vol.43, no.6, pp.503-505, 20 December 2004.
- [93] Saou-Wen Su, Kin-Lu Wong, Yuan-Tung Cheng and Wen-Shyang Chen, "Finite ground-plane effects on the ultra-wideband planar monopole antenna," *Microwave Opt. Technol. Lett.*, vol.43, no.6, pp. 535-537, 20 December 2004.
- [94] P.S.Hall, C.Wood, C.Garrett, "Wide bandwidth microstrip antennas for circuit integration", *IEE Electron. Lett.*, vol.15, pp. 458-460, 1970.
- [95] C.Wood, "Improved bandwidth of microstrip antenna using parasitic elements", *IEE Proc.*, Pt.H, vol. 127, pp.231-234, 1980.
- [96] A.G.Derneryd and I.Karlsson, "Broad band microstrip antenna element and array", *IEEE Trans. Antennas Propagat.*, vol. AP-24, pp. 140-141, 1981
- [97] N.Das and J.Chatterjee, "Conically depressed microstrip patch antenna", *IEE Proc.*, Pt.H, vol.130, pp.193-196, 1983.

- [98] A.Saban, "A new broadband stacked two layer antenna", Dig.Int. Symp. Antennas and Propagat., vol.1, pp.63-66, May 1983
- [99] P.S.Bhatnagar, J.P. Daniel, K.Mahadjoubi and C.Terret, "Experimental study on stacked microstrip Antennas", IEE Electron. Lett., vol.22, 864-865, 1985
- [100] M.Deepukarm J.George, C.K.Anandan, P.Mohanan and K.G.Nair, "Broadband dual frequency microstrip antenna", IeE Electron. Lett., vol.32, No.17, pp. 1442-1443., 1996
- [101] K.M Luck, K.F.Lee and Y.L.Chow, "Proximity coupled stacked circular disc microstrip antenna with slots", IEE Electron. Lett., vol.34, no.5, pp. 419-420,1998
- [102] K.M Luk, C.L.Mak, Y.L Chow and K.F Lee, " Broadband microstrip patch antenna", IEE Electron. Lett., vol.34, no.15 pp. 1442-1443, 1998
- [103] Y.X.Guo, K.M.Luk and K.F.Lee, "U-slot circular patch antenna with L-probe", IEE Electron. Lett., vol.35, no.20, pp. 1694-1695, 1999
- [104] Kin-Lu Wong, Saou-Wen Su, and Chia-Lun Tang- "Broadband Omnidirectional Metal-Plate Monopole Antenna"
- [105] W. L. Stutzman and G. A. Thiele, *Antenna Theory and Design*, 2nded. New York: Wiley, 1998, p. 172.
- [106] A Planar Inverted Cone Antenna, S.-Y. Suh and W. L. Stutzman. (2000, Sept. 8). <http://www.vtip.org/Licensing/disclosures/00-130.htm>
- [107] S.-Y. Suh, "A comprehensive investigation of new planar wideband antennas," Ph.D. dissertation, Virginia Polytech. Inst. State Univ., Blacksburg, VA, July 2002
- [108] Kawakami, H., and Sato, G.: 'Broadband characteristics of rotationally symmetric antennas and thin wire constructs', IEEE Trans. Antennas Propag., 1987, 35, pp. 26-32
- [109] Nakano, H., Ikeda, N., Wu, Y., Suzuki, R., Mimaki, H., and Yamauchi, J.: 'Realization of dual-frequency and wide-band VSWR performances using normal helical and inverted-F antennas', IEEE Trans. Antennas Propag., 1998, 46, pp. 788-793
- [110] Rogers, S.D., and Butler, C.M.: 'Cage antennas optimised for bandwidth', Electron. Lett., 2000, 36, (11), pp. 932-933

- [111] Cho, W., Kanda, M., Hwang, H., and Howard, M.W.: 'A disk-loaded thick cylindrical dipole antenna for validation of an EMC test site from 30 to 300 MHz', *IEEE Trans. Electromagn. Compat.*, 2000, 42, pp. 172–180
- [112] Brown, G.H., and Woodward, O.M.: 'Experimentally determined radiation characteristics of conical and triangular antennas', *RCA Rev.*, 1952, 13, (4), pp. 425–452
- [113] M. J. Ammann and Z. N. Chen, "A wide-band shorted planar monopole with bevel," *IEEE Trans. Antennas Propag.*, vol. 51, no. 4, pp. 901–903, Apr. 2003.
- [114] Agrawall, N.P., Kumar, G., and Ray, K.P.: 'Wide-band planar monopole antenna', *IEEE Trans. Antennas Propag.*, 1998, 46, pp.294–295
- [115] Ammann, M.J.: 'Square planar monopole antenna'. Presented at National Conf. Antennas & Propag., York, England, 1999, pp. 37–40
- [116] Chen, Z.N.: 'Impedance characteristics of planar bow-tie-like monopole antennas', *Electron. Lett.*, 2000, 36, (13), pp. 1100–1101
- [117] J. Michael Johnson and Yahya Rahmat-Samii "The Tab Monopole"
- [118] S. Honda, M. Ito, H. Seki, and Y. Jinbo, "A disc monopole antenna with 1:8 impedance bandwidth and omnidirectional radiation pattern," in *Proc. Int. Symp. Antennas Propagation*, Sapporo, Japan, pp. 1145–1148.
- [119] M. Hammoud, P. Poey, and F. Colombel, "Matching the input impedance of a broadband disc monopole," *Electron. Lett.*, vol. 29, pp. 406–407, Feb. 1993.
- [120] N. P. Agrawall, G. Kumar, and K. P. Ray, "Wide-band planar monopole antennas," *IEEE Trans. Antennas Propag.*, vol. 46, pp. 294–295, Feb.1998.
- [121] P. V. Anob, K. P. Ray, and G. Kumar, "Wideband orthogonal square monopole antennas with semi-circular base," in *Proc. IEEE Antennas Propagat. Soc. Int. Symp. Dig.*, vol. 3, Boston, MA, Jul. 2001, pp.294–297.
- [122] M. J. Ammann, "Control of the impedance bandwidth of wideband planar monopole antennas using a beveling technique," *Microwave Opt. Technol. Lett.*, vol. 30, pp. 229–232, Aug. 2001.

- [123] M. J. Ammann and Z. N. Chen, "Wideband monopole antennas for multi-band wireless systems," *IEEE Antennas Propagat. Mag.*, vol. 45, pp. 146–150, Apr. 2003.
- [124] S.-Y. Suh, W. L. Stutzman, and W. A. Davis, "Multi-broadband monopole disc antennas," in *Proc. IEEE Antennas Propagat. Soc. Int. Symp. Dig.*, vol. 3, Columbus, OH, pp. 616–619.
- [125] E. Antonino-Daviu, M. Cabedo-Fabres, M. Ferrando-Bataller, and A. Valero-Nogueira, "Wideband double-fed planar monopole antennas," *Electron. Lett.*, vol. 39, pp. 1635–1636, Nov. 2003.
- [126] State of the Art in Ultra-Wideband Antennas M. A. Peyrot-Solis 1 , 2, G.M. Galvan-Tejada1, H. Jardon-Aguilar 11 Department of Electrical Engineering, CINVESTAV-IPN, Mexico D.F., Mexico 2 Mexican Navy Research Institute, Mexico, D.F., Mexico Phone +52 (55) 50613767 E-mail: mpeyrot@cinvestav.mx
- [127] H. Schantz, "Introduction to ultra-wideband antennas". Ultra Wideband Systems and Technologies, 2003 IEEE Conference on 16-19 Nov. 2003, pp. 1-9.
- [128] K.-L. Wong, C.-H. Wu, and S.-W. Su, "Ultrawide-band square planar metal-plate monopole antenna with a trident-shaped feeding strip," *IEEE Trans. Antennas Propag.*, vol. 53, no. 4, pp. 1262–1268, Apr. 2005.
- [129] H. Schantz, "A Brief History of UWB Antennas". Aerospace and Electronic Systems Magazine, IEEE Volume 19, Issue 4, April 2004, pp.22-26.
- [130] K. Siwiak, P. Withington, S. Phelan, "Ultra-Wideband Radio: The Emergence of an Important New Technology", Vehicular Technology Conference, 2001, Volume 2, pp.1169-1172.
- [131] Federal Communications Commission, First Report and Order, Revision of Part 15 of the Commission's Rules Regarding Ultra- Wideband Transmission Systems, FCC 02-48, April 22, 2002.
- [132] Xuan Hui Wu, Zhi Ning Chen, M.Y.W. Chia, "Note on Antenna Design in UWB Wireless Communication Systems". Ultra Wideband Systems and Technologies, 2003 IEEE Conference on. 16-19 Nov. 2003, pp. 503-507.
- [133] Shun-Yun Lin and Kuang-Chih Huang "PRINTED PENTAGON MONOPOLE ANTENNA WITH A BAND-NOTCHED FUNCTION" Department of Electronics Engineering, Cheng Shiu University Kaohsiung, Taiwan 833, Republic of China

- [134] D. Porcino and W. Hirt, "Ultra-wideband radio technology: Potential and challenges ahead," *IEEE Commun. Mag.*, vol. 41, pp. 66–74, Jul. 2003.
- [135] H. M. Shen, R. W. P. King, and T. T. Wu, "V-conical antenna," *IEEE Trans. Antennas Propag.*, vol. 36, pp. 1519–1525, Nov. 1988.
- [136] K. Y. A. Lai, A. L. Sinopoli, and W. D. Burnside, "A novel antenna for ultra-wide-band applications," *IEEE Trans. Antennas Propag.*, vol. 40, pp. 755–760, Jul. 1992.
- [137] N. P. Agrawal, G. Kumar, and K. P. Ray, "Wide-band planar monopole antenna," *IEEE Trans. Antennas Propag.*, vol. 46, pp. 294–295, Feb. 1998.
- [138] M. J. Ammann, "Square planar monopole antenna," in *Proc. Inst. Elect. Eng. Nat. Conf. Antennas and Propagation*, 1999, pp. 37–40.
- [139] M. J. Ammann and Z. N. Chen, "Wideband monopole antennas for multiband wireless systems,
- [140] L.C. T. Chang and W. D. Burnside, "An ultrawide-bandwidth tapered resistive TEM horn antenna," *IEEE Trans. Antennas Propag.*, vol. 48, pp. 1848–1857, Dec. 2000.
- [141] T. Taniguchi and T. Kobayashi, "An omnidirectional and low-VSWR antenna for ultra-wideband wireless systems," in *Proc. IEEE Antennas and Propagation Soc. Int. Symp.*, vol. 3, Aug. 2003, pp. 460–463.
- [142] A. Kerkhoff and H. Ling, "Design of a planar monopole antenna for use with ultra-wideband (UWB) having a band-notched characteristic," in *Proc. IEEE Antennas and Propagation Soc. Int. Symp.*, vol. 1, Jun. 2003, pp. 830–833.
- [143] Y. Kim and D. H. Kwon, "CPW-fed planar ultra-wideband antenna having a frequency band notch function," *Electron. Lett.*, vol. 40, pp. 403–404, Apr. 2004.
- [144] J. Qiu, Z. Du, J. Lu, and K. Gong, "A band-notched UWB antenna," *Microw. Opt. Technol. Lett.*, vol. 45, pp. 152–154, Apr. 2005.
- [145] S.-W. Su, K.-L. Wong, and F.-S. Chang, "Compact printed ultra-wideband slot antenna with a band-notched operation," *Microw. Opt. Technol. Lett.*, vol. 45, pp. 128–130, Apr. 2005.
- [146] K.-L. Wong, Y.-W. Chi, C.-M. Su, and F.-S. Chang, "Band-notched ultra-wideband circular-disk monopole antenna with an arc-shaped slot," *Microw. Opt. Technol. Lett.*, vol. 45, pp. 188–191, May 2005.

- [147] G. R. Aiello and G. D. Rogerson, "Ultra-wideband wireless systems," *IEEE Microw. Mag.*, vol. 4, pp. 36–47, Jun. 2003.
- [148] T. Ogawa, A. Tomiki, and T. Kobayashi, "Development of two kinds of UWB sources for propagation, EMC and other experimental studies: Impulse radio and direct-sequence spread spectrum," in *Proc. IEEE Antennas and Propagation Soc. Int. Symp.*, vol. 4, Jun. 2003, pp. 273–276.
- [149] M. Hamalainen, V. Hovinen, R. Tesi, J. H. J. Iinatti, and M. Latva-aho, "On the UWB system coexistence with GSM900, UMTS/WCDMA, and GPS," *IEEE J. Select. Areas Commun.*, vol. 20, pp. 1712–1721, Dec. 2002.
- [150] H. G. Schantz, "Ultra wideband technology gains a boost from new antennas," *Antenna Syst. Technol.*, vol. 4, no. 1, Jan./Feb. 2001.
- [151] T. Yang and W. A. Davis, "Planar half-disk antenna structures for ultrawideband communications," in *Proc. IEEE Int. Symp. Antennas Propagation*, Jun. 2004, vol. 3, pp. 2508–2511.
- [152] Honda, S., Ito, M., Seki, H., and Jinbo, Y.: 'A disk monopole antenna with 1:8 impedance bandwidth and omni directional radiation pattern'. *Proc. ISAP92*, Sapporo, Japan, 1992, pp. 1145–1148 .
- [153] E. Antonino-Daviu, M. Cabedo-Fabre's, M. Ferrando-Bataller, and A. Valero-Nogueira, "Wideband double-fed planar monopole antennas," *Electron. Lett.*, vol. 39, no. 23, Nov. 2003.
- [154] Z. N. Chen, M. Y.W. Chia, and M. J. Ammann, "Optimization and comparison of broadband monopoles," *Proc. Inst. Elect. Eng. Microw. Antennas Propag.*, vol. 150, no. 6, Dec. 2003.
- [155] Jianxin Liang, *Student Member, IEEE*, Choo C. Chiau, *Student Member, IEEE*, Xiaodong Chen, *Member, IEEE*, and Clive G. Parini, *Member, IEEE* "Study of a Printed Circular Disc Monopole Antenna for UWB Systems"
- [156] K. S. Yee, "Numerical solution of initial boundary value problems involving Maxwell's equations in isotropic media," *IEEE Transactions on Antennas and Propagation*, AP-14, 4, pp. 302-307, 1966.
- [157] A. Taflove, "Review of the formulation and applications of the finite-difference time-domain method for numerical modeling of electromagnetic wave interactions with arbitrary structures," *Wave Motion*, 10, 6, pp. 547-582, 1988.

- [158] A. Taflove and M. E. Brodwin, "Numerical solution of steady state electromagnetic scattering problems using the time-dependent Maxwell's equations," *IEEE Transactions on Microwave Theory Techniques*, MTT-23, 8, pp. 623-630, 1975.
- [159] R. Holland, "THREDE: A free-field EMP coupling and scattering code," *IEEE Transactions on Nuclear Science*, NS-24, 6, pp. 2416-2421, 1977.
- [160] R. Holland, L. Simpson, and K. Kunz, "Finite-difference analysis of EMP coupling to lossy dielectric structures," *IEEE Transactions on Electromagnetic Compatibility*, EMC-22, 3, pp. 203-209, 1980.
- [161] D. E. Merewether, R. Fisher, and F. W. Smith, "On implementing a numeric Huygen's source scheme in a finite difference program to illuminate scattering bodies," *IEEE Transactions on Nuclear Science*, NS-27, 6, pp. 1829-1833, 1980.
- [162] A. Taflove and K. Umashankar, "Radar cross section of general three-dimensional scatterers," *IEEE Transactions on Electromagnetic Compatibility*, EMC-25, 4, pp. 433-440, 1983.
- [163] R. Holland and J. W. Williams, "Total-field versus scattered-field finite-difference codes: A comparative assessment," *IEEE Transactions on Nuclear Science*, NS-30, 6, pp. 4583-4588, 1983.
- [164] K. S. Kunz and R. J. Luebbers, *The Finite Difference Time Domain Method for Electromagnetics*, Boca Raton, FL, CRC Press, 1993.
- [165] J. Fang, "Time Domain Finite Difference Computation for Maxwell's Equations," PhD thesis, University of California at Berkeley, Berkeley, CA, 1989.
- [166] D. E. Merewether, "Transient currents on a body of revolution by an electromagnetic pulse," *IEEE Transactions on Electromagnetic Compatibility*, EMC-13, 2, pp. 41-44, 1971.
- [167] B. Engquist and A. Majda, "Absorbing boundary conditions for the numerical simulation of waves," *Mathematics of Computation*, 31, pp. 629-651, 1977.
- [168] E. L. Lindman, "'Free-space' boundary conditions for the time dependent wave equation," *Journal of Computational Physics*, 18, pp. 67-78, 1975.
- [169] G. Mur, "Absorbing boundary conditions for the finite-difference approximation of the time-domain electromagnetic-field equations,"

IEEE Transactions on Electromagnetic Compatibility, EMC-23, 4, pp. 377-382, 1981.

- [170] R. L. Higdon, "Absorbing boundary conditions for difference approximations to the multi-dimensional wave equations," *Mathematics of Computation*, 41, 176, pp. 437-459, 1986.
- [171] R. L. Higdon, "Numerical absorbing boundary conditions for the wave equation," *Mathematics of Computation*, 49, 179, pp. 65-90, 1987.
- [172] Z. P. Liao, H. L. Wong, B.-P. Yang, and Y.-F. Yuan, "A transmitting boundary for transient wave analysis," *Science Sinica*, Series A, 27, 10, pp. 1063-1076, 1984.
- [173] R. G. Keys, "Absorbing boundary conditions for acoustic media," *Geophysics*, 50, 6, pp. 892-902, 1985.
- [174] R. W. Ziolkowski, N. K. Madsen, and R. C. Carpenter, "Three dimensional computer modeling of electromagnetic fields: A global look back lattice truncation scheme," *Journal of Computational Physics*, 50, pp. 360-408, 1983.
- [175] J. C. Olivier, "On the synthesis of exact free space absorbing boundary conditions for the finite-difference time-domain method," *IEEE Transactions on Antennas and Propagation*, AP-40, 4, pp. 456-459, 1992.
- [176] J. De Moerloose and D. De Zutter, "Surface integral representation radiation boundary condition for the FDTD method," *IEEE Transactions on Antennas and Propagation*, AP-41, 7, pp. 890- 896, 1993.
- [177] E. N. M. Tromp and J. C. Olivier, "Synthesis of absorbing boundary conditions for the FDTD method: Numerical results," *IEEE Transactions on Antennas and Propagation*, AP-43, 2, pp.213-215, 1995.
- [178] F. Moglie, T. Rozzi, P. Marcozzi, and A. Schiavoni, "A new termination condition for the application of FDTD techniques to discontinuity problems in close homogenous waveguide," *IEEE Transactions on Microwave Theory Techniques*, MTT-2, 12, pp. 475-477, 1992.
- [179] E. A. Navarro, L. Gallart, J. L. Cruz, B. Gimeno, and V. Such, "Accurate absorbing boundary conditions for the FDTD analysis of H-plane wave guide discontinuities," *IEE Proceedings*, 141H, 1, pp. 59-61, 1994.

- [180] L. A. Viela, J. A. Pereda, A. Prieto, and A. Vegas, "FDTD multimode characterization of wave guide devices using absorbing boundary conditions for propagating and evanescent modes," *IEEE Microwave and Guided Wave Letters*, 4, 6, pp. 160- 162, 1994.
- [181] C. J. Railton, E. M. Daniel, D. L. Paul, and J. P. McGeehan, "Optimized absorbing boundary-conditions for the analysis of planar circuits using the finite-difference time-domain method," *IEEE Transactions on Microwave Theory Techniques*, MTT-41, 2, pp. 290-297, 1993.
- [182] V. Betz and R. Mittra, "A boundary condition to absorb both propagating and evanescent waves in a finite-difference time domain simulation," *IEEE Microwave and Guided Wave Letters*, 3, 6, pp. 182-184, 1993.
- [183] J. Fang, "Absorbing boundary conditions applied to model wave propagation in microwave integrated-circuits," *IEEE Transactions on Microwave Theory Techniques*, MTT-42, 8, pp. 1506- 1513, 1994.
- [184] J. G. Blaschak and G. A. Kriegsmann, "A comparative study of absorbing boundary conditions," *Journal of Computational Physics*, 77, pp. 109-139, 1988.
- [185] T. G. Moore, J. G. Blaschak, A. Taflove, and G. A. Kriegsmann, "Theory and application of radiation boundary operators," *IEEE Transactions on Antennas and Propagation*, AP-36, 12, pp. 1797-1812, 1988.
- [186] C. J. Railton and E. M. Daniel, "Comparison of the effect of discretisation on absorbing boundary algorithms in finite difference time domain method," *Electronics Letters*, 28, 20, pp. 1891-1893, 1992.
- [187] V. Betz and R. Mittra, "Comparison and evaluation of boundary conditions for the absorption of guided waves in an FDTD simulation," *IEEE Microwave and Guided Wave Letters*, 2, 12, pp. 499-501, 1992.
- [188] A. C. Cangellaris and D. B. Wright, "Analysis of the numerical error caused by the stair-stepped approximation of a conducting boundary in FDTD simulations of electromagnetic phenomena," *IEEE Transactions on Antennas and Propagation*, AP-39, 10, pp. 1518-1525, 1991.
- [189] R. Holland, "Pitfalls of staircase meshing," *IEEE Transactions on Electromagnetic Compatibility*, EMC-35, 4, pp. 434-439, 1993.
- [190] K. S. Kunz and K. M. Lee, "A three-dimensional finite-difference solution of the external response of an aircraft to a complex transient EM

- environment: I - The method and its implementation," *IEEE Transactions on Electromagnetic Compatibility*, EMC-20, 2, pp. 328-333, 1978.
- [191] K. S. Kunz and K. M. Lee, "A three-dimensional finite-difference solution of the external response of an aircraft to a complex transient EM environment: II - Comparison of predictions and measurements," *IEEE Transactions on Electromagnetic Compatibility*, EMC-20, 2, pp. 333-341, 1978.
- [192] P. Monk and E. Siili, "A convergence analysis of Yee's scheme on non-uniform grids," *SIAM Journal of Numerical Analysis*, 31,2, pp. 393-412, 1994.
- [193] P. Monk and E. Stili, "Error estimates for Yee's method on non-uniform grids," *IEEE Transactions on Magnetics*, 30, 5, pp. 3200-3203, 1994.
- [194] J. C. Kasher and K. S. Yee, "A numerical example of a two dimensional scattering problem using a subgrid," *Applied Computational Electromagnetics Society Journal and Newsletter*, 2, 2, pp. 75-102, 1987.
- [195] I. S. Kim and W. J. R. Hoefer, "A local mesh refinement algorithm for the time domain-finite difference method using Maxwell's curl equations," *IEEE Transactions on Microwave Theory Techniques*, MTT-38, 6, pp. 812-815, 1990.
- [196] S. S. Zivanovic, K. S. Yee, and K. K. Mei, "A sub gridding method for the time-domain finite-difference method to solve Maxwell's equations," *IEEE Transactions on Microwave Theory Techniques*, MTT-39, 3, pp. 471-479, 1991.
- [197] D. T. Prescott and N. V. Shuley, "A method for incorporating different sized cells into the finite-difference time-domain analysis technique," *IEEE Microwave and Guided Wave Letters*, 2, 11, pp. 434-436, 1992.
- [198] K. S. Kunz and L. Simpson, "A technique for increasing the resolution of finite-difference solutions of the Maxwell's equation," *IEEE Transactions on Electromagnetic Compatibility*, EMC-23, 4, pp. 419-422, 1981.
- [199] K. S. Yee, "Numerical solution to Maxwell's equations with non-orthogonal grids," Tech. Rep. UCRL-93268, Lawrence Livermore National Laboratory, 1987.
- [200] K. R. Umashankar, A. Taflove, and B. Beker, "Calculation and experimental validation of induced currents on coupled wires in an arbitrary shaped cavity," *IEEE Transactions on Antennas and Propagation*, AP-35, 11, pp. 1248-1257, 1987.

- [201] A. Taflove, K. R. Umashankar, B. Beker, F. Harfoush, and K. S. Yee, "Detailed FD-TD analysis of electromagnetic fields penetrating narrow slots and lapped joints in thick conducting screens," *IEEE Transactions on Antennas and Propagation*, AP-36, 2, pp. 247-257, 1988.
- [202] R. Holland and L. Simpson, "Implementation and optimization of the thin-strut formalism in THREDE," *IEEE Transactions on Nuclear Science*, NS-27, 6, pp. 1625-1630, 1980.
- [203] R. Holland and L. Simpson, "Finite-difference analysis EMP coupling to thin struts and wires," *IEEE Transactions on Electromagnetic Compatibility*, EMC-23, 2, pp. 88-97, 1981.
- [204] J. Gilbert and R. Holland, "Implementation of the thin-slot formalism in the finite-difference Eh@ code THREDII," *IEEE Transactions on Nuclear Science*, NS-28, 6, pp. 4269-4274, 1981.
- [205] K. R. Demarest, "A finite difference-time domain technique for modeling narrow apertures in conducting scatterers," *IEEE Transactions on Antennas and Propagation*, AP-35, 7, pp. 826-831, 1987.
- [206] C. D. Turner and L. D. Bacon, "Evaluation of a thin-slot formalism for finite-difference time-domain electromagnetics codes," *IEEE Transactions on Electromagnetic Compatibility*, EMC-30, 4, pp. 523-528, 1988.
- [207] D. J. Riley and C. D. Turner, "Hybrid thin-slot algorithm for the analysis of narrow apertures in finite-difference time-domain calculations," *IEEE Transactions on Antennas and Propagation*, AP-38, 12, pp. 1943-1950, 1990.
- [208] D. J. Riley and C. D. Turner, "The inclusion of wall loss in finite-difference time-domain thin-slot algorithms," *IEEE Transactions on Electromagnetic Compatibility*, EMC-33, 4, pp. 304-311, 1991.
- [209] J. H. Oates and R. T. Shin, "Small aperture modeling for EM1 applications using the finite-difference time-domain technique," *Journal of Electromagnetic Waves and Applications*, 9, 112, pp. 37-69, 1995.
- [210] B.-Z. Wang, "Small-hole formalism for the FDTD simulation of small-hole coupling," *IEEE Microwave and Guided Wave Letters*, 5, 1, pp. 15-17, 1995.
- [211] B.-Z. Wang, "Enhanced thin-slot formalism for the FDTD analysis of thin-slot penetration," *IEEE Microwave and Guided Wave Letters*, 5, 5, pp. 142-143, 1995.

- [212] A. Reineix and B. Jecko, "Analysis of microstrip patch antennas using finite difference time domain method," *IEEE Transactions on Antennas and Propagation*, AP-37, 11, pp. 1361-1369, 1989.
- [213] P. Leveque, A. Reineix, and B. Jecko, "Modeling dielectric losses in microstrip patch antennas: Application of FDTD method," *Electronics Letters*, 28, 6, pp. 539-540, 1992.
- [214] C. Wu, K.-L. Wu, Z.-Q. Bi, and J. Litva, "Accurate characterization of planar printed antennas using finite-difference time domain method," *IEEE Transactions on Antennas and Propagation*, AP-40, 5, pp. 526-533, 1992.
- [215] K. Uehara and K. Kagoshima, "FDTD method analysis of mutual coupling between microstrip antennas," *IEICE Transactions on Communications*, E76-B, 7, pp. 762-764, 1993.
- [216] T. Oonishi, T. Kashiwa, and I. Fukai, "Analysis of microstrip antennas on a curved surface using the conformal grids FDTD method," *Electronics and Communications in Japan, Part 1*, 76, 12, pp. 73-81, 1993.
- [217] T. Kashiwa, T. Onishi, and I. Fukai, "Analysis of microstrip antennas on a curved surface using the conformal grids FDTD method," *IEEE Transactions on Antennas and Propagation*, AP- 42, 3, pp. 423-427, 1994.
- [218] Y. Qian, S. Iwata, and E. Yamashita, "Optimal design of an offset-fed, twin-slot antenna element for millimeter-wave imaging arrays," *IEEE Microwave Guided Wave Letters*, 4, 7, pp. 232-234, 1994.
- [219] A. Reineix and B. Jecko, "A time domain theoretical method for the analysis of microstrip antennas composed by slots," *Annales des Telecommunications*, 48, 112, pp. 29-34, 1993.
- [220] A. Reineix, J. Paillol, and B. Jecko, "FDTD method applied to the study of radar cross section of microstrip patch antennas," *Annales des Telecommunications*, 48, 11/12, pp. 589-593, 1993.
- [221] A. Reineix, C. Melon, T. Monediere, and F. Jecko, "The FDTD method applied to the study of microstrip patch antennas with a biased ferrite substrate," *Annales des Telecommunications*, 49, 314, pp. 137-142, 1994.
- [222] R. Luebbers, L. Chen, T. Uno, and S. Adachi, "FDTD calculation of radiation patterns, impedance, and gain for a monopole antenna on a conducting box," *IEEE Transactions on Antennas and Propagation*, AP-40, 12, pp. 1577-1583, 1992.

- [223] L. Chen, T. Uno, S. Adachi, and R. J. Luebbers, "FDTD analysis of a monopole antenna mounted on a conducting box covered with a layer of dielectric," *IEICE Transactions on Communications*, E76-B, 12, pp. 1583-1586, 1993.
- [224] J. Toftgird, S. N. Hornsleth, and J. B. Andersen, "Effects on portable antennas of the presence of a person," *IEEE Transactions on Antennas and Propagation*, AP-41, 6, pp. 739-746, 1993.
- [225] M. A. Jensen and Y. Rahmat-Samii, "Performance analysis of antennas for hand-held transceivers using FDTD," *IEEE Transactions on Antennas and Propagation*, AP-42, 8, pp. 1106-1113, 1994.
- [226] M. A. Jensen and Y. Rahmat-Samii, "EM interaction of handset antennas and a human in personal communications," *Proceedings of the IEEE*, 83, 1, pp. 7-17, 1995.
- [227] H. Y. Chen and H. H. Wang, "Current and SAR induced in a human head model by electromagnetic fields irradiated from a cellular phone," *IEEE Transactions on Microwave Theory Techniques*, MTT-42, 12, pp. 2249-2254, 1994.
- [228] L. Martens, J. De Moerloose, D. De Zutter, J. De Poorter, and C. De Wagter, "Calculation of the electromagnetic fields induced in the head of an operator of a cordless telephone," *Radio Science*, 30, 1, pp. 283-290, 1995.

EXPERIMENTAL AND NUMERICAL METHODOLOGY

The chapter gives a brief description of basic facilities used for fabrication, experimental characterization and simulation studies of the antenna. The concluding section focuses on FDTD method and implementation for foretelling the antenna reflection and radiation characteristics. The fundamental mathematical concepts of FDTD and the theoretical aspects are outlined in Annexure 'A'.

3.1 Printed Antenna Fabrication and Characterisation.

Printed antennas are usually fabricated on microwave substrate materials using standard photolithographic techniques. Selection of proper substrate material is the essential part in Microstrip antenna design. The dielectric constant, loss tangent, homogeneity, isotropicity and dimensional strength of the substrate all are of importance. High loss tangent substrate adversely affects the efficiency of the antenna especially at high frequencies. The selection of dielectric constant of the substrate depends on the application of the antenna and the radiation characteristics specifications. High Dielectric constant substrates causes surface wave excitation and low bandwidth performance. After the proper selection of the substrate material a computer aided design of the geometry is initially made and a negative mask of the geometry to be generated is printed on a butter paper. A double side copper clad substrate of suitable dimension is properly cleaned using acetone and dried in order to avoid the discontinuity caused by the impurities. Any disparity in the etched structure will shift the resonant frequency from the predicted values,

especially when the operating frequency is very high. A thin layer of negative photo resist material is coated using spinning technique on copper surfaces and it is dried. The mask is placed onto the photo resist and exposed to UV light. After the proper UV exposure the layer of photo-resist material in the exposed portions hardens which is then immersed in developer solution for few minutes. The hardened portions will not be washed out by the developer. The board is then dipped in the dye solution in order to clearly view the hardened photo resist portions on the copper coating. After developing phase the unwanted copper portions are etched off using Ferric Chloride (FeCl_3) solution to get the required antenna geometry on the substrate. The etched board is rinsed in running water to remove any etchant. FeCl_3 dissolves the copper parts except underneath the hardened photo resist layer after few minutes. The laminate is then cleaned carefully to remove the hardened photo resist using acetone solution.

3.2 Measurement Techniques

The variation of the following antenna characteristics with different geometry and its controlling parameters were studied in detail.

- Resonant frequency
- Return loss
- Impedance bandwidth
- Radiation pattern
- Gain
- Efficiency

The measurement techniques of all the above parameters are discussed in the following sections.

3.2.1 Measurement of antenna Resonant frequency, Return loss and Bandwidth

The block diagram of the experimental set up for the measurement of the return loss characteristics using a Network Analyzer interfaced to a PC is shown in Figure (3-1). The two different types of Vector Network Analysers are briefly explained here.

HP 8510C Vector Network analyzer (VNA)

HP8510C is sophisticated equipment capable of making rapid and accurate measurements in frequency and time domain [1]. The NWA can measure the magnitude and phase of the S parameters. 32 bit microcontroller MC68000 based system can measure two port network parameters such as S_{11} , S_{12} , S_{22} , S_{21} and it's built in signal processor analyses the transmit and receive data and displays the results in many plot formats. The NWA consists of source, S parameter test set, signal processor and display unit. The synthesized sweep generator HP 83651B uses an open loop YIG tuned source to generate the RF stimulus. It can synthesize frequencies from 10 MHz to 50 GHz. The frequencies can be set in STEP mode or RAMP mode depending on the required measurement accuracy. The antenna under test is connected to the two port S parameter test set unit, HP8514B and incident and reflected wave at the port are then down converted to an intermediate frequency of 20MHz and fed to the detector. These signals are suitably processed to display the magnitude and phase information in the required format. These constituent modules are interconnected through GPIB system bus. An in-house developed MATLAB based data acquisition system coordinates the measurements and saves the data in the text format. Schematic diagram of HP8510C NWA and setup for reflection characteristic measurement is shown in Fig(3.1). HP 8510C NWA is mainly used for the antenna radiation pattern measurements.

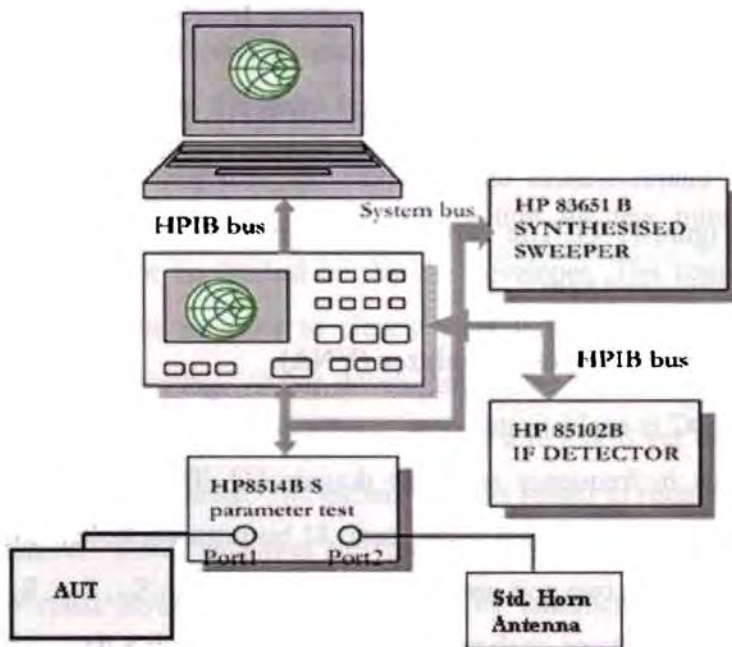


Fig.3.1 Experimental setup for antenna characterization

E8362B Programmable Network Analyzer (PNA)

The Agilent E8362B Vector Network Analyzer is a member of the PNA Series Network Analyzer platform and provides the combination of speed and precision for high frequency measurements. The operation range is from 10 MHz to 20 GHz. For antenna measurements it provides exceptional results with more points and faster measurement speed. It has 16,001 points per channel with $< 26 \mu\text{sec/point}$ measurement speed and 32 independent measurement channels. Built-in Windows XP operating system and other user interfaces makes measurement procedure much easier. Embedded help system with full manual, extensive measurement tutorials, and complete programming guide helps to carry out accurate measurement of antenna characteristics promptly. This instrument is used for reflection characteristics of the antenna presented in this thesis.

Crema Soft: Automated antenna measurement

The user friendly software *CremaSoft* is built in MATLAB^M environment. The powerful instrument control toolbox of the package is used for communicating with the stepper motor control and Network Analyzer using the GPIB interface. This automated software can be used for calibration, antenna measurements and material characterization of the substrate used for the antenna design.

Measurement of Antenna characteristics

The experimental procedures followed to determine the antenna characteristics are discussed in the following sections. Power is fed to the antenna from the S parameter test set of antenna through different cables and connectors. The connectors and cables will have its losses associated at higher microwave bands. Hence the instrument should be calibrated with known standards of open, short and matched loads to get accurate scattering parameters. There are many calibration procedures available in the network analyzer. Single port, full two port and TRL calibration methods are usually used. The two port passive or active device scattering parameters can be accurately measured using TRL calibration method. Return loss, VSWR and input impedance can be characterized using single port calibration method.

3.2.2 Return loss and 2:1 VSWR bandwidth

The return loss characteristic of the antenna is obtained by connecting the antenna to any one of the network analyzer port and operating the VNA in S_{11} or S_{22} mode. The calibration of the port is done for the frequency range of interest using the standard open, short and matched load. The calibrated instrument including the port cable is now connected to the device under test.

The frequency Vs reflection parameter (S_{11} or S_{22}) values is then stored on a computer using the ‘Crema Soft’ automation software.

The frequency corresponding to return loss minimum is taken as resonant frequency of the antenna. The range of frequencies for which the return loss value is within the -10dB (2:1 VSWR) points is usually treated as the bandwidth of the antenna. The antenna bandwidth is usually expressed as percentage of bandwidth, which is defined as

$$\%Bandwidth = \frac{\text{bandwidth}}{\text{centrefrequency}} * 100 \dots\dots\dots(3-1)$$

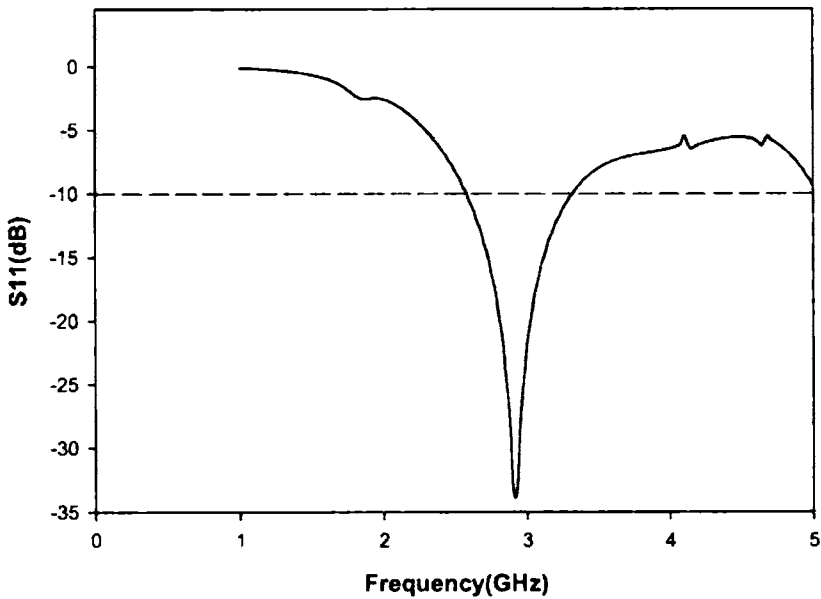


Fig.3.2 Return loss for impedance bandwidth

The 2:1 VSWR bandwidth is directly obtained from the reflection characteristics by noting the range of frequencies (Δf_r) over which the return loss (S_{11}) \leq -10 dB. The percentage bandwidth (% BW) is calculated as $\frac{\Delta f_r}{f_r} \times$

100%. A typical return loss plot is shown in fig.(3-2). The impedance curve of the test antenna fig.(3-3) can be plotted on the Smith Chart from the magnitude and phase of the return loss data.

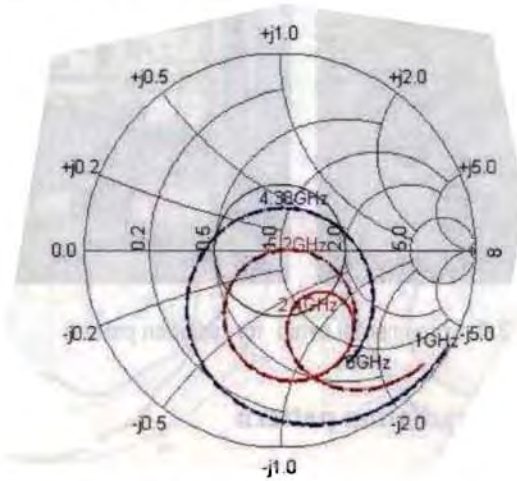


Fig. 3.3 Impedance curve on smith chart

3.2.3 Automated turn table assembly for far field measurement

A turn table is used for automatic 2D radiation pattern measurement. The turn table consists of a stepper motor driven rotating platform for mounting the Antenna under Test (AUT). An indigenously developed microcontroller based antenna positioner STIC 310C is used for radiation pattern measurement. The AUT is used as the receiver and a standard wideband ridged horn (1-18GHz) is used as transmitting antenna for radiation pattern measurements. The main lobe tracking for gain measurement and radiation pattern measurement is done using this setup. Antenna positioner is interfaced to the computer and with the in-house developed software '*Crema Soft*' automatic measurements can be carried out. To ensure far field criteria, the transmitter and receiver are separated by a distance greater than $2 * D^2 / \lambda$ where D is the maximum dimension of the antenna and λ is the minimum operating wavelength in free space.

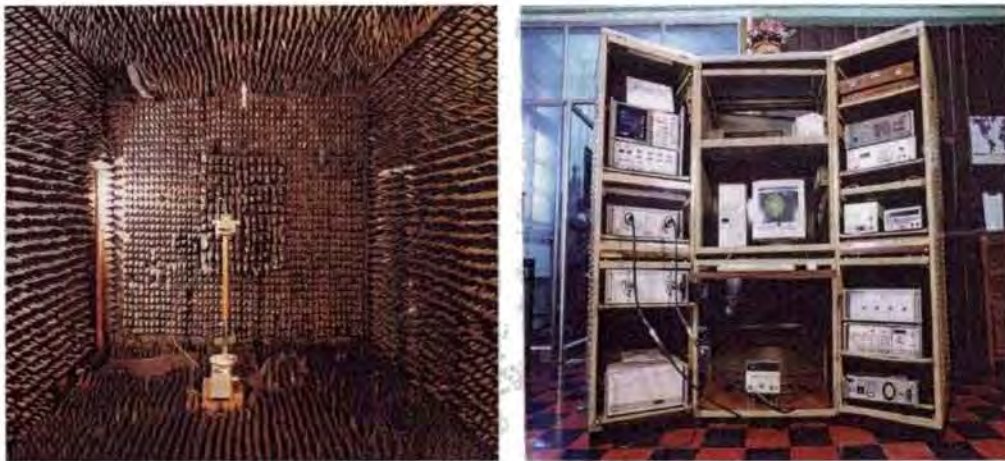


Fig 3.4 Experimental setup for radiation pattern

Measurement of antenna radiation pattern

The experimental set up for measurement of the antenna radiation pattern is shown in Figure (3-4). HP 8510C Network Analyser, interfaced to an IBM PC, is used for the pattern measurement. The PC is attached to a STIC 310C position controller. The antenna positioned along with the test antenna is kept at a distance $2 * D \frac{2}{\lambda}$ where 'd' is the distance between the transmitting and receiving antenna and ' λ ' is the wavelength corresponding to the largest frequency of operation. The AUT is used as the receiver and a standard wideband ridged horn (1-18GHz) is used as transmitting antenna for radiation pattern measurements. A wideband horn is used as the transmitter. The antennas are bore sighted and a THRU calibration is performed. After the bore sighting the Crema soft will automatically take the radiation pattern. The only input required for Crema soft are the start frequency, stop frequency step frequency, start angle, stop angle and step angle. The network analyser will measure the S21 data for the entire frequency for each step angle and store the data as an ASCII file. The radiation pattern for any desired frequency can be

easily plotted from these data. The process is repeated for co-polar and cross polar radiation pattern along E and H-plane respectively.

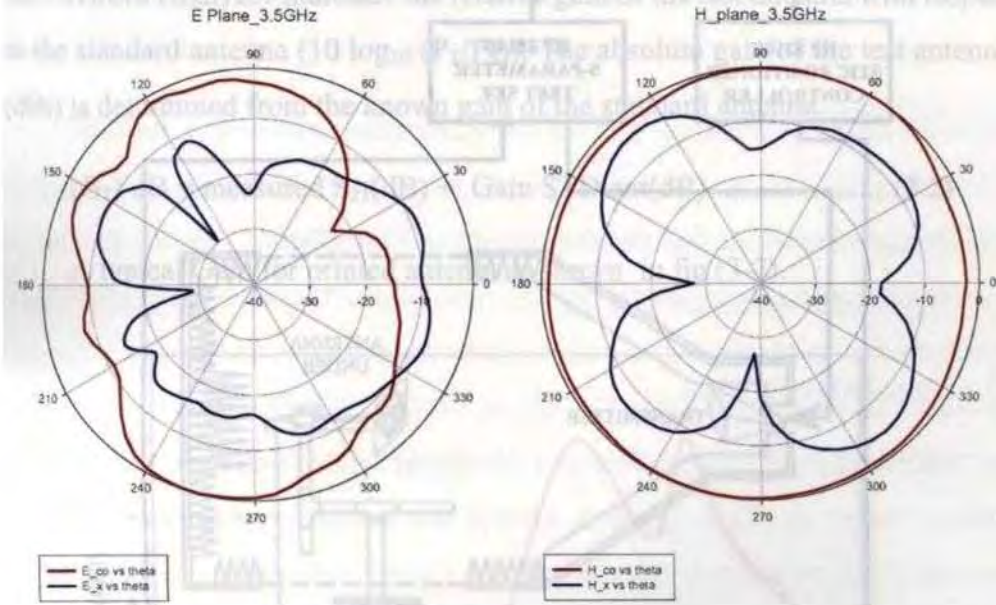


Fig. 3.5 Radiation pattern for E- Plane and H-Plane

Typical co-polar and cross-polar radiation patterns in the two principal planes of the test antenna (E-plane and H-plane) are shown in fig.(3-5). Appropriate gating can be applied in the time domain to minimise reflections and measurements are performed in the frequency domain. The entire measured data stored in ASCII format by *CREMA Soft* is further processed to yield the different radiation characteristics viz. half power beam width, cross- polar level, etc..

Most of the cases the radiation patterns are measured in an Anechoic chamber to simulate free space environment. Experimental set-up employed for the radiation pattern measurement is shown below.

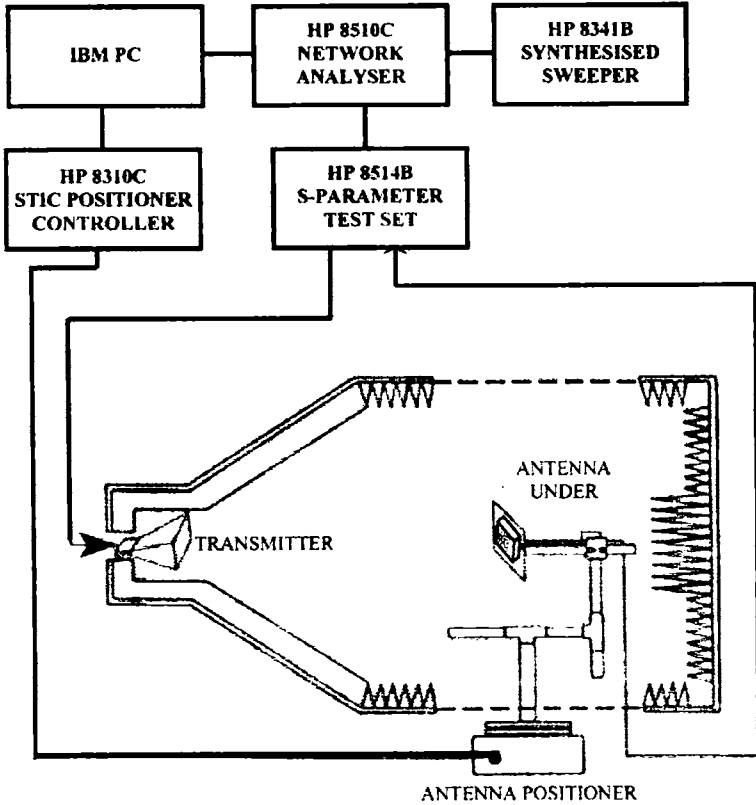


Fig. 3.6 Experimental Set up for measurement of radiation pattern / gain

3.2.4 Antenna Gain

The gain of the antenna under test is measured using the gain Transfer method [2-3]. The experimental setup is similar to the radiation pattern measurement setup. A standard antenna is placed in the antenna positioner and bore sighted. THRU calibration is made for the frequency range of interest. Standard antenna is then replaced by the AUT and the change in S_{21} is noted. Note that the AUT should be aligned so that the gain in the main beam direction is measured. This is the relative gain of the antenna with respect to the reference antenna. The absolute gain of the antenna is obtained by adding this relative gain to the gain of the standard antenna, provided by the manufacturer.

The standard antenna is replaced by the AUT maintaining the geometrical arrangement intact. The power received (P_T) is recorded. The plot displayed on the Network Analyzer indicates the relative gain of the test antenna with respect to the standard antenna ($10 \log_{10} (P_T/P_S)$). The absolute gain of the test antenna (dBi) is determined from the known gain of the standard antenna.

$$(G_T) \text{ dB} = \text{measured } S_{21}(\text{dB}) + \text{Gain STD ant}(\text{dB}) \dots \dots \dots (3.2)$$

A typical Gain for printed antenna is shown in fig.(3-7).

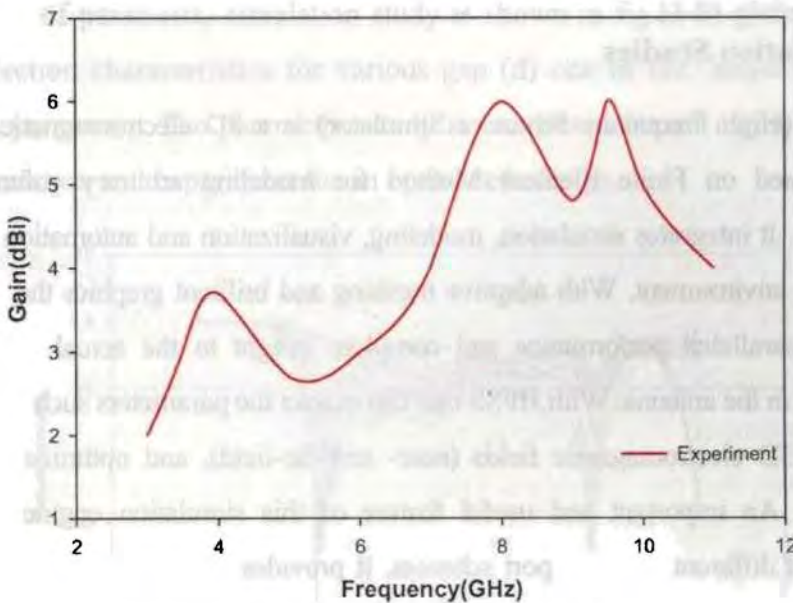


Fig. 3.7 Antenna Gain Measured

3.2.5 Antenna Efficiency

Efficiency of the antenna is measured using the Wheeler cap method [4-5]. The method involves making only two input impedance measurement of antenna under test: one with conducting cap enclosing the antenna and one without. For the Wheeler cap, a conducting cylindrical box is used whose radius is radian sphere of the antenna and to completely enclose the test antenna. Input

impedance of the test antenna is measured with and without the cap using E8362B PNA. Since the test antenna behaves like a series resonant RLC circuit near resonance, the efficiency is calculated by the following expression:

$$\text{Efficiency, } \eta = \frac{R_{no_cap} - R_{cap}}{R_{no_cap}} \dots\dots\dots (3-3)$$

R_{no_cap} = Input resistance of the antenna without Cap.

R_{cap} = Input resistance with Cap.

3.3 Simulation Studies

HFSS (High Frequency Structure Simulator) is a 3D electromagnetic field simulator based on Finite Element Method for modeling arbitrary volumetric structures [6]. It integrates simulation, modeling, visualization and automation in an easy to learn environment. With adaptive meshing and brilliant graphics the HFSS gives an unparalleled performance and complete insight to the actual radiation phenomenon in the antenna. With HFSS one can extract the parameters such as S, Y, Z, visualize 3D electromagnetic fields (near- and far-field), and optimize design performance. An important and useful feature of this simulation engine is the availability of different kinds of port schemes. It provides lumped port, wave port, incident wave scheme etc. The accurate simulation of coplanar waveguides and microstrip lines can be done using wave port. The parametric set up available with HFSS is highly suitable for Antenna engineer to optimize the desired dimensions. The first step in simulating a system in HFSS is to define the geometry of the system by giving the material properties and boundaries for 3D or 2D elements available in HFSS window. The suitable port excitation scheme is then given. A radiation boundary filled with air is then defined surrounding the structure to be simulated. Now, the simulation engine can be invoked by giving the proper frequency of

operations and the number of frequency points. Finally the simulation results such as scattering parameters, current distributions and far field radiation pattern can be displayed. The vector as well as scalar representation of E, H, J values of the device under simulation gives a good insight in to the antenna under analysis.

Various geometries under study for loading on the strip monopoles are Circular disc, Elliptical, Hexagonal, Octagonal, Rectangular. The parametric simulation using Ansoft-HFSS and analysis is done for optimizing the controlling parameters in each case of the above mentioned geometries. Example of parametric simulation study is shown in fig.(3-8) giving variation of reflection characteristics for various gap (d) one of the major controlling design parameter. The parametric study is conducted for all major parameters by simulation and experiment for an optimized design.

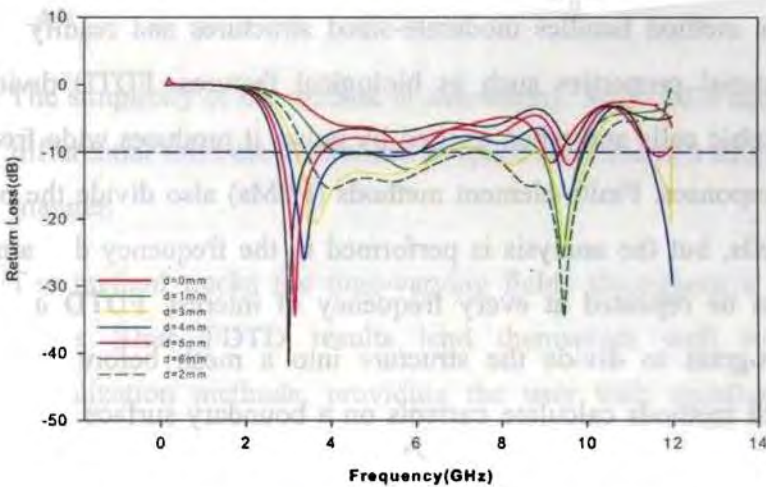


Fig. 3.9 Return loss variation for loaded monopole with 'd'

3.4 The FDTD method

Antenna analysis, an important part of design, requires a compromise between extensive calculations fabrication and measurement of prototypes,

which depends on working environment. One should minimize cost, which means reducing the time from the start of a design to completion of a working model. The ever increasing dynamic and versatile requirements of an antenna in mobile applications need a well developed antenna analysis in quickest possible time.

Analysis allows optimization of a design. We can design a number of antennas and adjust the dimensions until you find the best one. Again, you should be considering the costs of your time. At some point the incremental improvements are not worth the extra time for further analysis. For the Analysis and optimization FDTD (Finite-Difference Time-Domain) method is employed in the thesis.

The FDTD technique computes the fields on the structure in the time domain. This method handles moderate-sized structures and readily includes complex material properties such as biological features. FDTD divides the region into cubic cells and when excited by pulse, it produces wide frequency bandwidth responses. Finite-element methods (FEMs) also divide the problem into cubic cells, but the analysis is performed in the frequency domain. FEM analysis must be repeated at every frequency of interest. FDTD and FEMs require a program to divide the structure into a mesh before starting the solution. Both methods calculate currents on a boundary surface by using the equivalence theorem with the incident fields and then calculate the far-field radiation pattern from these boundary currents.

FDTD is an efficient tool for directly solving the Maxwell's equations using the finite difference techniques. The FDTD method is powerful yet simple algorithm that involves the discretization and solution of the derivative form of Maxwell's Curl equations in the time domain. The spatial and time

derivatives are approximated by centered differences, which are accurate to second order in time and space. Solution readily obtained by time stepping, where the new value for field components are calculated from previous value and this is called ‘Leap–Frog’ method.

If the discontinuities are too close to each other, the use of network concept will not be accurate due to the interactions of evanescent waves. To analyze the circuit accurately, the entire structure here to be simulated on one computation. In time domain analysis, broadband pulse may be used as excitation and frequency domain parameters calculated over the entire frequency range is by Fourier Transform (FT) of transient results.

The key attributes listed below combine to make the FDTD method a useful and powerful tool [7-10]. A more descriptive of FDTD is included in the Appendix ‘A’.

- The simplicity of the method is noteworthy. Maxwell’s equations in a differential form are discretized in space and time in a straightforward manner.
- The method tracks the time-varying fields throughout a volume of space. Thus FDTD results lend themselves well to scientific visualization methods, providing the user with excellent physical insight into the behaviour of electromagnetic fields.
- The method provides broadband response predictions about the system resonance. Far fields are derived from near fields.
- The geometric flexibility of the method permits the solution of a wide variety of radiation, scattering and coupling problems.

- Desired accuracy can be achieved by selecting suitable discretization parameters and boundary conditions.
- The method is extremely well suited for implementation on parallel computers.
- Personal computer capabilities have caught up with the requirements of FDTD for a wide range of modeling problems. Thus, even without any improvement in the fundamental algorithm, continuation of present trends will aid the generation of highly detailed electromagnetic wave models of volumetric complex structures of great engineering and scientific importance.

3.5 FDTD Implementation

The numerical algorithm for Maxwell’s curl equation defined by finite difference equation requires that time increment Δt have a specific bound relative to the lattice dimensions Δx , Δy and Δz . This bound is necessary to avoid numerical instability, an undesirable possibility of computed results to spuriously increase without the limit as time marching progresses. To ensure the computational stability it is necessary to satisfy a relation between the space increment and time increment. To ensure the stability of the time-stepping algorithm, Δt is chosen to satisfy the Courant-Friedrichs-Lewy (CFL) Stability criterion:

$$\Delta t \leq \frac{1}{V_{\max}} \frac{1}{\sqrt{1/\Delta x^2 + 1/\Delta y^2 + 1/\Delta z^2}} \dots\dots\dots(3.4)$$

V_{\max} is the maximum velocity of light in the computational volume. Typically V_{\max} will be the velocity of light in free space unless the entire volume is filled with

dielectric. In the present investigation the maximum time step is limited as 99.5% of the value given by the above equation.

The discretization of Maxwell's equations in space and time causes the variation of the phase constant of the propagating wave with frequency. For a fixed cell size different frequency components of a wave propagate at slightly different velocities. This phenomenon is referred to as numerical dispersion and is inherently present in the FDTD algorithm. Furthermore, velocity depends also on the angle of propagation with respect to the coordinate axis. This is called numerical anisotropy. For accurate and stable results, the grid dispersion error must be reduced to an acceptable level, which can be readily accomplished by reducing the cell size. Accuracy of computation can be ensured by selecting the grid size as 10 cells per wavelength ($\lambda/10$) or less at the highest frequency. In the analysis presented in the thesis the accuracy and stability are ensured by selecting $\Delta x, \Delta y, \Delta z \leq \lambda_{\min}/20$.

With the transient excitation in FDTD, impedance and scattering parameters over a wide frequency band can be calculated. One difficulty with FDTD is that for some applications, few thousands of time steps may be required for the transient fields to decay. This difficulty is common in the case of circuits having very high quality factor. One method to reduce the time steps required is to apply signal processing methods to predict the voltages and currents at later times from the results computed for early times. Instead of making FDTD calculations for the full number of time steps required for transients to dissipate, one might make actual FDTD calculations for some fraction of this total number of time steps, and use these results to predict those for the later times [11].

Applying the various prediction methods adds additional complexity to the FDTD calculation process. The prediction methods are complicated, and may require care and skill to obtain accurate results. Most of the methods described require the use to determine the order of the prediction process, related to the number of terms of whatever expansion function is used to approximate the FDTD time signal. A poor choice for the order of the prediction model can result in larger precision errors.

Another simple approach is to include a source with internal resistance to excite the problem. By employing source with internal resistance which matches with the characteristic impedance of the transmission line provided accurate results while greatly reduces the number of time steps required for convergence.

In this thesis the 3D-FDTD Modeler code is developed in Matlab 6.5 for, problem space set up, test object definition, EH algorithm, Absorbing radiation boundary condition (ABC), Data saver, FFT and far field transformation. The geometry is defined with estimated x , y , z , t for time step $n = 0$. Choice of cell size is very critical here as this has to be small enough to permit accurate results at highest frequency of interest adhering to the Nyquist criterion and yet be sufficiently large to keep the computing resources in manageable limit. All E and H components are initialized. The excitation Gaussian pulse is applied at feed point.

The E, H fields over the spatial grid inside the computational domain is updated. The outer radiation boundary condition is applied to absorb the scattered field at the outermost portion of the problem space. This is applied for say 4000 to 6000 step cycles ensuring the accuracy and stability of FDTD simulation without ringing. To ensure the stability of time stepping algorithm 'dt' is chosen to satisfy the courant stability criterion. Once this E, H field for

all the cycles are stored as a matrix, the post processing of this transient field data to extract required return loss (S11), radiation pattern etc. by FFT for visual presentation. This output processing may need the transformation of near field to far field radiation.

Cell Dimensions (mm)	$\Delta x = 0.5$ $\Delta y = 0.5$ $\Delta z = 0.4$
Time step	$\Delta t = 0.88$ ps
Number of time steps	6000
Simulation interval	4400 ps

The different parameters used for the FDTD calculations are given below.

Excitation	Gaussian Pulse Half width $T = 15$ ps Time delay $t_0 = 3T$
------------	-------------------------------------------------------------------

The numerical method described above is employed for the analysis of different antenna configurations. This time domain method is more suitable than the frequency domain method in designing the wide band antenna. Being a time domain technique, the FDTD method directly calculates the impulse response of an electromagnetic system. It implies that a single simulation can provide Ultra wideband temporal waveforms [12]. The results of the numerical analysis are validated through experiments and commercially available software and presented in chapter five.

The input impedance of the antenna is computed as ratio of the FFT of voltage derived from E field values at the feed point over the entire time steps,

to the FFT of current at the same point, derived from the H field values. Return Loss S_{11} (in dB) is then computed. Typical voltage and current waveforms at the feed point are shown in Figure (3-10). In FDTD calculations involving $R_s = 50 \Omega$, the voltage waveform is no longer purely Gaussian, since the voltage across the resistance is also included. It is observed during simulation that the system converges in ~ 6000 time steps for the present problem.

More details about the FDTD theory and its implementation for the present work is described in Appendix- A.

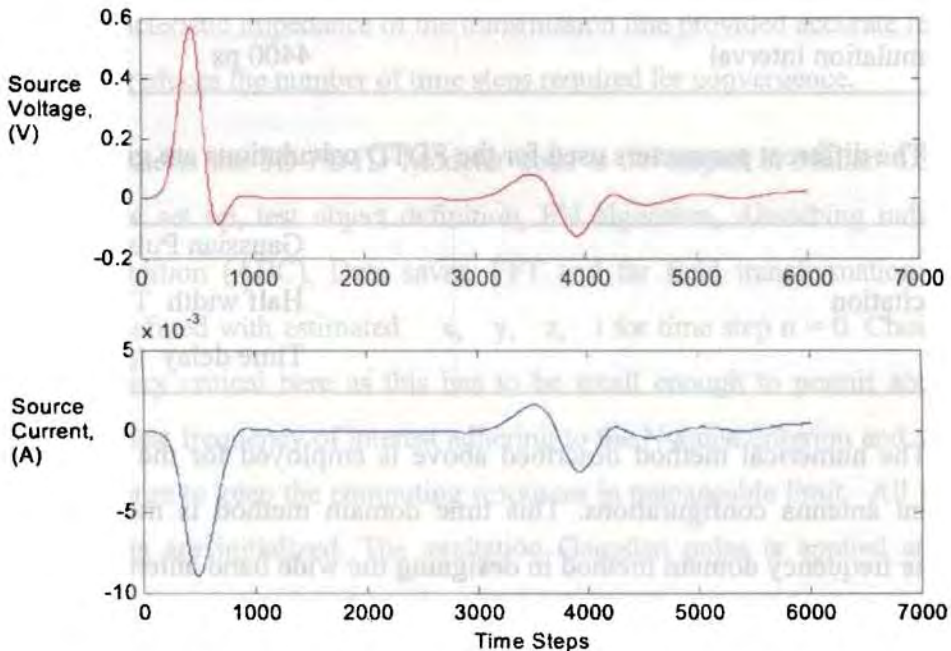


Fig. 3.10 Voltage and Current plot for step size of 6000 time steps.

3.6 References

- [1] HP8510C Network Analyzer operating and programming manual, Hewlett Packard, 1988.
- [2] C. A. Balanis, "Antenna Theory: Analysis and Design", Second Edition, John Wiley & Sons Inc. 1982.

- [3] John D. Kraus, "Antennas", Mc. Graw Hill International, second edition, 1988.
- [4] H.A Wheeler, "The Radian sphere around a small antenna", in Proc. IRE, August 1959, pp 1325-1331.
- [5] E.Newman, P.Hohley and C.H Walter, "Two methods for the measurement of antenna efficiency", IEEE trans. Antennas and Propogat.Vol.23, No.4, pp 457-461, July 1975.
- [6] HFSS User's manual, version 10, Ansoft Corporation, July 2005
- [7] K. S. Yee, "Numerical solution of initial boundary value problems involving Maxwell's equations in isotropic media," *IEEE Transactions on Antennas and Propagation*, AP-14, 4, pp. 302- 307, 1966.
- [8] A. Taflove, "Review of the formulation and applications of the finite-difference time-domain method for numerical modeling of electromagnetic wave interactions with arbitrary structures," *Wave Motion*, 10, 6, pp. 547-582, 1988.
- [9] A. Taflove and M. E. Brodwin, "Numerical solution of steady state electromagnetic scattering problems using the time-dependent Maxwell's equations," *IEEE Transactions on Microwave Theory Techniques*, MTT-23, 8, pp, 623-630, 1975.
- [10] K. S. Kunz and R. J. Luebbers, *The Finite Difference Time Domain Method for Electromagnetics*, Boca Raton, FL, CRC Press, 1993.
- [11] Enquist and Majada, "Absorbing Boundary Conditions for the Numerical simulation of waves", *Mathematics of computation*, Vol. 31, 1977, pp. 629-651.
- [12] A. Taflove and S. C. Hagness , *Computational Electrodynamics the Finite-Difference Time-Domain Method* , 2nd ed. Norwood, MA: Artech House, 2000.

INVESTIGATIONS ON ULTRA WIDE BAND (UWB) PRINTED MONOPOLES

Ultra Wide Band (UWB) technology is one of the most promising solutions for future communication systems due to its high-speed data rate and excellent immunity to multi-path interference. The un-licensing of ISM band gives an increased opportunity for wireless communications over short distances. This is the driving force behind work presented here. In this context, the UWB antenna design plays a unique role because it behaves like a band pass filter and reshapes the spectra of the pulses. Some of the critical requirements for UWB antenna are Ultra wide bandwidth, directional radiation patterns, constant gain and group delay over the entire band, high radiation efficiency and low profile.

Evolution of a Ultra wide band planar antenna from a simple microstrip transmission line is presented in this chapter. The chapter commences with the description of resonance and radiation characteristics of printed strip monopole antenna on an infinite ground plane. It is followed by a detailed study of the ground plane truncation effects on antenna radiation characteristics. The truncation of ground plane is effectively utilized to design a wide band printed strip monopole antenna. The detailed parametric analysis of wide band printed monopole is enabled to derive simple design equation for wide band performance. The finite length microstrip line is modified with a truncated ground plane to create a boundary discontinuity. It is found that this structure is

radiating to the surrounding. By properly adjusting the parameters of the antenna very large impedance bandwidth can be easily achieved with moderate radiation efficiency.

Experimental and theoretical analysis of compact monopole antenna derived from parametric analysis of a wide printed monopole is presented for application in broadband wireless communication systems. Thus this chapter highlights the step by step procedure to derive a broadband printed monopole antenna from a simple printed strip monopole antenna. Printed monopoles are conformal for modular design and can be fabricated along with the printed circuit board of the system, which make the design simpler and fabrication easier. The chapter concludes with some of the typical loaded strip monopole antenna designs along with its radiation characteristics suitable for wideband wireless communication gadgets. This is the basis for further fine tuning for achieving the goal of compact Ultra wide band antenna.

4.1 Characteristics of the Printed strip monopoles.

4.1.1 Printed Antenna design parameters

Fig. (4-1 a) is a finite open ended 50Ω microstrip transmission line etched on a substrate of $\epsilon_r=4.38$ and height 1.6 mm. The length of the microstrip line is 80 mm and width is 3 mm. The reflection studies show that this finite length transmission line is not resonating at all. The transmission studies show that this is a very good transmission line. So this can be used as a transmission line for transporting electromagnetic energy from one point to another. Since it is a transmission line the radiated energy from the structure is negligibly small and can not be used as a radiating element.

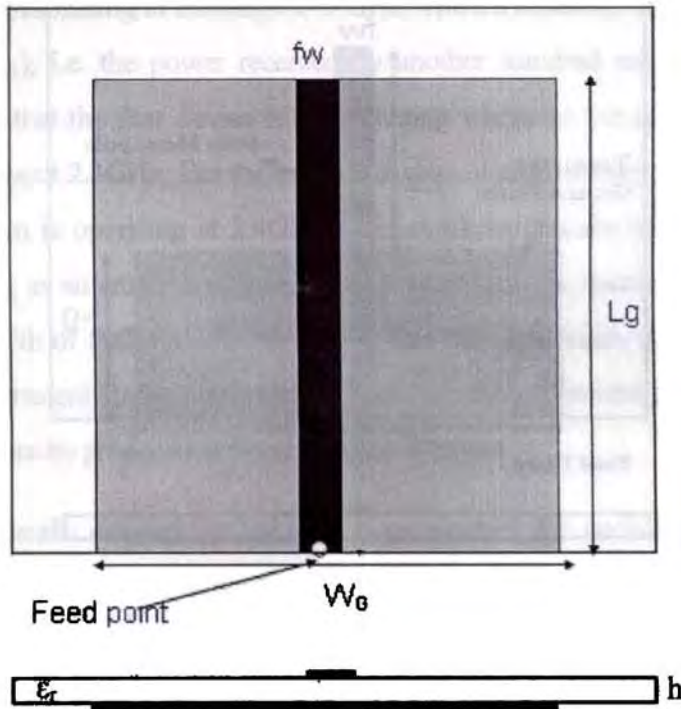


Fig.4.1(a) Geometry of printed Microstrip transmission line with substrate height ' h ' = 1.6mm , relative permittivity (ϵ_r)=4.38, feed width f_w =3mm, ground plane width ' W_g ' =65mm and Length ' L_g ' =80mm, Microstrip Tx line length = L_g = 80mm.

This finite length open circuited transmission line can be efficiently transformed as a radiating structure by modifying the structure. This is demonstrated in this section. Fig. 4.1 (b) is the modified structure of fig.4.1 (a). In this case the full ground plane of a microstrip line is truncated as shown in Fig. 4.1 (b). In this case the length and width of the ground plane is reduced to 18 mm X 65 mm. Only 18 mm of the top strip is having ground plane and the remaining part of the strip is without any ground plane. The reflection characteristics of both devices are shown in fig (4-2).

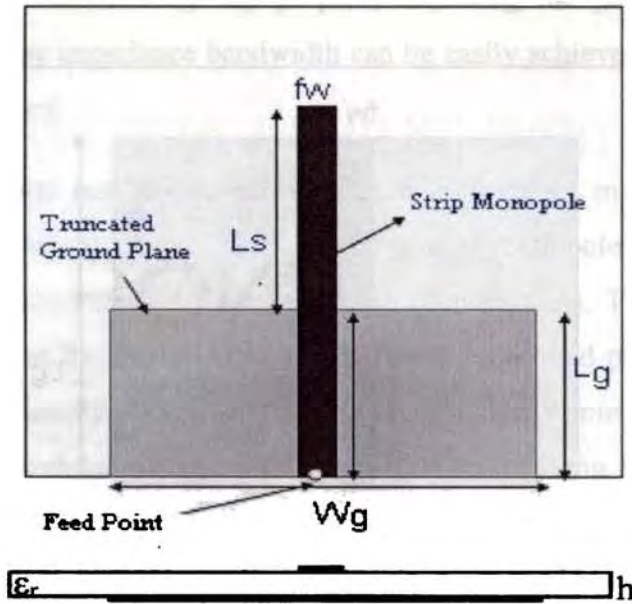
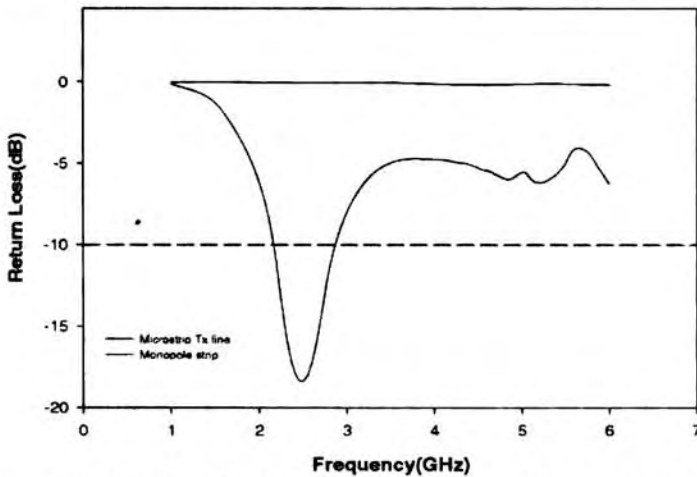


Fig.4-1(b) Geometry of printed strip Monopole antenna with substrate height ' h ' = 1.6mm, relative permittivity (ϵ_r) = 4.38, monopole strip length ' L_s ' = 25mm, feed width ' f_w ' = 3mm, truncated ground plane of width ' W_g ' = 65mm and length ' L_g ' = 18mm

4.1.2 Return Loss Characteristics



Figure(4-2) Return loss of (a) Finite length Microstrip transmission line with large ground plane on a substrate of height ' h ' = 1.6mm, relative permittivity (ϵ_r) = 4.38, strip length ' L_s ' = 59mm, strip width f_w = 3mm, ground plane width W_g = 65mm and length L_g = 80mm (b) Strip monopole on the same substrate with truncated ground plane. ' L_s ' = 25mm, W_g = 65mm, L_g = 18mm, f_w = 3mm, resonant frequency f_r = 2.4GHz.

It is very clear from the graph that first microstrip Tx line (antenna) in fig.4-1(a) is not at all resonating in the range 1- 5 GHz. The transmission characteristics of the antenna (S_{21}), i.e. the power received by another standard antenna kept at a distance shows that the first device is not radiating where as the second device is radiating near about 2.4GHz. But the monopole strip antenna shown in fig 4-1(b) of length $L_s=25\text{mm}$ is operating at 2.4GHz. This confirms that the second device is very well acting as an antenna. It is found that the antenna is resonating at 2.4GHz with a band width of 500MHz. So the percentage (%) Bandwidth of the antenna is 21%. This experiment shows a transmission line can be conveniently modified as a radiating structure by proper modification of the structure.

Next question is what are the design parameters for such a device? This question is answered in the following section.

To study the effect of the length of the dipole on the resonant frequency the monopole length 'Ls' is varied from 17mm to 30mm, keeping all the parameters as constant.

For the theoretical analysis the antenna is modeled using FDTD algorithm. Total computational domain used for the analysis of the antenna is $150 \times 180 \times 24$ cells. Δx , Δy , Δz in the computation domain are taken as 0.5mm. The discretization values are less than $\lambda/20$ at the maximum frequency of computation and gives good accuracy of the computed results. 10 air cells are assigned around the antenna geometry to simulate the practical condition in which antenna is immersed in the surrounding air. 10 cells are assigned for ABC at each side of the problem space. The layer just above the printed strip and just below the ground plane is assigned with effective dielectric constant to ensure the air-dielectric interface. A Gaussian pulse with pulse half width $T=15\text{ps}$ and time delay $t_0=3T$ is selected for the present analysis. According to the stability criteria the calculated time step is $\Delta t=0.95\text{ps}$.

Leubbers feed model is employed to implement the feeding system. Gaussian pulse is employed as the voltage sources for calculating the time domain response. The computed time domain response at the feed point is depicted in fig.(4-3). The electric field component is settled at around 6000 time steps. When the launched Gaussian pulse is complexly settled down in the computation domain the return loss value of the device is calculated. The time domain data are first converted to frequency domain by taking FFT and then return loss is calculated.

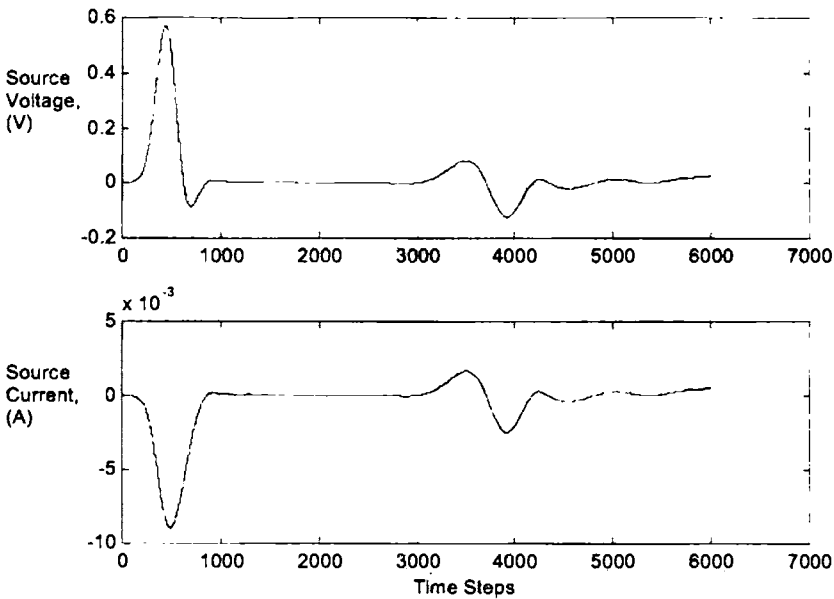


Fig. 4.3 Computed time domain response at feed point

The reflection characteristics simulated using FDTD are shown in figure (4-4). It is found that the resonant frequency ' f_r ' decreases with ' L_s ' of the monopole strip as expected. This shows that this device is working as a monopole antenna. For the experimental analysis a prototype of the antenna used in FDTD computation is fabricated using standard photolithographic techniques. Computed, experimental and simulated results are compared and discussed in following sections.

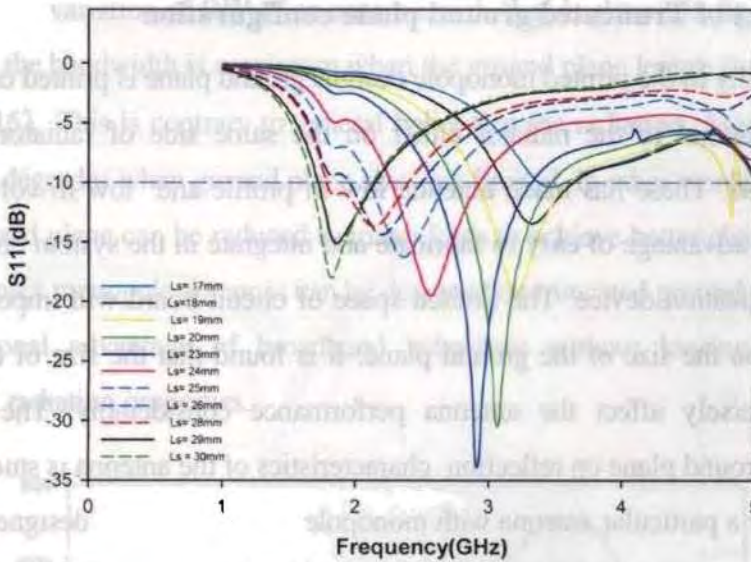


Fig.4.4 Return loss variation with frequency of strip monopole for different monopole length (FDTD Calculation) 'Ls', $W_g=65\text{mm}$, $L_g=18\text{mm}$, $fw=3\text{mm}$, $\epsilon_r=4.38$ and $h=1.6\text{mm}$.

The variation of measured resonant frequency with the monopole length 'Ls' is compared with FDTD in fig.(4-5). The results are in good agreement with FDTD prediction.

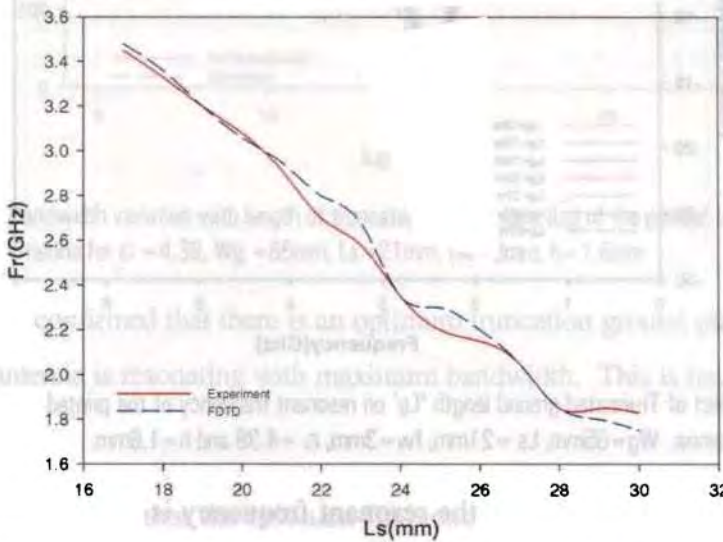


Fig. 4.5 Frequency variation with Strip length of monopole (Ls) of the printed strip monopole antenna for $L_g=18\text{mm}$, $W_g=65\text{mm}$, $fw=3\text{mm}$, $\epsilon_r=4.38$ and $h=1.6\text{mm}$.

4.1.3 Effect of Truncated ground plane configuration

Usually in the printed monopole designs ground plane is printed on the same substrate parallel to the radiator either on the same side of radiator or at the opposite side. These has made antenna low in profile and low in volume along with added advantage of easy to fabricate and integrate in the system circuit board of communication device. The limited space of circuit board will impose another constraint on the size of the ground plane. It is found that the size of the ground plane, adversely affect the antenna performance considerably. The effect of truncated ground plane on reflection characteristics of the antenna is studied in this section. For a particular antenna with monopole length ' L_s ' for a designed resonant frequency, the truncation ground plane length alone is varied to obtain its effects on the resonant frequency. The same is plotted in fig. (4-6).

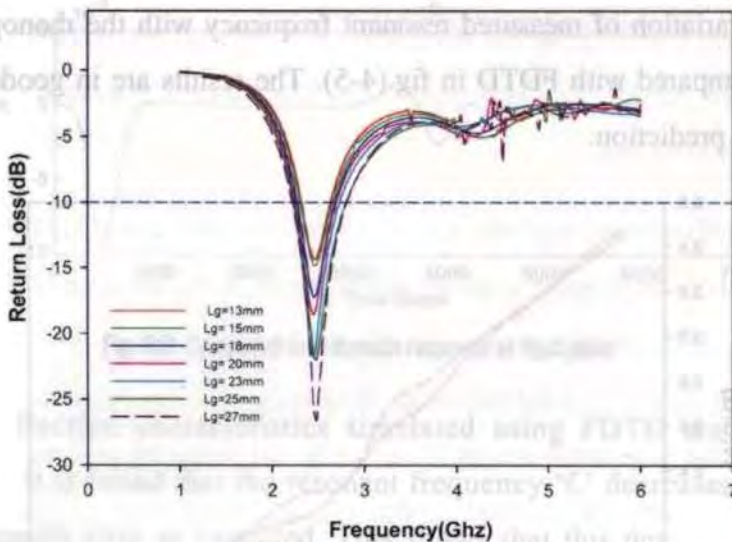


Fig. 4.6 Effect of Truncated ground length ' L_g ' on resonant frequency of the printed strip monopole antenna. $W_g=65\text{mm}$, $L_s=21\text{mm}$, $fw=3\text{mm}$, $\epsilon_r=4.38$ and $h=1.6\text{mm}$.

It is clear from the figure the resonant frequency is virtually independent of the length of ground plane of the antenna. The length is only affecting the matching and bandwidth of the antenna.

Typical variation of BW of an antenna with 'Lg' is shown in fig. (4-7). It is found that the bandwidth is maximum when the ground plane length is of the order 0.12 to 0.16λ . This is contrary to general belief that the radiation characteristic of monopole degrades when ground plane sizes are limited. In other words, the length of the ground plane can be reduced to many folds to achieve better characteristics. Thus compact monopole antennas can be designed on truncated ground planes with the additional advantage of broadband behaviour without losing its omnidirectional radiation properties.

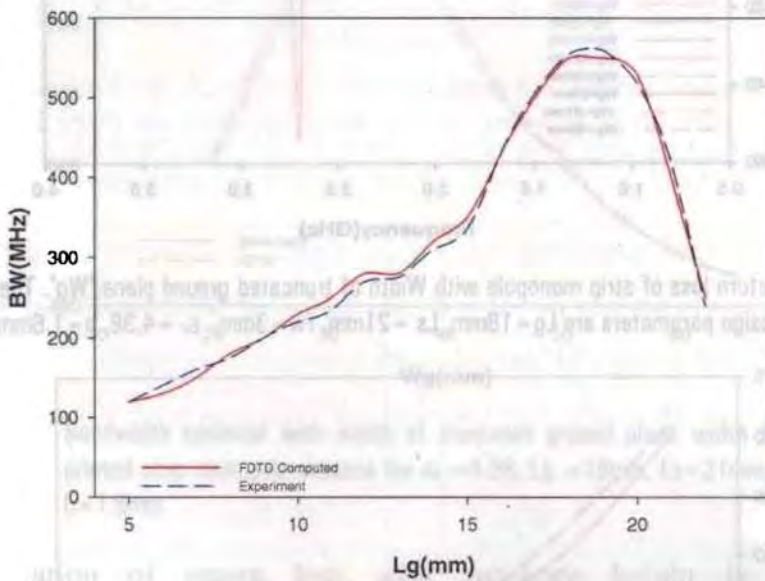


Fig. 4.7 Bandwidth variation with length of truncated ground plane (Lg) of the printed strip monopole antenna for $\epsilon_r = 4.38$, $W_g = 65\text{mm}$, $L_s = 21\text{mm}$, $fw = 3\text{mm}$, $h = 1.6\text{mm}$

So it is confirmed that there is an optimum truncation ground plane length for which the antenna is resonating with maximum bandwidth. This is happening when $L_g = 0.144\lambda$.

It is also found that the resonant frequency of the antenna depends on the ground plane width 'Wg'. However, this variation is in the expected line

compared to the dependence of resonant frequency on 'Lg'. This is demonstrated in fig. (4-8) and (4-9). For large ground plane width the resonant frequency is minimum as shown in fig.(4-9).

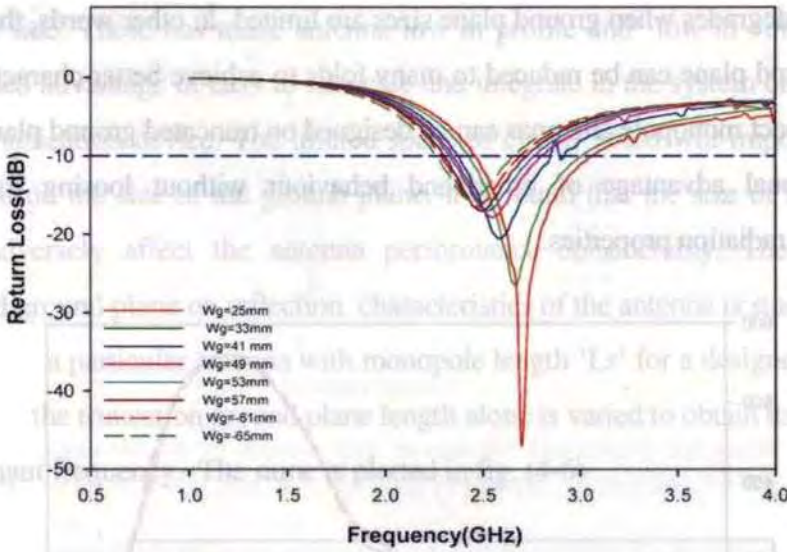


Fig. 4.8 Return loss of strip monopole with Width of truncated ground plane 'Wg'. The other design parameters are Lg = 18mm, Ls = 21mm, fw = 3mm, $\epsilon_r = 4.38$, h = 1.6mm.

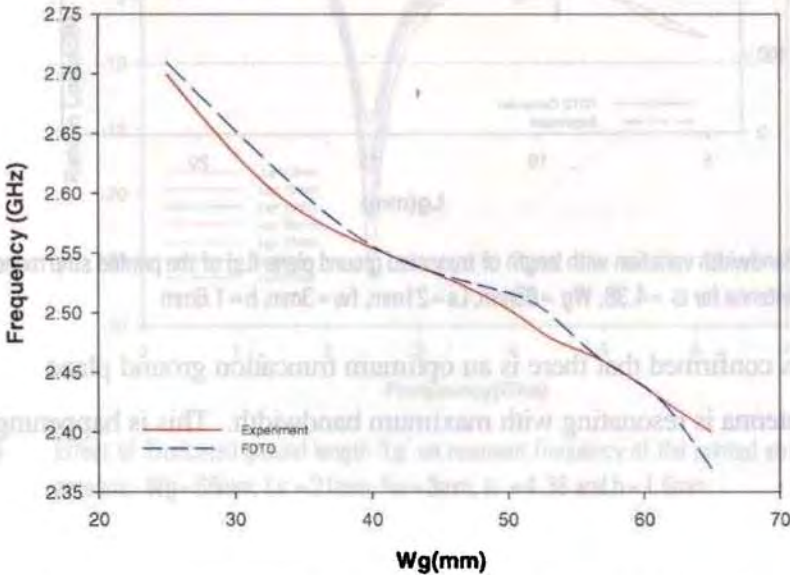


Fig.4.9 Frequency variation with Width of truncated ground plane (Wg) of the printed strip monopole antenna for $\epsilon_r = 4.38$, Lg = 18mm, Ls = 21mm, fw = 3mm, h = 1.6mm

The variation of BW of the antenna with 'Wg' for the optimum ground plane width is shown in fig.(4-10). It is found that the bandwidth of the antenna is maximum for an optimum value of the ground width (0.25 – 0.32 λ).

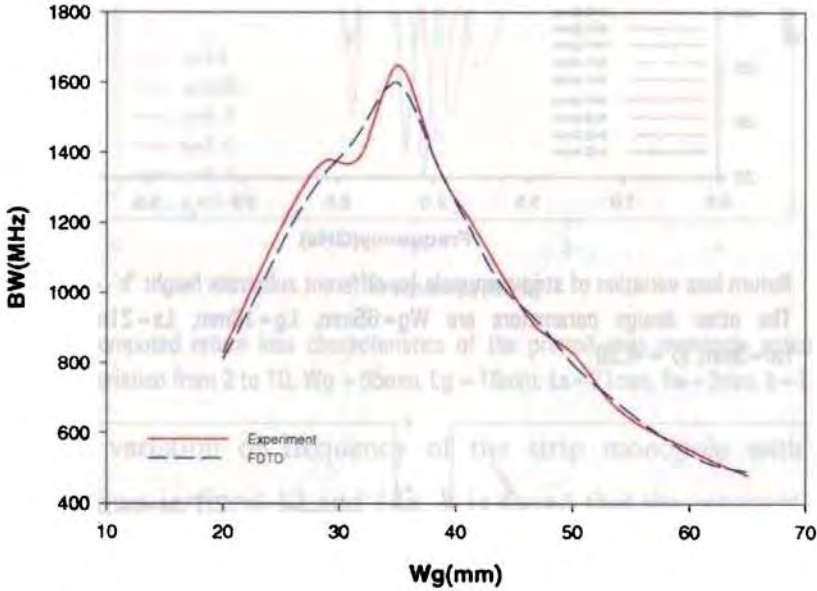


Fig. 4.10 Bandwidth variation with width of truncated ground plane width (Wg) of the printed strip monopole antenna for $\epsilon_r = 4.38$, $L_g = 18\text{mm}$, $L_s = 21\text{mm}$, $f_w = 3\text{mm}$, $h = 1.6\text{mm}$

Variation of return loss with substrate height is shown in fig.4-11. Variation of resonant frequency with substrate height is shown in fig.4-12(a). This shows that the variation resonant frequency with substrate height is negligibly small. The variation in the resonant frequency is from 2.4GHz to 2.7 GHz when h is varied from 0.6 mm to 2.4 mm. It is found that the resonant frequency is minimum for thin substrate and high for thick substrates.

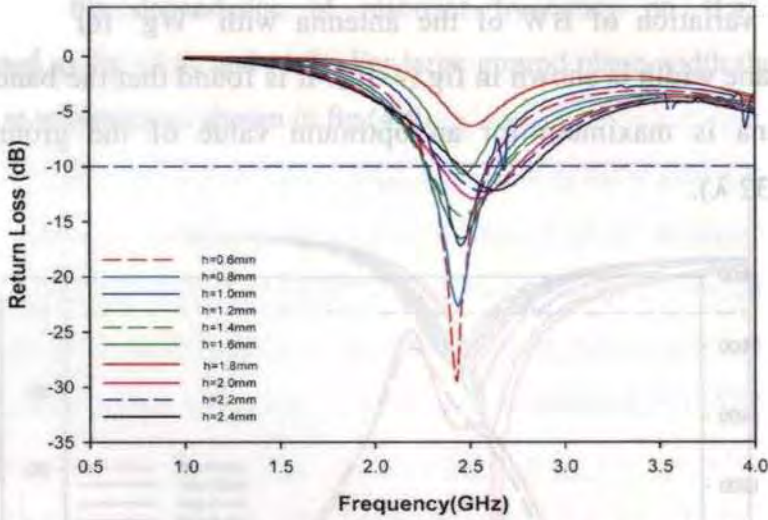


Fig. 4.11 Return loss variation of strip monopole for different substrate height ' h ' = 0.6 to 2.4mm. The other design parameters are $W_g=65\text{mm}$, $L_g=18\text{mm}$, $L_s=21\text{mm}$, $h=1.6\text{mm}$, $fw=3\text{mm}$, $\epsilon_r = 4.38$

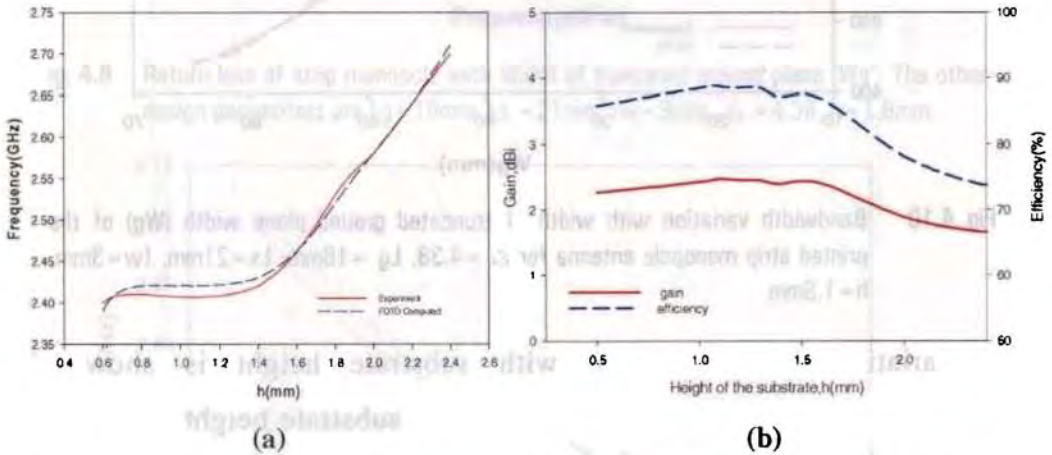


Fig. 4.12 (a) Resonant frequency ' F_r ' variation with substrate height (h) (b) Gain and Efficiency of strip monopole for different substrate height ' h ' = 0.6 to 2.4mm. The other design parameters are $W_g=65\text{mm}$, $L_g=18\text{mm}$, $L_s=21\text{mm}$, $h=1.6\text{mm}$, $fw=3\text{mm}$, $\epsilon_r = 4.38$.

The variation of gain and efficiency of the antenna with substrate height is shown in fig. 4-12(b). It is found that both gain and efficiency decreases with substrate height. This may be due to the excitation of surface waves in thick substrates.

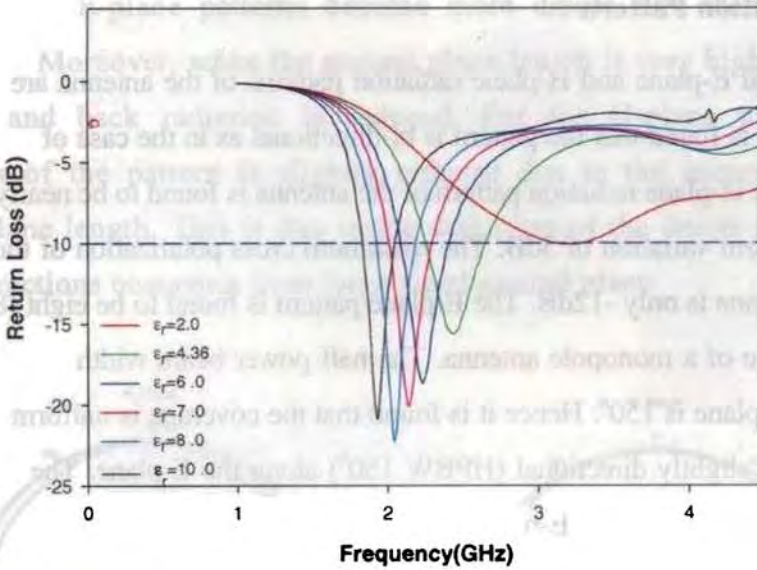


Fig. 4.13 Computed return loss characteristics of the printed strip monopole antenna for ϵ_r variation from 2 to 10, $W_g = 65\text{mm}$, $L_g = 18\text{mm}$, $L_s = 21\text{mm}$, $fw = 3\text{mm}$, $h = 1.6\text{mm}$.

Typical variation of frequency of the strip monopole with dielectric constant is shown in fig. 4-13 and 14a. It is found that the resonant frequency decreases with dielectric constant of the substrate. Moreover, it is found that the gain is optimum for a particular antenna. For this design the gain is maximum when of ϵ_r is in the range of 8-9 as demonstrated in fig. 4.14(b).

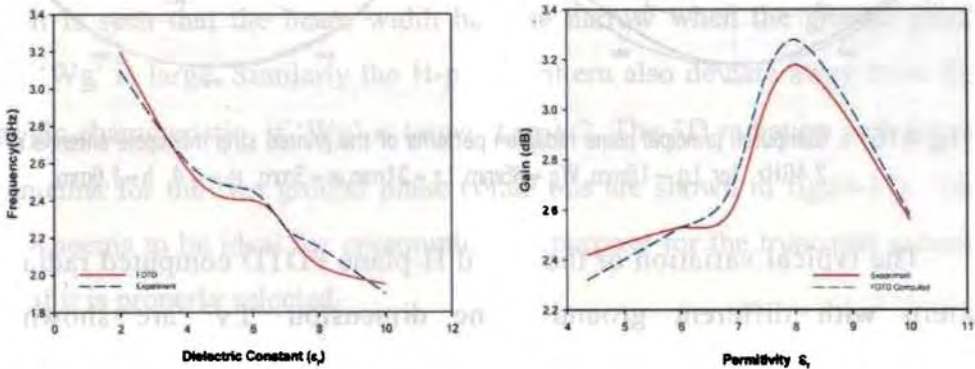


Fig. 4.14(a) Resonant Frequency variation (b) Computed and Measured Gain of the printed strip monopole antenna for variation of $\epsilon_r = 4.38$ to 10, $W_g = 65\text{mm}$, $L_g = 18\text{mm}$, $L_s = 21\text{mm}$, $fw = 3\text{mm}$, $h = 1.6\text{mm}$

4.1.4 Radiation Pattern

Typical E-plane and H-plane radiation patterns of the antenna are shown in fig.(4-15). It is found that the pattern is bi-directional as in the case of a monopole antenna. The H-plane radiation pattern of the antenna is found to be nearly uniform with maximum variation of 3dB. The maximum cross polarization of the antenna along this plane is only -12dB. The E-plane pattern is found to be eight (8) shaped as in the case of a monopole antenna. The half power beam width of the antenna along the E-plane is 150° . Hence it is found that the coverage is uniform along the H-plane and slightly directional (HPBW 150°) along the E-plane. The worst case cross polarization along the E-plane is -10dB.

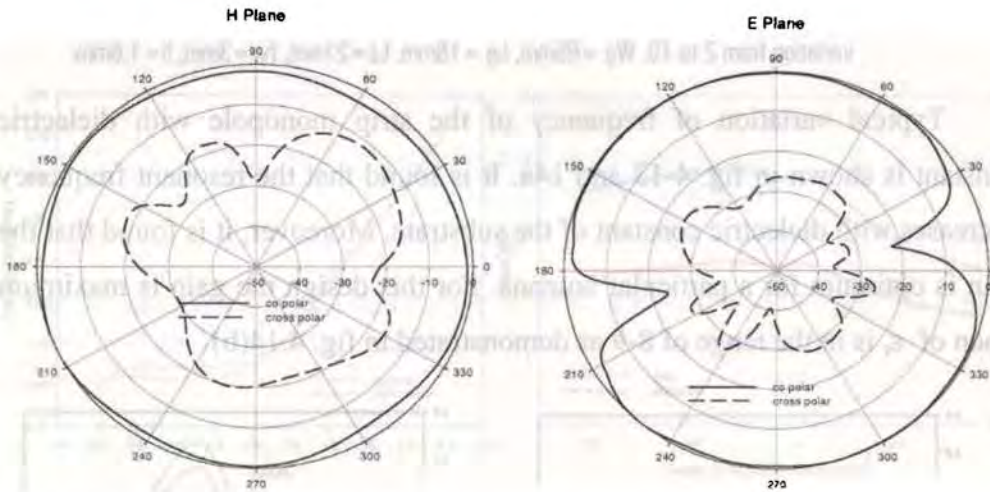


Fig. 4.15 Computed principal plane radiation patterns of the printed strip monopole antenna at 2.4GHz for $L_g = 18\text{mm}$, $W_g = 65\text{mm}$, $L_s = 21\text{mm}$, $w = 3\text{mm}$, $\epsilon_r = 4.4$, $h = 1.6\text{mm}$.

The typical variation of the E and H-plane FDTD computed radiation pattern with different ground plane dimension 'L_g' are shown in fig.(4-16). Radiation characteristics studies reveal the ground plan length variation affects the nulls of the E-plane pattern where as the beam width is varied slightly in the H-plane pattern. When the ground plane length is

very low the E-plane patterns become more dipole like than classical monopoles. Moreover, when the ground plane length is very high it acts as reflector and back radiation is reduced. For the H-plane pattern the broadness of the pattern is slightly reduced due to the increase in the ground plane length. This is due to the distortion of the image due to the edge diffractions occurring from large sized ground plane

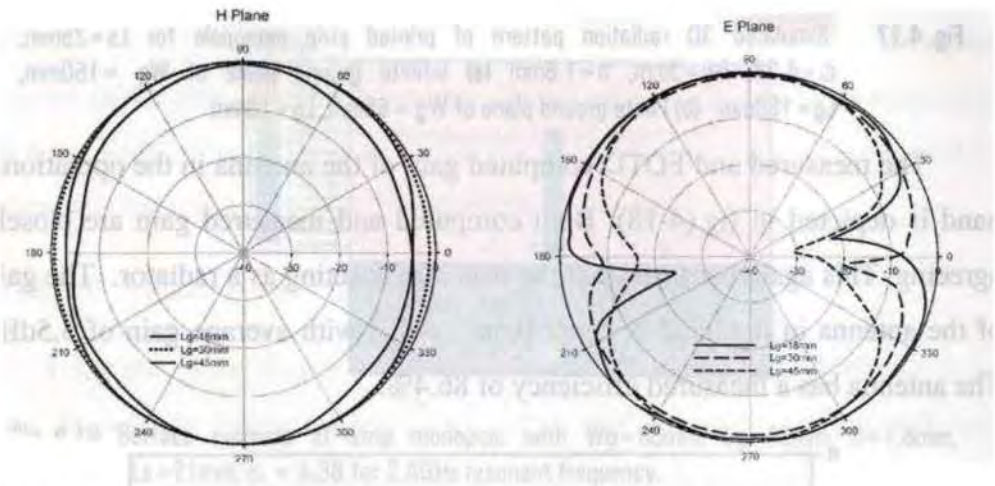


Fig. 4.16 Variation of principal plane radiation patterns of the printed strip monopole antenna at 2.4GHz due to 'Lg' $W_g = 65\text{mm}$, $L_s = 21\text{mm}$, $w = 3\text{mm}$, $\epsilon_r = 4.4$, $h = 1.6\text{mm}$

It is seen that the beam width become narrow when the ground plane width 'Wg' is large. Similarly the H-plane pattern also deviate away from the isotropic characteristic if 'Wg' is larger than $\lambda/2$. The 3D radiation patterns of the antenna for the two ground plane conditions are shown in fig.(4-17). The pattern seems to be ideal for communication purpose for the truncated ground plane if it is properly selected.

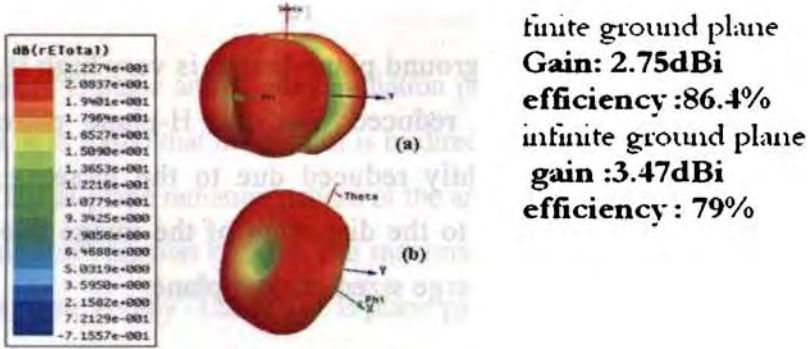


Fig. 4.17 Simulated 3D radiation pattern of printed strip monopole for $L_s=25\text{mm}$, $\epsilon_r=4.38$, $f_w=3\text{mm}$, $h=1.6\text{mm}$ (a) Infinite ground plane of $W_g = 150\text{mm}$, $L_g = 150\text{mm}$ (b) Finite ground plane of $W_g = 65\text{mm}$, $L_g = 18\text{mm}$

The measured and FDTD computed gain of the antenna in the operational band is depicted in fig.(4-18). Both computed and measured gain are closely agreeing. This again confirms that the structure is acting as a radiator. The gain of the antenna in the band is better than 2.4 dBi with average gain of 3.5dBi. The antenna has a measured efficiency of 86.4%.

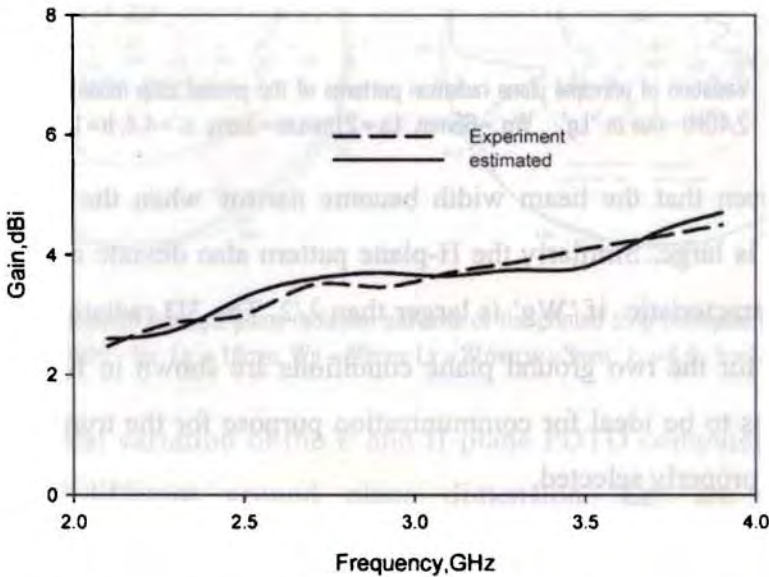


Fig. 4.18 Experimental and FDTD computed gain of the wide band printed strip monopole antenna

4.1.5 Inferences

The simulated surface current distribution of a typical monopole antenna above a finite ground plane is shown in Fig. 4-19. The length of the strip monopole is $\lambda_d/4$ and width f_w is 3mm. From the figure it is very clear that there is quarter wavelength variation of field along the strip.

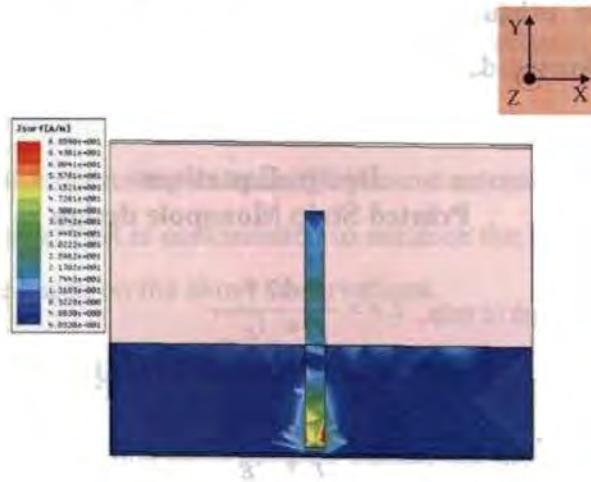


Fig. 4.19 Surface currents of strip monopole with $W_g=65\text{mm}$, $L_g=18\text{mm}$, $h=1.6\text{mm}$, $L_s=21\text{mm}$, $\epsilon_r = 4.38$ for 2.4GHz resonant frequency.

From the surface current distribution it can be inferred that the surface current at the tip of the monopole is minimum. Maximum surface current is observed near the feed point. The simulated current distributions confirm that antenna is resonant with quarter wavelength current variation along the strip. But there is no current variation on the finite ground plane at the resonant frequency. But it can be observed that at the edges along the width of the ground plane there is feeble current which varies with the dimensions of the ground plane.

This strip monopole is strongly radiating at the resonant frequency of 2.4GHz as seen from the current density plot. At the fundamental resonance, the electric field is vertically polarized along Y-direction. Feeble current along the

truncated edges of the ground plane are opposite in phase and cancel at the far field. There is little radiation from the ground plane at this frequency. This monopole with truncated ground plane exhibits similar radiation characteristics to a half wavelength dipole. The edge currents on the ground plane truncation can be effectively utilized to design microstrip fed printed dipoles.

From the exhaustive experimental, FDTD computations and simulation studies the following design equation are derived for an optimized printed strip monopole.

Design Equations Printed Strip Monopole design

$$\text{Length of strip, } L_s = \frac{0.42 * c}{f_r * \sqrt{\epsilon_{eff}}}$$

$$\text{Width of Gnd plane, } W_g = \frac{1.38 * c}{f_r * \sqrt{\epsilon_{ref}}}$$

$$\text{Length of Gnd plane, } L_g = \frac{0.36 * c}{f_r * \sqrt{\epsilon_{ref}}}$$

$$\text{Effective dielectric constant, } \epsilon_{eff} = \frac{\epsilon_r + 1}{2} (1 + 0.3 * h)$$

$$\text{Resonant frequency (GHz), } f_r = 3 + \frac{2}{\sqrt{\epsilon_{ref}}} \left[\frac{21}{L_s} + \frac{65}{W_g} + \frac{18}{L_g} - 3 \right]$$

The width of the monopole is set as width of 50Ω microstrip feed line. Since the field components are not confined to the substrate alone effective dielectric constant 'ε_{eff}' has to be used in calculation. Where 'c' is the velocity of electromagnetic wave in free space. The constants in the above equations are derived from exhaustive parametric analysis.

The above investigations conclude with the observations a) The ground plane dimensions of the feed line of a microstrip excited printed monopole plays a crucial role in the resonance and radiation characteristics of the printed monopole antenna. b) The ground plane truncation can be effectively utilized to control the impedance bandwidth of the antenna. c) The ground plane can be properly tailored to generate an additional resonance near the fundamental mode which can be effectively used to broaden the bandwidth of the printed strip monopole.

As in the case of a microstrip antenna the present antenna is offering very low band width. The next part is concentrated to enhance the bandwidth of this planar strip monopole based on the above observations.

Printed Wide Monopole Antennas.

From our earlier studies it is found that the bandwidth of a strip monopole is 21%. In order to widen the band width of printed monopole antenna, different geometries are tried as radiating elements and elaborately discussed in this section .

It is a well known concept that the bandwidth of wire antenna can be increased by increasing the diameter or thickness of the wire. This concept is tried here to enhance the bandwidth by increasing the size of the monopole by different sizes and geometries.

The direct loading of various simple geometries like Rectangular, Elliptical , Circular, Octagon , Hexagon were tried as printed monopole. It is theoretically predicted that all geometries upon loading will result in wide band antennas. Rectangular is found to be most simple for better parametric control, fabrication, testing and theoretical analysis and hence the investigation is started with rectangular shape. It is remarkable that, all designs are looking for a wider

matching impedance bandwidth without loss of omni-directional radiation pattern. Here the theoretical analysis is performed by 3D-FDTD method and the results are verified with experiments and simulations.

4.2 Wide Rectangular Strip Monopole.

4.2.1 Printed Antenna design parameters

The geometry of the wide rectangular strip monopole is shown in fig.(4-20). Here a rectangular patch of length 'Sl' and width 'Sw' is directly loaded on a strip at a distance 'd' from the ground plane. In this case the overall length of the antenna 'Sl+d' is same as the length of the earlier strip monopole antenna. There is a small gap 'd' is introduced to achieve matching.

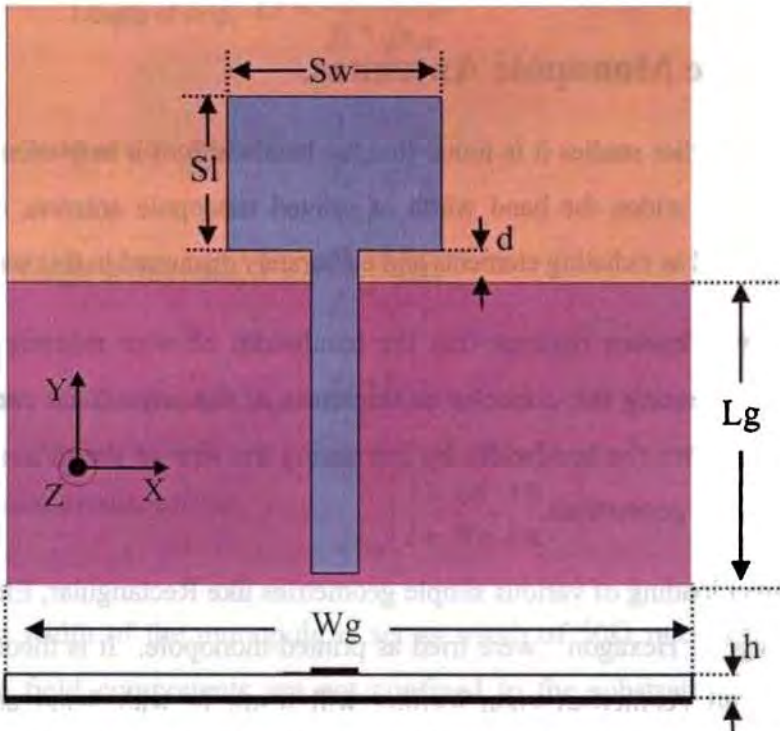


Fig.4.20 Geometry of Wide Rectangular strip monopole with truncated ground width ' W_g '=45mm, Length ' L_g '=20mm, gap ' d '=3mm, patch width ' S_w '=14mm, patch width ' S_l '=10mm Substrate height h =1.6mm, substrate ϵ_r =4.38

4.2.2 Return Loss Characteristics

Variation of return loss of a typical wide rectangular strip monopole is shown in fig.(4-21) along with the strip monopole antenna of same length of a rectangular strip monopole shown in fig.(4-20). Fig.(4-21) shows that the strip monopole with $L_s=13\text{mm}$ is resonating at 3.2GHz with a bandwidth of 500MHz which is approximately 21%. The same antenna with wide rectangular patch of equivalent strip length of $L_s=13\text{mm}$ has mean frequency of 4.5GHz with band width of 6GHz. This shows that it is an ideal method to enhance the bandwidth of strip monopole by widening the strip.

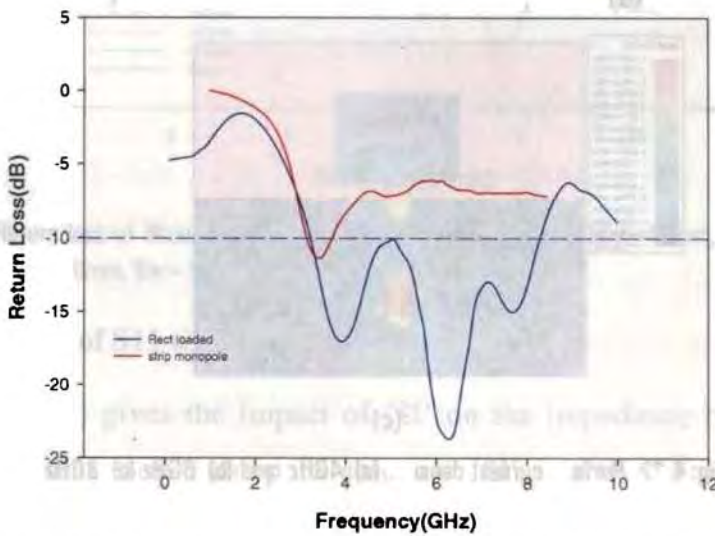


Fig. 4-21 Return loss of strip monopole $L_s=13\text{mm}$ for 3.2GHz and Wide Rectangular strip monopole with gap ' d ' = 3mm, ' W_g ' = 45mm, ' L_g ' = 20mm, ' sl ' = 10mm, $Sw = 14\text{mm}$, $h=1.6\text{mm}$, $\epsilon_r = 4.38$

From the resonance curve it can be seen that the antenna is resonating at three frequencies. The lower frequency is due to the total length (L_g+Sl+d), mid frequency due to ($Sl+d$) and the higher frequency is due to the (Sl). A current density plot of the proposed antenna at frequency band of operation is

illustrated in fig. (4-22a,b,c). It is seen from the plotted results that the respective resonant lengths corresponds to 4, 6 and 8GHz bands.

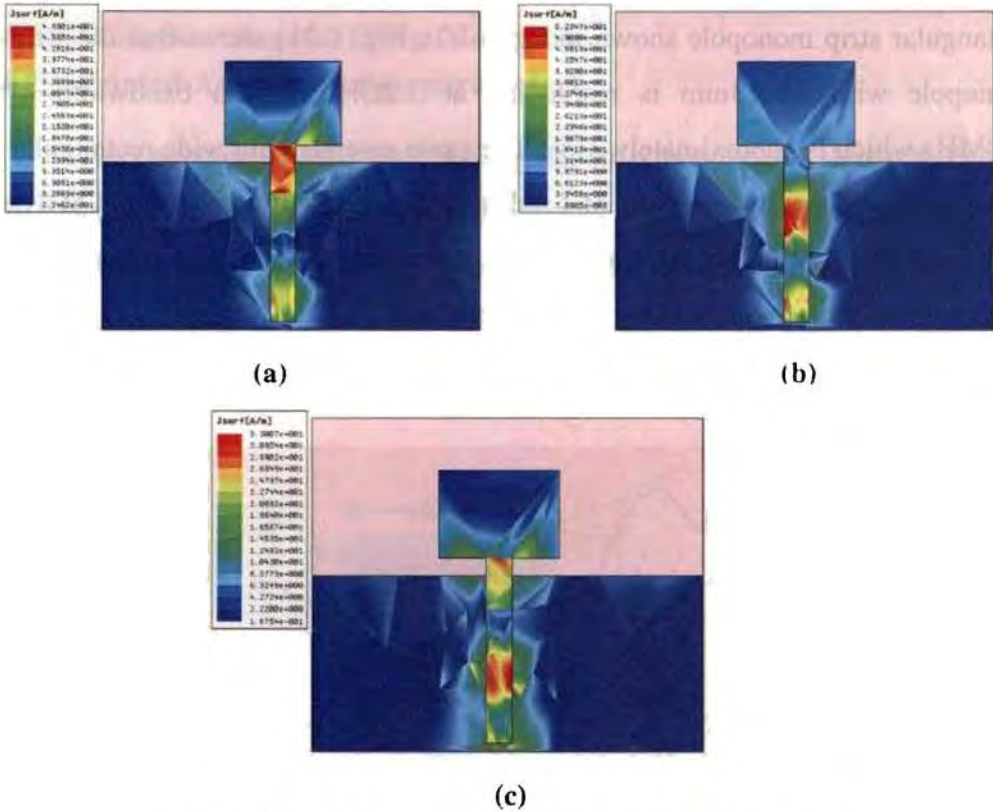


Fig. 4.22 Surface current density (a) 4GHz and (b) 6GHz (c) 8GHz

4.2.3 Parametric Analysis

(a) Variation of S11 with 'd'

Fig. (4-23) gives the impact of 'd' on the impedance bandwidth. This is one of the main parameter controlling the impedance matching between the feed, truncated ground and radiating patch. The gap 'd' between the edge of the truncated ground and the rectangular strip, therefore decides the impedance bandwidth. This is the fundamental parameter for widening the bandwidth. It is evident from the following figure that the optimal value of

'd' for maximum bandwidth is 3mm. The bandwidth is from 3GHz to 8.4GHz.

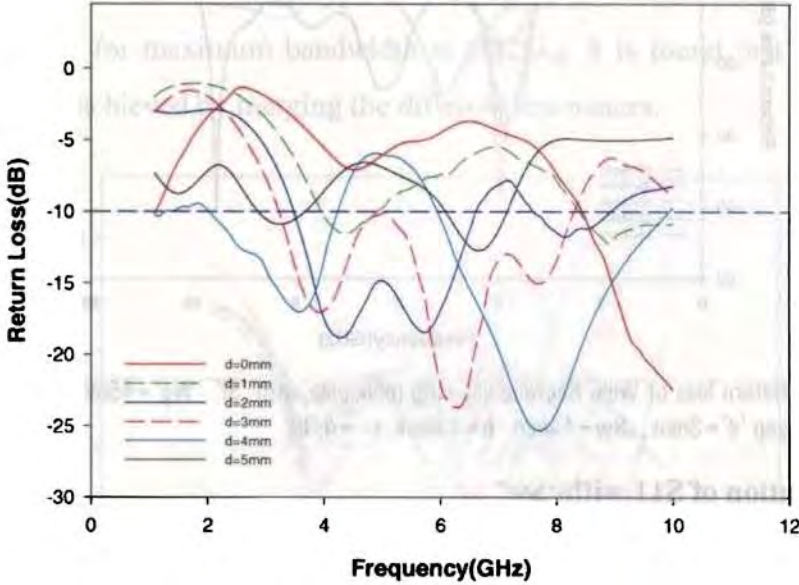


Fig.4.23 Return loss of Wide Rectangular strip monopole with 'd' , 'Wg' =45mm, 'Lg' =20mm, 'Sl' = 10mm, Sw = 14mm, h = 1.6mm, $\epsilon_r = 4.38$.

(b) Variation of S11 with 'Sl'

Fig. (4-24) gives the impact of 'Sl' on the impedance bandwidth of wide rectangular strip monopole antenna. 'Sl' is varied from 10mm to 19mm keeping all other parameters kept constant. It is evident from figure that the optimal value of 'Sl' for maximum bandwidth is $0.33\lambda_d$. Since the optimum value of 'Sl' is chosen as $0.33\lambda_d$, the antenna is fabricated and tested experimentally. These results are compared with FDTD analysis for the following results in fig.(4-24).

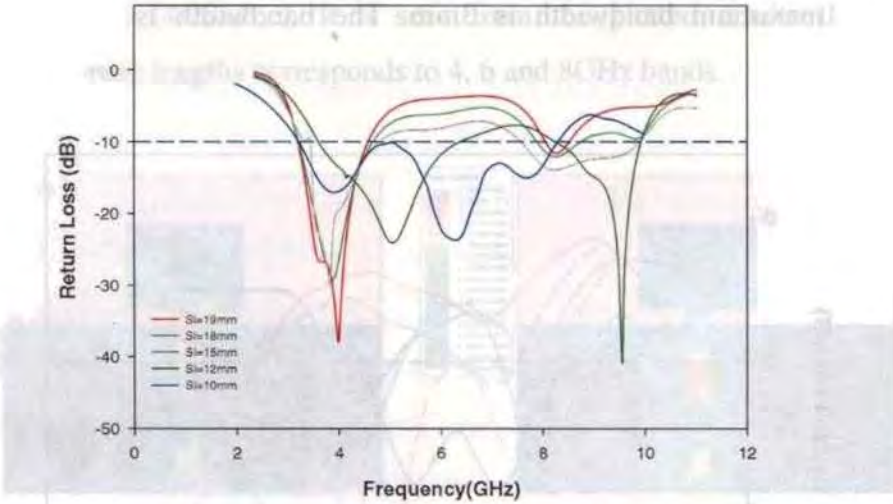


Fig.4.24 Return loss of Wide Rectangular strip monopole with 'Sl' 'Wg' =45mm, Lg =20mm, gap 'd'=3mm , Sw=14mm h=1.6mm, $\epsilon_r = 4.38$

(c) Variation of S11 with 'Sw'

Keeping 'Sl' as optimized dimension ($0.33\lambda_d$), the 'Sw' is varied for further optimization. The fig.(4-25) shows the variation of return loss. From the above variations, the rectangular geometry with Sw=14mm ($0.46\lambda_d$), giving good impedance performance is selected.

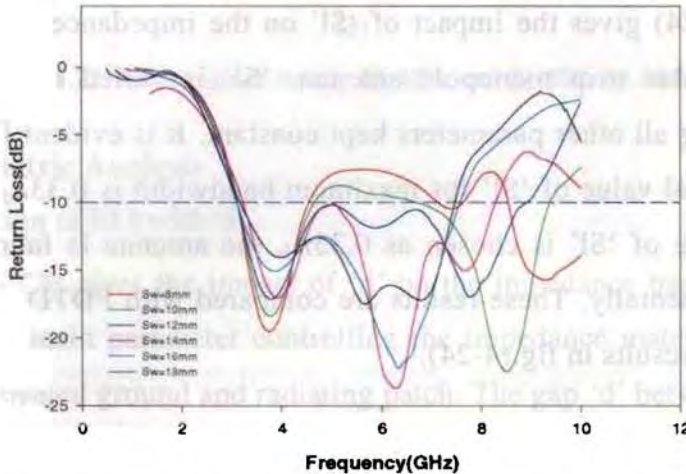


Fig.(4-25) Return loss of Wide Rectangular strip monopole with 'Sw' 'Wg' =45mm, Lg =20mm, gap 'd'=3mm , 'sl'=10mm, h=1.6mm, $\epsilon_r = 4.38$

(d) Variation of S11 with 'Lg'

Fig. (4-26) gives the impact of truncated ground dimension 'Lg' on the impedance bandwidth for this type of loading. It is evident that the optimal value of 'Lg' for maximum bandwidth is $0.625\lambda_d$. It is found that maximum bandwidth is achieved by merging the different resonances.

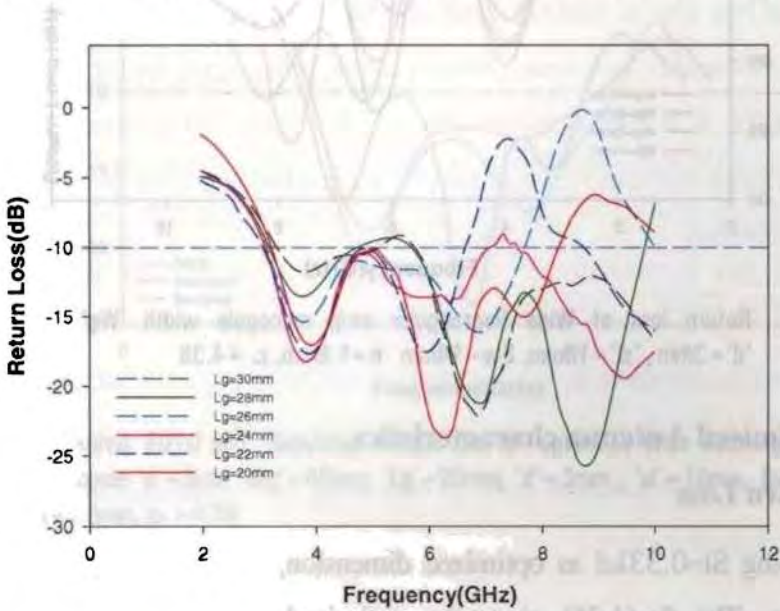


Fig.4.26 Return loss of Wide Rectangular strip monopole with 'Lg' 'Wg'=45mm, gap'd' = 3mm, 'sl' = 10mm, Sw = 14mm, h = 1.6mm, $\epsilon_r = 4.38$

(e) Variation of S11 with 'Wg'

Fig. (4-27) gives the impact of truncated ground dimension 'Wg' on the impedance bandwidth wide strip monopole antenna. It is evident that the optimal value of 'Wg' = $1.4\lambda_d$ for maximum bandwidth for the already optimized $Lg = 0.625\lambda_d$ at the mean resonant frequency. Since the optimum value of 'Wg' is chosen as $1.4\lambda_d$ for further optimizations.

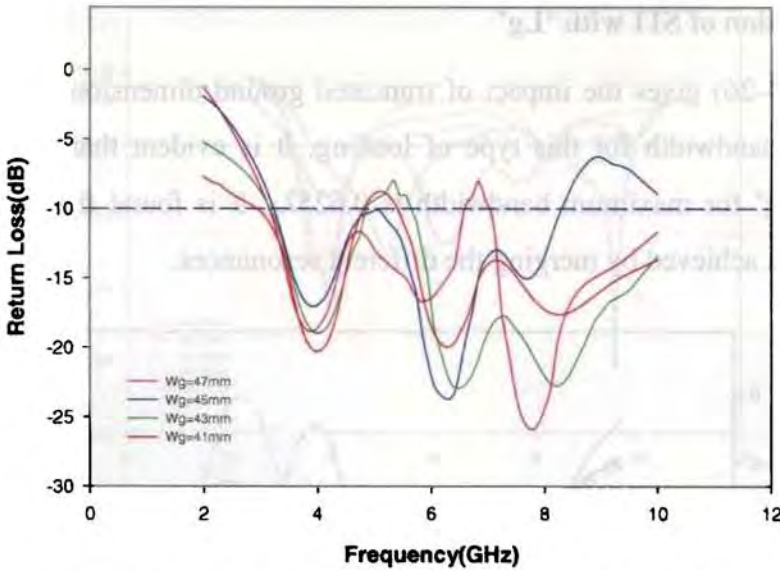


Fig.4.27 Return loss of Wide Rectangular strip monopole width 'Wg', 'Lg'=20mm, 'd'=3mm, 'sl'=10mm, Sw=14mm h=1.6mm, $\epsilon_r = 4.38$

4.2.4 Optimised Antenna characteristics

(a) Return Loss

Keeping $Sl=0.33\lambda_d$ as optimized dimension, the 'Sw' is varied for further optimization. The fig.(4-25) gives the optimized 'Sw'=14mm on impedance bandwidth. Similarly the truncated ground dimension is also optimized as $Wg=1.4\lambda_d$ and $Lg=0.625\lambda_d$.

For the theoretical analysis the antenna is modeled using FDTD algorithm. Total computational domain used for the analysis of the antenna is $120 \times 100 \times 24$ cells. Δx , Δy , Δz in the computation domain are taken as 0.5mm. 10 cells are assigned for ABC at each side of the problem space. A Gaussian pulse with pulse half width $T=15ps$ and time delay $t_0=3T$ is selected for the present analysis. According to the stability criteria the calculated time step is $\Delta t=0.95ps$. Leubbers feed model is employed to implement the feed. The electric field component is settled at around 5000 time steps. This return loss variation with frequency for

FDTD, experimental and Simulation in fig.(4-28) and compared for good agreement on results.

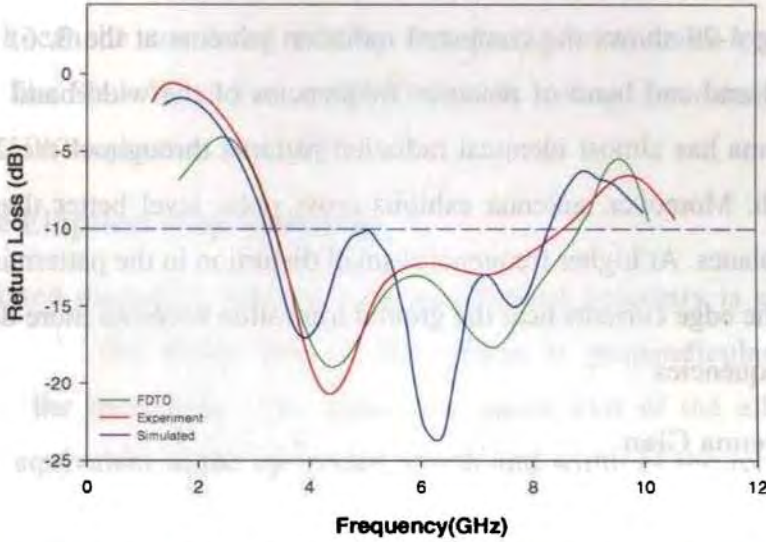


Fig.4.28 Measured, FDTD and Simulated Return loss of optimized Wide Rectangular strip monopole 'd'=3mm 'Wg'=45mm, 'Lg'=20mm, 'd'=3mm, 'sl'=10mm, Sw=14mm h=1.6mm, $\epsilon_r = 4.38$

(b) Radiation Pattern

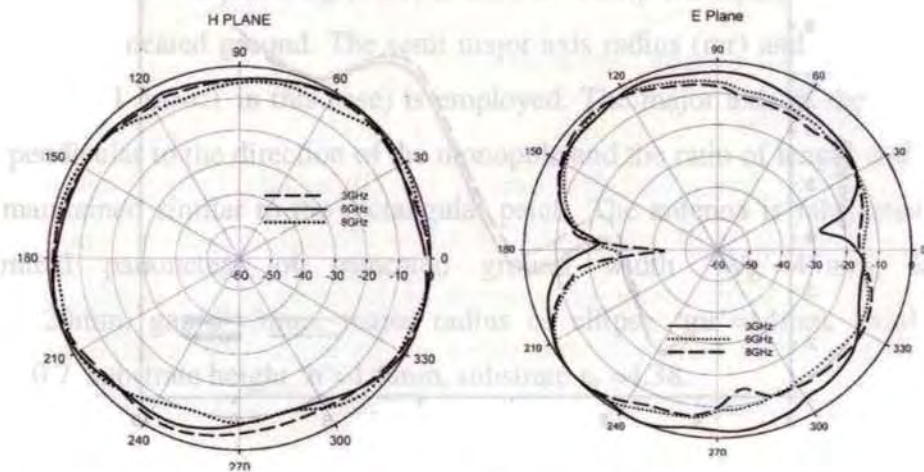


Fig. 4.29 H and E plane radiation pattern at 3, 6 and 8GHz, 'd'=3mm 'Wg'=45mm, 'Lg'=20mm, 'd'=3mm, 'sl'=10mm, Sw=14mm h=1.6mm, $\epsilon_r = 4.38$

The inference obtained from the above discussion concluded that the radiation pattern of a wide band printed strip monopole over a truncated ground plane is nearly omni directional in one plane and figure of eight in the other plane. Fig 4-29 shows the computed radiation patterns at the 3, 6, 8 GHz for start, mid and end band of resonant frequencies of the wide band monopole. The antenna has almost identical radiation patterns throughout the 2:1 VSWR bandwidth. Moreover, antenna exhibits cross polar level better than 20dB in both the planes. At higher frequencies small distortion in the pattern is observed because the edge currents near the ground truncation becomes more dominant at higher frequencies

(c) Antenna Gain

Gain of the antenna computed and measured using gain transfer method is shown in Fig 4.30. Antenna exhibits an peak gain of 7.5dBi in the operating band. At higher frequencies gain is increased considerably due to the slight directional characteristics.

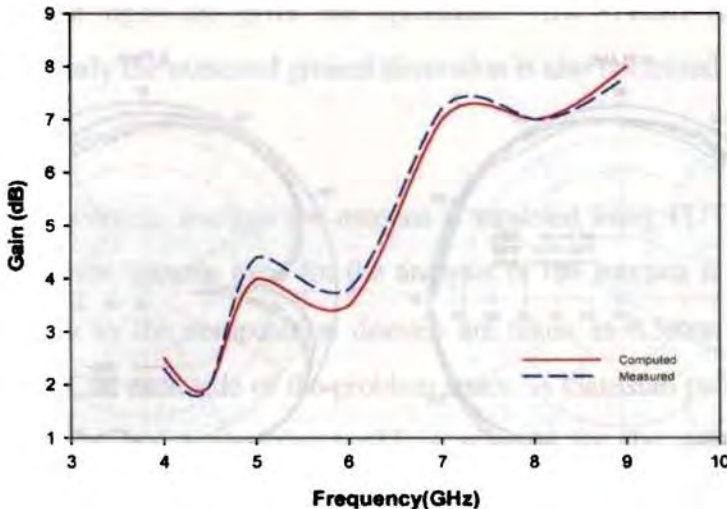


Fig.4.30 Gain of the optimized Wide Rectangular strip monopole

The optimization is carried out for all the controlling parameters studied above. This gives a performance near to the UWB and best suited for further fine tuning as seen from the above parametric analysis, gain and radiation patterns. It can be concluded that by introducing some more controlling parameters like Slow Wave Factor (SWF) there is a scope for extending this antenna for UWB operation (3-11 GHz).

4.3 Wide Elliptical strip monopole

A printed monopole antenna with an elliptical geometry is shown in fig.(4-31). Here the major axis of the ellipse is perpendicular to the direction of the monopole. The major and minor axis of the ellipse are selected as equivalent to the optimized length and width of the rectangular patch under study in 4.2.1. The performance of this loaded monopole antenna is studied in this section and compared with the optimum rectangular loaded strip.

4.3.1 Printed Antenna design parameters

An Elliptical patch fig.(4-31) is used as a strip monopole at a gap of 'd' from the truncated ground. The semi major axis radius (mr) and axial ratio(ar) more than 1 ($ar < 1$ in this case) is employed. The major axis of the ellipse is perpendicular to the direction of the monopole and the ratio of length and width is maintained similar to the rectangular patch. The antenna is fabricated with nominal parameters of truncated ground width 'Wg'=45mm, length 'Lg'=20mm, gap 'd'=3mm, major radius of ellipse 'mr'=14mm, axial ratio 'ar'=0.7, substrate height 'h'=1.6mm, substrate $\epsilon_r = 4.38$.

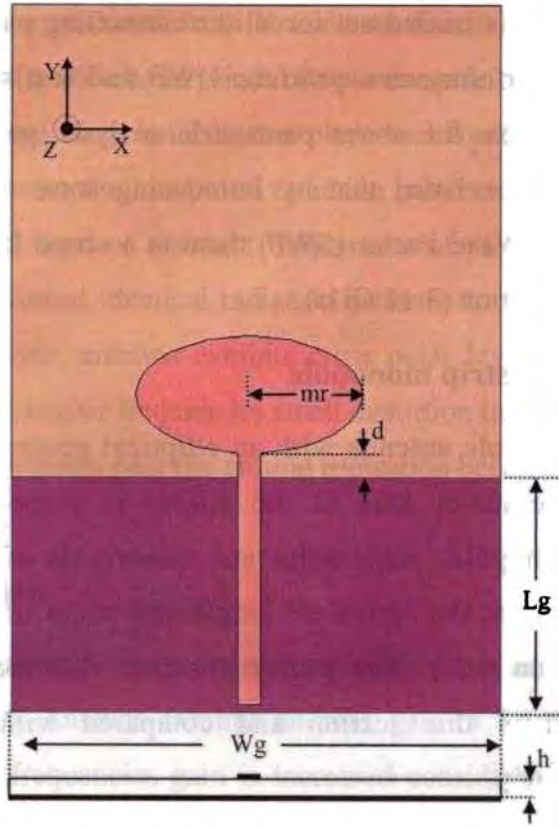


Fig. 4.31 Geometry of wide elliptical strip monopole ' $W_g=45\text{mm}$, ' $L_g=20\text{mm}$, gap ' $d=1\text{mm}$, major radius of ellipse ' $mr=14\text{mm}$, axial ratio ' $ar=0.7$, $h=1.6\text{mm}$, $\epsilon_r=4.38$

4.3.2 Optimised Antenna characteristics

(a) Return Loss

The return loss characteristics of an elliptically loaded antenna is compared with a strip monopole of same overall length as shown in fig.(4-16). The strip monopole antenna is resonating at 3.2GHz with a bandwidth of 21%. But when the shape of the monopole is altered as an ellipse, it is resonating at two resonant frequencies at 3.5 and 5.8GHz with a total bandwidth of 4GHz and 80%.

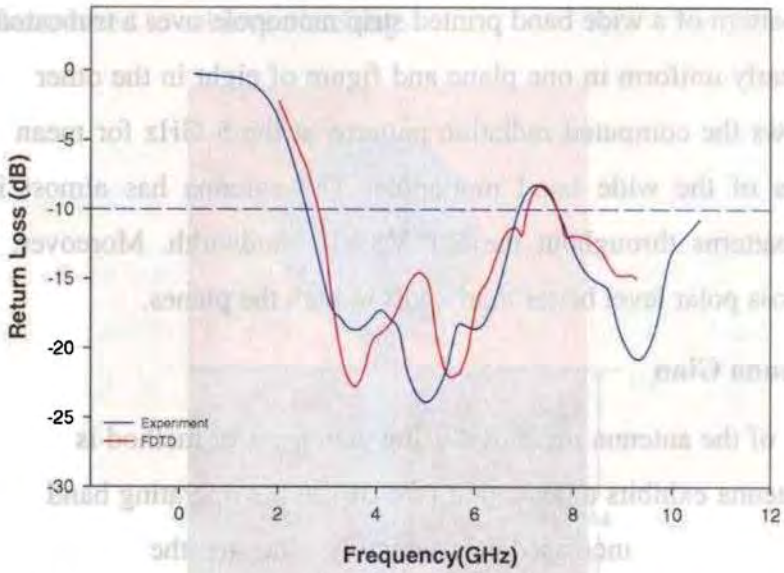


Fig. 4.32 Computed and measured Return loss of Printed monopole loaded with elliptical patch 'Lg' = 20mm, 'Wg' = 45mm, 'mr' = 14mm, 'ar' = 0.7, h = 1.6mm, $\epsilon_r = 4.38$.

(b) Radiation Pattern

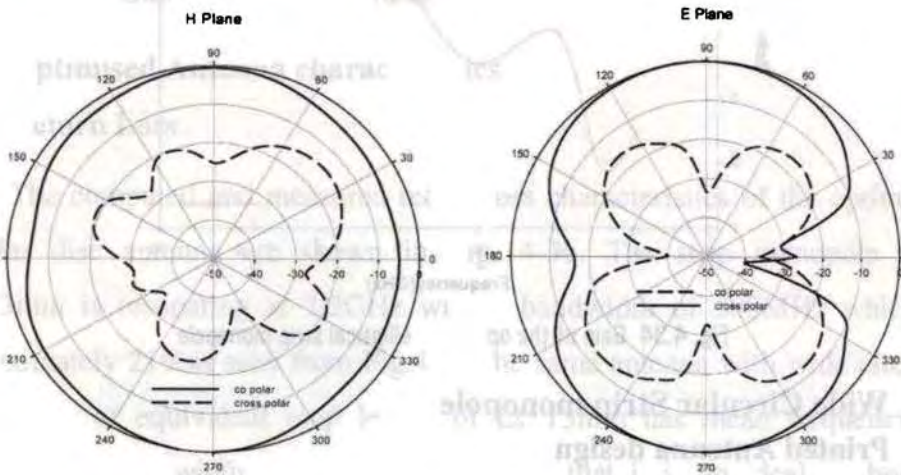


Fig. 4.33 H and E plane radiation pattern of the above antenna at 5GHz

The inference obtained from the above discussion concluded that the radiation pattern of a wide band printed strip monopole over a truncated ground plane is nearly uniform in one plane and figure of eight in the other plane. Fig (4-33) shows the computed radiation patterns at the 5 GHz for mean resonant frequencies of the wide band monopole. The antenna has almost identical radiation patterns throughout the 2:1 VSWR bandwidth. Moreover, antenna exhibits cross polar level better than 20dB in both the planes.

(c) Antenna Gain

Gain of the antenna measured using gain transfer method is shown in Fig (4-34). Antenna exhibits a peak gain of 6 dBi in the operating band. At higher frequencies gain is increased considerably due to the slight directional characteristics.

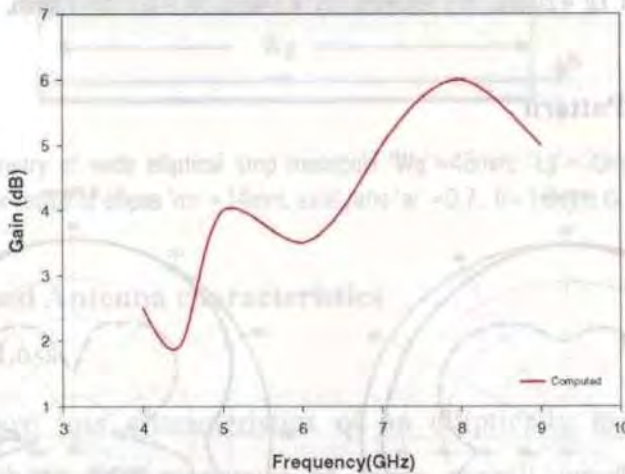


Fig. 4.34 Gain of the optimized elliptical strip monopole

4.4 Wide Circular Strip monopole

4.4.1 Printed Antenna design parameters

The geometry of the wide circular strip monopole is shown in fig.(4-35). Here the monopole is a circular disc of radius ' r ' on a strip at a distance ' d ' from the ground plane. In this case the over all length of the antenna ($2r+d$) is

equivalent to the length of the earlier strip monopole antenna. There is a small gap d is introduced to achieve matching.

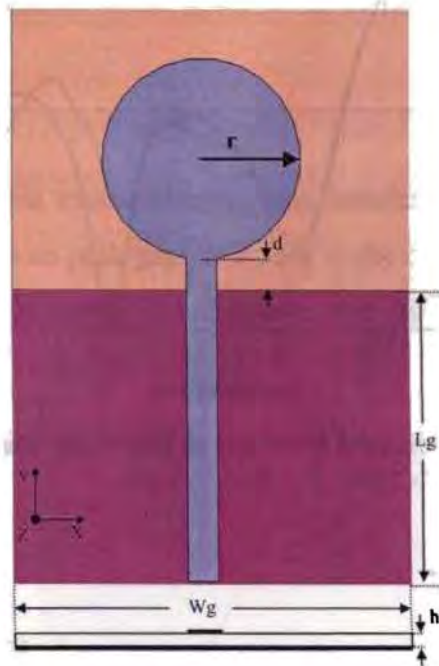


Fig.4.35 Geometry of Wide circular strip monopole loaded ' W_g '=45mm, ' L_g '=20mm, gap ' d '=3mm, radius of disc ' r '=10mm, h =1.6mm, ϵ_r =4.38

4.4.2 Optimised Antenna characteristics

(a) Return Loss

The computed and measured return loss characteristics of the optimized circular disc antenna are shown in Fig, 4-36. The strip monopole with $L_s=13\text{mm}$ is resonating at 3.2GHz with a bandwidth of 500MHz which is approximately 21% as seen from Fig.4-3. The same antenna with wide circular monopole of equivalent strip length of $L_s=13\text{mm}$ has mean frequency of 5GHz with band width of 6GHz. This shows that it is an ideal method to enhance the bandwidth of strip monopole by widening the strip.

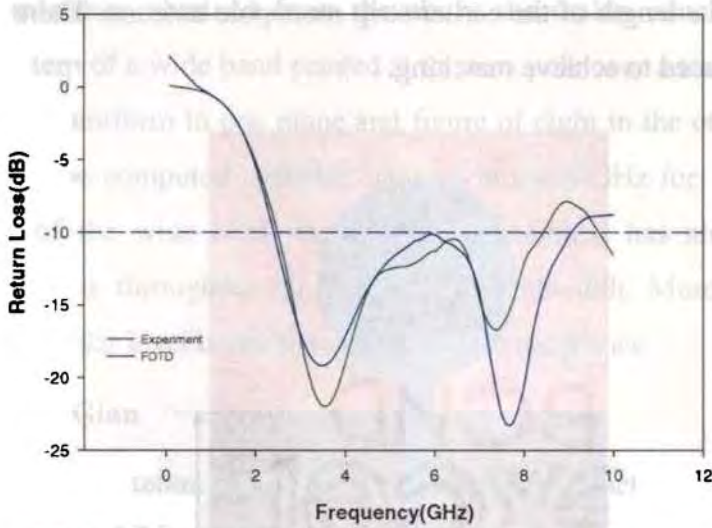


Fig.4.36 Computed and measured Return loss of Wide circular strip monopole ' L_g ' = 20mm, ' W_g ' = 45mm, ' r ' = 10mm, h = 1.6mm, ϵ_r = 4.38

(b) Radiation Pattern

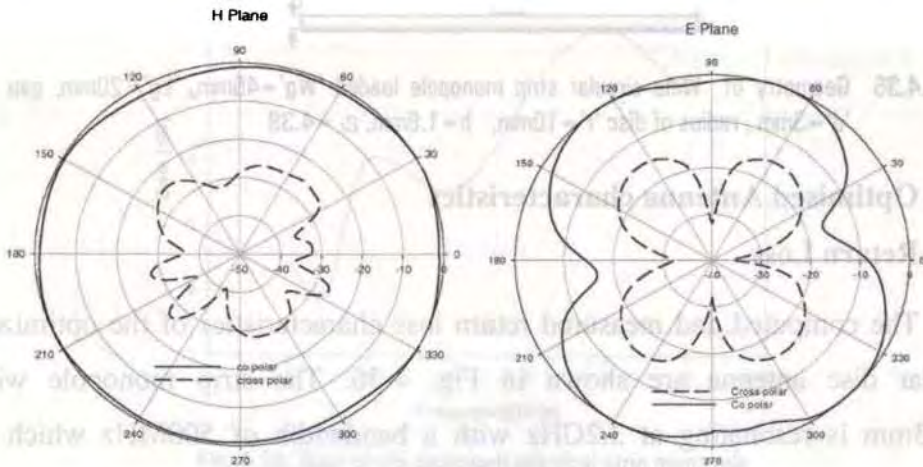


Fig. 4.37 H and E plane radiation pattern of the above antenna at 6 GHz

The inference obtained from the above radiation patterns concluded that the radiation pattern of a wide band printed strip monopole over a truncated ground plane is nearly uniform in one plane and figure of eight in the other plane. Fig 4.37 shows the computed radiation patterns at the 6GHz

for mean resonant frequency of the wide band monopole. The antenna has almost identical radiation patterns throughout the 2:1 VSWR bandwidth. Moreover, antenna exhibits cross polar level better than 20dB in both the planes.

(c) Antenna Gain

Gain of the antenna measured using gain transfer method is shown in fig. (4.38). Antenna exhibits an peak gain of 7.5dBi in the operating band. At higher frequencies gain is increased considerably due to the slight directional characteristics.

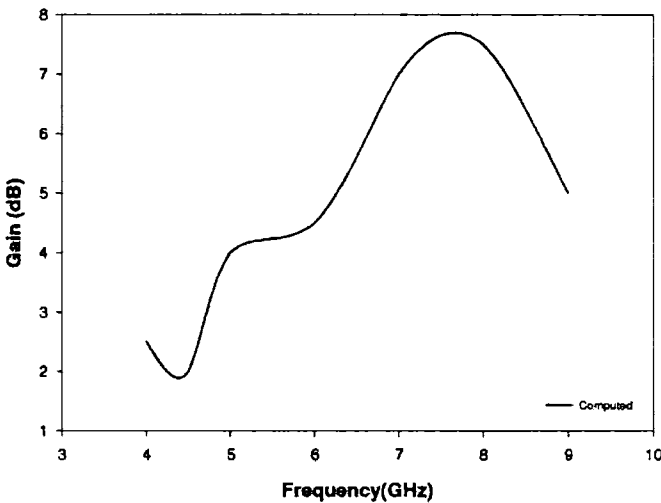


Fig.4.38 Gain of the optimized circular strip monopole

The optimization is carried out for all the controlling parameters studied above. It can be seen that the sizes of the circular disc affect the operating frequency. The operating frequency decreases with the 'r', which is similar to a dipole, of course the bandwidth is not wide enough to cover the entire UWB region.

4.5 Wide Octagonal Strip Monopole

4.5.1 Printed Antenna design parameters

The geometry of the wide Octagonal strip monopole is shown in fig. (4-33). Here the monopole is a Octagon of side 'a' on a strip at a distance 'd' from the ground plane. In this case the overall length of the antenna ($2.4a+d$) is equivalent to the length of the earlier strip monopole antenna. There is a small gap 'd' is introduced to achieve impedance matching. Fig.(4-28) shows the optimized reflection characteristics of the antenna. This shows clearly that the BW can also be increased by this method.

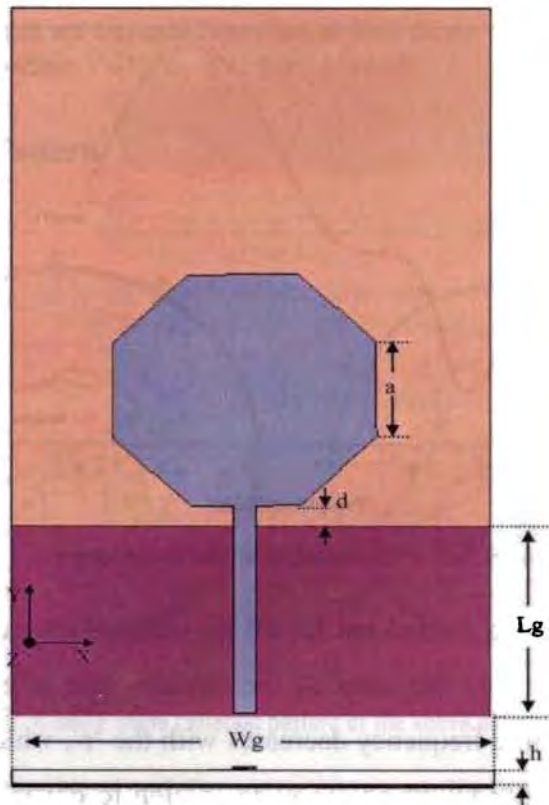


Fig.4.39. Geometry of Wide Octagon strip monopole ' $Wg=45\text{mm}$, Length ' $Lg=20\text{mm}$, gap ' $d=3\text{mm}$, side length ' $a=9\text{mm}$, $h=1.6\text{mm}$, $\epsilon_r=4.38$

4.5.2 Optimised Antenna characteristics

(a) Return Loss

The strip monopole with $L_s=13\text{mm}$ is resonating at 3.2GHz with a bandwidth of 500MHz which is approximately 21% as seen from Fig.(4-3). The same antenna with wide Octagonal monopole of equivalent strip length of $L_s=13\text{mm}$ has mean frequency of 4GHz with band width of 3.5GHz which is approximately 90% . Fig.(4-40) shows that it is also a method to enhance the bandwidth of strip monopole by widening the strip.

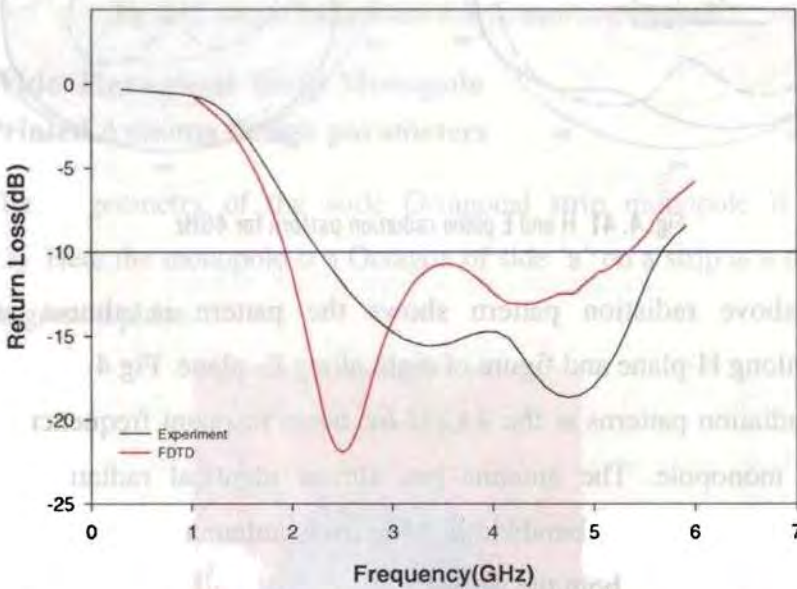


Fig.4.40 Computed and measured Return loss of Wide Octagon strip monopole ' $L_g=20\text{mm}$, ' $W_g=45\text{mm}$, ' $a=10\text{mm}$, $h=1.6\text{mm}$, $\epsilon_r=4.38$

The optimization is carried out for all the controlling parameters studied above. It can be seen that the sizes of the Octagon strip affect the operating frequency. The low operating frequencies decrease regularly with the increasing of ' a ', which is similar to a dipole.

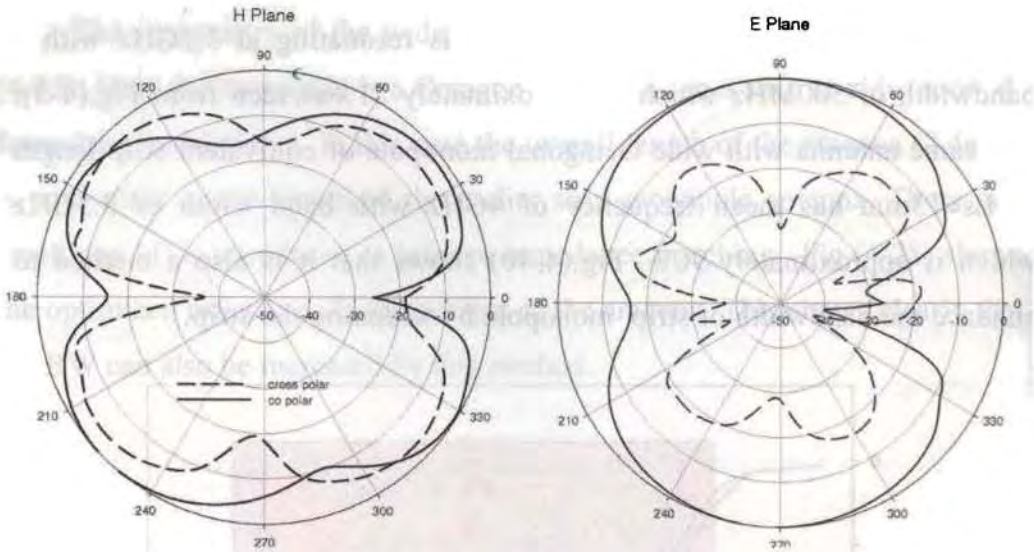
(b) Radiation Pattern

Fig. 4. 41 H and E plane radiation pattern for 4GHz

The above radiation pattern shows the pattern is almost uniform directional along H-plane and figure of eight along E- plane. Fig 4-41 shows the measured radiation patterns at the 4 GHz for mean resonant frequencies of the wide band monopole. The antenna has almost identical radiation patterns throughout the 2:1 VSWR bandwidth. Moreover, antenna exhibits cross polar level better than 15dB in both the planes.

(c) Antenna Gain

Gain of the antenna measured using gain transfer method is shown in Fig 4.42. Antenna exhibits a peak gain of 5.5dBi in the operating band. At higher frequencies gain is increased considerably due to the slight directional characteristics.

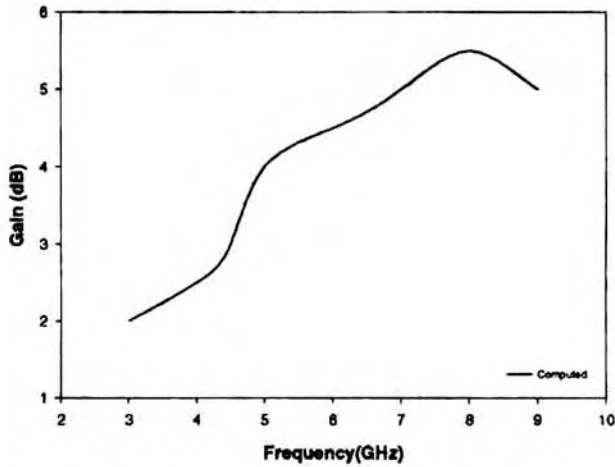


Fig. 4.42 Gain of the optimized Wide Octagon strip monopole

4.6 Wide Hexagonal Strip Monopole

4.6.1 Printed Antenna design parameters

The geometry of the wide Octagonal strip monopole is shown in fig.(4-33). Here the monopole is a Octagon of side 'a' on a strip at a distance 'd' from the ground plane.

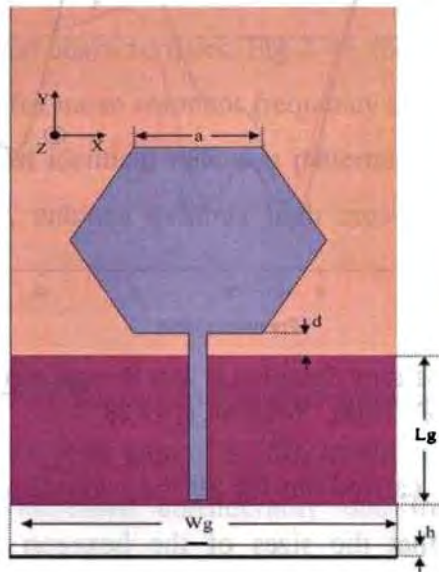


Fig.4.43 Geometry of wide Hexagon strip monopole ' W_g '=45mm, ' L_g '=20mm, gap ' d '=1mm, side length ' a '=10mm, h =1.6mm, ϵ_r =4.38

In this case the overall length of the antenna ($1.7a+d$) is equivalent to the length of the earlier strip monopole antenna. There is a small gap d is introduced to achieve matching. Fig.(4-28) shows the optimized reflection characteristics of the antenna. This shows clearly that the BW can also be increased by this method.

4.6.2 Optimised Antenna characteristics

(a) Return Loss

The strip monopole with $L_s=13\text{mm}$ is resonating at 3.2GHz with a bandwidth of 500MHz which is approximately 21% as seen from Fig.4-3. The same antenna with wide Hexagonal monopole of equivalent strip length of $L_s=13\text{mm}$ has mean frequency of 4.5GHz with band width of 4GHz which is approximately 85%. This shows that it can also enhance the bandwidth of strip monopole by widening the strip.

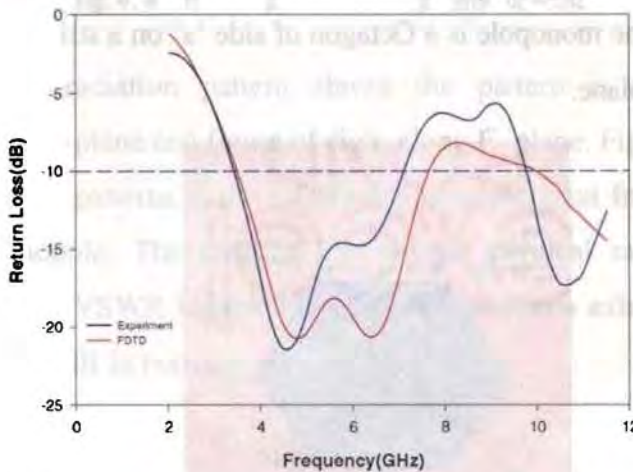


Fig. 4-44 Computed and measured Return loss of Wide Hexagon strip monopole ' $L_g = 20\text{mm}$, ' $W_g = 45\text{mm}$, ' $a = 10\text{mm}$, $h = 1.6\text{mm}$, $\epsilon_r = 4.38$

The optimization is carried out for all the controlling parameters studied above. It can be seen that the sizes of the hexagon affect the operating frequency. The low operating frequencies decrease regularly with the increasing of ' a ', which is similar to a dipole. However, the optimised hexagonal strip

antenna offered a band width of 3.8 GHz with a 85% band width of average frequency of band at 4.5 GHz.

(b) Radiation Pattern

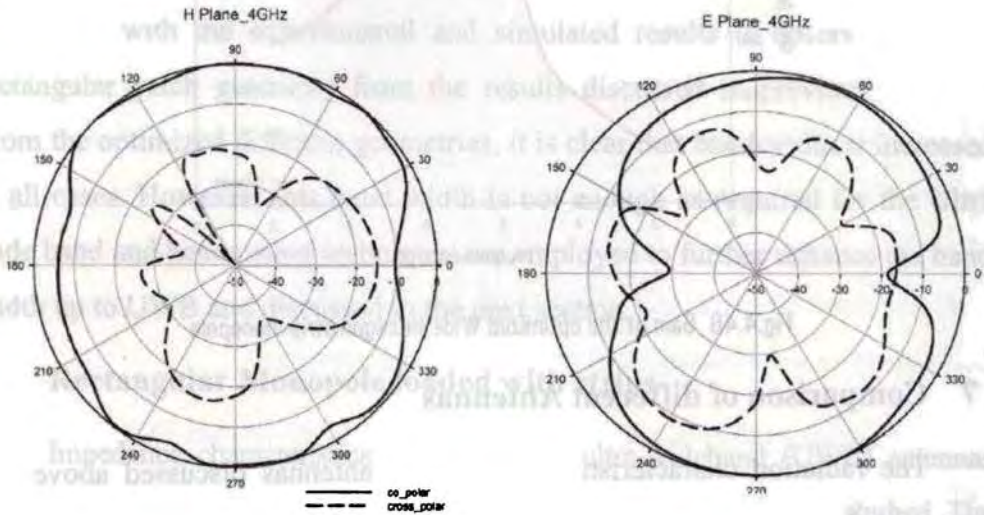


Fig. 4-45 H and E plane radiation pattern for 4 GHz

The above radiation pattern shows the pattern is slightly away from desired omni directional characteristics. Fig 4-45 shows the measured radiation patterns at the 4 GHz for mean resonant frequency of the wide band monopole. The antenna has almost identical radiation patterns throughout the 2:1 VSWR bandwidth. Moreover, antenna exhibits high cross polar level which is not encouraging.

(c) Antenna Gain

Gain of the antenna measured using gain transfer method is shown in Fig 4.46. Antenna exhibits a peak gain of 5.5dBi in the operating band. At higher frequencies gain is increased considerably due to the slight directional characteristics.

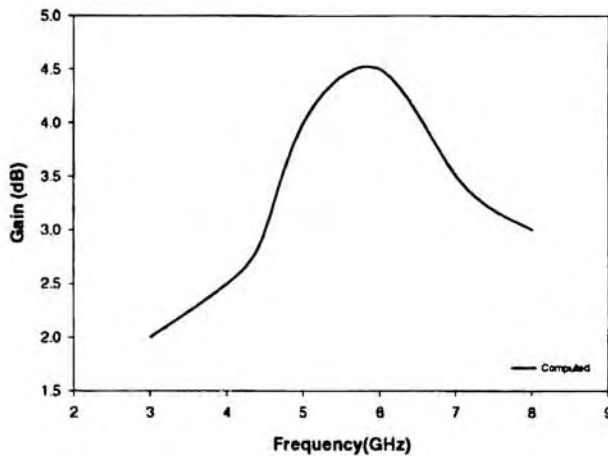


Fig.4.46 Gain of the optimized Wide Hexagon strip monopole

4.7 Comparison of different Antennas

The radiation characteristics of different antennas discussed above are summarized in Table (4-1).

Table (4-1)

No	Antenna Type	BW (GHz)	Bw %	Gain (dB)	Efficiency %	Cross polarisation	HPBW H-Plane	HPBW E-Plane
1	Rectangular	6	130	7.8	87	27dB	360°	90°
2	Elliptical	4.1	80	6	84	22dB	360°	85°
3	Circular	5.8	120	7.5	88	25dB	360°	90°
4	Octagonal	3.5	90	5.4	81	18dB	340°	80°
5	Hexagonal	3.9	85	5	79	15dB	330°	80°

In the above section we already conducted studies on different types of geometries for radiation characteristics. The comparison of the same is done and gist of the salient features is given in Table (4-1). Impedance bandwidth, % bandwidth, Gain, Efficiency, cross polarization, half power beam width are compared and it is found that Rectangular is most suitable and also for better

parametric control, fabrication , testing, simple structure and theoretical analysis. It is remarkable that, all designs are looking for a wider matching impedance bandwidth without loss of omni-directional radiation pattern. Here the theoretical analysis is carried out by 3D-FDTD method and the good agreement with the experimental and simulated results is observed for the rectangular patch geometry from the results discussed in previous sections. From the optimized different geometries, it is clear that band width is increased in all cases. However, this band width is not enough as required for the Ultra wide band and hence other techniques are employed to further enhance the band width up to UWB and discussed in the next section.

4.8 Rectangular Monopole loaded with strips

Impedance characteristics of a group of ultra-wideband (UWB) antennas with different geometries are theoretically (FDTD) and experimentally studied. The validity is again confirmed with simulation studies using Ansoft-HFSS. The details of the simulation and experiment results are presented and discussed. For the sake of analysis, here we divide the UWB frequency into three “sub” bands. They are (a) lower UWB Band covering frequencies between 3 and 5 GHz, (b) mid UWB Band covering frequencies between 5 and 8 GHz and (c) upper UWB Band covering frequencies between 8 and 11 GHz. Ideally, the impedance bandwidth at these three bands should have a return loss of less than -10 dB.

The printed wide rectangular patch monopole is analyzed and optimized in the previous section offers good radiation characteristics for a wide band of frequencies. In pursuit of stringent impedance and radiation requirements in Ultra Wide band antennas, different geometries are analyzed using FDTD analysis for enhancing the bandwidth up to the extent of covering the entire Ultra Wide Band (3.1GHz-10.6GHz).

This investigations leading to a compact printed monopole with strips on the patch [1] having Slots on ground plane is presented in this chapter. This procedure is successfully applied to reduce the dimensions of Rectangular patch antenna using the discontinuities such as Defected Ground Structure (DGS) and Defected Microstrip Structure (DMS) [1-3]. Since it has more discontinuities providing larger targets for EM wave, the net result in area reduction can be as high as 50% in certain cases. The DGS is realized by etching slots in the truncated ground plane of the printed monopole. The slot perturbs the field distribution in the ground plane. This give rise to the effective increase in the series capacitance and inductance of transmission line for an increased effective length and lower resonant frequency. This property of DGS is effective for miniaturization of printed planar antennas.

Rectangular patch top loaded monopole antenna is first optimized for UWB by adding strips to radiating patch and then by incorporating two symmetric slots on the ground plane. Combination of slot on the ground and strips on the monopole is presented as combo model, which is the final outcome of this thesis. The effect of various controlling parameters on the impedance bandwidth of the antenna is studied extensively for optimizing the geometry.

4.8.1 Printed Antenna design parameters

(a) Rectangular monopole with one strip

A single strip of length 'L1' and width 'W1' is added at the bottom of the patch on one side of the rectangular ($g_1=0\text{mm}$) as shown in fig (4-47). The idea here is to produce additional resonance at higher frequency due to the resonance of this simple strip. So the length of the strip is selected as for the first resonance is nearly at about 9 GHz where the main rectangular strip is not resonating. When a strip is added at one end of the patch it is found that there is a tendency of resonance at higher frequency. This aspect is demonstrated in fig. (4-48).

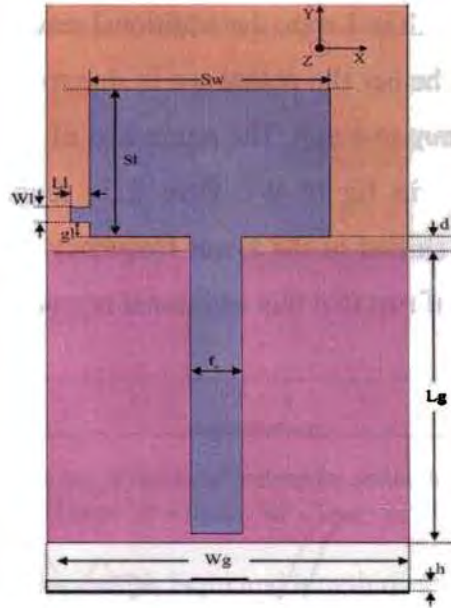


Fig.4.47 Geometry of Printed Rectangle monopole with one left strip, substrate of height $h=1.6\text{mm}$, dielectric constant $(\epsilon_r) = 4.38$. Truncated ground length ' L_g ', width ' W_g ', Feed gap ' d ', feed width ' f_w ', rectangular patch length ' S_l ', width ' S_w ', Left strip length ' L_l ', width ' W_l ', gap of strip from lower edge of patch -left ' g_l '

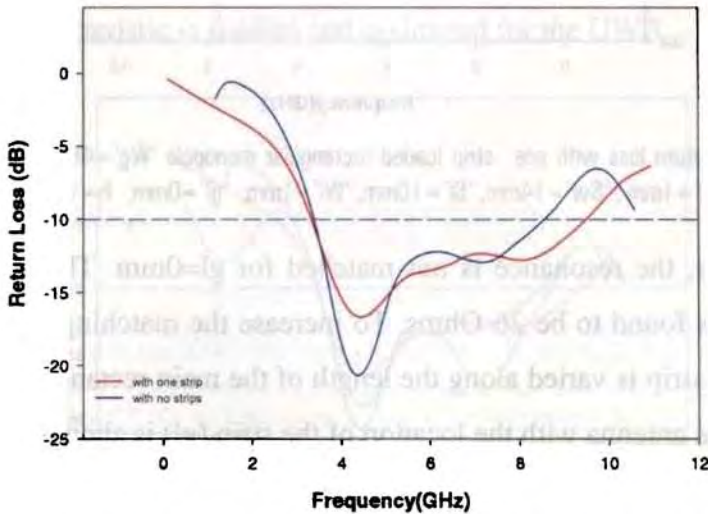


Fig.4.48 Return loss with and without strip loaded rectangular monopole ' $W_g=45\text{mm}$ ', ' $L_g=20\text{mm}$ ', ' $d=1\text{mm}$ ', ' $S_w=14\text{mm}$ ', ' $S_l=10\text{mm}$ ', ' $L_l=4\text{mm}$ ', ' $W_l=1\text{mm}$ ', ' $g_l=0\text{mm}$ ', $h=1.6\text{mm}$, $\epsilon_r = 4.38$.

When the strip length is 1 mm, the additional resonance is found to be at 9.2 GHz. To confirm whether the resonance is due to this additional strip its length is varied from 1 mm to 4 mm. The return loss of the antenna for different strip lengths are shown in fig (4-49). Here it is found that the additional resonance frequency is shifted to the lower frequency region with increase of the strip length. This confirms that this additional resonance is due to the newly added strip.

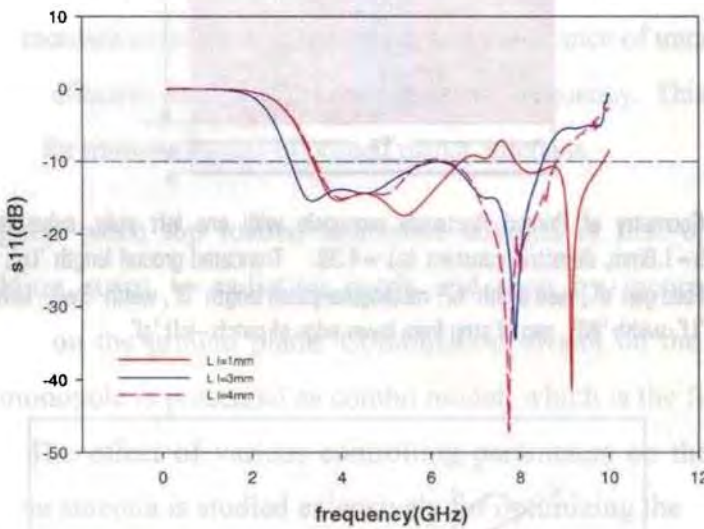


Fig.4.49 Return loss with one strip loaded rectangular monopole ' $W_g=45\text{mm}$ ', ' $L_g=20\text{mm}$ ', ' $d=1\text{mm}$ ', ' $Sw=14\text{mm}$ ', ' $Sl=10\text{mm}$ ', ' $Wl=1\text{mm}$ ', ' $gl=0\text{mm}$ ', $h=1.6\text{mm}$, $\epsilon_r=4.38$.

However, the resonance is not matched for $gl=0\text{mm}$. The impedance at this location is found to be 26 Ohms. To increase the matching the location of the additional strip is varied along the length of the main rectangular patch. The response of the antenna with the location of the strip (gl) is shown in fig. (4-50). It is well evident that **when** the strip location is $gl=1\text{mm}$ from the bottom the impedance at this frequency is improved and the band width of the antenna is extended up to 9.6 GHz.

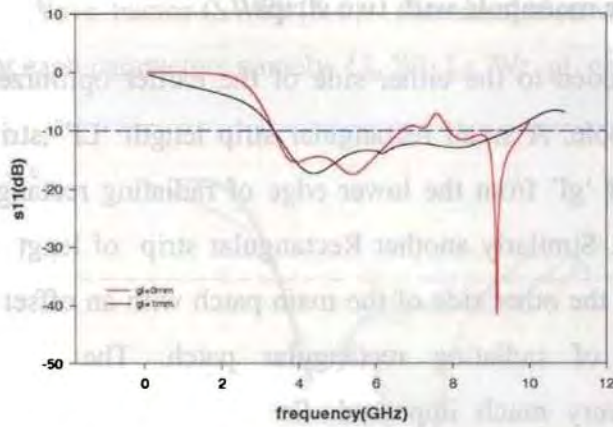


Fig.4.50 Return loss with one strip loaded rectangular monopole ' $W_g=45\text{mm}$ ', ' $L_g=20\text{mm}$ ', ' $d=1\text{mm}$ ', ' $Sw=14\text{mm}$ ', ' $Sl=10\text{mm}$ ', ' $Wl=1\text{mm}$ ', ' $Ll=1\text{mm}$ ', $h=1.6\text{mm}$, $\epsilon_r=4.38$.

Now another Strip of width 1mm and length of 4mm is added on the same side at ' $gl=1\text{mm}$ ' and 4mm respectively. Because of the mutual coupling of the strip the impedance characteristic was worsened as seen from fig.(4-51). To mitigate this effect the second Strip is shifted to the other side as in fig. (4-52). The nominal offset ' gr ' from the bottom of the rectangular patch. Now the return loss characteristic is studied and optimized for the UWB.

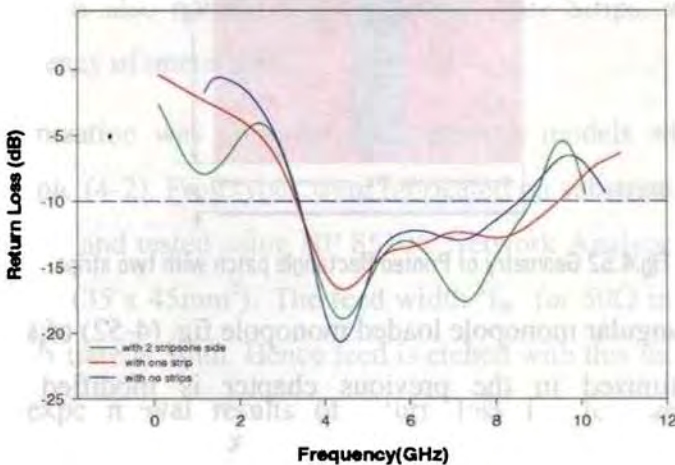


Fig. 4-51 Return loss with and without strip loaded rectangular monopole ' $W_g=45\text{mm}$ ', Length ' $L_g=20\text{mm}$ ', ' $d=1\text{mm}$ ', ' $Sw=14\text{mm}$ ', ' $Sl=10\text{mm}$ ', ' $Ll=4\text{mm}$ ', ' $Wl=1\text{mm}$ ', ' $gl=1\text{mm}$ ' and 4mm, $h=1.6\text{mm}$, substrate $\epsilon_r=4.38$.

(b) Rectangular monopole with two strips

Strips are added to the either side of the earlier optimized rectangular wide band monopole. A small rectangular strip length ' L_l ', strip width ' W_l ' placed at a gap of ' g_l ' from the lower edge of radiating rectangular patch as shown in fig.4-52. Similarly another Rectangular strip of length ' L_r ', width ' W_r ' is added on the other side of the main patch with an offset of ' g_r ' from the lower edge of radiating rectangular patch. The input impedance characteristic is very much improved. So for further studies this type of configuration is selected.

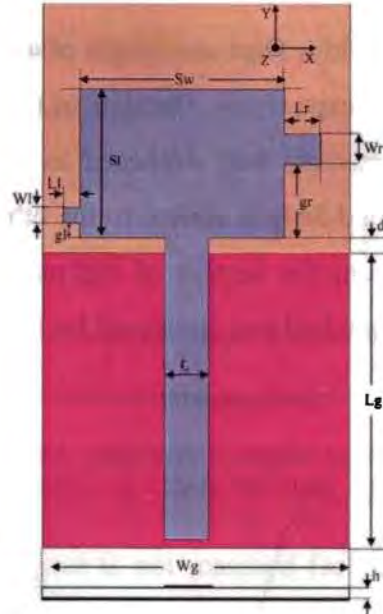


Fig.4.52 Geometry of Printed Rectangle patch with two strips.

The Rectangular monopole loaded monopole fig. (4-52) of size $S_l=10\text{mm}$, $S_w=14\text{mm}$ optimized in the previous chapter is modified by attaching asymmetrically strips of size $(L_l \times W_l)$ and $(L_r \times W_r)$ at a distance of ' g_l ' and ' g_r ' respectively from the lower edge of rectangular patch. This Defected Microstrip Structure (DMS) structure actually results in discontinuities for

increased Slow Wave Factor (SWF) [5-6]. The simulation was carried out for optimization of each parameters namely Ll, Wl, Lr, Wr, gl, gr.

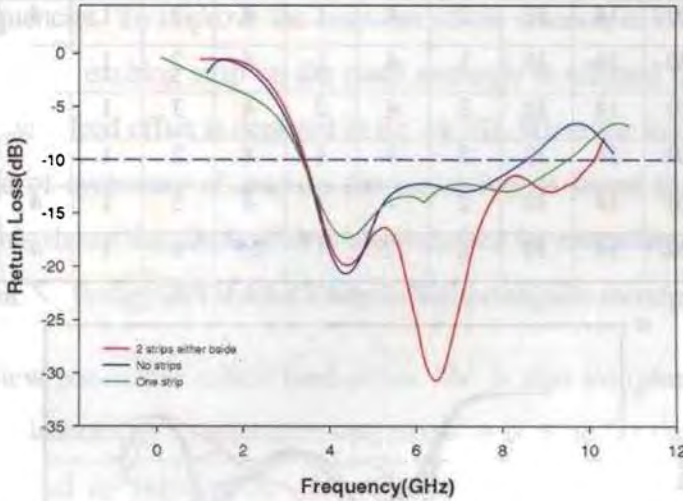


Fig. 4.53 Return loss with two strip either side on rectangular monopole. 'Wg'=45mm, 'Lg=20mm', 'd=1mm', 'Sw'=14mm, width 'Sl'=10mm, 'Ll'=4mm, 'Wl'=1mm, 'Lr'=4mm, 'Wr'=2mm, 'gl'=1mm, 'gr'=3mm, h=1.6mm, $\epsilon_r=4.38$.

From the analysis two Strip are sufficient to produce UWB operation. So in this thesis Strips are restricted to two in order to avoid the further complications. It is also noticed that by adding more Strips, we can further extend the frequency of operation

The optimization was done for the following models with parameters described in Table (4-2). Prototypes were fabricated on substrate with $\epsilon_r=4.38$, height 'h'=1.6mm and tested using HP 8510C Network Analyzer. The overall size of antenna is (35 x 45mm²). The feed width 'f_w' for 50Ω input impedance on the above substrate is 3mm. Hence feed is etched with this fact in mind. The variations in experimental results of return loss for few antenna models fabricated as per the design parameters in Table (4-2) are shown in Fig.(4-54) .

Table(4-2)

Model No.	Wg (mm)	Lg (mm)	Sl (mm)	Sw (mm)	d (mm)	LI (mm)	WI (mm)	Lr (mm)	Wr (mm)	gl (mm)	gr (mm)	h (mm)	ϵ_r
1	45	20	14	10	2	4	1	4	2	1	4	1.6	4.38
2	45	20	14	10	1	4	1	4	2	1	4	1.6	4.38
3	45	20	14	10	3	4	2	4	3	1	4	1.6	4.38
4	45	20	14	10	3	4	1	4	2	1	4	1.6	4.38
5	45	20	14	10	2	4	1	4	3	1	4	1.6	4.38
6	45	20	14	10	2	2.5	1	2.5	2	1	4	1.6	4.38

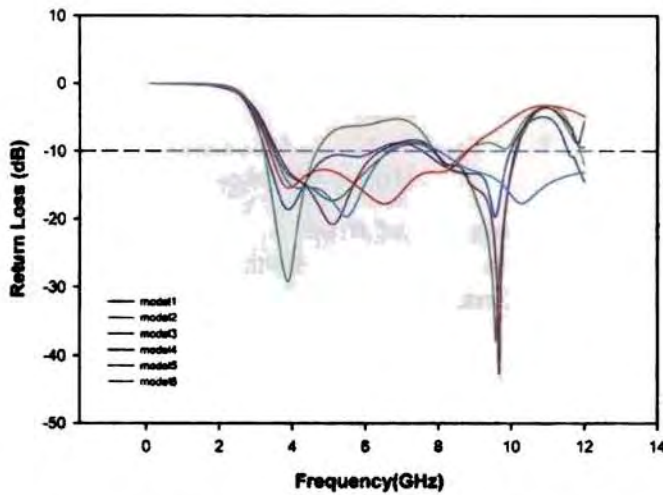


Fig. 4.54 Return loss variation for various models (1-6) of strip loaded rectangular monopole with different parameters as given in Table (5-1).

From the exhaustive theoretical and simulation studies revealed that the antenna performance is better when the separation distance 'd' is near to 2mm. If 'd' is large the capacitive coupling between the ground and radiating patch is small and this will degrade the performance. This is mainly affected at the centre band.

From the above fig. (4-54), it is very clear that return loss characteristics for model-1 has maximum bandwidth very close to UWB requirement. Hence this is selected as basic model to improve upon by further parametric optimization.

(c) Rectangular monopole with two strips and offset

But from the figure it is found that this deteriorated the behavior of the antenna at lower frequencies. To improve the response of the antenna at lower frequencies the location of the exciting strip on the main rectangle is offsetted from the centre. The antenna with feed offset is depicted in fig. (4-55). When the feed offset is 1mm from the line of symmetry of antenna the return loss is found to be very much improved. This shows that feed offset is also required for extending the band width of the antenna. So for the later studies a feed offset rectangular monopole is used.

So a new parameter called feed offset 'fo' is also introduced during this process of optimizations. Parametric optimization is done for the following the models described in Table (4-3). Models are fabricated on substrate with $\epsilon_r = 4.38$, $h = 1.6\text{mm}$ for all cases and the overall size of antenna is $(35 \times 45)\text{mm}^2$.

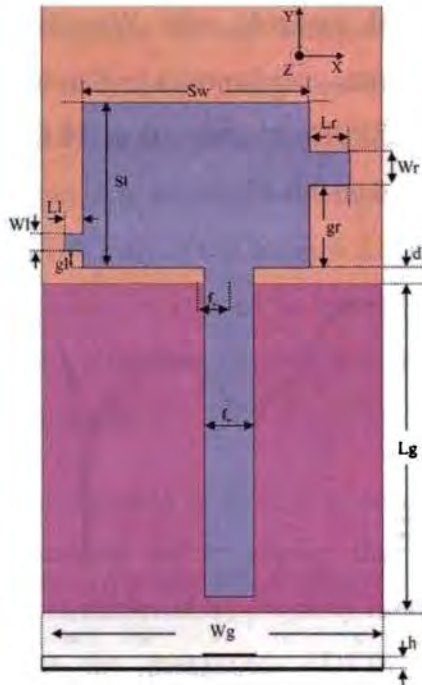


Fig.4.55 Geometry of Printed Rectangle patch with two strips with feed offset

Table (4-3)

Model No.	Wg (mm)	Lg (mm)	Sl (mm)	Sw (mm)	d (mm)	Ll (mm)	Wl (mm)	Lr (mm)	Wr (mm)	gl (mm)	gr (mm)	h (mm)	fo (mm)
1	45	20	14	10	1	4	1	4	2	1	4	1.6	1
2	45	20	14	10	2	2.5	1	2.5	2	1	4	1.6	1.5
3	45	20	14	10	2	2.5	1	2.5	2	0	4	1.6	2
4	45	20	14	10	2	2.5	1	2.5	2	1	4	1.6	2

The return loss analysis for all the above antennas in Table (4-3) are shown in fig.(4-56) and discussed here. It is again observed that the input impedance is minimum at the centre and maximum at the edges. So the matching can be conveniently adjusted by locating the feed location. So by simply offsetting the feed any required impedance condition can be easily achieved. This aspect is very clear from fig. (4-56). The best match is obtained when 'fo' is slightly offset by 1mm. Model-1 is best optimized for UWB applications with controlling parameters of Strip UWB monopole with $W_g=45\text{mm}$, $fo=1\text{mm}$, $Ll=4\text{mm}$, $Lr=4\text{mm}$, $gl=1\text{mm}$, $wr=2\text{mm}$, $wl=1\text{mm}$, $Lg=20\text{mm}$ giving an impedance bandwidth starting from 2.85GHz to more than 10.6GHz. Hence the further investigations were conducted on this Model-1.

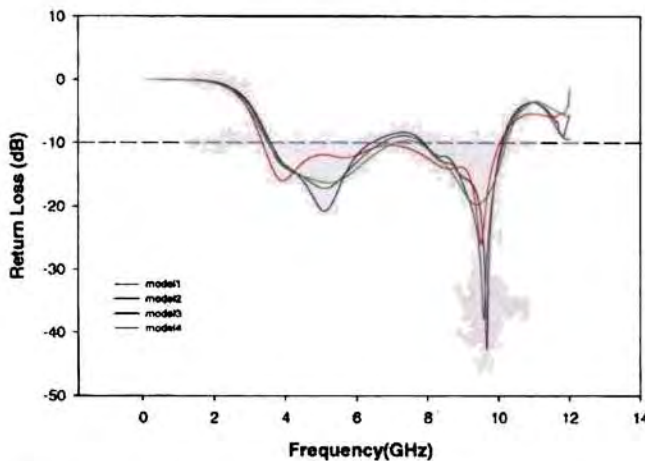


Fig.4.56 Return loss variation for various models (1-4) optimized strip loaded rectangular monopole with different parameters as given in Table (5-2).

4.8.2 Return Loss Characteristics of the optimized Antenna

These antenna characteristics are computed using FDTD code implemented in MATLABTM. The built in FFT function of the MATLAB is used to extract the frequency domain characteristics. The entire computational domain is divided into Yee cells of dimensions $\Delta x = \Delta y = \Delta z = 0.3\text{mm}$ and maximum frequency of operation is selected as 12GHz so that spatial discretization is less than $\lambda/20$ of the maximum frequency of operation. The substrate is discretized as 6 cells in the Z direction and 10 air cells were assigned on each side of the substrate periphery to ensure the practical condition of surrounding air. The layer of cell just above the printed strip monopole and underneath the ground plane is assigned with effective dielectric constant to ensure the air dielectric interface. 10 cells are assigned surrounding the antenna to truncate the problem space with ABC which ensures the complete absorption of any incident wave at the truncation boundary. Microstrip feed is modeled using Leubber's technique as outlined in Appendix-A. The input Gaussian pulse facilitates to extract the wideband characteristics of the printed strip monopole antenna. From the near field data far field radiation pattern and gain of the antenna are computed as outlined in Appendix-A. Sinusoidal excitation is used to extract the field components at the resonant frequency. The following sections describe the experimental and theoretical observations in detail.

The return loss characteristics of the optimized antenna is shown in fig. (4-57). FDTD analysis carried out to predict the antenna characteristics. Here the ultra-wide band is achieved by properly merging the three resonant modes, as evident from the measured, FDTD, simulated return loss characteristics in fig. (4-57).

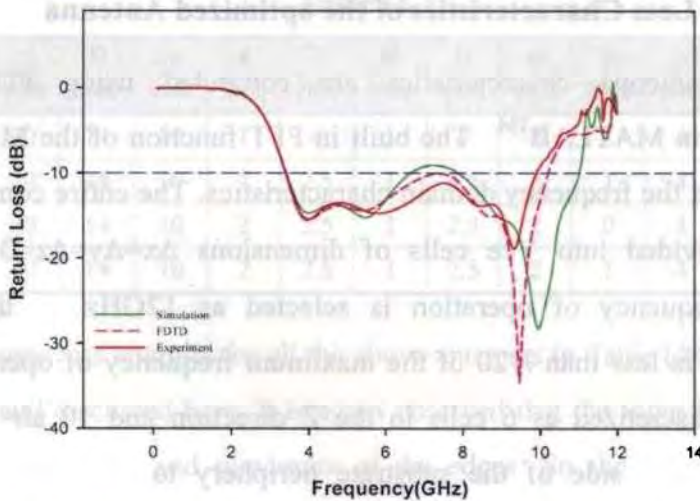


Fig.4.57 Return loss for optimized strip loaded wide rectangular strip monopole 'Wg' = 45mm, 'Lg = 20mm', 'd = 1mm', 'Sl' = 14mm, 'Sw' = 10mm, 'Ll' = 4mm, 'Wl' = 1mm, 'Lr' = 4mm, 'Wr' = 2mm, 'gl' = 1mm, 'gr' = 4mm, 'fo' = 1mm, h = 1.6mm, $\epsilon_r = 4.38$.

A reasonably good agreement between experimental results, simulated and theoretical analysis using FDTD codes. This authenticates the design. However, the further miniaturization for achieving the compactness is investigated through design variants.

The fabricated optimized UWB monopole antenna has a small electrical length $(35 \times 45) \text{ mm}^2$ and a measured bandwidth ranging from 3-11 GHz. The top and bottom strip has the size of $(4 \times 1) \text{ mm}^2$ and $(4 \times 2) \text{ mm}^2$ respectively, tells that longer strips can reduce the lower edge frequency by increasing the overall size of the antenna frequencies.

The frequency f_r can be estimated by the longest effective current path $L = \lambda_d/2$, where λ_d is the wavelength inside the substrate at f_r . From the electric current distribution on the antenna at the lowest frequency of 3 GHz, it is seen that the majority of the electric currents is concentrated on the right portion of the upper radiator due to 'Lr'

Distribution of surface electric currents density (J_{surf}) on antenna at 3 resonant modes are shown in fig.(4-58a-c) and the resonance is explained.

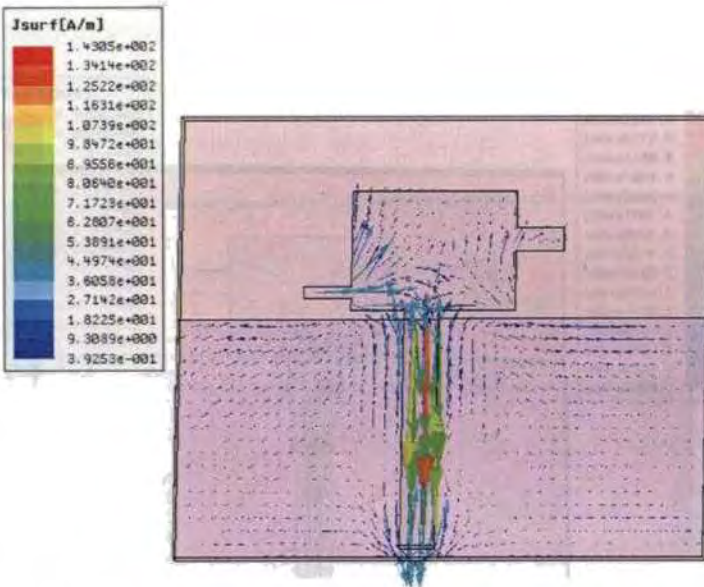
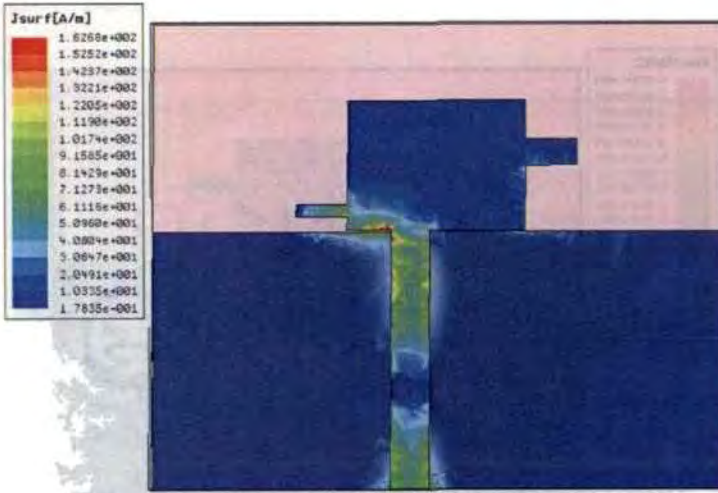


Fig. 4.58a J - surface for 4.68GHz i.e. the first resonant frequency of the strip loaded UWB rectangular monopole antenna, $W_g=45\text{mm}$, $f_0=1\text{mm}$, $Ll\&Lr=4\text{mm}$, $g_l=1\text{mm}$, $g_r=4\text{mm}$, $w_r=2\text{mm}$, $w_l=1\text{mm}$, $L_g=20\text{mm}$, $d=1\text{mm}$

The 1st resonant frequency at 4.685GHz corresponds to $\lambda_d/4$ of 9.5mm. The resonant length as seen from the current is $(Sw-fw)/2+Ll=\lambda_d/4$. This has been validated by simulated and measured results.

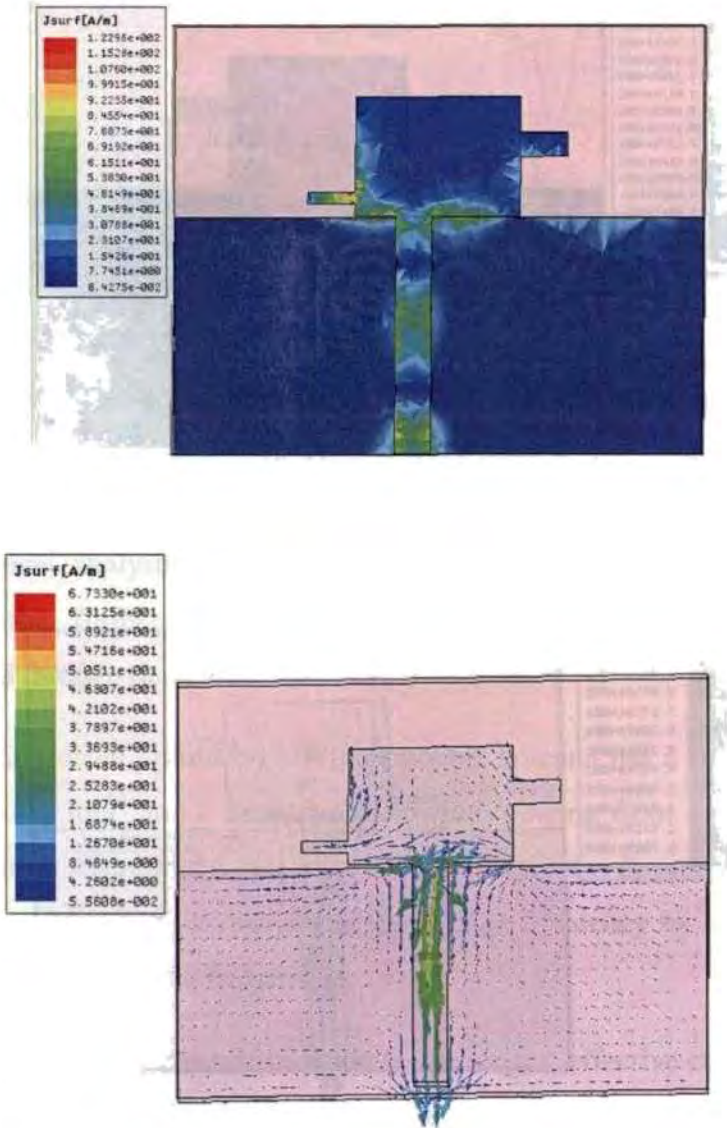


Fig. 4.58b J- surface for 7.95GHz i.e. the i.e. the 2nd resonant frequency of the strip loaded UWB rectangular monopole antenna ,Wg=45mm, fo=1mm, Ll&Lr=4mm, gl=1mm, gr=4mm, wr=2mm, wl=1mm, Lg=20mm, d=1mm

The 2nd resonant frequency at 7.95GHz corresponds to $\lambda_d/4$ of 5.5mm. The resonant length as seen from the current is $(S_w-f_w)/2 = \lambda_d/4$. This has been validated by simulated and measured results.

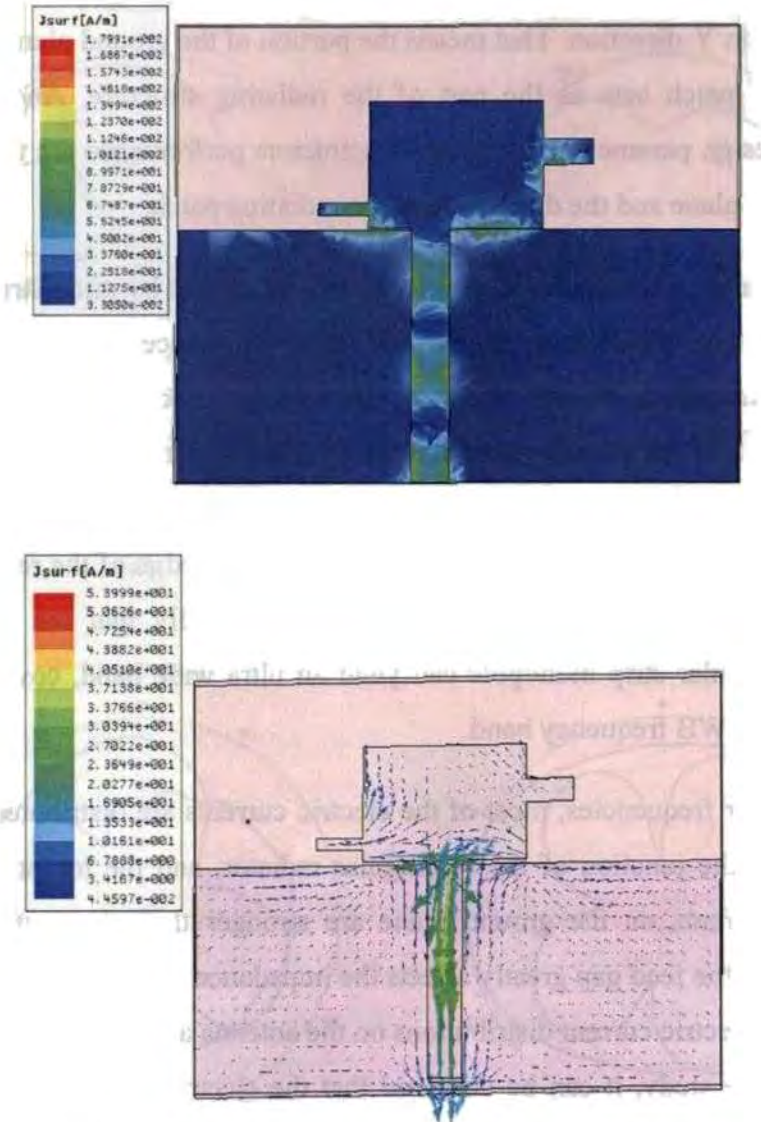


Fig. 4.58c J - surface for 10.34GHz i.e. the 3rd resonant frequency of the strip loaded UWB rectangular monopole antenna, $W_g=45\text{mm}$, $f_o=1\text{mm}$, $Ll\&Lr=4\text{mm}$, $g_l=1\text{mm}$, $g_r=4\text{mm}$, $w_r=2\text{mm}$, $w_l=1\text{mm}$, $L_g=20\text{mm}$, $d=1\text{mm}$

This 3rd resonant frequency at 10.34GHz corresponds to $\lambda_d/2$ of nearly 9 mm. The resonant length as seen from the current is (g_r+l_r+d) therefore corresponds to $\lambda_d/2$. This has been validated by simulated and measured results.

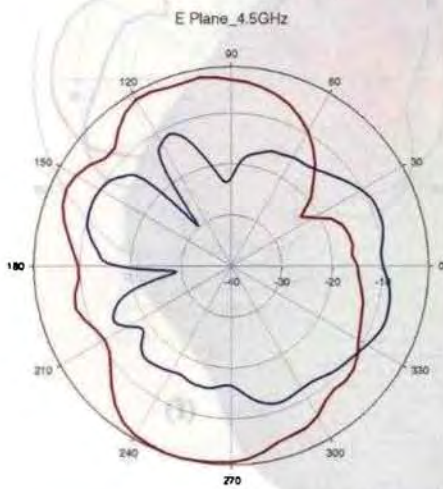
On the ground plane, the current is mainly distributed on the upper edge along the L_g in Y-direction. That means the portion of the ground plane close to the radiating patch acts as the part of the radiating structure. Another two important design parameters that affect the antenna performance are the length of the ground plane and the dimension of the radiating patch.

The printed Rectangular strip monopole antenna fed by microstrip line is investigated here. It has been shown that the performance of the antenna in terms of its frequency domain characteristics is mostly dependent on the feed gap, the length of the ground plane and the dimension of the antenna. The first resonant frequency is directly associated with the dimension of the rectangular strip because the current is mainly distributed along the edge of the rectangular strip. It is demonstrated numerically and experimentally that the proposed printed rectangular strip monopole can yield an ultra wide band, covering the FCC defined UWB frequency band.

At higher frequencies, most of the electric currents are distributed on the feeding strip, the junction of the rectangular radiator, and the top strip. As a result, the currents on the ground plane are stronger than those at 3 GHz. Consequently, the feed gap greatly affects the impedance matching. Fig. (4-58a-d) shows the electric current distributions on the antenna at 4.68, 7.95 and 10.34 GHz. From the study, it can be observed that the electric currents are mainly concentrated around the feeding strip at all the frequencies. Thus, the ground plane significantly affects the impedance and radiation performance of this Rectangular strip loaded monopole UWB antenna (Ant.I).

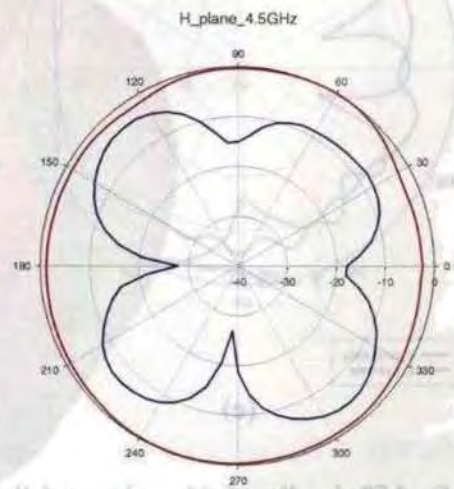
4.8.3 Radiation Pattern

The experimental results of 2D radiation pattern in E-plane and H-plane for co and cross polarization are shown in fig.(4-59a-f) for different modes.



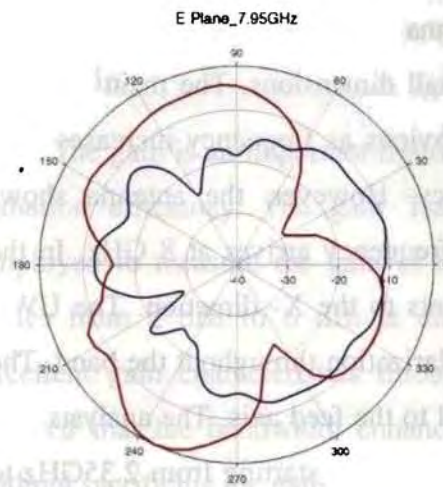
— E_{co} vs theta
— E_x vs theta

(a)



— H_{co} vs theta
— H_x vs theta

(b)



— E_{co} vs theta
— E_x vs theta

(c)



— H_{co} vs theta
— H_x vs theta

(d)

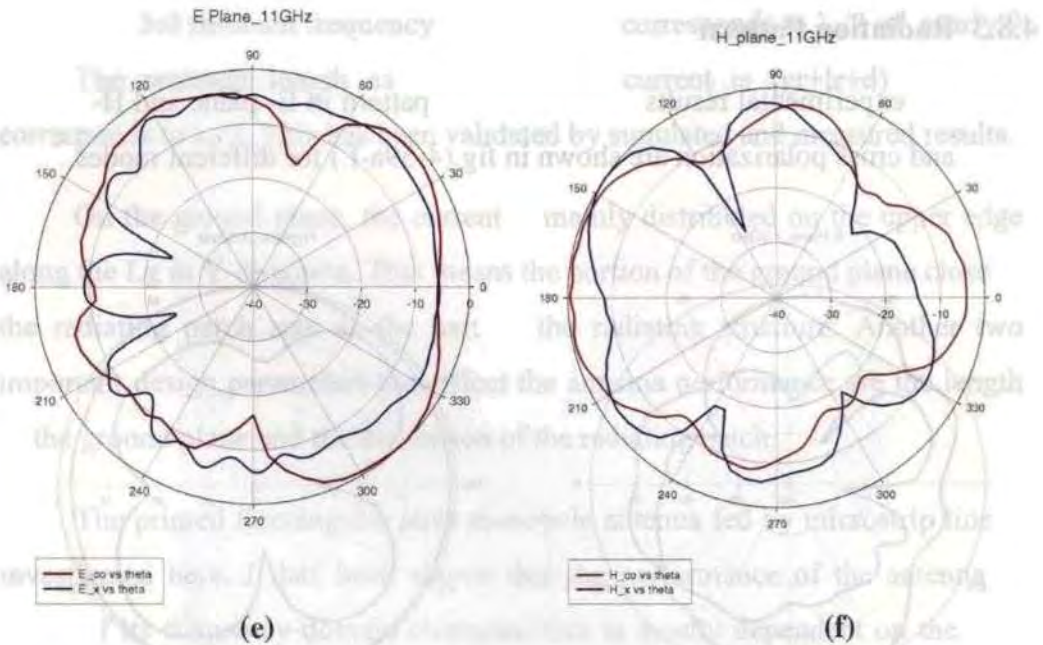


Fig. 4.59a-f Normalised E- plane and H-plane radiation pattern at 4.5GHz,7.95GHz and 11GHz for optimized strip loaded rectangular monopole 'Wg'=45mm, 'Lg=20mm', 'd'=1mm, 'Sl'=14mm, 'Sw'=10mm, 'Ll'=4mm, 'Wl'=1mm, 'Lr'=4mm, 'Wr'=2mm, 'gl'=1mm, 'gr'=4mm, 'fo'=1mm, h=1.6mm, $\epsilon_r=4.38$.

In the lower frequency band, the antenna has uniform radiation pattern in the azimuth plane due to its electrically small dimensions. The main beam in the X-direction becomes more and more obvious as frequency increases. The cross polarization increases with frequency. However, the antenna shows slightly higher gain in other directions as frequency arrives at 8 GHz. In the higher frequency band, the main beam points to the X- direction. The UWB strip monopole is found to exhibit linear polarization throughout the band. The polarization is vertical (Y-direction) parallel to the feed axis. The analysis also confirms the results giving an impedance bandwidth starting from 2.35GHz to more than 11GHz.

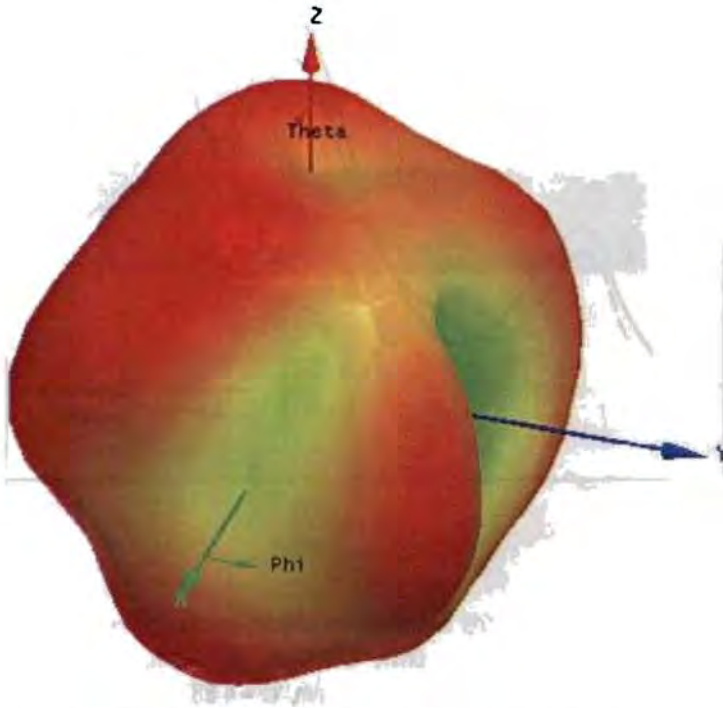


Fig. 4.60 The simulated 3D radiation pattern for optimized strip loaded rectangular monopole ' $W_g=45\text{mm}$ ', ' $L_g=20\text{mm}$ ', ' $d=1\text{mm}$ ', ' $Sl=14\text{mm}$ ', ' $Sw=10\text{mm}$ ', ' $Ll=4\text{mm}$ ', ' $Wl=1\text{mm}$ ', ' $Lr=4\text{mm}$ ', ' $Wr=2\text{mm}$ ', ' $gl=1\text{mm}$ ', ' $gr=4\text{mm}$ ', ' $fo=1\text{mm}$ ', $h=1.6\text{mm}$, $\epsilon_r=4.38$.

4.8.4 Gain

The gain is an important figure of merit of an antenna as a measure of its radiation efficiency. The gain Transfer method explained in chapter 3 is employed to measure the gain of the Antenna Under Test (AUT). The gain varies from 2 dBi to 6 dBi at different band for various geometries. The excellent gain characteristics throughout the band is noteworthy. It is also inferred that the bandwidth enhancement of monopole to UWB is achieved without sacrificing the gain.

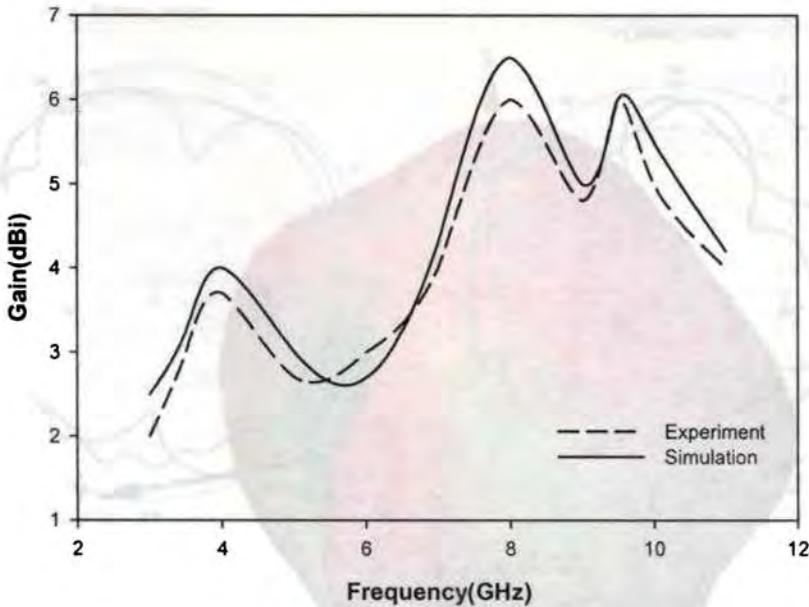


Fig. 4.61 The Gain for optimized strip loaded rectangular monopole 'Wg' = 45mm, 'Lg' = 20mm, 'd' = 1mm, 'Sl' = 14mm, 'Sw' = 10mm, 'Ll' = 4mm, 'Wl' = 1mm, 'Lr' = 4mm, 'Wr' = 2mm, 'gl' = 1mm, 'gr' = 4mm, 'fo' = 1mm, h = 1.6mm, $\epsilon_r = 4.38$.

The measured and simulated gains are shown in Fig. (4-61). The gain is measured along the peak direction. The measured gain error is within 0.5 dBi. The measured gain above 3 GHz frequency range has an average 3.5 dBi or more. The slight discrepancies between the simulated and measured gains can be attributed to the substrate loss and effect of connector which are not incorporated in the simulation. However, the simulated and measured gains have a similar tendency.

4.8.5 Compactness

By adding strips to the radiator or modifying the shapes of radiator as well as the ground plane, the ultra wide band is achieved. The size of the printed antenna is shrunk to $(35 \times 45) \text{ mm}^2$ from the normal size of $(50 \times 50) \text{ mm}^2$ or more. However, the impedance characteristics of the printed designs

may suffer from strong ground-plane effects. The photo of the prototype of optimized Strip loaded Rectangular Monopole fabricated and characterized is shown in figure (4-62) to illustrate the compactness.

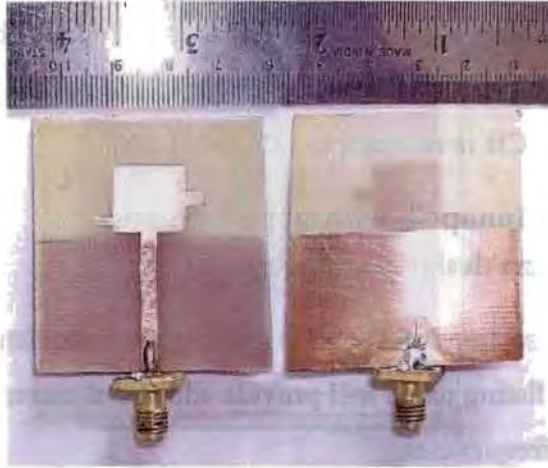


Fig. 4.62 The top and bottom view of the prototype 'Wg'=45mm, 'Lg'=20mm', 'd'=1mm', 'Sl'=14mm, 'Sw'=10mm, 'Ll'=4mm, 'Wl'=1mm, 'Lr'=4mm, 'Wr'=2mm, 'gl'=1mm, 'gr'=4mm, 'fo'=1mm, h=1.6mm, $\epsilon_r = 4.38$, Overall size (35 X 45mm²).

4.8.6 Effect of Truncated ground plane configuration

The parametric study is carried out by simulation as well as experiments for practical applications. The major parameters controlling the size of the antenna are the length (Lg), width (Wg), gap (d) and feed offset (fo).

In addition, the printed UWB antenna consisting of a planar radiator and system ground plane is essentially an unbalanced design, where the electric currents are distributed on both the radiator and the ground plane so that the radiation from the ground plane is inevitable. Therefore, the performance of the printed UWB antenna is significantly affected by the shape of the ground plane [17], [18]. Such a ground-plane effect causes severe practical engineering problems such as design complexity and

deployment difficulty. Therefore, this work presents a technique to reduce the ground-plane effect on the performance of a small printed UWB antenna. The printed antenna is designed to cover the UWB band of 3.1–10.6 GHz, in particular, the lower band of 3.1–5 GHz. The attempt is successful by asymmetrically attaching a strip to the radiator to reduce the ground-plane effect on the performance and thus the overall size of the antenna printed onto a 1.6mm thick PCB is reduced to (35 X 45) mm².

4.9 Rectangular Monopole with slotted ground

4.9.1 Printed Antenna design parameters

In the previous section it is found that addition of two Strips on either side of the rectangular radiating patch will provide additional current path which are resonating at higher frequencies.

A single slot of length 'y' and width 'x' is added on one side of the truncated ground plane edge at $Vx/2$ from the line of symmetry. This geometry is shown in fig (4-63). The idea here is to produce additional resonance at higher frequency due to the resonance of this simple slot. So the size of the slot is selected as for the first resonance at about 9 GHz. When a slot is added at one side of ground edge, it is found that there is a tendency of resonance at higher frequency. This aspect is demonstrated in fig.(4-64). When the slot width is 3mm the additional resonance is found to be at 9 GHz. To confirm whether the resonance is due to this additional strip its length is varied from 1 mm to 3 mm. The return loss of the antenna for different slot widths is shown in fig (4-64).

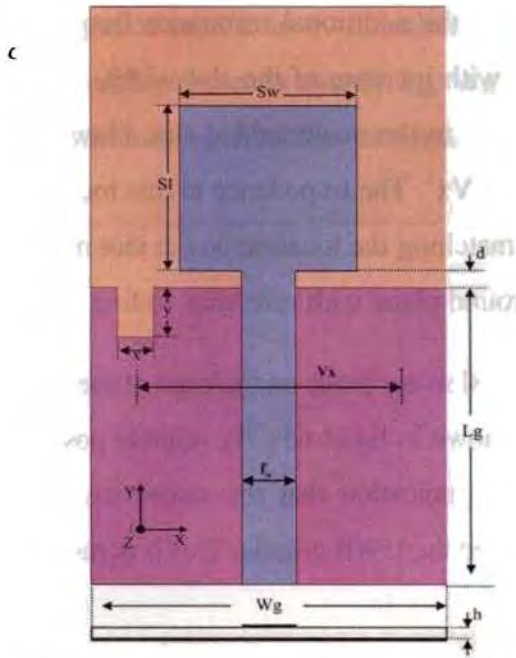


Fig.4.63 Geometry of Rectangle Monopole with one slot on ground. Truncated ground length 'Lg', width 'Wg', rectangular patch length 'Sl', width 'Sw', Feed gap 'd', Slot on ground plane -width 'x', height 'y', slot 'Vx/2' from centre line, Substrate height $h=1.6\text{mm}$, substrate $\epsilon_r = 4.38$.

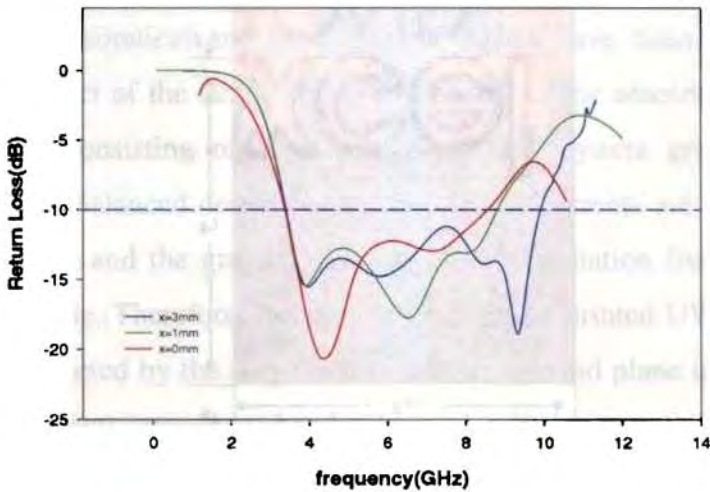


Fig.4.64 Return loss characteristics of Rectangle Monopole with one slot on ground, $W_g=45\text{mm}$, $d=2\text{mm}$, $L_g=18\text{mm}$, $Sw=14\text{mm}$, $Sl=10\text{mm}$, 'y' = 3mm, $V_x=18\text{mm}$, $h=1.6\text{mm}$, $\epsilon_r = 4.38$.

Here it is found that the additional resonance frequency is shifted to the lower frequency region with increase of the slot width. This confirms that this additional resonance is due to the newly added slot. However, the resonance is not matched for arbitrary ' V_x '. The impedance at this location is found to be 35 Ohms. To increase the matching the location of the slot need to be varied along the edge of truncated ground plane with reference to line of symmetry.

Now the symmetric slots are made on the edge of the truncated ground close to the radiating patch as shown in fig.(4-65). By suitably positioning the optimized size slots, there is strong indication that the return loss characteristic getting extended further and covered the UWB criteria. This is demonstrated in fig.(4-66)

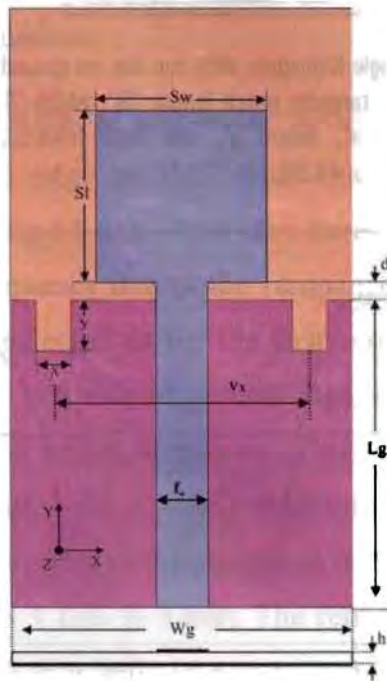


Fig.4.65 Geometry of Rectangle Monopole with Two slots on ground.

The Rectangular monopole of size $Sl=10\text{mm}$, $Sw=14\text{mm}$ optimized in the previous chapter is modified by cutting slots of size $(x \times y)$ symmetrically on the

truncated ground at separation of 'Vx' in X-direction. The simulation was carried out for optimization of each parameters namely Lg, Wg, Sl, Sw, x, y, and 'Vx'. The geometry of the antenna along with other parameters are shown in fig.(4-65).

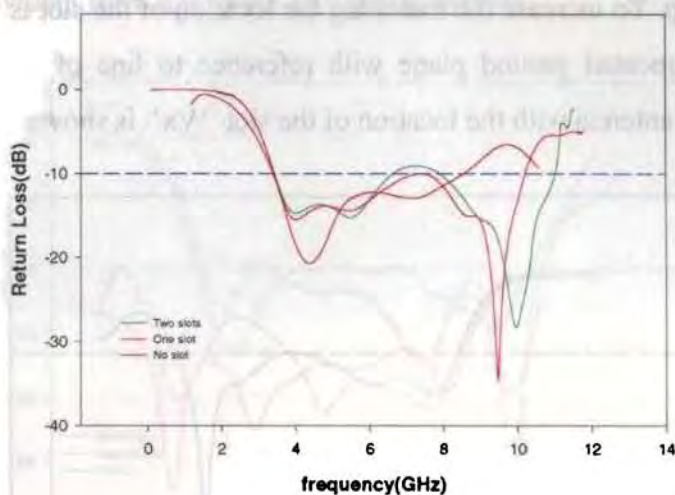


Fig.4.66 Return loss characteristics of Rectangle Monopole with one, two and no slot on ground, $W_g=45\text{mm}$, $d=2\text{mm}$, $L_g=18\text{mm}$, $Sw=14\text{mm}$, $Sl=10\text{mm}$, $'y'=3\text{mm}$, $V_x=18\text{mm}$, $h=1.6\text{mm}$, $\epsilon_r=4.38$.

Detailed theoretical and experimental studies have been conducted to optimize the effect of the slot on the ground plane of the antenna. The printed UWB antenna consisting of a planar radiator and system ground plane is essentially an unbalanced design, where the electric currents are distributed on both the radiator and the ground plane so that the radiation from the ground plane is inevitable. Therefore, the performance of the printed UWB antenna is significantly affected by the shape and size of the ground plane in terms of the operating frequency, impedance bandwidth, and radiation patterns [17], [18].

Here the objective of the work was to optimize the antenna for UWB applications with special emphasis on the size of the antenna. It is observed that by properly selecting the slot parameters the overall size of the antenna can be

reduced to $30 \times 45 \text{mm}^2$. The following sections deals the optimization procedure to obtain a compact UWB antenna.

One more slot is made symmetrically on the other side of the main rectangular strip. To increase the matching the location of the slot is varied along the edge of truncated ground plane with reference to line of symmetry. The response of the antenna with the location of the slot 'Vx' is shown in fig. (4-67).

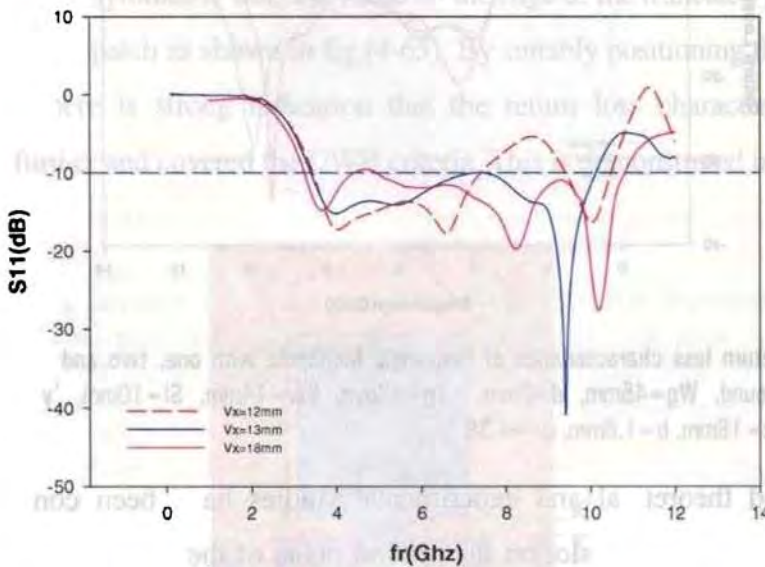


Fig.4.67 Return loss characteristics of Rectangle Monopole with two slot on ground, $W_g=45\text{mm}$, $d=2\text{mm}$, $L_g=18\text{mm}$, $S_w=14\text{mm}$, $S_l=10\text{mm}$, ' y ' = 3mm, $h=1.6\text{mm}$, $\epsilon_r=4.38$.

From the above result in fig.(4-67), the impedance matching for the antenna with parameters $W_g=45\text{mm}$, Feed gap $d=2\text{mm}$, $L_g=18\text{mm}$, regular rectangular patch of $S_w=14\text{mm}$, $S_l=10\text{mm}$, two symmetric slots on ground edge with ' x ' = 1mm, ' y ' = 3mm, the optimum location is $V_x=18\text{mm}$, on a substrate of height $h=1.6\text{mm}$, dielectric constant $\epsilon_r=4.38$. The overall size of the UWB antenna is $30 \times 45 \text{mm}^2$ and further fine tuning by parameter optimization is done on this.

4.9.2 Return Loss Characteristics

The return loss characteristics of the optimized antenna is shown in fig.(5-14). The ultra-wide band is achieved by properly merging the three resonant modes, as evident from the return loss characteristics.

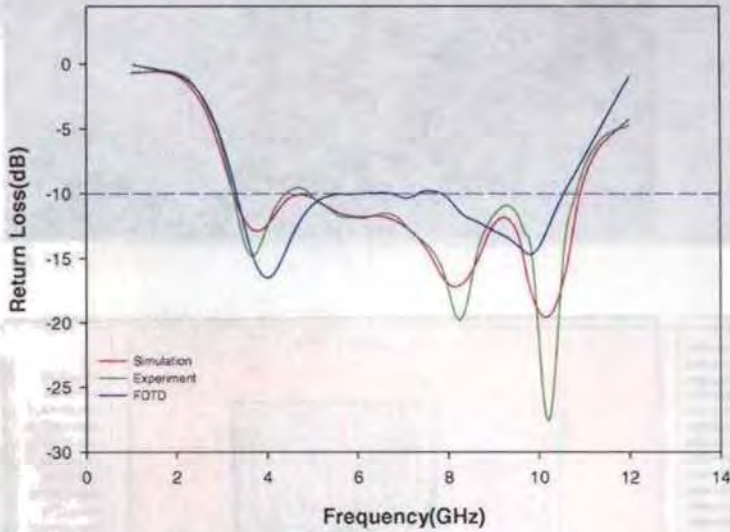


Fig. 4.68 Return loss characteristics for optimized Rectangle Monopole with two slot on ground UWB antenna, $W_g=45\text{mm}$, $d=2\text{mm}$, $L_g=18\text{mm}$, $Sw=14\text{mm}$, $Sl=10\text{mm}$, ' x ' = 1mm, ' y ' = 3mm, $V_x=18\text{mm}$, $h=1.6\text{mm}$, $\epsilon_r=4.38$, overall size $(30 \times 45)\text{mm}^2$.

The simulated and FDTD results are in agreement with the experimental observations and the antenna is radiating EM energy from 3.1 to 10.6 GHz. The reasonable match between the experimental results, simulated and theoretical analysis using FDTD codes authenticates the design. There has been a reduction in overall size from $35 \times 45 \text{mm}^2$ to $30 \times 45\text{mm}^2$. However, the further miniaturization for achieving the compactness is investigated through design variants in next section.

Distribution of surface electric currents density (J_{surf}) on antenna at 3 resonant modes are shown in fig.(5-7a) to (5-7c).

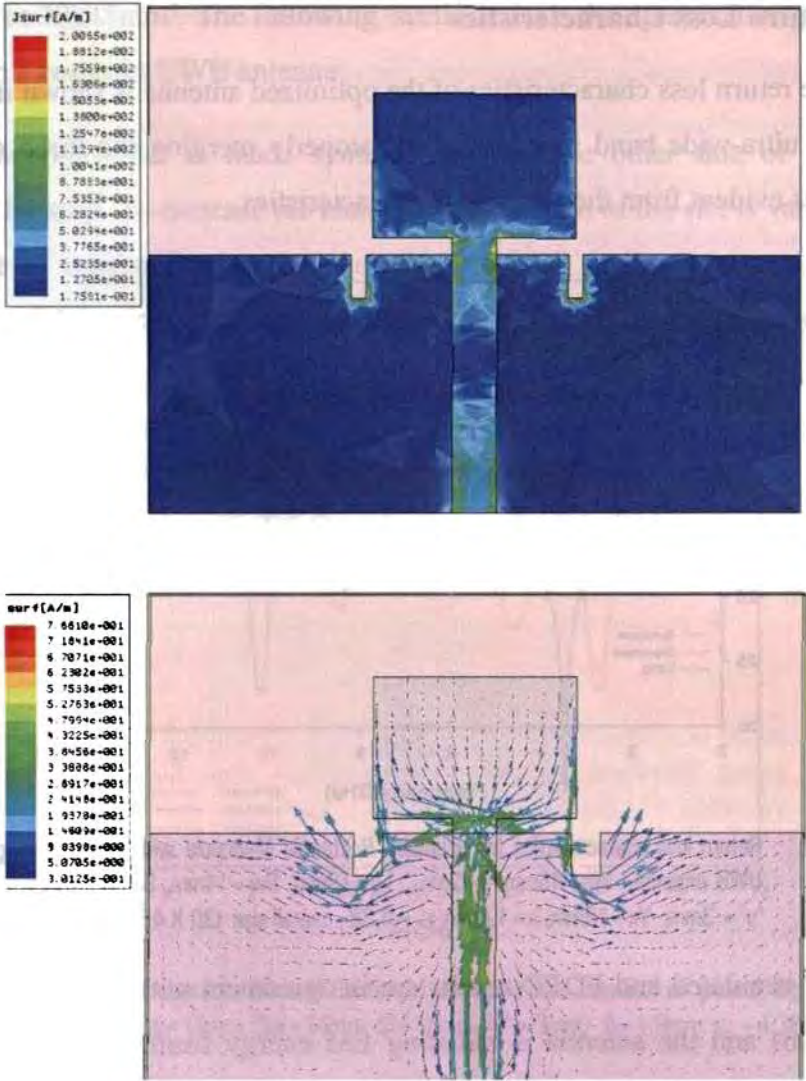


Fig.4-69a Current distribution at 4GHz for Printed UWB rectangular monopole with ground slots $W_g = 45\text{mm}$, $d = 2\text{mm}$, $L_g = 18\text{mm}$, $Sw = 14\text{mm}$, $Sl = 10\text{mm}$, $x = 2\text{mm}$, $y = 3\text{mm}$, $V_x = 15\text{mm}$, $\epsilon_r = 4.38$, $h = 1.6\text{mm}$

The 1st resonant frequency at 4GHz is because of the resonance of the current path $(Sw/2+d)$ which is approximately corresponds to $\lambda/4$. This is evident from the fig.(4-69a).

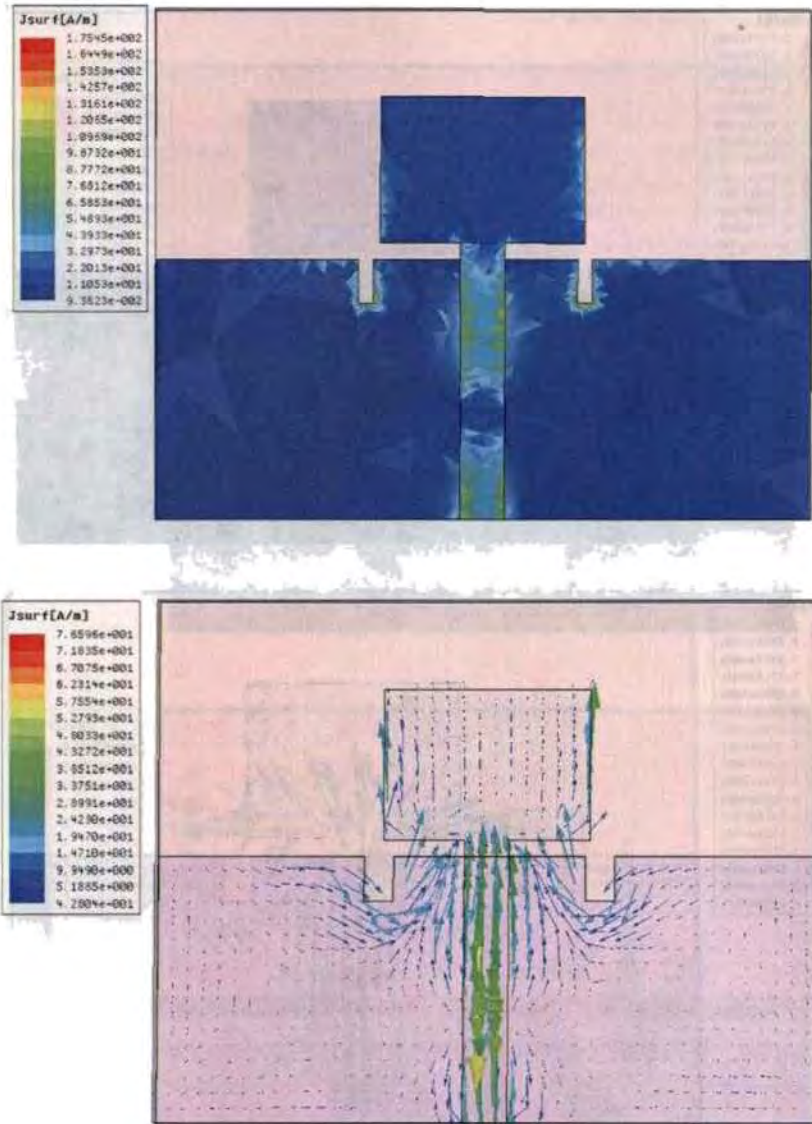


Fig.4.69b Current distribution at 6.5GHz for Printed UWB rectangular monopole with ground slots $W_g=45\text{mm}$, $d=2\text{mm}$, $L_g=18\text{mm}$, $Sw=14\text{mm}$, $Sl=10\text{mm}$, $x=2\text{mm}$, $y=3\text{mm}$, $V_x=15\text{mm}$, $\epsilon_r=4.38$, $h=1.6\text{mm}$

The 2nd resonant frequency at 6.5GHz corresponds to $\lambda/2$. This resonant length as seen from the current distribution is $(Sl+d+y)$. This has been validated by simulation and experiment.

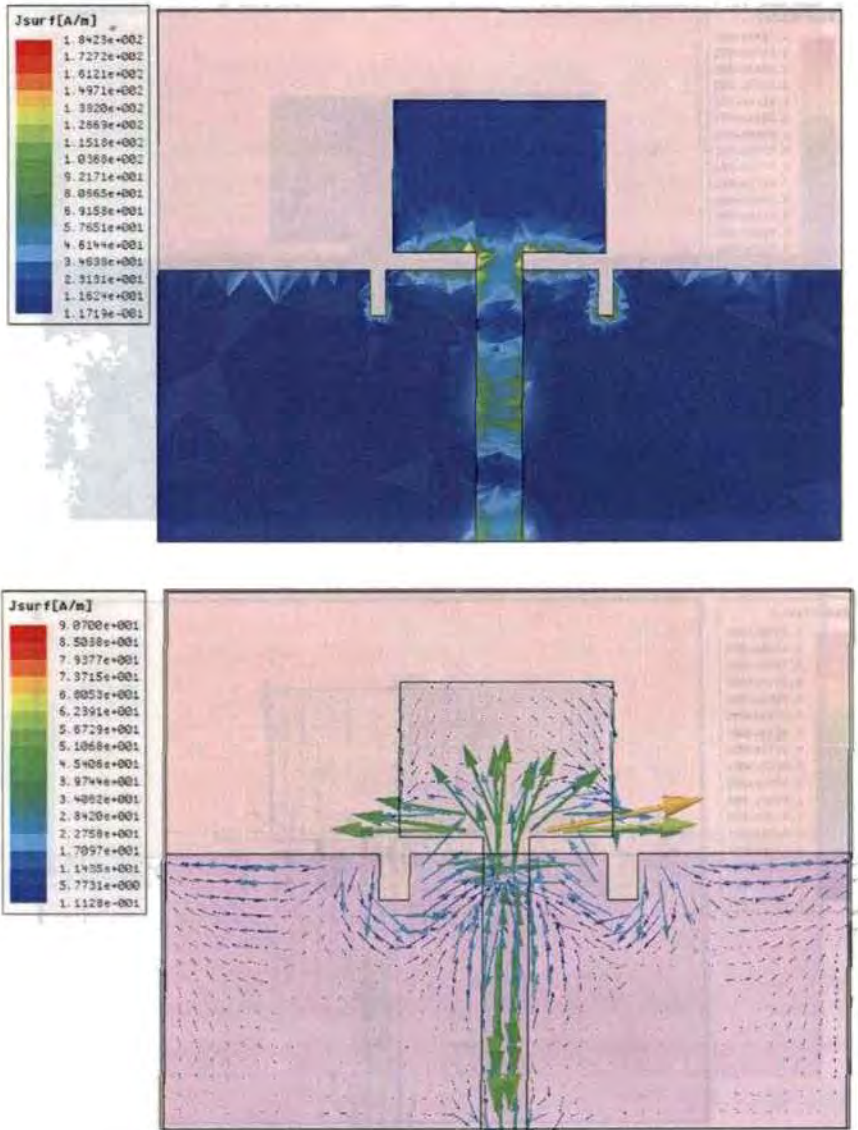


Fig.4.69c Current distribution at 8GHz for Printed UWB rectangular monopole with ground slots $W_g = 45\text{mm}$, $d = 2\text{mm}$, $L_g = 18\text{mm}$, $S_w = 14\text{mm}$, $S_l = 10\text{mm}$, $x = 2\text{mm}$, $y = 3\text{mm}$, $V_x = 15\text{mm}$, $\epsilon_r = 4.38$, $h = 1.6\text{mm}$

The 3rd resonant frequency at 8GHz corresponds to $\lambda d/2$. This resonant length corresponds to $(S_w/2 + x + y)$. This is shown in fig. (4-69c).

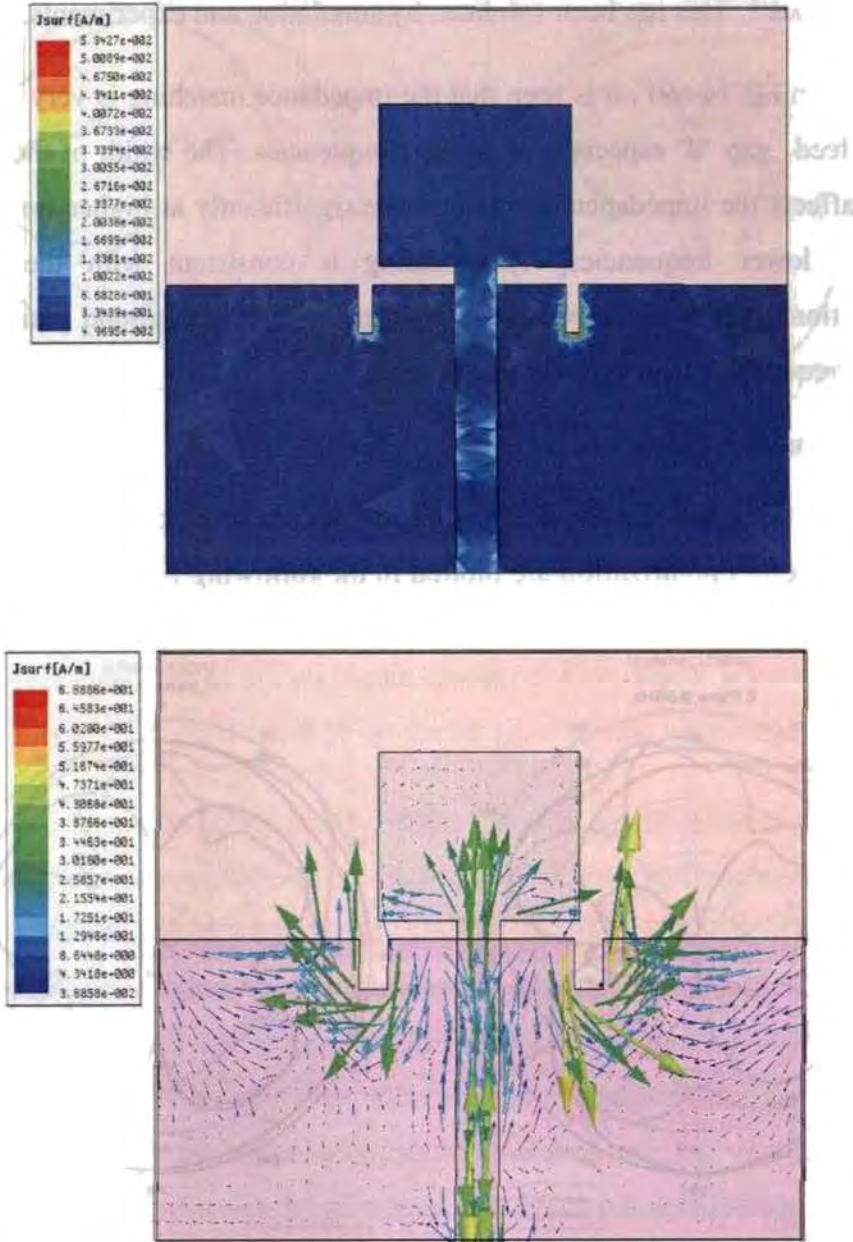


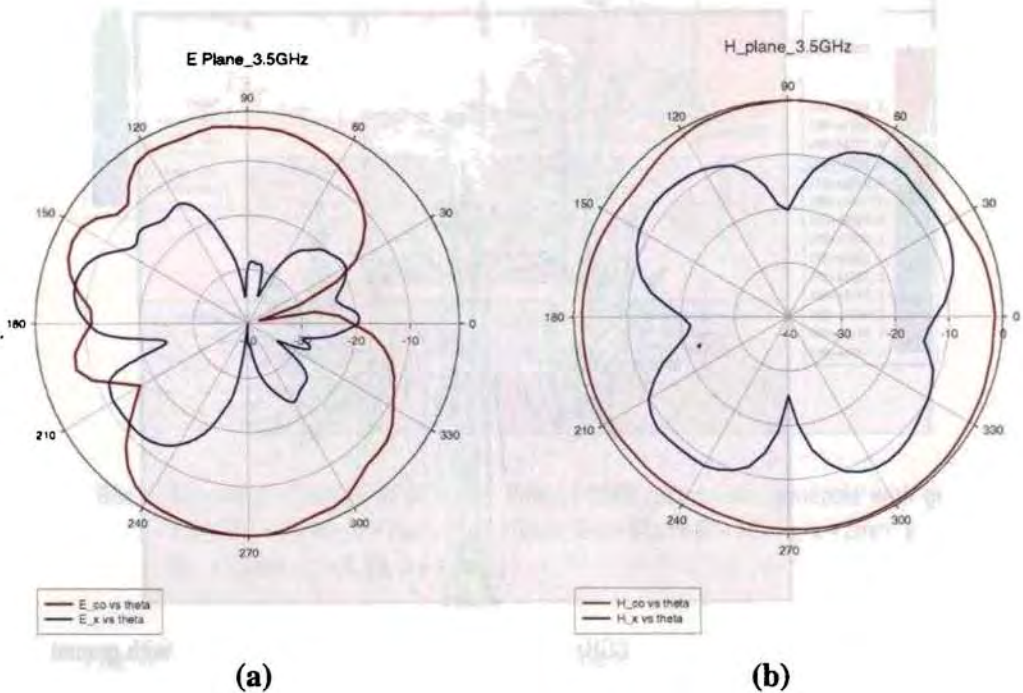
Fig.4.69 d Current distribution at 10GHz for Printed UWB rectangular monopole with ground slots $W_g = 45\text{mm}$, $d = 2\text{mm}$, $L_g = 18\text{mm}$, $S_w = 14\text{mm}$, $S_l = 10\text{mm}$, $x = 2\text{mm}$, $y = 3\text{mm}$, $V_x = 15\text{mm}$, $\epsilon_r = 4.38$, $h = 1.6\text{mm}$

The 4th resonant frequency at 10.0 GHz is due to the path $(2y+x+d)$, which is $\lambda d/2$. This has been validated by simulation and experiments.

From fig. (4-69), it is seen that the impedance matching is very sensitive to the feed gap 'd' especially at higher frequencies. The width of the ground plane affects the impedance matching more significantly at higher frequencies than at lower frequencies. This finding is consistent with the current distributions, where more current is concentrated on the ground plane at the higher frequencies than at lower frequencies.

4.9.3 Radiation Pattern

The measured results of 2D radiation pattern in E- plane and H- plane for co and cross polarization are plotted in the following figs.(4-70a-f)



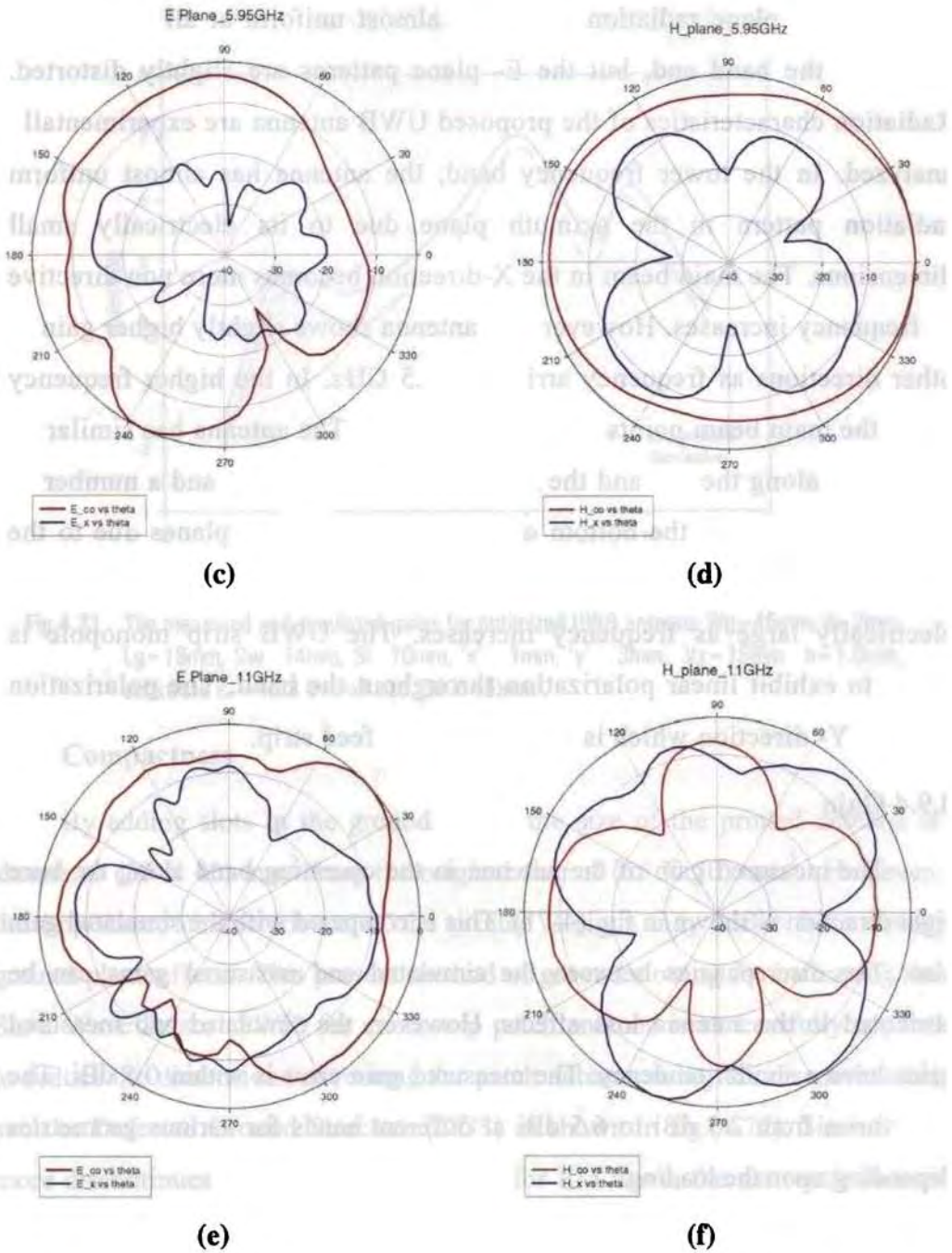


Fig.4.70a-f Radiation characteristics for optimized UWB antenna has $W_g=45\text{mm}$, $d=2\text{mm}$, $L_g=18\text{mm}$, $Sw=14\text{mm}$, $Sl=10\text{mm}$, $'x'=1\text{mm}$, $'y'=3\text{mm}$, $V_x=18\text{mm}$, $h=1.6\text{mm}$, $\epsilon_r=4.38$.

The H- plane radiation pattern is almost uniform at all frequencies except at the band end, but the E- plane patterns are slightly distorted. Radiation characteristics of the proposed UWB antenna are experimentally analyzed. In the lower frequency band, the antenna has almost uniform radiation pattern in the azimuth plane due to its electrically small dimensions. The main beam in the X-direction becomes more non directive as frequency increases. However, the antenna shows slightly higher gain in other directions as frequency arrives at 9.5 GHz. In the higher frequency band, the main beam points to the X- direction. The antenna has similar E-plane cuts along the XZ and the Y Z planes up to 7 GHz, and a number of side lobes appear at the bottom of the XZ and the Y Z planes due to the diffractions from the edge of the ground plane, which becomes more electrically large as frequency increases. The UWB strip monopole is found to exhibit linear polarization throughout the band. The polarization is along Y- direction which is the direction of feed strip.

4.9.4 Gain

The measured gain of the antenna in the operating band along the bore sight direction is shown in fig. (4-71). This is compared with the simulated gain also. The discrepancies between the simulated and measured gains can be attributed to the antenna loss effects. However, the simulated and measured gains have a similar tendency. The measured gain error is within 0.5 dBi. The gain varies from 2.5 dBi to 6.5 dBi at different bands for various geometries depending upon the loading.

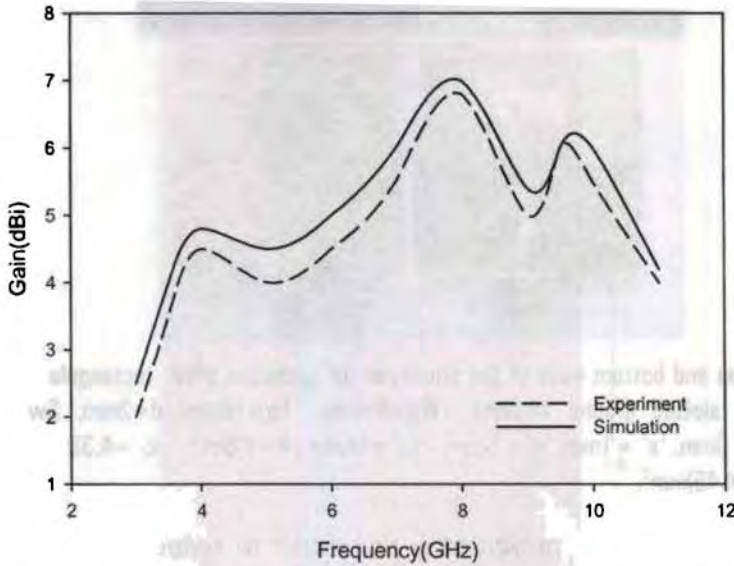


Fig.4.71 The measured and simulated gains for optimized UWB antenna $W_g=45\text{mm}$, $d=2\text{mm}$, $L_g=18\text{mm}$, $Sw=14\text{mm}$, $Sl=10\text{mm}$, $'x'=1\text{mm}$, $'y'=3\text{mm}$, $V_x=18\text{mm}$, $h=1.6\text{mm}$, substrate $\epsilon_r=4.38$ Overall size $(30 \times 45)\text{mm}^2$

4.9.5 Compactness

By adding slots in the ground plane, the size of the printed antenna is shrunk to $(30 \times 40)\text{mm}^2$ from the original size of $(65 \times 50)\text{mm}^2$. However, the impedance characteristics of the printed designs may suffer from strong ground-plane effects. This present method of ground slotting for increasing the Slow Wave Factor (SWF) for microstrip patch antenna is successfully applied to reduce the dimensions of rectangular patch antenna using the discontinuities such as Defected Ground Structure (DGS) as shown in fig.(4-72). Since it has more discontinuities providing larger targets for EM wave, the net result in area reduction of nearly 30%.



Fig.4.72 The top and bottom view of the prototype of optimized UWB rectangular monopole with slotted ground antenna $W_g=45\text{mm}$, $L_g=18\text{mm}$, $d=2\text{mm}$, $S_w=14\text{mm}$, $S_l=10\text{mm}$, 'x' = 1mm, 'y' = 3mm, 'Vx' = 18mm, $h=1.6\text{mm}$, $\epsilon_r=4.38$ Overall size $(30 \times 45)\text{mm}^2$.

Therefore, this work presented a technique to reduce the ground-plane effect on the performance of a small printed UWB antenna. The printed antenna is designed to cover the UWB band of 3.1–10.6 GHz, in particular, the lower band of 3.1–5 GHz. By cutting a rectangular slot (notch) vertically from the ground plane, the overall size of the antenna printed onto a 1.6mm thick PCB is reduced to $(30 \times 45)\text{mm}^2$.

4.10 Combo model with strips and ground slots

4.10.1 Printed Antenna design parameters

The previous studies show that introduction of strips to the radiating patch can extend the operation of the antenna to the UWB spectrum. Similarly the addition of slots on the ground plane can effectively reduce the size of the ground plane to achieve the same operating condition. This section deals with the combined effect of strip on the patch and slots on the ground plane to provide UWB operations with still reduced size for better compactness. The geometry of the Combo model antenna (Ant.III) along with other parameters are shown in fig.(4-73).

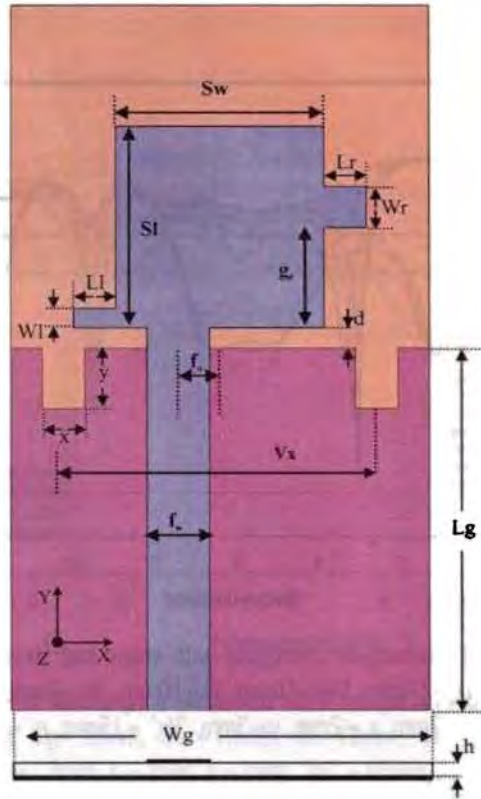


Fig.4.73 Geometry of Combo Model Rectangle Monopole with strips and slots on ground , Truncated ground length ' L_g ', width ' W_g ', rectangular patch length ' S_l ', width ' S_w ', Slot on ground plane –width ' x ', height ' y ', Left strip length ' L_l ', width ' W_l ', Right strip length ' L_r ', width ' W_r ', gap of strip from lower edge of patch –left ' g_l ', right ' g_r ', separation of slots ' V_x '. feed offset ' f_o ' , Substrate with $\epsilon_r = 4.38$, $h = 1.6\text{mm}$.

4.10.2 Parametric Analysis

Having studied the return loss and radiation characteristics of the strip type (Ant.I) and slot type (Ant.II) antenna optimised for the UWB operation, the controlling parameters for the proposed combination of Strips & Slots (Combo Model Ant.III) are studied in depth for thorough understanding of the effect of each parameters on performance of the antenna as described in following sections (a) – (l).

(a) Effect of 'd'

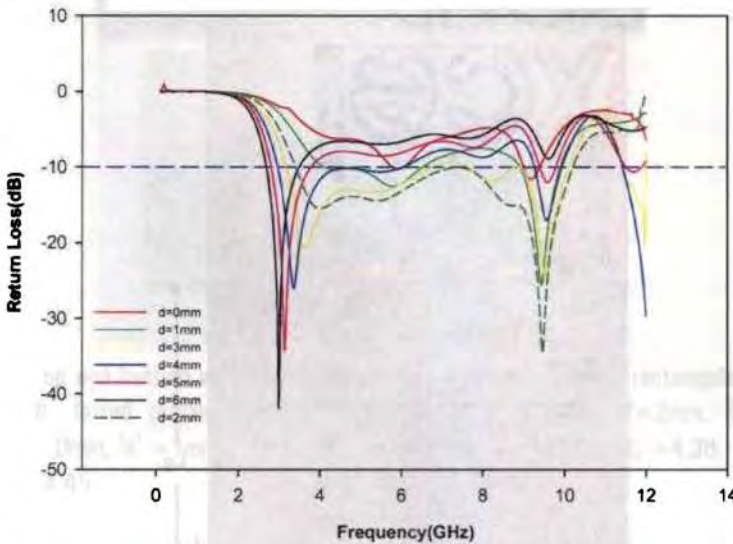


Fig.4.74. Return Loss of Rectangular monopole with strips and slots for 'd', $W_g=20\text{mm}$, $L_l=L_r=2\text{mm}$, $L_g=18\text{mm}$, $S_w=10\text{mm}$, $S_l=10\text{mm}$, $W_r=2\text{mm}$, $W_l=1\text{mm}$, $g_l=0\text{mm}$, $g_r=4\text{mm}$, $'fo' = -2\text{mm}$. $x = 2\text{mm}$, $y = 3\text{mm}$, $'Vx' = 15\text{mm}$, $\epsilon_r = 4.38$, $h = 1.6\text{mm}$

The lower resonant frequency falls with increase of the gap 'd' as seen from the above fig.(4-74). This can be ascribed to the extended current path due to increase of the 'd'. The lower resonant bandwidth decreases with increase in 'd' presumably due to less coupling effect with increasing 'd'.

The gap 'd' has not much impact on the upper resonant frequency but has strong impact on the higher frequency impedance matching. This is very clear from the fig(4-74) that the upper -10dB cut off frequency for UWB operation is maximum for optimized value of $d = 2\text{mm}$. The UWB impedance matching is just possible with $d = 3\text{mm}$, however the bandwidth is comparatively less. The impedance matching deteriorates for $d < 2\text{mm}$ and $d > 3\text{mm}$ and the antenna performance degrades to that of a dual band antenna. Therefore the impedance matching is very sensitive to the feed gap 'd' especially at higher frequencies.

(b) Effect of 'Wg'

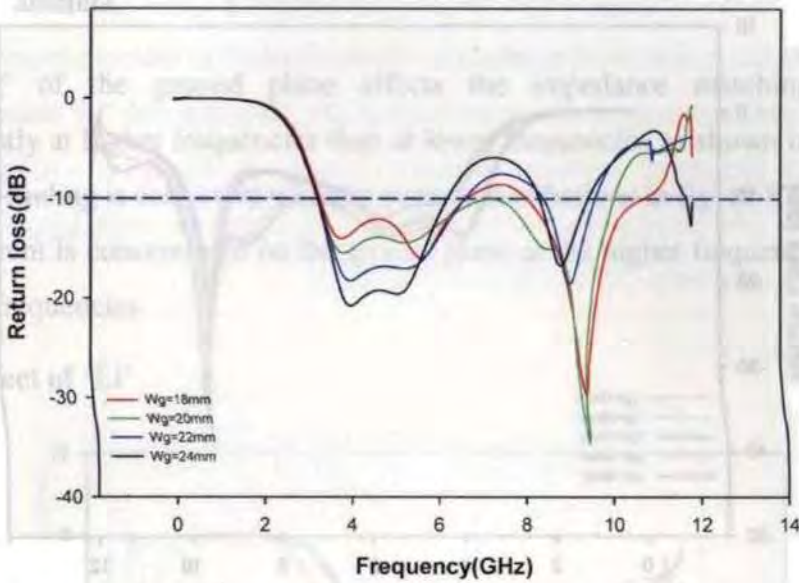


Fig.4-75 Return Loss of Rectangular monopole with strips and slots for 'Wg', $d=2\text{mm}$, $L_l=L_r=2\text{mm}$, $L_g=18\text{mm}$, $S_w=10\text{mm}$, $S_l=10\text{mm}$, $W_r=2\text{mm}$, $W_l=1\text{mm}$, $g_l=0\text{mm}$, $g_r=4\text{mm}$, $f_0=-2\text{mm}$, $x=2\text{mm}$, $y=3\text{mm}$, $V_x=15\text{mm}$, $\epsilon_r=4.38$, $h=1.6\text{mm}$

Return loss characteristics (S11) for the ground width "Wg" varying from 18 to 24mm is shown in the above fig.(4-75). The lower resonant frequency has not much impact on the width of ground plane "Wg" as evident from the figure. This can be ascribed to the no change in current path due to increase of the 'Wg'. However, mid band frequency is affected by width of ground plane. The optimum ground plane width is selected as 20mm.

The "Wg" has much impact on the upper resonant frequency. The upper resonant frequency decreases with increase in "Wg". Operation band is maximum for optimized value of $W_g=20\text{mm}$. The UWB impedance matching is just possible with $W_g=20\text{mm}$ for other cases the band merging does not take place. The impedance matching deteriorates for both $W_g < 20\text{mm}$ and $W_g > 20\text{mm}$ and the antenna performance degrades to that of a dual band antenna.

(c) Effect of 'Lg'

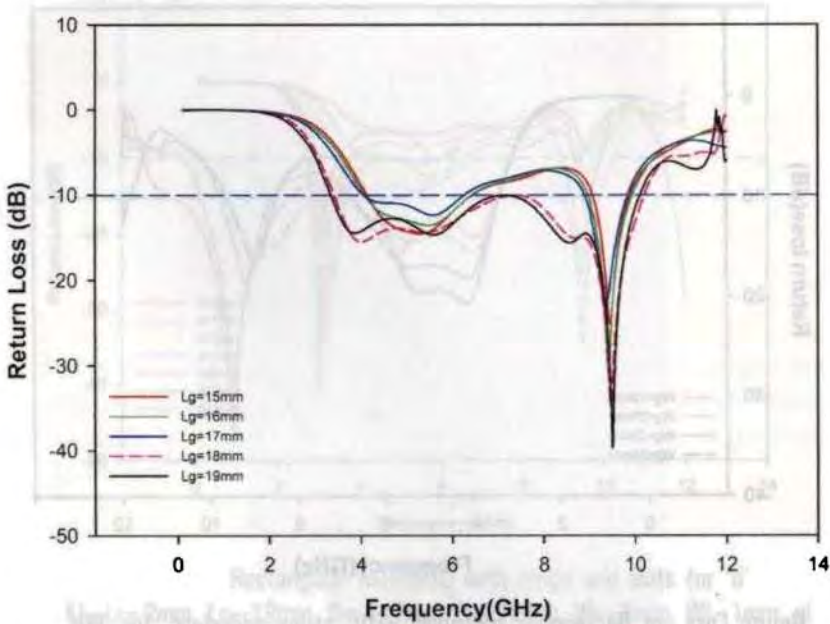


Fig.4.76 Return Loss of Rectangular monopole with strips and slots for 'Lg', $W_g=20\text{mm}$, $d=2\text{mm}$, $L_l=L_r=2\text{mm}$, $S_w=10\text{mm}$, $S_l=10\text{mm}$, $W_r=2\text{mm}$, $W_l=1\text{mm}$, $g_l=0\text{mm}$, $g_r=4\text{mm}$, $f_0=-2\text{mm}$, $x=2\text{mm}$, $y=3\text{mm}$, $V_x=15\text{mm}$, $\epsilon_r=4.38$, $h=1.6\text{mm}$

The lower resonant frequency has much impact on the length of ground plane "Lg" as seen from the above return loss characteristics (S11) for ground length "Lg" varying from 15 to 19mm fig.(4-76). This can be due to the increase in current path due to increase of the 'Lg' at the threshold of $\sim 0.7\lambda_{gd}$. The first resonance is strong at 4GHz and the 2nd resonance at 8GHz play a vital role in pulling the strong 4th resonance at the upper band cause merging the band resulting in UWB characteristic.

The "Lg" has not much impact on the upper resonant frequency. A slight decrease in resonant frequency 'fr' is noticed with increase in "Lg". The UWB impedance matching is just possible with Lg=18mm for all other cases the band merging does not take place. The impedance matching deteriorates for both

$L_g < 18\text{mm}$ and $L_g > 18\text{mm}$ and the antenna performance degrades to that of a dual band antenna.

' L_g ' of the ground plane affects the impedance matching more significantly at higher frequencies than at lower frequencies as shown in fig.(4-76). This finding is consistent with the current distributions in fig. (4-87), where more current is concentrated on the ground plane at the higher frequencies than at lower frequencies

(d) Effect of ' L_l '

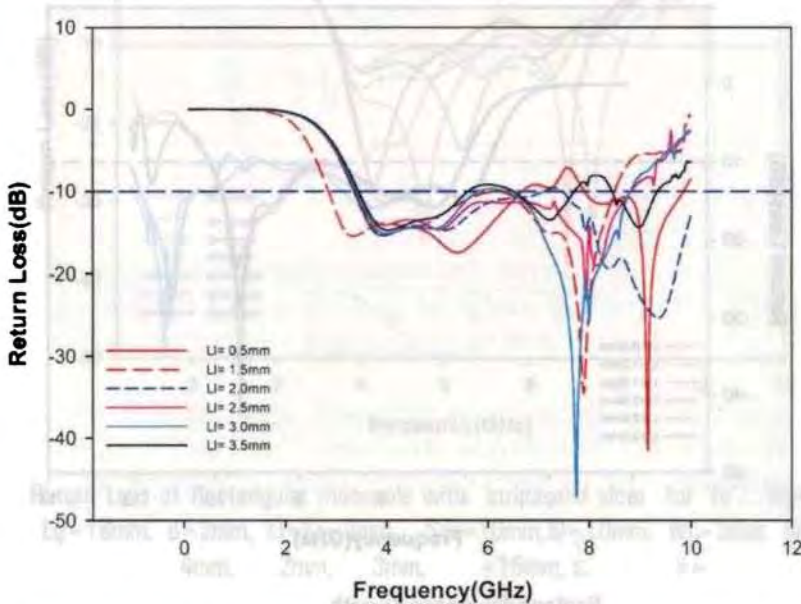


Fig.4.77 Return Loss of Rectangular monopole with strips and slots for ' L_l ', $W_g=20\text{mm}$, $L_g=18\text{mm}$, $d=2\text{mm}$, $L_r=2\text{mm}$, $S_w=10\text{mm}$, $S_l=10\text{mm}$, $W_r=2\text{mm}$, $W_l=1\text{mm}$, $g_l=0\text{mm}$, $g_r=4\text{mm}$, $f_0=-2\text{mm}$. $x=2\text{mm}$, $y=3\text{mm}$, ' V_x ' = 15mm , $\epsilon_r=4.38$, $h=1.6\text{mm}$

This a very important controlling parameter as seen from the fig.(4-77). There is a upward shift in the upper resonant frequency while the lower band has not much impact on ' L_l '. The transition shift takes place at the optimized ' L_l ' value of 2mm .

The lower resonant frequency is nearly independent and upper resonant frequency falls with increase or decrease of the left strip arm length “Ll” about the optimized value as seen from the above fig.(4-77). This can be ascribed to the extended current path due to increase of the ‘Ll’ The gap ‘Ll’ has not much impact on the upper resonant frequency except at the upper -10dB cut off frequency. The large impedance matching is just possible with $Ll=2.0\text{mm}$ and deteriorates for both $Ll<2.0\text{mm}$ and $Ll>2.0\text{mm}$.

(e) Effect of ‘Lr’

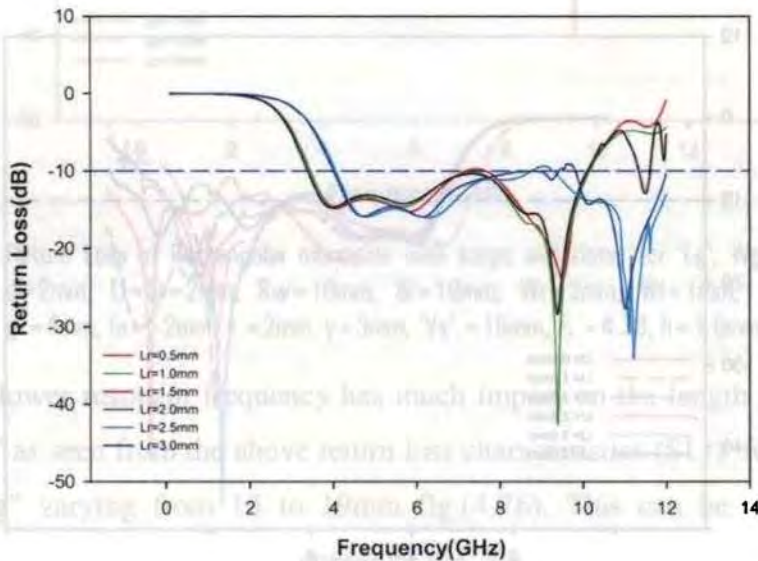


Fig. 4.78 Return Loss of Rectangular monopole with strips and slots for ‘Lr’, $Wg=20\text{mm}$, $Lg=18\text{mm}$, $d=2\text{mm}$, $Ll=2\text{mm}$, $Sw=10\text{mm}$, $Sl=10\text{mm}$, $Wr=2\text{mm}$, $Wl=1\text{mm}$, $gl=0\text{mm}$, $gr=4\text{mm}$, $fo=-2\text{mm}$, $x=-2\text{mm}$, $y=3\text{mm}$, $Vx=15\text{mm}$, $\epsilon_r=4.38$, $h=1.6\text{mm}$

‘Lr’ is also very important controlling parameter as seen from the fig.(4-78). Here both the bands are influenced by ‘Lr’, There is a upward shift in the lower and upper resonant frequency. The transition shift takes place at the optimized ‘Lr’ value of 2mm. The entire band gets shifted by 0.75GHz in lower band and 1.5GHz in the upper band. So ‘Lr’ is a very critical design parameter.

The lower resonant frequency falls with increase of the right strip arm length “ L_r ” as seen from the above figure for ‘ L_r ’ varied from 0.5 to 3mm. This may be due to the increased current path due to ‘ L_r ’. The gap ‘ L_r ’ has not much impact on the upper resonant frequency except at the upper cut off frequency.

(f) Effect of ‘ f_0 ’

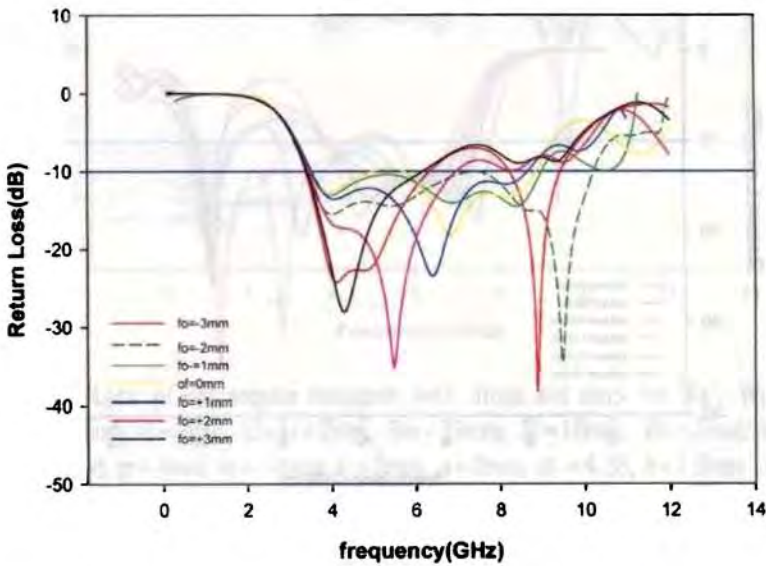


Fig.4.79 Return Loss of Rectangular monopole with strips and slots for ‘ f_0 ’, $W_g=20\text{mm}$, $L_g=18\text{mm}$, $d=2\text{mm}$, $L_l=L_r=2\text{mm}$, $Sw=10\text{mm}$, $Sl=10\text{mm}$, $Wr=2\text{mm}$, $Wl=1\text{mm}$, $gl=0\text{mm}$, $gr=4\text{mm}$, $x=2\text{mm}$, $y=3\text{mm}$, ‘ V_x ’ = 15mm , $\epsilon_r=4.38$, $h=1.6\text{mm}$

The lower cutoff frequency has not much impact on the feed offset as seen from fig.(4-79). This means there is no change in current path due to increase or decrease of the ‘ f_0 ’. The positive feed offset means shift of the feed strip towards right side with respect to the centre line. The feed offset mainly changes the impedance value.

The ‘ f_0 ’ has strong impact on the upper resonant frequency which decreases with increase or decrease with respect to the optimized offset

value 'fo'. The UWB impedance matching is just possible only with 'fo' = -2mm for all other cases two distinct bands are observed. The impedance matching deteriorates for both $fo < -2\text{mm}$ and $fo > -2\text{mm}$ and the antenna performance degrades to that of a dual band antenna as seen from fig.(4-79).

(g) Effect of 'SI'

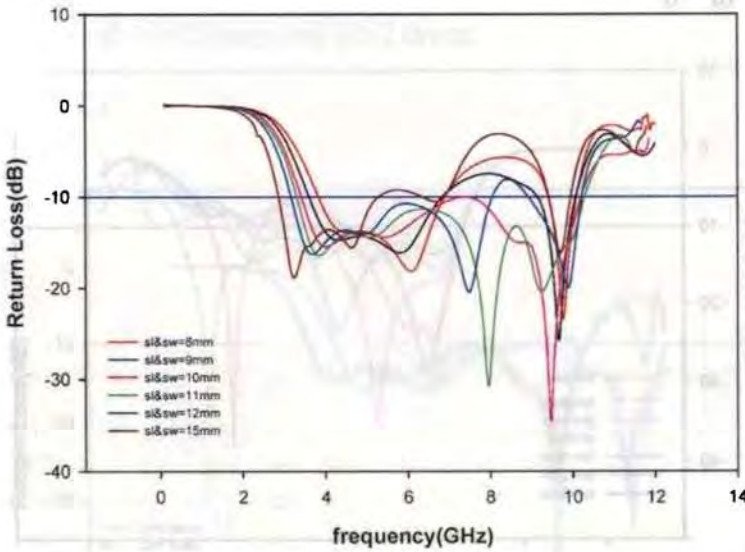


Fig.4.80 Return Loss of Rectangular monopole with strips and slots for 'SI &Sw', $Wg=20\text{mm}$, $Lg=18\text{mm}$, $d=2\text{mm}$, $Ll=Lr=2\text{mm}$, 'fo' = -2mm, $Wr=2\text{mm}$, $Wl=1\text{mm}$, $gl=0\text{mm}$, $gr=4\text{mm}$, $x=2\text{mm}$, $y=3\text{mm}$, 'Vx' = 15mm, $\epsilon_r=4.38$, $h=1.6\text{mm}$

The lower resonant frequency falls with increase in dimension of the patch(Sw &SI) as seen from the above fig.(4-80).

The patch dimension has not much impact on the upper resonant frequency except the upper cut off frequency. The bandwidth is maximum for optimized value of $SI=Sw=10\text{mm}$ and 11mm . The impedance matching deteriorates for $SI=Sw$ above 11mm and below 10mm and the antenna performance degrades to that of a dual band antenna. Therefore

UWB impedance matching is possible with this combination of patch dimension.

(b) Effect of 'Vx'

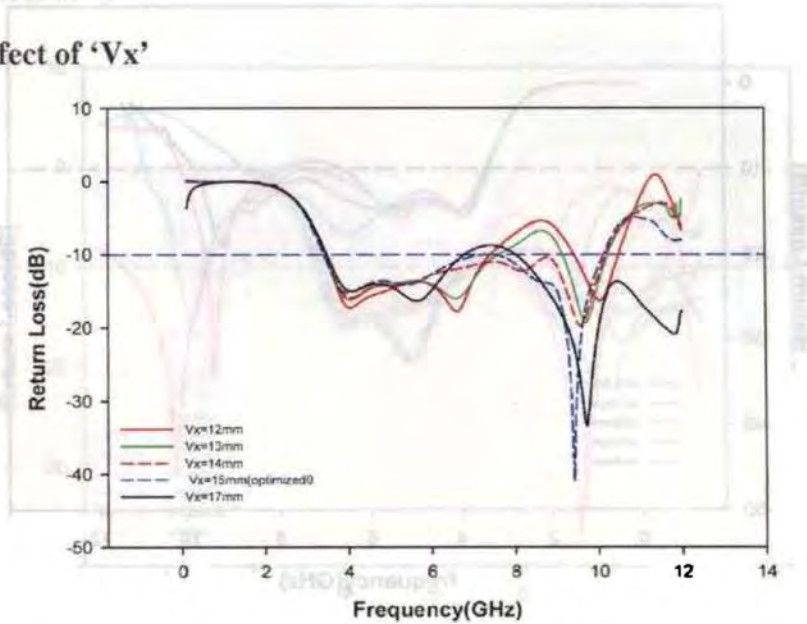


Fig.4.81 Return Loss of Rectangular monopole with strips and slots for 'Vx', $W_g=20\text{mm}$, $L_g=18\text{mm}$, $d=2\text{mm}$, $L_l=L_r=2\text{mm}$, $S_w=10\text{mm}$, $S_l=10\text{mm}$, $W_r=2\text{mm}$, $W_l=1\text{mm}$, $g_l=0\text{mm}$, $g_r=4\text{mm}$, $f_0=-2\text{mm}$, $x=2\text{mm}$, $y=3\text{mm}$, $\epsilon_r=4.38$, $h=1.6\text{mm}$

The lower resonant frequency has not much impact on the slot gap vector as seen from the above fig. (4-81). The "Vx" has strong impact on the middle resonant frequency which decreases the UWB characteristics with increase or decrease with respect to the optimized value 'Vx'. UWB operation with maximum bandwidth is optimized for $V_x = 15\text{mm}$. The UWB impedance matching is just possible only with $V_x=\lambda_d$ for other cases the proper band merging does not take place.

(i) Effect of 'x'

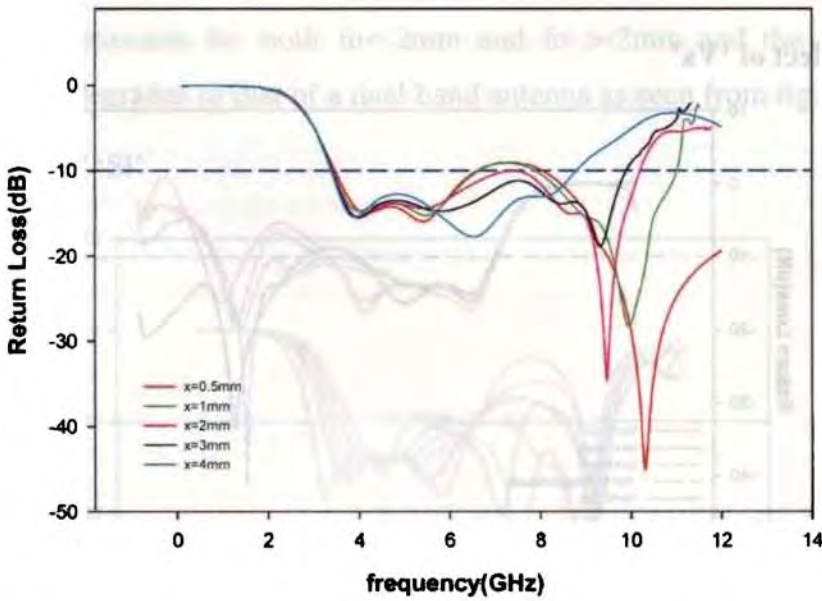


Fig.4.82 Return Loss of Rectangular monopole with strips and slots for 'x', $W_g = 20\text{mm}$, $L_g = 18\text{mm}$, $d = 2\text{mm}$, $L_l = L_r = 2\text{mm}$, $S_w = 10\text{mm}$, $S_l = 10\text{mm}$, $W_r = 2\text{mm}$, $W_l = 1\text{mm}$, $g_l = 0\text{mm}$, $g_r = 4\text{mm}$, $f_0 = -2\text{mm}$, $V_x = 15\text{mm}$, $y = 3\text{mm}$, $\epsilon_r = 4.38$, $h = 1.6\text{mm}$.

The lower resonant frequency is independent of rectangular slot width in ground plane 'x' as seen from the above fig.(4-82) Return loss characteristics (S11) for the slot width "x" varying from 0 to 4mm. This can be ascribed to the no change in current path due to increase of the 'x'.

The rectangular slot height 'x' has much impact on the upper resonant frequency and inversely proportional to 'x'. However -10dB bandwidth for UWB operation is maximum only with very small 'x'. The optimized value of 'x' is chosen as $0.12 \lambda_d$.

(j) Effect of 'y'

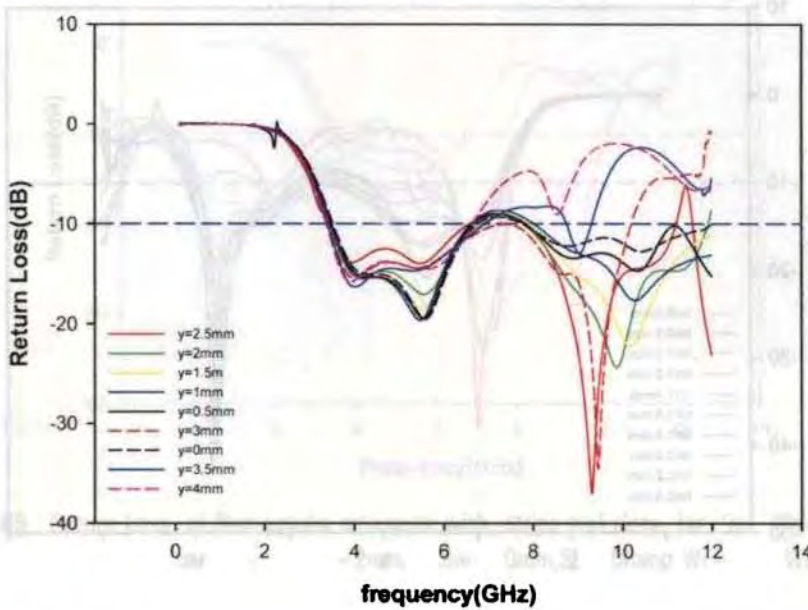


Fig.54.83 Return Loss of Rectangular monopole with strips and slots for 'y', $W_g=20\text{mm}$, $L_g=18\text{mm}$, $d=2\text{mm}$, $L_l=L_r=2\text{mm}$, $S_w=10\text{mm}$, $S_l=10\text{mm}$, $W_r=2\text{mm}$, $W_L=1\text{mm}$, $g_l=0\text{mm}$, $g_r=4\text{mm}$, $f_0=-2\text{mm}$, $V_x=15\text{mm}$, $x=2\text{mm}$, $\epsilon_r=4.38$, $h=1.6\text{mm}$.

The lower resonant frequency is independent of rectangular slot height in ground plane 'y' as seen from the above fig.(4-83). This means no change in the current path due to 'y' for lower resonance. The rectangular slot height 'y' has much impact on the upper resonant frequency and its cutoff value. The UWB impedance matching is just possible only with $y=3\text{mm}$.

(k) Effect of 'h'

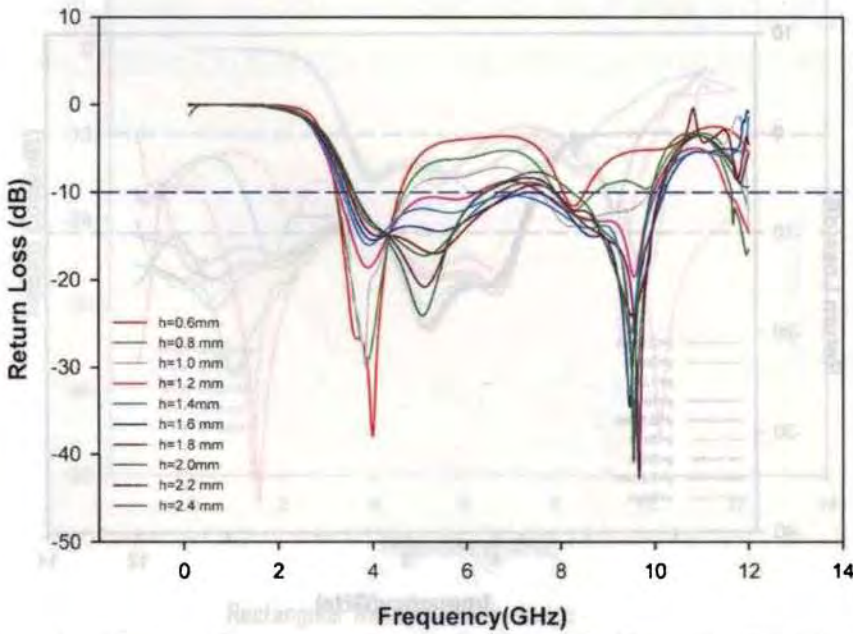


Fig.4.84 Return Loss of Rectangular monopole with strips and slots for 'h', $W_g=20\text{mm}$, $L_g=18\text{mm}$, $d=2\text{mm}$, $L_l=L_r=2\text{mm}$, $S_w=10\text{mm}$, $S_l=10\text{mm}$, $W_r=2\text{mm}$, $W_L=1\text{mm}$, $g_l=0\text{mm}$, $g_r=4\text{mm}$, $f_0=-2\text{mm}$, $V_x=15\text{mm}$, $x=2\text{mm}$, $y=3\text{mm}$, $\epsilon_r=4.38$.

The impedance response is also affected by the height of substrate. The change in the 'h' leads to a shift in the characteristic impedance of the feeding strip from $50\ \Omega$. This causes the drastic impedance mismatch at the input level resulting in sudden fall in bandwidth. Therefore independent optimization is required for UWB operation for a given substrate of specified height.

c

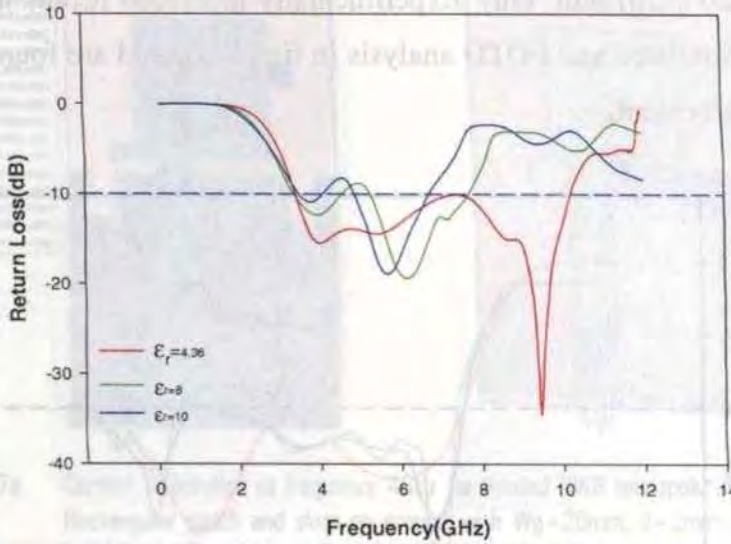
(I) Effect of ' ϵ_r '

Fig.4.85 Return Loss of Rectangular monopole with strips and slots for ' ϵ_r '. $W_g=20\text{mm}$, $L_g=18\text{mm}$, $d=2\text{mm}$, $L_l=L_r=2\text{mm}$, $S_w=10\text{mm}$, $S_l=10\text{mm}$, $W_r=2\text{mm}$, $W_l=1\text{mm}$, $g_l=0\text{mm}$, $g_r=4\text{mm}$, $f_o=-2\text{mm}$, ' V_x ' = 15mm , $x=2\text{mm}$, $y=3\text{mm}$, $h=1.6\text{mm}$.

The impedance response is also affected by the dielectric constant ' ϵ_r ' as shown in fig.(4-85). The dielectric constant leads to a shift in the characteristic impedance of the feeding strip from $50\ \Omega$. This causes the drastic impedance mismatch at the input level resulting in sudden fall in bandwidth.

4.10.3 Optimized Printed UWB Combo Antenna

The optimization was done for the following model with different controlling parameters $W_g=20\text{mm}$, Feed gap $d=2\text{mm}$, strip length $L_l=L_r=2\text{mm}$, $L_g=18\text{mm}$, Regular rectangular Patch of $S_w=10\text{mm}$, $S_l=10\text{mm}$, strip widths $W_r=2\text{mm}$, $W_l=1\text{mm}$, strip gap from patch bottom edge left- $g_l=0\text{mm}$, right- $g_r=4\text{mm}$, feed offset $f_o=-2\text{mm}$, slot width $x=2\text{mm}$, slot height $y=3\text{mm}$, separation between slots in x direction $V_x=15\text{mm}$. Model fabricated on substrate with $\epsilon_r=4.38$, $h=1.6\text{mm}$ size and tested using HP

8510C Network Analyzer. With the said parameters the overall size of antenna is (20×30) mm² only. Experimentally measured results are plotted along with simulated and FDTD analysis in fig.(4-86) and are found to be in very good agreement.

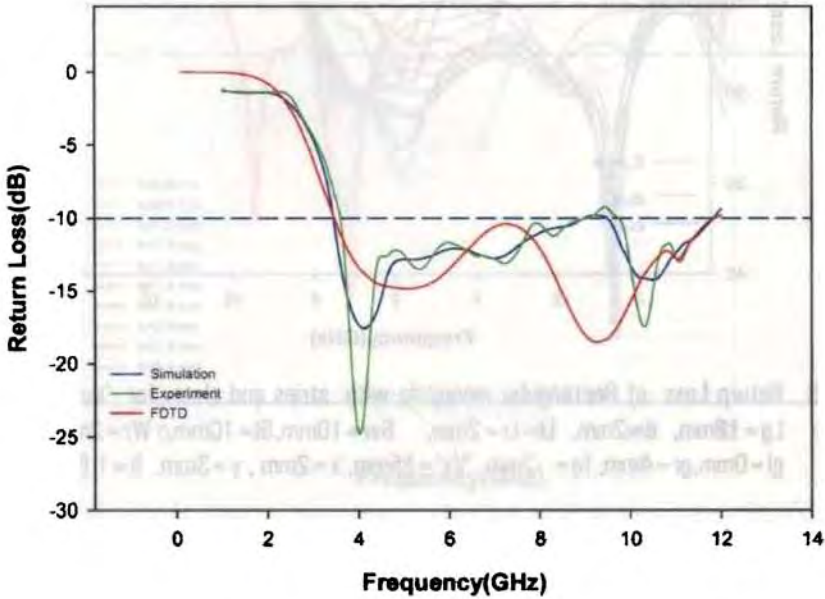


Fig.4.86 Optimised Return loss for Printed UWB Rectangular monopole with strips and slots
 $W_g = 20$ mm, $d = 2$ mm, $L_l = L_r = 2$ mm, $L_g = 18$ mm, $S_w = 10$ mm, $S_l = 10$ mm, $W_r = 2$ mm,
 $W_l = 1$ mm, $g_l = 0$ mm, $g_r = 4$ mm, $f_o = -2$ mm, $x = 2$ mm, $y = 3$ mm, $V_x = 15$ mm, $\epsilon_r = 4.38$,
 $h = 1.6$ mm

This optimized findings in fig.(4-86) is consistent with the surface current distributions in Fig. (4-87a-e), studied in detail for different resonant frequencies. It is seen that more current is concentrated on the ground plane at the higher frequencies than at lower frequencies.

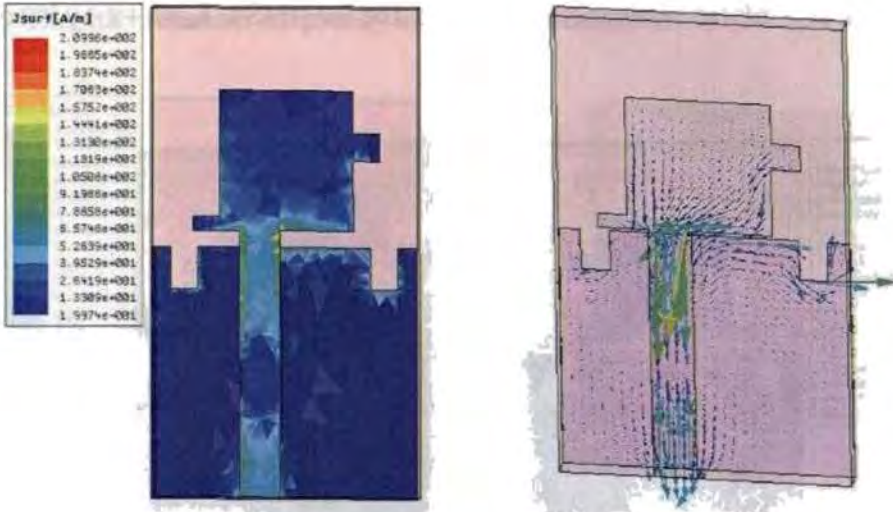


Fig. 4.87a Current distribution at frequency 4GHz for Printed UWB monopole with strips on Rectangular patch and slots on ground with $W_g=20\text{mm}$, $d=2\text{mm}$, $L_l=L_r=2\text{mm}$, $L_g=18\text{mm}$, $S_w=10\text{mm}$, $S_l=10\text{mm}$, $W_r=2\text{mm}$, $W_l=1\text{mm}$, $g_l=0\text{mm}$, $g_r=4\text{mm}$, $f_o = -2\text{mm}$, $x = 2\text{mm}$, $y = 3\text{mm}$, $V_x = 15\text{mm}$, $\epsilon_r = 4.38$, $h = 1.6\text{mm}$

This 1st resonant at 4 GHz corresponds to the length $(S_w-f_w)/2 + g_r+L_r+d = \lambda_d/4$. This has been validated by simulated and measured results.

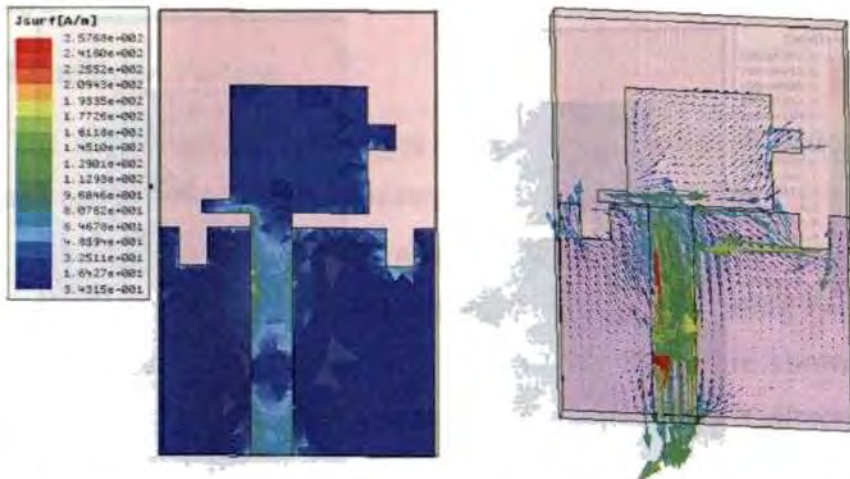


Fig.4.87b Current distribution at frequency 6GHz for Printed UWB monopole with strips on Rectangular patch and slots on ground with $W_g=20\text{mm}$, $d=2\text{mm}$, $L_l=L_r=2\text{mm}$, $L_g=18\text{mm}$, $S_w=10\text{mm}$, $S_l=10\text{mm}$, $W_r=2\text{mm}$, $W_l=1\text{mm}$, $g_l=0\text{mm}$, $g_r=4\text{mm}$, $f_o = -2\text{mm}$, $x = 2\text{mm}$, $y = 3\text{mm}$, $V_x = 15\text{mm}$, $\epsilon_r = 4.38$, $h = 1.6\text{mm}$

The 2nd 6GHz resonance is due to the length $(Sw-f_w)/2 + x + y$ is equal to $\lambda_d/4$.

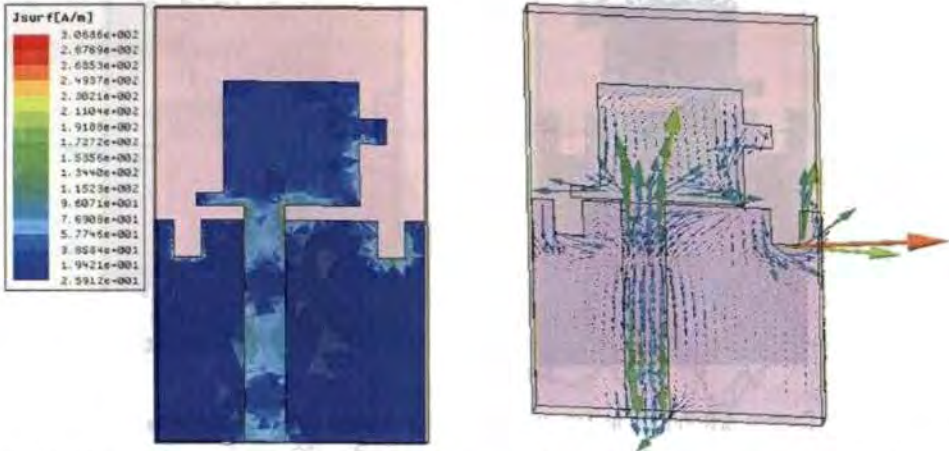


Fig.4.87c Current distribution at higher frequency 8.75GHz for Printed UWB monopole with strips on Rectangular patch and slots on ground with $W_g=20\text{mm}$, $d=2\text{mm}$, $L_l=L_r=2\text{mm}$, $L_g=18\text{mm}$, $Sw=10\text{mm}$, $Sl=10\text{mm}$, $Wr=2\text{mm}$, $Wl=1\text{mm}$, $gl=0\text{mm}$, $gr=4\text{mm}$, $f_o=-2\text{mm}$, $x=2\text{mm}$, $y=3\text{mm}$, $V_x=15\text{mm}$, $\epsilon_r=4.38$, $h=1.6\text{mm}$

The 3rd resonant frequency at 8.75GHz corresponds to $(Sw/2 + f_o + y) = \lambda_d/2$.

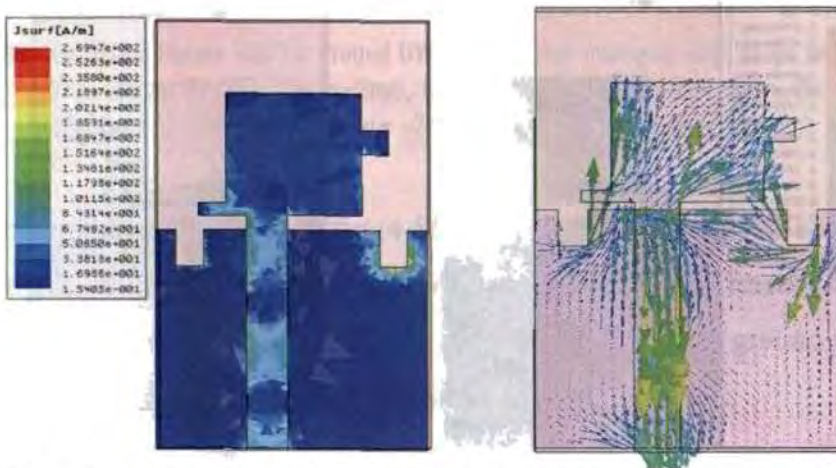


Fig.4.87d Current distribution at higher frequency 9.5GHz for Printed UWB monopole with strips on Rectangular patch and slots on ground with $W_g=20\text{mm}$, $d=2\text{mm}$, $L_l=L_r=2\text{mm}$, $L_g=18\text{mm}$, $Sw=10\text{mm}$, $Sl=10\text{mm}$, $Wr=2\text{mm}$, $Wl=1\text{mm}$, $gl=0\text{mm}$, $gr=4\text{mm}$, $f_o=-2\text{mm}$, $x=2\text{mm}$, $y=3\text{mm}$, $V_x=15\text{mm}$, $\epsilon_r=4.38$, $h=1.6\text{mm}$

The 4th resonant frequency at 9.5GHz corresponds to $(Sl-2gl+Wl)=\lambda_d/2$

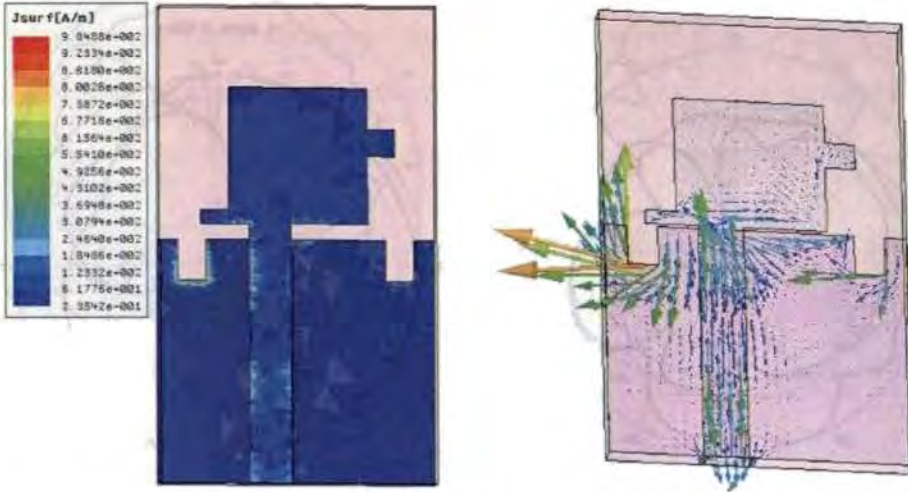
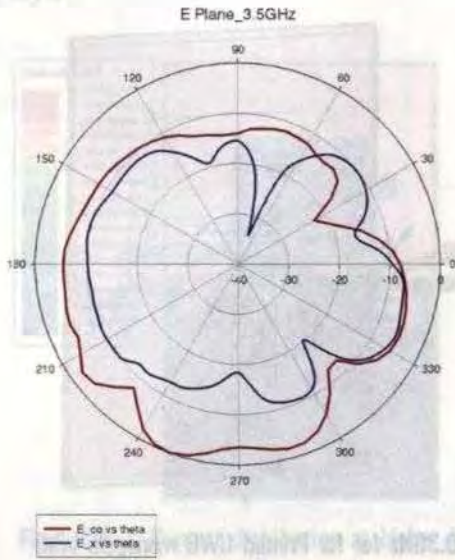


Fig.4-87e Current distribution at higher frequency 10.3GHz for for Printed UWB monopole with strips on Rectangular patch and slots on ground with $Wg=20\text{mm}$, $d=2\text{mm}$, $Ll=Lr=2\text{mm}$, $Lg=18\text{mm}$, $Sw=10\text{mm}$, $Sl=10\text{mm}$, $Wr=2\text{mm}$, $Wl=1\text{mm}$, $gl=0\text{mm}$, $gr=4\text{mm}$, $fo=-2\text{mm}$, $x=2\text{mm}$, $y=3\text{mm}$, $Vx=15\text{mm}$, $\epsilon_r=4.38$, $h=1.6\text{mm}$

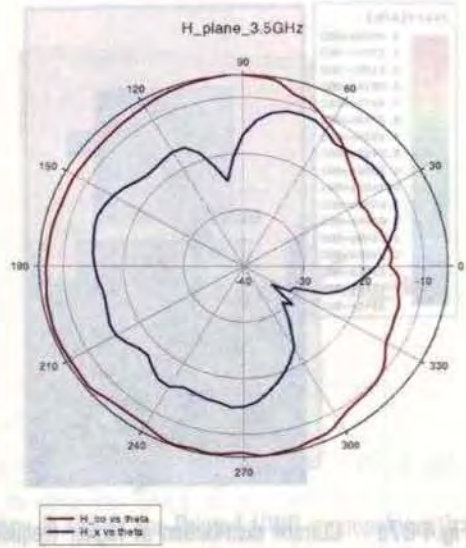
The 5th resonant frequency at 10.34GHz corresponds to $(Sw/2 -fo+Ll+y+d-Wl) = \lambda_d/2$.

4.10.4 Radiation Pattern

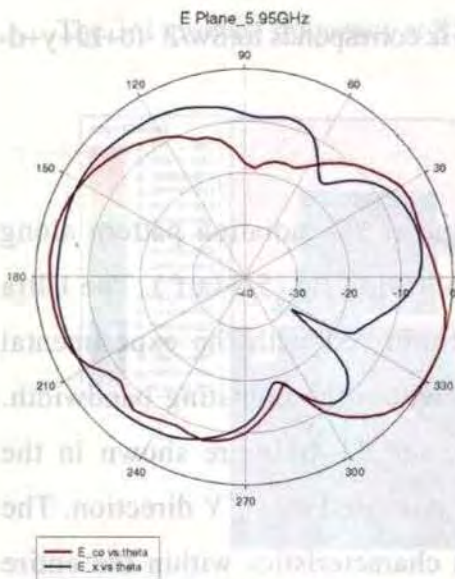
The experimental copolar and crosspolar 2D radiation pattern along E- plane and H- plane are shown in the following fig.(5-34a-f). The Ultra Wide Band behavior of the antenna is confirmed with the experimental radiation patterns at different frequencies within the operating bandwidth. Measured radiation patterns at 3.5, 5.95, and 11 GHz are shown in the Figure (4.88a-f). The antenna is vertically polarized along Y direction. The antenna exhibits monopole type radiation characteristics within the entire UWB range.



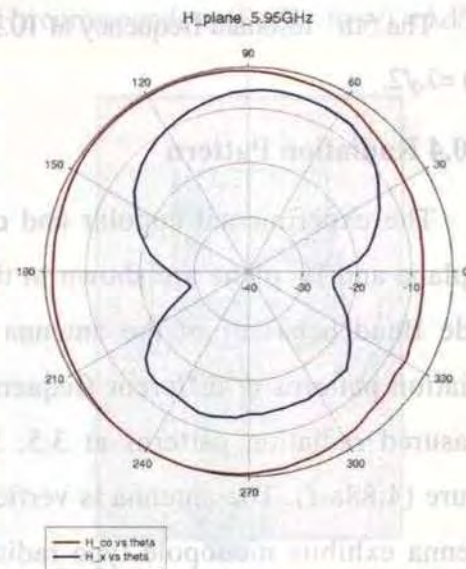
(a)



(b)



(c)



(d)

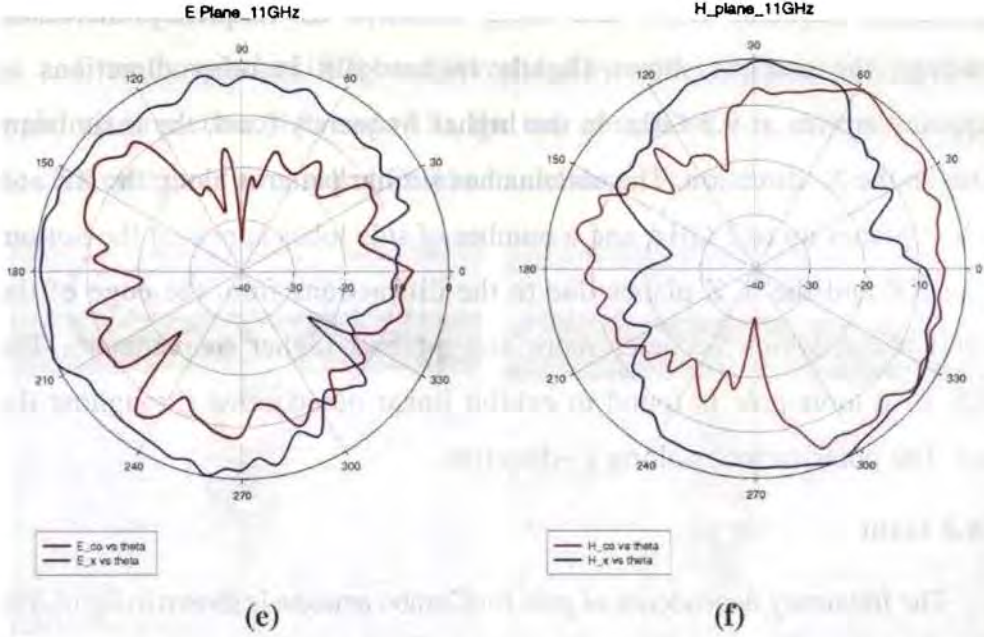


Fig.4.88a-f E-plane and H-plane Radiation pattern for Printed Rectangular UWB monopole with strips and slots on ground, $W_g=20\text{mm}$, $d=2\text{mm}$, $L_l=L_r=2\text{mm}$, $L_g=18\text{mm}$, $S_w=10\text{mm}$, $S_l=10\text{mm}$, $W_r=2\text{mm}$, $W_l=1\text{mm}$, $g_l=0\text{mm}$, $g_r=4\text{mm}$, $f_o=-2\text{mm}$, $x=-2\text{mm}$, $y=3\text{mm}$, $V_x=15\text{mm}$, $\epsilon_r=4.38$, $h=1.6\text{mm}$

These patterns are better compared to the measured ones for Ant I and II, which were presented in 4.8 and 4.9. The radiation patterns are nearly uniform in H-plane. However, at higher frequencies they exhibit more ripples. The radiation patterns of all the antennas are very much similar in horizontal plane.

The H- plane radiation pattern is almost uniform at all frequencies except at the band end. However, the E- plane pattern is slightly distorted but seems to be stable in the entire band. Radiation characteristics of the proposed UWB antenna are experimentally analyzed. Each pattern is normalized with respect to the peak gain along the corresponding plane. In the lower frequency band, the antenna has uniform radiation pattern in the azimuth plane due to its electrically small dimensions. The main beam in the

X-direction becomes more and more directive as frequency increases. However, the antenna shows slightly higher gain in other directions as frequency arrives at 9.5 GHz. In the higher frequency band, the main beam points to the X- direction. The antenna has similar patterns along the XZ and the Y Z planes up to 7 GHz, and a number of side lobes appear at the bottom of the XZ and the Y Z planes due to the diffractions from the edge of the ground plane, which becomes more and more at higher frequencies . The UWB strip monopole is found to exhibit linear polarization throughout the band. The polarization is along y –direction.

4.10.5 Gain

The frequency dependence of gain for Combo antenna is shown in fig.(4-89). The maximum gain of 7.4dBi is observed at the higher frequency. The measured gain is in good agreement with simulated gain as seen from the figure.

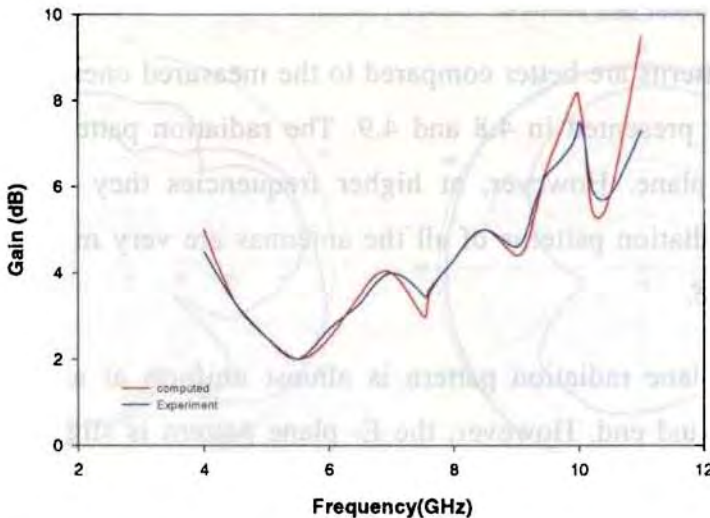


Fig.4.89 The measured and simulated gains for Printed Rectangular UWB monopole with strips and slots on ground, $W_g=20\text{mm}$, $d=2\text{mm}$, $L_l=L_r=2\text{mm}$, $L_g=18\text{mm}$, $S_w=10\text{mm}$, $S_l=10\text{mm}$, $W_r=2\text{mm}$, $W_l=1\text{mm}$, $g_l=0\text{mm}$, $g_r=4\text{mm}$, $f_o=-2\text{mm}$, $x=2\text{mm}$, $y=3\text{mm}$, $V_x=15\text{mm}$, $\epsilon_r=4.38$, $h=1.6\text{mm}$

4.10.6 Compactness

Even though the UWB band is realized by adding strips or cutting slot as explained in section (4.8) and (4.9), the true compactness is achieved through the combination of two, called Combo model described in this section (4.10).

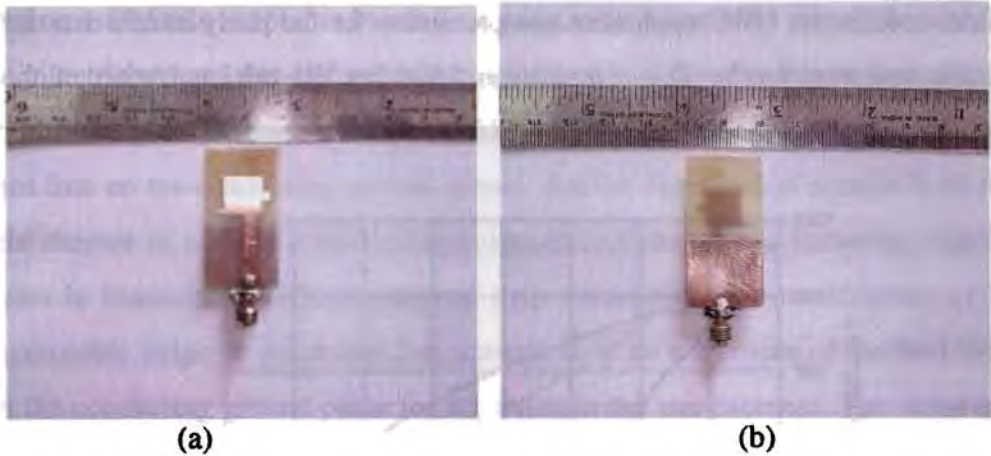


Fig.4.90a,b The top and bottom view of the prototype Printed UWB monopole (size 20X 30mm²). Rectangular monopole with strips and slots on ground, $W_g=20\text{mm}$, $d=2\text{mm}$, $L_l=L_r=2\text{mm}$, $L_g=18\text{mm}$, $S_w=10\text{mm}$, $S_l=10\text{mm}$, $W_r=2\text{mm}$, $W_L=1\text{mm}$, $g_l=0\text{mm}$, $g_r=4\text{mm}$, $f_o=-2\text{mm}$, $x=-2\text{mm}$, $y=3\text{mm}$, $V_x=15\text{mm}$, $\epsilon_r=4.38$, $h=1.6\text{mm}$

The physical size and shape of the antenna fabricated and tested is shown in photograph fig.(4-90) highlighting the prints on the either side of the substrate.

4.10.7 Efficiency

Typical approaches for realizing electrically small antennas involve adding inductance to reduce the inherent capacitance in small antennas. Sometimes a top loading structure is introduced to provide additional inductance and capacitance [6]. This approach leads to an antenna with low efficiency, low gain, or narrow bandwidth. In this thesis, we investigate small UWB antennas with a top-loading structure that retains desirable properties. The measured efficiency using the wheeler cap method is found to be 88% average across the UWB band.

4.10.8 Phase response and Group delay.

The antenna designed has got good phase linearity as seen from the fig.(4-91). The group delay for the reflected signal fig.(4-92) is quite stable and well within the 1.2ns except for 1.7ns at 5.2GHz (s5150-5350MHz) band for HIPERLAN ,which is seldom used in the UWB applications as precaution for the likely interference for existing operating bands. The compactness following the miniaturization of the antenna is one of the main reasons for this excellent performance.

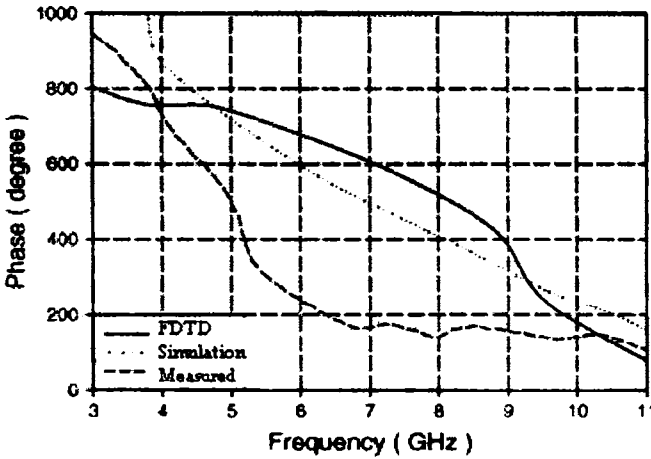


Fig. 4.91 Phase Response characteristic

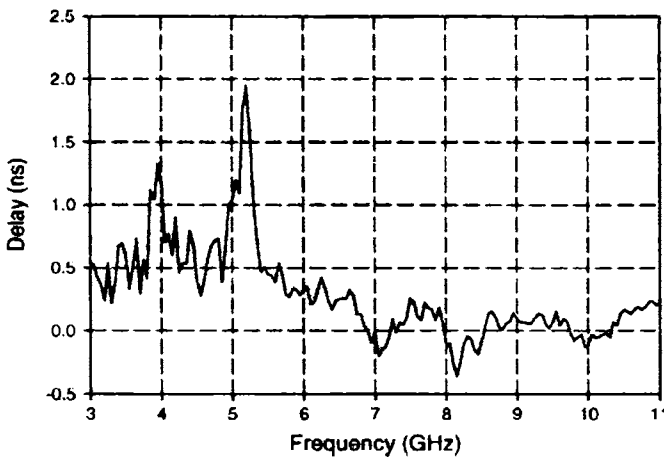


Fig. 4-92 measured group delay characteristics

4.11 Conclusion

The thesis has reported on the investigation on various designs of printed planar monopole antennas for UWB applications. Three different antenna designs (designated here as Ant I, II and III) are proposed. Ant- I described in section 4.8 of this chapter is basically a wide rectangular strip monopole with 2 asymmetric strips. Ant-II described in section 4.9 of this chapter, is basically a wide rectangular strip monopole with 2 symmetric slots on either side of the feed line on the conducting ground plane. Ant-III described in section 4.10 of this chapter is a combination (Combo) model of above two antennas, which again is basically a wide rectangular strip monopole with combination of 2 asymmetric strips on patch and 2 symmetric slots on either side of the feed line on the conducting ground plane for achieving better compactness. The strips on radiating patch and slots on the ground plane have been optimized after exhaustive experimental and simulation studies. All these above described antennas with strips, slots or Combo model (Ant I, II and Ant III) exhibit Ultra wide bandwidth. The systematic evolution of a compact UWB antenna is consolidated and presented in different sections of the chapter.

The calculated radiation patterns are near uniform in horizontal plane in the operating band. However, at higher frequencies they exhibit more ripples. The obtained results indicate that Ant-III is most compact among the three and considered to be most suitable for UWB applications compared to the printed planar monopole antennas Ant-I and II. The planar format, which makes them a more suitable at UWB microwave applications. Optimal design provides an antenna of overall size $(20 \times 30) \text{ mm}^2$, which could be the smallest planar antenna reported to satisfy the specification for $VSWR < 2$ at 3.1 to 10.6 GHz. Measured results have been presented for the return loss and gain patterns as a function of frequency. The proposed antenna features compact size, wide

impedance bandwidth, and consistent radiation patterns over the ultra wideband frequency spectrum as seen from the results. The characteristics of the proposed antenna, in frequency domain are measured and compared with simulation and FDTD computations.

Recently, several broadband monopole configurations, such as circular, rectangular, elliptical, pentagonal and hexagonal, have been proposed for UWB applications [4]–[7]. These broadband monopoles feature wide operating bandwidths, satisfactory radiation properties, simple structures and ease of fabrication. However, they are not planar structures because their ground planes are perpendicular to the radiators. As a result, they are not suitable for integration with a printed circuit board.

A compact and low-profile printed strip & Ground slot (Combo type monopole) with direct feed is presented. It is a good candidate for UWB application and can be integrated with transceivers, mobile phones, laptops etc.. Parametric studies have been done for further investigations to provide the design engineers with useful design information.

A comparison of the proposed antenna in the thesis with the recent reported UWB antenna is given in the Table (4-4). Usually, such printed antennas have the broad impedance bandwidth with compact size of around (40 X 50) mm². By slotting the radiator and/or modifying the shapes of radiator as well as the ground plane, the size of the printed antenna is reported to have shrunk to (30 X 30)mm² [12]–[16]. But in this case reported in thesis the size is (20 X 30) mm² for achieving UWB performance which can directly go into handheld terminals of futuristic UWB mobile services.

Table 4.4 Comparison of performance of recent Printed Antennas reported

Sl.No.	Type of UWB Antenna	size	Bandwidth	Maximum Peak Gain	Efficiency
1	Strip monopole	(68X65)mm ²	800MHz	3.6dBi	82%
2	Dumbbell shaped	(65X65)mm ²	1.120GHz	4.5dBi	75%-85%
3	Loaded monopoles	(40X65)mm ²	3.6- 9GHz	6dBi	79%-87%
4	Printed antenna	(40X50)mm ²	3.1- 10.6GHz	4.5dBi	75%-85%
5	Branched Monopole	(35X65)mm ²	2.95- 11.6GHz	5dBi	79%-90%
6	CPW rhombic	(30X20)mm ²	3.1- 11.9GHz	6.54dBi	76%-85%
7	strip loaded Rectangle monopole	(35X45)mm ²	3.1- 11.8GHz	5.1dBi	84%-90%
8	Rectangle monopole with slots on GND	(30X45)mm ²	3.1- 11.2GHz	6.2dBi	80%-87%
9	Combo type UWB Antenna (proposed)	(20X30)mm ²	3.1- 12.0GHz	7.4dBi	85%-94%

4.12 References

- [1] J.S. Lim, Y.T. Lee, C.S.Kim, D.Ahn and S. Nam, "A vertically Periodic Defected Ground Structure and its applications in reducing the size of microwave circuits" *IEEE microwave and Wireless Components letters*, Vol.12, No.12, December 2002, pp.479-481.
- [2] J.A. Tirando-Mendez, H. Jardon-Aguilar, F.Iturbide-Sanchez, I Gracia – Ruiz, V.Molina-Lopaz and R. Acevo-Herrera, "A Proposed Defected Microstrip Structure (DMS) Behavior for reducing Rectangular patch antenna size", *Microwave and optical Technology Letters*, Vol.43, No.6, December 2004, pp. 481-484.

- [3] J.A. Tirando-mendez, H.jardon –Aguiliar and F. Iturbide-Sanchez, “Application of the Defected Microstrip Structure as a Tuning Technique for Rectangular Printed Antenna ,” *Microwave and optical Technology Letters*, Vol.48, No.2, February 2006, pp. 370-373.
- [4] J.A. Tirando-mendez, H.jardon –Aguiliar and F. Iturbide-Sanchez, “Application of the Defected Microstrip Structure as a Tuning Technique for Rectangular Printed Antenna ,” *Microwave and optical Technology Letters*, Vol.48, No.2, February 2006, pp. 370-373
- [5] C. Waldschmidt and K. D. Palmer, “Loaded wedge bow-tie antenna using linear profile,” *Electron. Lett.*, vol. 37, no. 4, pp. 208–209, Feb. 2001.
- [6] D. Uduwawala, M. Norgren, P. Fuks, and A. W. Gunawardena, “A deep parametric study of resistor-loaded bow-tie antennas for ground-penetrating radar applications using FDTD,” *IEEE Trans. Geosci. Remote Sensing*, vol. 48, no. 4, pp. 732–742, Apr. 2004.
- [7] R. L. Li and V. F. Fusco, “Broadband semi loop antenna,” *Microw. Opt. Technol. Lett.*, vol. 34, no. 4, pp. 233–234, Aug. 2002. [8] F.-R. Hsiao and K.-L.Wong, “Omnidirectional planar folded dipole antenna,” *IEEE Trans. Antennas Propag.*, vol. 52, no. 7, pp. 1898–1902, Jul. 2004.
- [9] K.-L. Wong, C.-H. Wu, and S.-W. Su, “Ultrawide-band square planar metal-plate monopole antenna with a trident-shaped feeding strip,” *IEEE Trans. Antennas Propag.*, vol. 53, no. 4, pp. 1262–1268, Apr. 2005.
- [10] J. Qiu, Z. Du, J. Lu, and K. Gong, “A case study to improve the impedance bandwidth of a planar monopole,” *Microw. Opt. Technol. Lett.*, vol. 45, no. 2, pp. 124–126, Apr. 2005.
- [11] M. J. Ammann and Z. N. Chen, “A wide-band shorted planar monopole with bevel,” *IEEE Trans. Antennas Propag.*, vol. 51, no. 4, pp. 901–903, Apr. 2003.
- [12] A. V. Nogueira, M. F. Bataller, and M. Cabedo-Fabres, “A wideband arrow head planar monopole antenna for multi-service mobile systems,” *Microw. Opt. Technol. Lett.*, vol. 37, no. 3, pp. 188–190, May 2003.
- [13] N. Behdad and K. Sarabandi, “A compact antenna for ultra wide-band applications,” *IEEE Trans. Antennas Propag.*, vol. 53, no. 7, pp. 2185–2192, Jul. 2005.

- [14] T. Yang and W. A. Davis, "Planar half-disk antenna structures for ultrawideband communications," in *Proc. IEEE Int. Symp. Antennas Propagation*, Jun. 2004, vol. 3, pp. 2508–2511.
- [15] D. H. Kwon and Y. Kim, "CPW-fed planar ultrawideband antenna with hexagonal radiating elements," in *Proc. IEEE Int. Symp. Antennas Propagation*, Jun. 2004, vol. 3, pp. 2947–2950.
- [16] J. Liang, C. C. Chiau, X. Chen, and C. G. Parini, "Printed circular ring monopole antennas," *Microw. Opt. Technol. Lett.*, vol. 45, no. 5, pp. 372–375, Jun. 5, 2005.
- [17] H. S. Choi, J. K. Park, S. K. Kim, and J. Y. Park, "A new ultra-wideband antenna for UWB applications," *Microw. Opt. Technol. Lett.*, vol. 40, no. 5, pp. 399–401, Mar. 5, 2004.
- [18] K. Chung, H. Park, and J. Choi, "Wideband microstrip-fed monopole antenna with a narrow slit," *Microw. Opt. Technol. Lett.*, vol. 47, no. 4, pp. 400–402, Nov. 20, 2005.
- [19] Z. N. Chen, "Impedance characteristics of planar bow-tie-like monopole antennas," *Electron. Lett.*, vol. 36, no. 13, pp. 1100–1101, June 2000.

CONCLUSION AND FUTURE SUGGESTED WORKS

5.1 Thesis Highlights.

A compact UWB antenna developed which can directly go into futuristic mobile handsets is basically a loaded printed monopole. The work started with a simple strip monopole printed on a truncated ground plane. Various bandwidth enhancement techniques are explored. The effect of each controlling parameter is studied in detail. Using the methodology outlined in the thesis a compact UWB antenna operating from 3.1 to 11GHz is designed and tested. The antenna performance was excellent.

5.2 Inferences on experimental and theoretical observations.

The radiation characteristics of different printed wide band and ultra wide band monopole antennas are studied experimentally and numerically. From the detailed experimental investigations, it is concluded that loaded strip monopole can successfully be used for wide band and ultra wide band applications. It is observed that by suitably trimming the antenna parameters UWB operation can be easily achieved by merging different resonances. From table (4-1) and figure (4-21), it is clear that the band width of strip monopole has increased by 130% for the Rectangular patch loading. The same is revealed for the cases of other loading patches such as Elliptical, Circular disc, Octagon and Hexagon as detailed in chapter 4. It is quite evident from the table(4-1) and figure (4-28).

Section 4.2 to 4.7 shows the optimized feed point, truncated ground, patch shape and size for wide band applications. From these observations, it can be concluded that top loading with a gap 'd' is effectively be used for band width enhancement of antenna. All the techniques offered 80% to 130% bandwidth.

The effect of permittivity of substrate used for fabricating the patch on the bandwidth of antenna is also studied. The bandwidth enhancement is achieved without deteriorating the radiation characteristics.

The work started with simulation and experimental study right from the simple strip monopole in chapter-4. The study has evolved certain empirical formula for design of a printed monopole for single band antenna for mobile operating band of 1800MHz and 2400MHz. The search for wide band printed antenna continued by suitably loading the monopole antenna by resonant geometries directly loading.

The direct loading of various geometries like elliptical, circular, octagonal, hexagonal and rectangular were presented. It is found that all geometries upon loading has resulted in widening the bandwidth. For the performance in Ultra Wide Band (UWB) applications, rectangular loading is found to be most suitable. It is remarkable that, all designs are looking for a wider matching impedance bandwidth without loss of omni-directional radiation pattern. Here the theoretical analysis is carried out by 3D-FDTD method and the good agreement with the experimental and simulated results as observed and reported in chapter 4.

5.3 Salient features of the antenna and applications

Prametric analysis using HFSS is employed to achieve UWB antenna. The optimized prototype model is fabricated , tested and reported in chapter 4.

The experimental and theoretical results are found to be in good agreement. The radiation patterns are almost omni-directional. The overall dimension of this printed UWB antennas is only **35X45mm²** .

It is also noticed that wide band width can be achieved using slots of suitable dimension on the truncated ground plane. The optimized prototype antenna is fabricated , tested and reported in chapter 4. The experimental and theoretical results are found to be in good agreement. Here also the radiation patterns are almost omni-directional. The overall dimension of this printed UWB antennas is **30X45mm²** .

Broad bandwidth and antenna miniaturization can be simultaneously achieved by the suitable combination of the strip and slots. This is demonstrated at the concluding part of chapter-4. The experimental and theoretical results are found to be in good agreement. The radiation patterns at each resonant frequency are almost omni-directional. The overall dimension of this printed UWB antennas is now reduced to **20X30mm²**

5.4 Suggestions for future work

1. The other techniques for widening the bandwidth like beveling, gap loading, resistor loading, multi-feed etc.. can be tried on the optimized model reported in the thesis to further enhance the band width and miniaturization. Some other technique of implementing the Defected Microstrip structure (DMS), Defected Ground Structure (DGS) can be applied to realize the goal of still compact UWB antenna.
2. The other geometries like elliptical, circular disc, octagon, and hexagon can also be used for similar study for UWB performance analysis as these structures may be specifically suitable for certain

applications due its physical feature and special electrical characteristics.

3. Possibility of reducing the size of the antenna by meta material loading is another interesting area. It is reported that meta material can reduce the size of the antenna to sub miniature wavelength. This aspect can provide very interesting results.
4. This type of antennas is only an opening in the field of low power UWB antennas for futuristic gadgets. It could be thought as wearable antennas. Lots of scope for such wearable antennas with much more bandwidth for use on human body itself to correct the sensitivity of mind and transform the personality itself. This could be an effective tool to treat so called obsessive traits of human behaviour termed in medical science. A detailed study in this direction is sure to reveal more on the Electromagnetic effect on the metals being worn on the human body like gold and silver ornaments, wrist watches and copper plates as 'Raksha' etc..

Appendix -A

FDTD METHOD

Finite Difference Time Domain (FDTD) method proposed by Yee in 1966 is extensively used many areas of science and technology. FDTD, a technique that discretizes the problem domain in both time and space gives time and frequency domain information of the electromagnetic problem of interest. FDTD provides a direct solution of time dependant Maxwell's equation for electric and magnetic field intensities in a finite, piecewise homogenous media. Due to the lack of analytical preprocessing and modeling, FDTD is a potential tool for planar antenna problems. Moreover, this analysis approach can be used to include the effect of finite ground plane and substrate parameters which is very important in the present investigation, especially where printed monopole with truncated ground plane is the focus of this work. Specifically, certain characteristic strengths of FDTD attract the investigators to apply this algorithm in the antenna design and analysis. Following are the striking features of this powerful modelling, simulation and analysis tool.

- From the mathematical point of view, it is a direct implementation of Maxwell's curl equations. Therefore, analytical processing of Maxwell's equations is almost negligible.
- It can model complex antenna geometries and feed and other structures.
- It can model any type of materials of importance to electromagnetic technology, including conductors, dielectrics, dispersive and non linear medium.

- Impulsive excitations in Time Domain gives a broadband response in frequency domain in a single FDTD run through concurrently run Fourier transform.
- The complex near field information is an intrinsic part of FDTD model and the near to far field transformation offers the calculation of far field radiation pattern in single FDTD run.
- FDTD is accurate: It is good model of the physical world. The ready availability of time domain and frequency domain data provides a deep physical insight to the problem in different perspectives. Visualization of fields in time provides a clear insight to the actual physics behind the antenna radiation.

A.1 Discretization in FDTD

The FDTD method originally proposed by K.S. Yee [1], is an explicit finite difference scheme using central differences on a Cartesian grid staggered in both space and time. A full three – dimensional FDTD cell (Yee lattice) is shown in Figure (A-1) wherein, the Electric fields lie along the midpoint of the cell edges and the Magnetic fields lie along the centre of the cell faces. Yee defines the grid coordinates (i, j, k) as

$$(i, j, k) = (i\Delta x, j\Delta y, k\Delta z) \dots\dots\dots (A.1)$$

where Δx , Δy and Δz are the actual grid separations.

Any function of space and time is written as

$$F^n(i, j, k) = F(i\Delta x, j\Delta y, k\Delta z, n\Delta t) \dots\dots\dots (A.2)$$

where Δt is the time increment, n is the time index and $\Delta x, \Delta y, \Delta z$ is the space increment along the three coordinate axes.

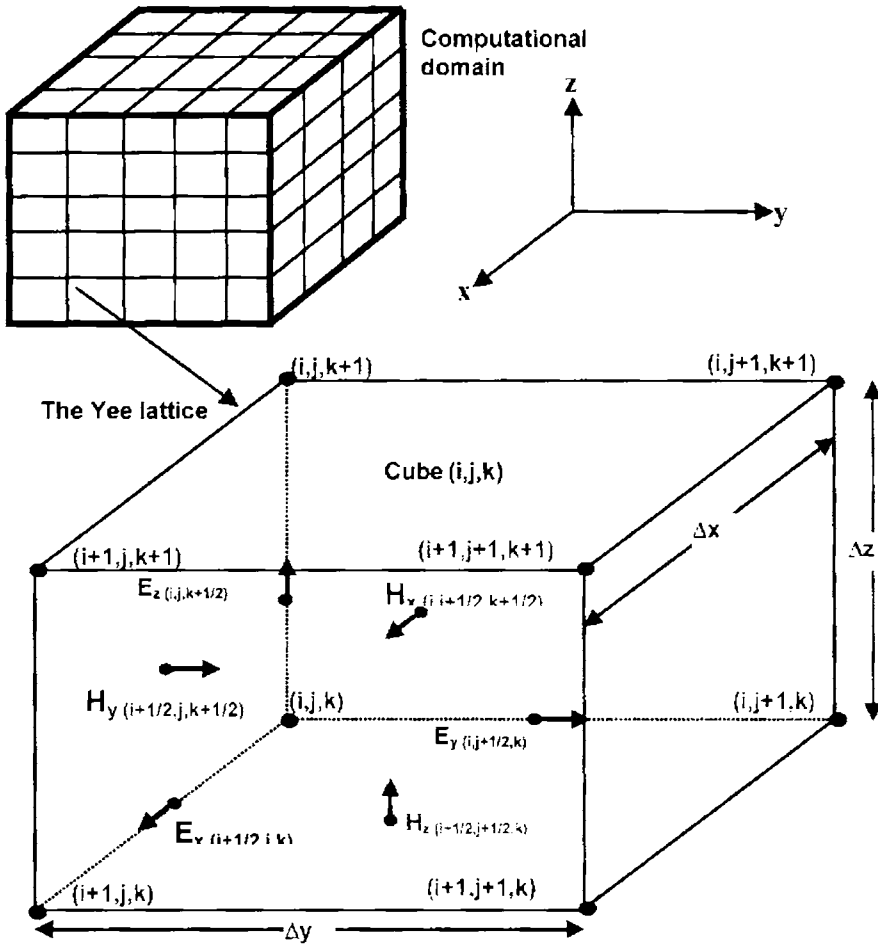


Fig. (A-1) The three - dimensional staggered mesh FDTD cell (Yee lattice) in the computational domain

The spatial and temporal derivatives of F are written using central finite difference approximations as follows.

$$\frac{\partial F^n(i, j, k)}{\partial x} = \frac{F^n(i+1/2, j, k) - F^n(i-1/2, j, k)}{\Delta x} \dots\dots\dots (A.3.a)$$

$$\frac{\partial F^n(i, j, k)}{\partial t} = \frac{F^{n+1/2}(i, j, k) - F^{n-1/2}(i, j, k)}{\Delta t} \dots\dots\dots (A.3.b)$$

The starting point of the FDTD algorithm is the differential form of Maxwell's curl equations for an isotropic medium [Eqn A.4 (a-b)].

$$\nabla \times \vec{E} = -\mu \frac{\partial \vec{H}}{\partial t} \dots\dots\dots (A.4.a)$$

$$\nabla \times \vec{H} = \sigma \vec{E} + \epsilon \frac{\partial \vec{E}}{\partial t} \dots\dots\dots (A.4.b)$$

These can be written as six scalar equations in Cartesian coordinates [Eqn. A.5 (a-f)].

$$\frac{\partial H_x}{\partial t} = \frac{1}{\mu} \left(\frac{\partial E_y}{\partial z} - \frac{\partial E_z}{\partial y} \right) \dots\dots\dots (A.5.a)$$

$$\frac{\partial H_y}{\partial t} = \frac{1}{\mu} \left(\frac{\partial E_z}{\partial x} - \frac{\partial E_x}{\partial z} \right) \dots\dots\dots (A.5.b)$$

$$\frac{\partial H_z}{\partial t} = \frac{1}{\mu} \left(\frac{\partial E_x}{\partial y} - \frac{\partial E_y}{\partial x} \right) \dots\dots\dots (A.5.c)$$

$$\frac{\partial E_x}{\partial t} = \frac{1}{\epsilon} \left(\frac{\partial H_z}{\partial y} - \frac{\partial H_y}{\partial z} - \sigma E_x \right) \dots\dots\dots (A.5.d)$$

$$\frac{\partial E_y}{\partial t} = \frac{1}{\epsilon} \left(\frac{\partial H_x}{\partial z} - \frac{\partial H_z}{\partial x} - \sigma E_y \right) \dots\dots\dots (A.5.e)$$

$$\frac{\partial E_z}{\partial t} = \frac{1}{\epsilon} \left(\frac{\partial H_y}{\partial x} - \frac{\partial H_x}{\partial y} - \sigma E_z \right) \dots\dots\dots (A.5.f)$$

Equations A.3.a and A.3.b are applied to the six scalar equations (A.5.a to A.5.f), resulting in six coupled explicit finite difference equations (A.6.a to A.6.f), in free space.

$$\begin{aligned}
 H_x^{n+1/2}(i, j+1/2, k+1/2) &= H_x^{n-1/2}(i, j+1/2, k+1/2) \\
 &+ \left[\frac{\Delta t}{\mu \Delta z} \right] (E_y^n(i, j+1/2, k+1) - E_y^n(i, j+1/2, k)) \\
 &- \left[\frac{\Delta t}{\mu \Delta y} \right] (E_z^n(i, j+1, k+1/2) - E_z^n(i, j, k+1/2)) \dots\dots\dots (A.6a)
 \end{aligned}$$

$$\begin{aligned}
 H_y^{n+1/2}(i+1/2, j, k+1/2) &= H_y^{n-1/2}(i+1/2, j, k+1/2) \\
 &+ \left[\frac{\Delta t}{\mu \Delta x} \right] (E_z^n(i+1, j, k+1/2) - E_z^n(i, j, k+1/2)) \\
 &- \left[\frac{\Delta t}{\mu \Delta z} \right] (E_x^n(i+1/2, j, k+1) - E_x^n(i+1/2, j, k)) \dots\dots\dots (A.6b)
 \end{aligned}$$

$$\begin{aligned}
 H_z^{n+1/2}(i+1/2, j+1/2, k) &= H_z^{n-1/2}(i+1/2, j+1/2, k) \\
 &+ \left[\frac{\Delta t}{\mu \Delta y} \right] (E_x^n(i+1/2, j+1, k) - E_x^n(i+1/2, j, k)) \\
 &- \left[\frac{\Delta t}{\mu \Delta x} \right] (E_y^n(i+1, j+1/2, k) - E_y^n(i, j+1/2, k)) \dots\dots\dots (A.6c)
 \end{aligned}$$

$$\begin{aligned}
 E_x^{n+1}(i+1/2, j, k) &= E_x^n(i+1/2, j, k) \\
 &+ \left[\frac{\Delta t}{\epsilon \Delta y} \right] (H_z^{n+1/2}(i+1/2, j+1/2, k) - H_z^{n+1/2}(i+1/2, j-1/2, k)) \\
 &- \left[\frac{\Delta t}{\epsilon \Delta z} \right] (H_y^{n+1/2}(i+1/2, j, k+1/2) - H_y^{n+1/2}(i+1/2, j, k-1/2)) \dots\dots\dots (A.6d)
 \end{aligned}$$

$$\begin{aligned}
 E_y^{n+1}(i, j+1/2, k) &= E_y^n(i, j+1/2, k) \\
 &+ \left[\frac{\Delta t}{\epsilon \Delta z} \right] (H_x^{n+1/2}(i, j+1/2, k+1/2) - H_x^{n+1/2}(i, j+1/2, k-1/2)) \\
 &- \left[\frac{\Delta t}{\epsilon \Delta x} \right] (H_z^{n+1/2}(i+1/2, j+1/2, k) - H_z^{n+1/2}(i-1/2, j+1/2, k)) \dots\dots\dots (A.6e)
 \end{aligned}$$

$$\begin{aligned}
 E_z^{n+1}(i, j, k+1/2) &= E_z^n(i, j, k+1/2) \\
 &+ \left[\frac{\Delta t}{\epsilon \Delta x} \right] \left(H_y^{n+1/2}(i+1/2, j, k+1/2) - H_y^{n+1/2}(i-1/2, j, k+1/2) \right) \\
 &- \left[\frac{\Delta t}{\epsilon \Delta y} \right] \left(H_x^{n+1/2}(i, j+1/2, k+1/2) - H_x^{n+1/2}(i, j-1/2, k+1/2) \right) \dots\dots\dots (A.6f)
 \end{aligned}$$

\vec{H} and \vec{E} are evaluated at alternate half time steps using equations (A.6.a-f), such that all field components are calculated in each time step Δt . The updated new value of a field component at any layer thus depends upon its value in the previous step and the previous value of the components of the other field at the adjacent spatial points. Table A.1 indicates the spatial and temporal relation of the E and H nodes in the Yee lattice. The discretization in space and time and the leap-frog time integration employed in the FDTD method proposed by Yee is shown in fig.A-2.

Table A.1 Spatial and temporal relation of the E and H

		x	y	z	t
E node	E_x	$i+1/2$	j	k	n
	E_y	i	$j+1/2$	k	n
	E_z	i	j	$k+1/2$	n
H node	H_x	i	$j+1/2$	$k+1/2$	$n\pm 1/2$
	H_y	$i+1/2$	j	$k+1/2$	$n\pm 1/2$
	H_z	$i+1/2$	$j+1/2$	k	$n\pm 1/2$

$$E_{y,i,j,k}^{n+1} = E_{y,i,j,k}^n + \frac{\Delta t}{\epsilon \Delta z} (H_{x,i,j,k+1}^{n+1/2} - H_{x,i,j,k}^{n+1/2}) - \frac{\Delta t}{\epsilon \Delta x} (H_{z,i+1,j,k}^{n+1/2} - H_{z,i,j,k}^{n+1/2}) \dots\dots (A.7e)$$

$$E_{z,i,j,k}^{n+1} = E_{z,i,j,k}^n + \frac{\Delta t}{\epsilon \Delta x} (H_{y,i,j,k}^{n+1/2} - H_{y,i,j,k}^{n+1/2}) - \frac{\Delta t}{\epsilon \Delta y} (H_{x,i,j+1,k}^{n+1/2} - H_{x,i,j,k}^{n+1/2}) \dots\dots (A.7f)$$

To facilitate the implementation of the algorithm in a digital computer, the indices of the field components are renamed, eliminating the ½ index notation as suggested by Sheen *et al.* [2]. This allows the value of each field component to be stored in a three-dimensional array, with the array indices corresponding to the spatial indices. Figure A.2 differentiates the notations proposed by Yee and Sheen, in deriving the H_z component according to equation (A.6.c). Equations (A.6.a-f) may be therefore re-written as (A.7.a-f), forming the basis of the computer implementation of the FDTD scheme in this thesis.

A.2 Boundary conditions

Most of the Electromagnetic problems are unbounded or associated with open space regions. In the FDTD implementation of such problems requires exhaustive computational efforts and unlimited computational resources. Due to limited computational resources, the simulation domain requires truncation, which may introduce spurious fields from the boundaries unless appropriate measures are taken. Size of the computational domain is selected based on the problem under analysis. The Boundary condition should ensure that the outgoing wave is completely absorbed at the boundary, making domain appear infinite in extend with minimum numerical back reflection. The first most widely used ABC was devised by Mur in 1981 [3]. This boundary condition is derived from a one-way wave equation. However, the attenuation of waves incident on the Mur ABC degrades as the incident angle (away from the normal) increases until at the grazing angle, the boundary becomes perfectly reflecting. Hence for most of the

simulations using Mur’s first order ABC at least 20 cells are required between the boundary and the radiating structure. As the number of cells between the radiator and boundary is increased the outward propagating wave from the radiator approaches to the normal incidence at the truncated boundary and are subsequently absorbed better than the waves at the near grazing angle. In 1994, Berenger [4] derived a new boundary condition referred to as a Perfectly Matched Layer (PML) which reduces reflections several orders of magnitude below other techniques. It uses a modified set of Maxwell’s equations in which fields at the ABC-simulation space interface are split into two components and an artificial anisotropic material is introduced within the ABC. The result is a PML wave impedance perfectly matched to the simulation space and independent of incident angle. Incident waves are attenuated in the direction normal to the layers as they propagate through the artificial medium. Reflection coefficients as low as –80 dB have been demonstrated [5] for both 2-D and 3-D FDTD simulations.

Apart from ABC and PML, the implementation of the truncated ground plane printed monopole antennas involves simple boundary conditions such as Perfect Electric Conductor (PEC) and Dielectric interface boundary.

Perfect Electric Conductor (PEC) boundary

The PEC boundary is used to represent ideal conductors. This type of boundary condition deliberately reflects all incident wave energy back into the computational domain, thus limiting its size. The boundary conditions at a perfect electric conductor are such that the electric field components tangential to the surface must be zero, stated mathematically where \vec{n} is a surface normal vector,

$$\vec{n} \times \vec{E} = 0 \quad \dots\dots\dots (A.8)$$

in the Yee cell formulation the electric fields calculated at points on the surface of a PEC are always tangential to the surface. Thus by using the Yee cell in the FDTD scheme, the boundary condition at the surface of a PEC can be satisfied by simply setting $E_{tan} = 0$, they will remain *nearly* zero throughout the iterations. In materials finite conductivity, the update equation for the electric field component is

$$E^n = E^{n-1} \left[\frac{1 - \sigma\Delta t / 2\epsilon}{1 + \sigma\Delta t / 2\epsilon} \right] + \left[\frac{1}{1 + \sigma\Delta t / 2\epsilon} \right] \left[\frac{\Delta t}{\epsilon} \right] (\nabla \times H^{n-1/2}) \dots\dots\dots(A.9)$$

when $\sigma \gg 1$ in the above equation, $E^n \cong E^{n-1}$. In the FDTD iteration procedure, once the boundary conditions on the tangential fields are satisfied, the boundary conditions on the normal fields will be automatically valid. PEC boundaries are used in the present investigation to model the finite ground plane and metallic strip of the printed strip monopole antenna.

Dielectric interface boundary

While modelling the monopole printed on a dielectric substrate at the interface between two media (Air and Dielectric) the discretization of Maxwell’s equation become invalid. This is because in the difference equation only single value for material constants (ϵ and μ) are used, but in actual case there are two separate values on either side of the interface (ϵ_1, μ_1 of air and ϵ_2, μ_2 of the dielectric). By applying the equivalent parameter approach introduced by Zhang and Mei [6] the condition at the interface is approximated as

$$\epsilon_{eff} = \frac{\epsilon_1 + \epsilon_2}{2} \dots\dots\dots(A.10)$$

a detailed description of the Boundary condition applied for the truncation of the computational domain is presented in the following section.

A.2.1 First order Mur’s ABC

Mur’s first order ABC is derived from differential equations. Differential based ABC’s are generally obtained by factoring the wave equation and by allowing a solution that permits only outgoing waves. Mur’s ABC was proposed after the theoretical work by Enquist and Majda [7]. It provides satisfactory absorption for a great variety of problems and is extremely simple to implement. Mur’s first order ABC looks back one step in time and one cell into the space location. For the structure considered in the thesis, the pulses on the radiating monopoles will be normally incident to the outer boundary mesh walls and this leads to simple approximate boundary condition that the tangential electric field at the outer boundary obeys one dimensional wave equation in the direction normal to the mesh wall. For the x normal wall the one dimensional wave equation can be written as

$$\left(\frac{\partial}{\partial x} - \frac{1}{c} \frac{\partial}{\partial t} \right) E_{tan} = 0 \dots\dots\dots (A.11)$$

by imposing above equation on a wave normally incident on planar surface, absorbing condition for a normal incident wave with out reflection can be obtained as

$$\frac{\partial E(x,t)}{\partial x} = \frac{1}{c} \frac{\partial E(x,t)}{\partial t} \text{ Where } x=\Delta x/2, t= (n+1/2) \Delta t \dots\dots\dots (A.12)$$

for updating of the electric field at

$$x = \Delta x / 2, t = (n + 1) \Delta t$$

in finite-difference form it can be written as follows:

$$\frac{E_1^{n+1/2} - E_0^{n+1/2}}{\Delta x} = \frac{1}{c} \frac{E_{1/2}^{n+1} - E_{1/2}^n}{\Delta t} \tag{A.13}$$

In this form, the finite-difference approximation is accurate to the second order in x and t . But the values at the half grid points and half time steps are not available, and can be averaged as

$$E_m^{n+1/2} = \frac{E_m^{n+1} + E_m^n}{2} \tag{A.14}$$

$$E_{m+1/2}^n = \frac{E_{m+1}^n + E_m^n}{2} \tag{A.15}$$

The equations A.11, A.12 and A.13 yields a explicit finite difference equation

$$E_0^{n+1} = E_1^n + \left(\frac{c\Delta t - \Delta x}{c\Delta t + \Delta x} \right) (E_1^{n+1} - E_0^n) \tag{A.16}$$

Where E_0 represents the tangential electric field component on the mesh wall and E_1 represents the tangential electric field component on node inside of the mesh wall. Similar expressions are obtained for the other absorbing boundaries by using the corresponding normal directions for each wall. But while implementing the Mur's first order boundary conditions for truncated ground plane printed monopole it should be noted that boundary walls are far enough from the radiating monopole to ensure the normal incidence at the boundary walls. For the oblique incidence case the wave will reflected from the boundary walls.

A.2.2 Bergner's PML ABC

Berenger's perfectly matched layer (PML) type of has been the most widely accepted [8-9] and is set to revolutionize the FDTD method. In the

perfectly matched layer (PML) truncation technique, an artificial layer of absorbing material is placed around the outer boundary of the computational domain. The goal is to ensure that a plane wave that is incident from FDTD free space to the PML region at an arbitrary angle is completely absorbed there without reflection. This is the same as saying that there is complete transmission of the incident plane wave at the interface between free space and the PML region. Thus the computational region and the PML region are said to be perfectly matched.

In the present investigation of printed monopole with truncated ground plane Mur's first order ABC requires a large computational domain to ensure normal incidence which increases the computational efforts and time. Hence FDTD method with PML concept is implemented by introducing Electric Flux Density (D) in discretized Maxwell's equations as proposed by Sullivan [10].

Initially the implementation of PML concept in FDTD is described and then discretized Maxwell's equations are derived. The iterative FDTD algorithm presented in this section does not use separate computer codes for PML section, but the generalized equation can be used for both normal media and PML by suitably enabling or disabling some medium dependent parameters in the equations.

Consider the following Maxwell's equations,

$$\frac{\partial D}{\partial t} = \frac{1}{\sqrt{\epsilon_0 \mu_0}} \nabla_x H \quad \dots\dots\dots (A.17)$$

$$D(\omega) = \epsilon^*, (\omega) E(\omega) \quad \dots\dots\dots (A.18)$$

Where $\epsilon^*, (\omega) = \epsilon_r + \frac{\sigma}{j\omega\epsilon_0} \quad \dots\dots\dots (A.19)$

$$\frac{\partial H}{\partial t} = -\frac{1}{\sqrt{\epsilon_0 \mu_0}} \nabla_x E$$

Consider a transverse magnetic wave (TM) propagating in a medium. The E and H field components are Ez, Hx and Hy. Now the above equations are reduced to

$$\frac{\partial D_z}{\partial t} = \frac{1}{\sqrt{\epsilon_0 \mu_0}} \left(\frac{\partial H_y}{\partial x} - \frac{\partial H_x}{\partial y} \right) \dots\dots\dots (A.20a)$$

$$D(\omega) = \epsilon^* (\omega) E(\omega) \dots\dots\dots (A.20b)$$

$$\frac{\partial H_x}{\partial t} = -\frac{1}{\sqrt{\epsilon_0 \mu_0}} \frac{\partial E_z}{\partial y} \dots\dots\dots (A.20c)$$

$$\frac{\partial H_y}{\partial t} = \frac{1}{\sqrt{\epsilon_0 \mu_0}} \frac{\partial E_z}{\partial x} \dots\dots\dots (A.20d)$$

If a wave is propagating in medium A and it impinges upon medium B, the amount of reflection is dictated by the intrinsic impedances of the two media

$$\Gamma = \frac{\eta_A - \eta_B}{\eta_A + \eta_B} \dots\dots\dots (A.21)$$

which are determined by the dielectric constant and permeability of the respective media

$$\eta = \sqrt{\frac{\mu}{\epsilon}} \dots\dots\dots (A.22)$$

Up to now, it is assumed that μ is a constant, so when a propagating pulse travels from ϵ_1 to ϵ_2 , it sees a change in impedance and reflects a portion of the pulse. However, if μ changed with ϵ so that η remains a constant, Γ would

be zero and no reflection will occur. This still doesn't solve the problem, because the pulse will continue propagating in the new medium. Hence the medium must be lossy so that the pulse will die out before it hits the boundary. This is accomplished by making both ϵ and μ of Eq. (A.22) complex because the imaginary part represents attenuation or loss.

by applying Fourier transform to the Eqn. A.20.a-A.20.d

$$j\omega D_z = c_0 \left(\frac{\partial H_y}{\partial x} - \frac{\partial H_x}{\partial y} \right) \dots\dots\dots (A.23a)$$

$$D_z(\omega) = \epsilon^*_r(\omega) E_z(\omega) \dots\dots\dots (A.23b)$$

$$j\omega H_x = -c_0 \frac{\partial E_z}{\partial y} \dots\dots\dots (A.23c)$$

$$j\omega H_y = c_0 \frac{\partial E_z}{\partial x} \dots\dots\dots (A.23d)$$

It should be noted that ϵ and μ are eliminated from the spatial derivatives in the above equations for the normalized units. Instead of putting them back to implement the PML, we will add fictitious dielectric constants and permeabilities.

$$j\omega D_z \epsilon^*_{Fz}(x) \epsilon^*_{Fz}(y) = c_0 \left(\frac{\partial H_y}{\partial x} - \frac{\partial H_x}{\partial y} \right) \dots\dots\dots (A.24a)$$

$$D_z(\omega) = \epsilon^*_r(\omega) E_z(\omega) \dots\dots\dots (A.24b)$$

$$j\omega H_x \mu^*_{Fx}(x) \mu^*_{Fx}(y) = -c_0 \frac{\partial E_z}{\partial y} \dots\dots\dots (A.24c)$$

$$j\omega H_y \mu^*_{Fy}(x) \mu^*_{Fy}(y) = c_0 \frac{\partial E_z}{\partial x} \dots\dots\dots (A.24d)$$

It is worth noting that the fictitious values added in the equations have nothing to do with the real values of $\epsilon^*, (\omega)$ which specify the medium.

Sacks et al. [11] showed that there are two conditions to form a PML:

The impedance going from the background medium to the PML must be constant

$$\eta_0 = \eta_m = \sqrt{\frac{\mu^*_{Fx}}{\epsilon^*_{Fx}}} = 1 \tag{A.25}$$

In the direction perpendicular to the boundary the relative dielectric constant and relative permeability must be the inverse of those in the other directions

That is,

$$\epsilon^*_{Fx} = \frac{1}{\epsilon^*_{Fy}} \tag{A.26}$$

$$\mu^*_{Fx} = \frac{1}{\mu^*_{Fy}} \tag{A.27}$$

Each of these is a complex quantity of the form

$$\epsilon^*_{Fm} = \epsilon_{Fm} + \frac{\sigma D_m}{j\omega\epsilon_0} \text{ for } m=x \text{ or } y \tag{A.28}$$

$$\mu^*_{Fm} = \mu_{Fm} + \frac{\sigma H_m}{j\omega\mu_0} \text{ for } m=x \text{ or } y \tag{A.29}$$

The following selection of parameters satisfies Eq. A.26 and A.27

$$\epsilon_{Fm} = \mu_{Fm} = 1 \tag{A.30}$$

$$\frac{\sigma D_m}{\epsilon_0} = \frac{\sigma H_m}{\mu_0} = \frac{\sigma D}{\epsilon_0} \tag{A.31}$$

Substituting these values in (A.28)

$$\eta_0 = \eta_m = \sqrt{\frac{\mu^*_{Fx}}{\epsilon^*_{Fx}}} = \sqrt{\frac{1 + \sigma(x) / j\omega\epsilon_0}{1 + \sigma(x) / j\omega\epsilon_0}} = 1 \dots\dots\dots (A.32)$$

If σ increases gradually as it goes into the PML, (A.24.a -A.24.d) will cause Dz and Hy to be attenuated.

The PML is first implemented in the X direction. Therefore, the x dependent values of ϵ^*_F and μ^*_F will be retained.

$$j\omega D_z \epsilon^*_{Fz}(x) = c_0 \left(\frac{\partial H_y}{\partial x} - \frac{\partial H_x}{\partial y} \right) \dots\dots\dots (A.33)$$

$$j\omega H_x \mu^*_{Fx}(x) = -c_0 \frac{\partial E_z}{\partial y} \dots\dots\dots (A.34)$$

$$j\omega H_y \mu^*_{Fy}(x) = c_0 \frac{\partial E_z}{\partial x} \dots\dots\dots (A.35)$$

$$j\omega \left(1 + \frac{\sigma_D(x)}{j\omega\epsilon_0} \right) D_z = c_0 \left(\frac{\partial H_y}{\partial x} - \frac{\partial H_x}{\partial y} \right) \dots\dots\dots (A.36)$$

$$j\omega \left(1 + \frac{\sigma_D(x)}{j\omega\epsilon_0} \right)^{-1} H_x = -c_0 \frac{\partial E_z}{\partial y} \dots\dots\dots (A.37)$$

using the values of (A.33 and A.34)

$$j\omega \left(1 + \frac{\sigma_D(x)}{j\omega\epsilon_0} \right) H_y = c_0 \frac{\partial E_z}{\partial x} \dots\dots\dots (A.38)$$

In the above equations the permeability of Hx is the inverse of that of Hy. Therefore the second requirement for the PML is fulfilled. Now the above equations have to be put into the FDTD formulation. Consider the left side of (A.33)

$$j\omega \left(1 + \frac{\sigma_D(x)}{j\omega\epsilon_0} \right) D_z = j\omega D_z + \frac{\sigma_D(x)}{\epsilon_0} D_z$$

Moving to the time domain, and then taking the finite difference approximations,

$$\begin{aligned} \frac{\partial D_z}{dt} + \frac{\sigma_D(i)}{\epsilon_0} D_z &\equiv \frac{D_z^{n+1/2}(i,j) - D_z^{n-1/2}(i,j)}{\Delta t} + \frac{\sigma_D(i)}{\epsilon_0} \frac{D_z^{n+1/2}(i,j) + D_z^{n-1/2}(i,j)}{2} \\ &= D_z^{n+1/2}(i,j) \frac{1}{\Delta t} \left[1 + \frac{\sigma_D(i)\Delta t}{2\epsilon_0} \right] - D_z^{n-1/2}(i,j) \frac{1}{\Delta t} \left[1 - \frac{\sigma_D(i)\Delta t}{2\epsilon_0} \right] \end{aligned}$$

if this is substituted into Eq. (A.29) along with the spatial derivatives,

$$\begin{aligned} D_z^{n+1/2}(i,j) &= g\beta(i)D_z^{n-1/2}(i,j) + \\ &g\gamma(i)0.5 \left[H_y^n(i+1/2,j) - H_y^n(i-1/2,j) - H_y^n(i,j+1/2) - H_y^n(i,j-1/2) \right] \dots \text{(A.39)} \end{aligned}$$

the parameters $gi2(i)$ and $gi3(i)$ are given by

$$gi2(i) = \frac{1}{1 + \sigma_D(i)\Delta t / 2\epsilon_0} \dots \text{(A.40)}$$

$$gi3(i) = \frac{1 - \sigma_D(i)\Delta t / 2\epsilon_0}{1 + \sigma_D(i)\Delta t / 2\epsilon_0} \dots \text{(A.41)}$$

Similarly H_y can be formulated as,

$$H_y^{n+1}(i+1/2,j) = f\beta(i+1/2)H_y^n(i+1/2,j) + f\gamma(i+1/2)0.5 \left[E_z^{n+1/2}(i+1,j) - E_z^{n+1/2}(i,j) \right] \dots \text{(A.42)}$$

where

$$fi2(i+1/2) = \frac{1}{1 + \sigma_D(i+1/2)\Delta t / (2\epsilon_0)} \dots \text{(A.43)}$$

$$f3(i+1/2) = \frac{1 - \sigma_D(i+1/2)\Delta t / (2\epsilon_0)}{1 + \sigma_D(i+1/2)\Delta t / (2\epsilon_0)} \dots\dots\dots (A.44)$$

These parameters are calculated at i+1/2 positions due to the 1/2 cell position of the H component. (A.29) can be written as,

$$j\omega H_x = -c_0 \left[\frac{\partial E_z}{\partial y} + \frac{\sigma_D(x)}{\epsilon_0} \frac{1}{j\omega} \frac{\partial E_z}{\partial y} \right] \dots\dots\dots (A.45)$$

The spatial derivative will be written as,

$$\frac{\partial E_z}{\partial y} \cong \frac{E_z^{n+1/2}(i,j+1) - E_z^{n+1/2}(i,j)}{\Delta x} = -\frac{curl_e}{\Delta x} \dots\dots\dots (A.46)$$

implementing this into FDTD gives

$$\frac{H_x^{n+1}(i,j+1/2) - H_x^n(i,j+1/2)}{\Delta t} = -c_0 \left[\frac{-curl_e}{\Delta x} - \frac{\sigma_D(x)}{\epsilon_0} \Delta t \sum_{n=0}^T \frac{curl_e}{\Delta x} \right] \dots\dots\dots (A.47)$$

The extra t in front of the summation is the part of the approximation of the time domain integral.

$$\begin{aligned} H_x^{n+1}(i,j+1/2) &= H_x^n(i,j+1/2) + \frac{c_0 \Delta t}{\Delta x} curl_e + \frac{\Delta t c_0}{\Delta x} \frac{\sigma_D(x) \Delta t}{\epsilon_0} I_{Hx}^{n+1/2}(i,j+1/2) \\ &= H_x^n(i,j+1/2) + \frac{c_0 \Delta t}{\Delta x} curl_e + \frac{\sigma_D(x) \Delta t}{2\epsilon_0} I_{Hx}^{n+1/2}(i,j+1/2) \dots\dots\dots (A.48) \end{aligned}$$

(A.32) is implemented as the following series of equations:

$$curl_e = \left[E_z^{n+1/2}(i,j) - E_z^{n+1/2}(i,j+1) \right] \dots\dots\dots (A.49)$$

$$I_{Hx}^{n+1/2}(i,j+1/2) = I_{Hx}^{n-1/2}(i,j+1/2) + curl_e \dots\dots\dots (A.50)$$

$$H_x^{n+1}(i,j+1/2)=H_x^n(i,j+1/2)+0.5curl_e+fil(i)I_{Hc}^{n+1/2}(i,j+1/2) \dots\dots\dots (A.51)$$

With

$$fil(i) = \frac{\sigma(i)\Delta t}{2\epsilon_0} \dots\dots\dots (A.52)$$

In calculating the f and g parameters, it is not necessary to actually vary conductivities. Instead, we calculate an auxiliary parameter,

$$x_n = \frac{\sigma\Delta t}{2\epsilon_0} \dots\dots\dots (A.53)$$

that increases as it goes into the PML. The f and g parameters are then calculated:

$$x_n(i) = 0.333 \left(\frac{i}{length_pml} \right)^3 \quad i=1,2, \dots\dots, length_pml \dots\dots\dots (A.54)$$

$$fil(i) = x_n(i) \dots\dots\dots (A.55)$$

$$gi2(i) = \left(\frac{1}{1 + x_n(i)} \right) \dots\dots\dots (A.56)$$

$$gi3(i) = \left(\frac{1 - x_n(i)}{1 + x_n(i)} \right) \dots\dots\dots (A.57)$$

The factor 0.333 is found empirically to be the largest number that remained stable. The cubic factor is also found empirically to be the most effective variation.

The parameters vary in the following manner:

fil(i) from 0 to 0.333

gi2(i) from 1 to 0.75

gi3(i) from 1 to 0.5

Throughout the main problem space, g_1 is zero, while g_2 and g_3 are 1. Therefore, there is a transition from the main part of the program to the PML. The above equations refer to the implementation of PML in x direction. Now the PML is to be implemented in y direction. Therefore instead of (A.33) one can write

$$j\omega \left(1 + \frac{\sigma_D(x)}{j\omega\epsilon_0}\right) \left(1 + \frac{\sigma_D(y)}{j\omega\epsilon_0}\right) D_z = c_0 \left(\frac{\partial H_y}{\partial x} - \frac{\partial H_x}{\partial y}\right) \dots\dots\dots (A.58a)$$

$$j\omega \left(1 + \frac{\sigma_D(x)}{j\omega\epsilon_0}\right)^{-1} \left(1 + \frac{\sigma_D(y)}{j\omega\epsilon_0}\right) H_x = c_0 \left(-\frac{\partial E_z}{\partial y}\right) \dots\dots\dots (A.58b)$$

$$j\omega \left(1 + \frac{\sigma_D(x)}{j\omega\epsilon_0}\right) \left(1 + \frac{\sigma_D(y)}{j\omega\epsilon_0}\right)^{-1} H_y = c_0 \frac{\partial E_z}{\partial x} \dots\dots\dots (A.58c)$$

Employing the same procedure in the previous section D, and H values becomes

$$D_z^{n+1/2}(i,j) = g_3(i)g_3(j)D_z^{n-1/2}(i) + g_2(i)g_2(j)0.5 \begin{bmatrix} H_y^n(i+1/2,j) - H_y^n(i-1/2,j) \\ -H_x^n(i,j+1/2) + H_x^n(i,j-1/2) \end{bmatrix}$$

In Y direction, H_y will require an implementation similar to the one used for H_x in the x direction.

$$curl_e = \left[E_z^{n+1/2}(i+1,j) - E_z^{n+1/2}(i,j)\right] \dots\dots\dots (A.59a)$$

$$I_{Hy}^{n+1/2}(i+1/2,j) = I_{Hy}^{n-1/2}(i+1/2,j) + curl_e \dots\dots\dots (A.59b)$$

$$H_y^{n+1}(i+1/2,j) = f_3(i+1/2)H_y^n(i+1/2,j) - f_2(i+1/2)0.5curl_e + f_1(j)I_{Hy}^{n+1/2}(i+1/2,j) \dots\dots\dots (A.60a)$$

Finally, H_x in the x direction becomes

$$\text{curl}_e = [E_z^{n+1/2}(i, j) - E_z^{n+1/2}(i, j+1)]$$

$$I_{H_x}^{n+1/2}(i, j+1/2) = I_{H_x}^{n-1/2}(i, j+1/2) + \text{curl}_e$$

$$H_x^{n+1}(i, j+1/2) = ff3(j+1/2)H_x^n(i, j+1/2) + ff2(j+1/2)0.5\text{curl}_e + fi1(i)I_{H_x}^{n+1/2}(i, j+1/2)$$

The full set of parameters associated with the PML are,

- fi1(i)&fj1(j) from 0 to 0.333
- fi2(i), gi2(i), fj2(j) and gj2(j) from 1 to 0.75
- fi3(i), gi3(i), fj3(j) and gj3(j) from 1 to 0.5

The PML can be turn off in the main part of the problem space by setting fi1 and fj1 to 0, and other parameters to 1.

The free space equations for D and H in three dimensions are,

$$\frac{\partial D_x}{\partial t} = \frac{1}{\sqrt{\epsilon_0 \mu_0}} \left(\frac{\partial H_z}{\partial y} - \frac{\partial H_y}{\partial z} \right) \dots\dots\dots (A.61a)$$

$$\frac{\partial D_y}{\partial t} = \frac{1}{\sqrt{\epsilon_0 \mu_0}} \left(\frac{\partial H_x}{\partial z} - \frac{\partial H_z}{\partial x} \right) \dots\dots\dots (A.61b)$$

$$\frac{\partial D_z}{\partial t} = \frac{1}{\sqrt{\epsilon_0 \mu_0}} \left(\frac{\partial H_y}{\partial x} - \frac{\partial H_x}{\partial y} \right) \dots\dots\dots (A.61c)$$

$$\frac{\partial H_x}{\partial t} = \frac{1}{\sqrt{\epsilon_0 \mu_0}} \left(\frac{\partial E_y}{\partial z} - \frac{\partial E_z}{\partial y} \right) \dots\dots\dots (A.61d)$$

$$\frac{\partial H_y}{\partial t} = \frac{1}{\sqrt{\epsilon_0 \mu_0}} \left(\frac{\partial E_z}{\partial x} - \frac{\partial E_x}{\partial z} \right) \dots\dots\dots (A.61e)$$

$$\frac{\partial H_z}{\partial t} = \frac{1}{\sqrt{\epsilon_0 \mu_0}} \left(\frac{\partial E_x}{\partial y} - \frac{\partial E_y}{\partial x} \right) \dots\dots\dots (A.61f)$$

The development of the PML for three dimensions closely follows the two dimensional version. The only difference is that we have to deal with three directions instead of two.

For instance (A.58.a) becomes

$$j\omega \left(1 + \frac{\sigma_x(x)}{j\omega\epsilon} \right) \left(1 + \frac{\sigma_y(y)}{j\omega\epsilon_0} \right) \left(1 + \frac{\sigma_z(z)}{j\omega\epsilon_0} \right)^{-1} D_z = c_0 \left(\frac{\partial H_y}{\partial x} - \frac{\partial H_x}{\partial y} \right) \dots\dots\dots (A.62)$$

$$\begin{aligned} j\omega \left(1 + \frac{\sigma_x(x)}{j\omega\epsilon} \right) \left(1 + \frac{\sigma_y(y)}{j\omega\epsilon_0} \right) D_z &= c_0 \left(1 + \frac{\sigma_z(z)}{j\omega\epsilon_0} \right) \left(\frac{\partial H_y}{\partial x} - \frac{\partial H_x}{\partial y} \right) \\ &= c_0 \text{curl}_z h + c_0 \frac{\sigma_z(z)}{\epsilon_0} \frac{1}{j\omega} \text{curl}_z h \dots\dots\dots (A.63) \end{aligned}$$

$$\text{Let } I_{Dz} = \frac{1}{j\omega} \text{curl}_z h \dots\dots\dots (A.64)$$

Which is an integration when it goes to the time domain. Thus above Eq. becomes

$$j\omega \left(1 + \frac{\sigma_x(x)}{j\omega\epsilon} \right) \left(1 + \frac{\sigma_y(y)}{j\omega\epsilon_0} \right) D_z = c_0 \left(\text{curl}_z h + \frac{\sigma_z(z)}{\epsilon_0} I_{Dz} \right) \dots\dots\dots (A.65)$$

The implementation of this into FDTD parallels that of the two dimensional PML, except the right side contains the integration term I_{Dz} . Following previous procedure the equation can be written as

$$\text{curl}_z h = \begin{bmatrix} H_y^n(i+1/2, j, k+1/2) - H_y^n(i-1/2, j, k+1/2) \\ H_x^n(i, j+1/2, k+1/2) + H_x^n(i, j-1/2, k+1/2) \end{bmatrix} \dots\dots\dots (A.66a)$$

$$I^n_{Dz}(i, j, k+1/2) = I^{n-1}_{Dz}(i, j, k+1/2) + \text{curl}_z h \dots\dots\dots (A.66b)$$

$$D^{n+1/2}_z(i, j, k+1/2) = gi3(i)gj3(j)D^{n-1/2}_z(i, j, k+1/2) + gi2(i)gj2(j)0.5(curl_h + gk1(k)I^n_{Dz}(i, j, k+1/2)) \dots\dots\dots (A.66c)$$

The I_{Dz} is a three dimensional array that is dimensioned throughout the problem space, but used only at two edges. The three dimensional implementation will have a total of six such arrays, which increases the computational burden. For this reason, I_{Dz} will be broken up into small three-dimensional arrays, defined at the low values of k and one defined at the high values of k. Similarly equations for D_x , D_y , H_x , H_y , H_z can be derived. In the iterative FDTD algorithm, values of D are computed first and then E is computed as,

$$E_x = g_{ax} D_x$$

$$E_y = g_{ay} D_y$$

$$E_z = g_{az} D_z$$

$$\text{Where } g_{ax} = g_{ay} = g_{az} = 1 / (\epsilon_r + (\sigma * dt / \epsilon_0))$$

This is a medium dependent parameter. In the case of PECs (Perfect Electric Conductor), one can easily define it by making g_{ax} , g_{ay} and g_{az} as zero so that the respective field components of E becomes zero, thus the boundary conditions for PEC are automatically assigned in the computation. The components of H are computed from the computed E values.

For the analysis of printed monopole antenna presented in the thesis the above mentioned PML based FDTD technique is implemented using MATLABTM. This MATLAB based code can be used for extracting antenna characteristics such as return loss, radiation pattern, gain and efficiency.

A.3.1 Numerical dispersion and stability criteria

The numerical algorithm for Maxwell’s curl equation defined by finite difference equation requires that time increment Δt have a specific bound relative to the lattice dimensions Δx , Δy and Δz . This bound is necessary to avoid numerical instability, an undesirable possibility of computed results to spuriously increase without the limit as time marching progresses. To ensure the computational stability it is necessary to satisfy a relation between the space increment and time increment. To ensure the stability of the time-stepping algorithm, Δt is chosen to satisfy the Courant-Friedrichs-Lewy (CFL) Stability criterion:

$$\Delta t \leq \frac{1}{V_{\max}} \frac{1}{\sqrt{1/\Delta x^2 + 1/\Delta y^2 + 1/\Delta z^2}} \dots\dots\dots (A.67)$$

V_{\max} is the maximum velocity of light in the computational volume. Typically V_{\max} will be the velocity of light in free space unless the entire volume is filled with dielectric. These equations will allow the approximate solution of E and H in the volume of the computational domain or mesh. In the present investigation the maximum time step is limited as 99.5% of the value given by the above equation.

The discretization of Maxwell’s equations in space and time causes the variation of the phase constant of the propagating wave with frequency. For a fixed cell size different frequency components of a wave propagate at slightly different velocities. This phenomenon is referred to as numerical dispersion and is inherently present in the FDTD algorithm. Furthermore, velocity depends also on the angle of propagation with respect to the coordinate axis. This is called numerical anisotropy. For accurate and stable results, the grid dispersion error must be reduced to an acceptable level, which can be readily accomplished by reducing the cell size. Accuracy of computation can be

ensured by selecting the grid size as 10 cells per wavelength ($\lambda/10$) or less at the highest frequency. In the analysis presented in the thesis the accuracy and stability are ensured by selecting $\Delta x, \Delta y, \Delta z \leq \lambda_{\min}/20$.

A.3.2 Luebbers feed model for fast FDTD convergence

With the transient excitation in FDTD, impedance and scattering parameters over a wide frequency band can be calculated. One difficulty with FDTD is that for some applications, few thousands of time steps may be required for the transient fields to decay. This difficulty is common in the case of circuits having very high quality factor. One method to reduce the time steps required is to apply signal processing methods to predict the voltages and currents at later times from the results computed for early times. Instead of making FDTD calculations for the full number of time steps required for transients to dissipate, one might make actual FDTD calculations for some fraction of this total number of time steps, and use these results to predict those for the later times [12].

Applying the various prediction methods adds additional complexity to the FDTD calculation process. The prediction methods are complicated, and may require care and skill by the use to obtain accurate results. Most of the methods described require the use to determine the order of the prediction process, related to the number of terms of whatever expansion function is used to approximate the FDTD time signal. A poor choice for the order of the prediction model can result in larger precision errors.

Another simple approach is to include a source with internal resistance to excite the problem. By employing source with internal resistance which matches with the characteristic impedance of the transmission line provided accurate results while greatly reduces the number of time steps required for convergence.

A.3.3 Resistive source model

FDTD transient calculations are often excited by a hard voltage source, whose internal source resistance is zero ohms. These sources are very easy to implement in an FDTD code. The electric field at the mesh edge where the source is located is determined by some function of time rather than by the FDTD update equations. A common choice is a Gaussian pulse, but other functions may also be used. The Gaussian pulse is significantly greater than zero amplitude for only a very short fraction of the total computation time, especially for resonant geometries such as many antennas and micro strip circuits.

Once the pulse amplitude drops the source voltage becomes essentially zero, the source effectively becoming a short circuit. Thus, any reflections from the antenna or circuit which return to the source are totally reflected. The only way the energy introduced into the calculation space can be dissipated is through radiation or by absorption by lossy media or lumped loads. For resonant structures, there are frequencies for which this radiation or absorption process requires a relatively long time to dissipate the excitation energy. Using a source with an internal resistance to excite the FDTD calculation provides an additional loss mechanism for the calculations.

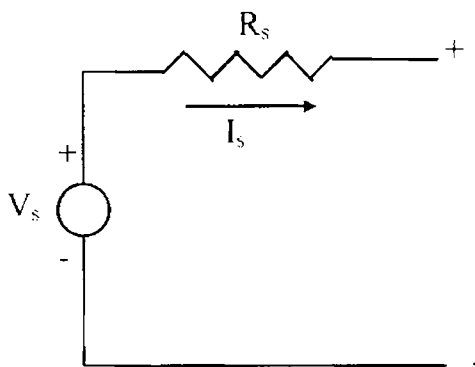


Fig A.5 FDTD source with source resistance

Consider that it is desired to excite an FDTD calculation with a voltage source that corresponds to an electric field E in the z direction at a certain mesh location $i_s \Delta x, j_s \Delta y, k_s \Delta z$, described using the usual Yee notation. The corresponding equivalent circuit for a voltage source which includes an internal source resistance R_s is illustrated in Fig. A.5. If the source resistance R_s is set to zero then the usual FDTD electric field at the source location is simply given by

$$E_s^n(i_s, j_s, k_s) = \frac{V_s(n\Delta t)}{\Delta z} \dots\dots\dots (A.68)$$

V_s is any function of time, often a Gaussian pulse.

However, with the source resistance included, the calculation of the source field $E_s^n(i_s, j_s, k_s)$ at each time step is complicated slightly. To determine the terminal voltage V of Fig. A.4 and, thus, the FDTD electric source field $E_s^n(i_s, j_s, k_s)$, the current through the source must be determined. This can be done by Ampere's circuital law, taking the line integral of the magnetic field around the electric field source location. The current through the source is then given by

$$I_s^{n-1/2} = (H_x^{n-1/2}(i_s, j_{s-1}, k_s) - H_x^{n-1/2}(i_s, j_s, k_s))\Delta x + (H_y^{n-1/2}(i_s, j_s, k_s) - H_y^{n-1/2}(i_{s-1}, j_s, k_s))\Delta y \dots\dots\dots (A.69)$$

so that by applying Ohm's law to the circuit of Fig. A.4 the electric source field is given by

$$E_s^n(i_s, j_s, k_s) = \frac{V_s(n\Delta t)}{\Delta z} + \frac{I_s^{n-1/2} R_s}{\Delta z} \dots\dots\dots (A.70)$$

if $R_s=0$, in this equation, then the usual hard-voltage source results. The value of the internal resistance does not appear to be critical. A reasonable choice for

R_s is to use the value of the characteristic impedance of the transmission line. In the thesis R_s is selected as 50Ω .

A.3.4 Staircase transition for microstrip line feed

The microstrip excitation presented in the thesis is implemented by using Luebber's [43] approach of stair cased FDTD mesh transition from electric field sources location to the full width of the microstrip transmission line. Compared to the "hard" voltage source excitation this approach provides accurate results with reduced computational time. For implementing the stair cased transition in microstrip line the substrate is discretized in order to incorporate more than one Yee cell. A gap feed model can be obtained by applying the excitation field between the microstrip line and the ground plane using a stair cased mesh transition as shown in Fig. A.6

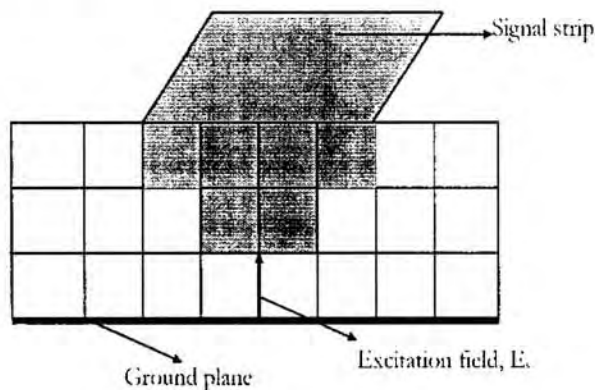


Fig. A.6 Stair cased feed model for microstrip line in FDTD

A.3.5 Excitation source modeling.

Proper excitation of the computational domain excites a field distribution closely resembling that of the physical structure. On the other hand, improper excitation leads to spurious solutions. For the antenna analysis in time-domain a narrow pulse is usually used as the excitation pulse to extract the frequency-

domain parameters in the entire frequency range of interest by Fourier transform of the transient results. The frequency band of interest decides the width of the pulse. A narrow pulse ensures wide band performance. To avoid the unnecessary noise appearing in the FDTD generated response, the excitation pulse and its spectrum must have a smooth roll off and low side lobes.

A sine wave or a Gaussian pulse can be used as the input signal for the 3D FDTD method. However, a Gaussian pulse plane wave is the most widely specified incident field as it provides a smooth roll off in frequency content and is simple to implement. In addition, the frequency spectrum of a Gaussian pulse is also Gaussian and will therefore provide frequency domain information from dc to the desired cut off frequency by adjusting the pulse width. The Gaussian input is of the form

$$g(t) = e^{-\left(\frac{(t-t_0)^2}{T^2}\right)} \dots\dots\dots (A.71)$$

where t_0 is the pulse delay and T relates to the Gaussian half width, which sets the required cut off frequency. Writing in the discrete form,

$$g(n\Delta t) = e^{-\left(\frac{(n\Delta t-t_0)^2}{T^2}\right)} \dots\dots\dots (A.72)$$

where $T = N \Delta t$ and $t_0 = 3T$. Thus the pulse is sampled N times in a pulse half width T . The Gaussian pulse and its spectrum are shown in Figure A.7. It is evident from the figure that the pulse provides relatively high signal levels up to the desired frequency. The parameter N can be changed to achieve sharper frequency roll off. In the FDTD method, all functions are assumed to be causal. Therefore, to satisfy the initial condition of zero excitation at the zeroth time step, the time of origin of the Gaussian pulse must be shifted by t_0 ($t_0 \gg 1$). To ensure proper initial value conditions a time delayed Gaussian pulse $t_0=3*T$ is employed in the thesis.

In order to simulate a voltage source excitation in a Microstrip fed structure, a vertical electric field E_s can be imposed in between the ground plane and the microstrip line as shown in Fig A.5. This electric field is defined using the Equn.A.55 with the voltage source as Gaussian pulse.

$$V_s = e^{-\left(\frac{(t-t_0)^2}{T^2}\right)} \dots\dots\dots (A.73)$$

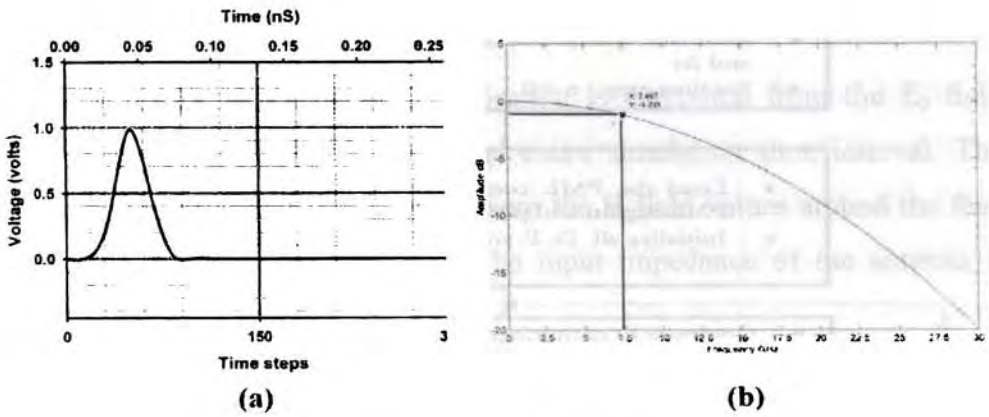


Fig. A.7 (a) Gaussian pulse (b) Gaussian spectrum

Gaussian pulse is usually used for the extracting the antenna characteristics such as return loss, impedance bandwidth, input impedance etc. Sinusoidal excitation is usually used to extract the radiation characteristics at a particular frequency of interest. A sinusoidal function of the following form is usually used for extracting the near field data at a particular frequency.

$$E(t) = E_0 \sin(2\pi ft)$$

Where E_0 determines the peak amplitude and ' $t=n*\Delta t$ ' is the current instant of time.

A.3.6 Flowchart of Yee algorithm

MATLAB based numerical code is developed for the parametric analysis of the antenna. The Flow chart used for extracting the antenna reflection characteristics are depicted in Fig.A.8

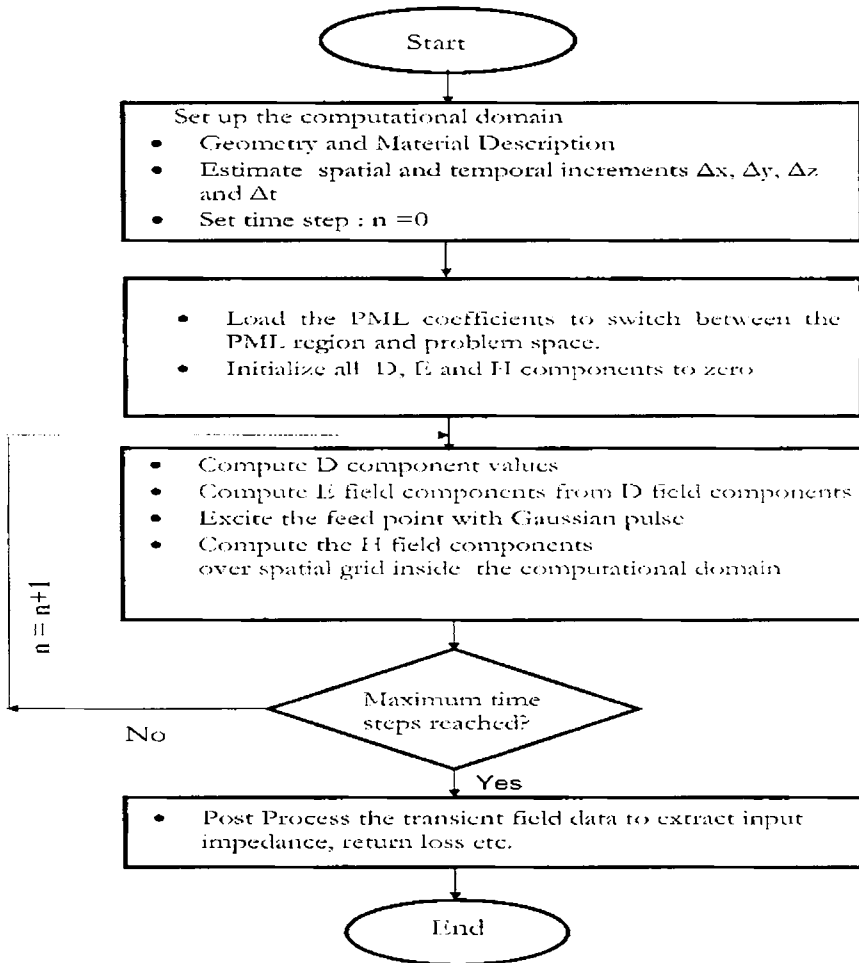


Fig.A.8. The FDTD flow chart

A.4 Antenna characteristics using FDTD

FDTD algorithm performs the transient analysis of the antenna under investigation. Fourier transform of the transient data gives the frequency

domain information over the frequency range of interest. Current and voltage samples are taken from the fixed points in the FDTD grid and Fast Fourier Transform (FFT) is used to compute the frequency domain information. Since for our analysis FFT can provide results with good accuracy FFT is used instead of DFT. By suitably post processing this information the reflection characteristics can be extracted as outlined in the section below.

A.4.1 Reflection characteristics

A.4.1.1 Return loss, Resonant frequency and 2:1 VSWR Band width

The voltage at the input port location is computed from the E_z field components at the feed point over the entire simulation time interval. The current at the feed point is calculated from the H field values around the feed point using Ampere’s circuital law. The input impedance of the antenna is computed from the Eqn A.58

$$Z_{in}(\omega) = \frac{FFT(V^n, P)}{FFT(I^{n-1}, P)} \dots\dots\dots (A.74)$$

Where P is the suitable Zero padding used for taking FFT, $V^n = E_z^n * \Delta z$ and I^{n-1} is given by equation A.54.

Since microstrip line is modeled using Leubber’s staircase approach as explained in previous section, the internal impedance of source resistance R_s is taken as the characteristic impedance (Z_0) of microstrip line.

Reflection coefficient is given as

$$\Gamma(\omega) = \frac{Z_{in} - Z_0}{Z_{in} + Z_0} \dots\dots\dots (A.75)$$

Return loss in dB, $S_{11} = 20 \log_{10} \Gamma(\omega) \dots\dots\dots (A.76)$

The return loss computed in the above process is processed for extracting the fundamental resonant frequency and 2:1 VSWR bandwidth corresponding to the -10dB return loss.

A.4.1.2 Radiation characteristics

Theoretical analysis procedure for predicting the radiation characteristics of the antenna usually employs formulating the theoretical model of the antenna and applying different numerical approximations. But the main problem with these approximations is that discrepancies may occur due to the inaccurate modeling and approximations. Moreover, most of the modeling techniques use modeling the current on the conducting surface to predict the radiation characteristics. Even though the computational time is less, wide band performance can not be achieved using these techniques, while using FDTD transient calculations can be done more efficiently for most of the antenna geometries than by applying frequency domain methods. FDTD is capable of computing transient far zone radiations of the antennas excited by non sinusoidal sources using transient near to far field transformation [13]. Hence from one FDTD computation wide band gain and radiation characteristics can be extracted. But using these transient near to far field transformation computational effort is more if number of frequencies involved is high. In applications requiring transient results in wideband frequency domain the fully transient approach involving Fast Fourier Transform is more desirable than applying a Discrete Fourier Transform in every time step. This method utilizes computing the transient far field Electric and Magnetic vector potentials on closed surface in the computational domain by running summation at each time step [14]. Procedure employed in this thesis for computing the radiation characteristics of the antenna is presented in the following section.

A.4.1.3 Principal plane radiation patterns.

To extract the radiation pattern at the resonant frequency a sinusoidal source is used as the excitation source. Initially using the Gaussian pulse the resonant frequency of the antenna is extracted and thus obtained resonant frequency f_r is used for FDTD run for pattern computation. The source voltage for pattern computation is given by

$$V(n\Delta t) = \sin(2\pi f_r n\Delta t)$$

A near field transformation surface layer is selected just above the printed monopole layer as the transformation layer for field computations. The surface S is chosen to be in the near field of radiating monopole with proper dimensions to ensure that tangential E field components are negligible outside this boundary. Usually a rectangular surface as shown in Fig.A.9 is chosen for the easy implementation of near to far field transformation algorithm.

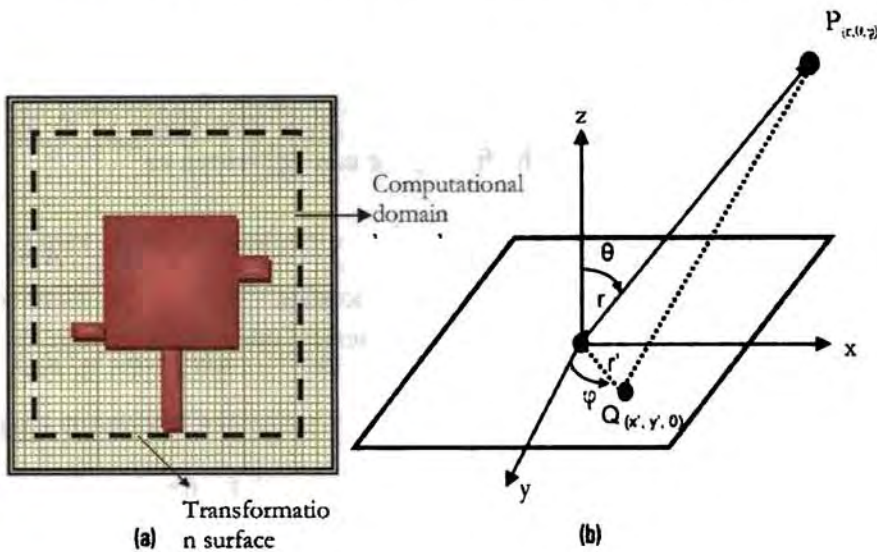


Fig A.9. Radiation pattern computation using FDTD.

- (a) Near field transformation surface
- (b) Spatial point Q in near field and far field point P.

The tangential near field Electric and Magnetic Field vectors on this surface are sampled and converted to equivalent surface currents.

$$\bar{J}_s = \bar{a}_n \times \bar{H}_A \dots\dots\dots (A.77)$$

$$\bar{M}_s = \bar{E}_A \times \bar{a}_n \dots\dots\dots (A.78)$$

Where \bar{a}_n is the unit outward normal from the transformation surface ($\bar{a}_n = \bar{z}$). The far field at any point outside this transformation surface is computed from the electric and magnetic vector potential derived from the surface current equivalence principle. The far field E field vectors tangential to the direction of propagation is given by

$$E_\theta = -\mu \frac{\partial A_\theta}{\partial t} - \frac{1}{c} \frac{\partial F_\phi}{\partial t} \dots\dots\dots (A.79)$$

$$E_\phi = -\mu \frac{\partial A_\phi}{\partial t} + \frac{1}{c} \frac{\partial F_\theta}{\partial t} \dots\dots\dots (A.80)$$

where A and F represents magnetic and electric vector potentials and θ and ϕ denotes the coordinates in the spherical coordinate system. Suppressing the $e^{j\omega t}$ variation [14] the electric field in the free space can be written as

$$E(r, \theta, \phi) = j\omega\eta_0.(F_\theta.\bar{a}_\phi - F_\phi.\bar{a}_\theta) \dots\dots\dots A.81$$

E_θ and E_ϕ are derived by transforming into spherical coordinate system as

$$E_\theta = j\omega\eta_0.(F_x.Sin(\phi) - F_y.Cos(\phi)) \dots\dots\dots (A.82)$$

$$E_\phi = j\omega\eta_0.Cos(\theta).(F_x.Cos(\phi) + F_y.Sin(\phi)) \dots\dots\dots (A.83)$$

Following assumptions are made for the near to far field transformation

- The antenna radiates into the $z > 0$ and $z < 0$ region from the aperture in the $z = 0$ plane
- r is in the far field i.e ($r \gg (x'^2 + y'^2)^{1/2}$) & $k_0 r \gg 1$
- Transformation surface dimensions are proper so that tangential electric fields are negligible outside the transformation aperture boundary.

Eqn A.81 now becomes

$$E = j \cdot \exp(-jkr) / (\lambda r) \cdot \left(\begin{pmatrix} \cos(\theta) \cdot (f_x \cos(\phi) + f_y \sin(\phi)) \bar{a}_\phi \\ -(f_x \sin(\phi) - f_y \cos(\phi)) \bar{a}_\theta \end{pmatrix} \right) \dots (A.84)$$

Where

$$f_x = \iint_S E_x(x', y', 0) \cdot \exp(jk(x' \sin(\theta) \cos(\phi) + y' \sin(\theta) \sin(\phi))) \cdot dx' dy'$$

The E field components $E_x(x', y', 0)$ can be computed by the technique proposed by Zimmerman et.al [15] as

$$E_{x(x', y', z'=0)} = (1/N) \sum_{n=1}^N E_x(n) \cdot \exp(j2\pi n/N) \dots (A.85)$$

Where $E(n)$ correspond to the corresponding tangential electric field components E_x^n and E_y^n sampled at the point on the transformation surface point $Q(x', y', 0)$ at the n^{th} time step. N corresponding to time steps for one period of sinusoidal excitation frequency. From the E_θ and E_ϕ values obtained using the above computation the E-plane and H-plane pattern can be derived. A complete flow chart illustrating the radiation pattern computation algorithm is illustrated in the Fig A.10

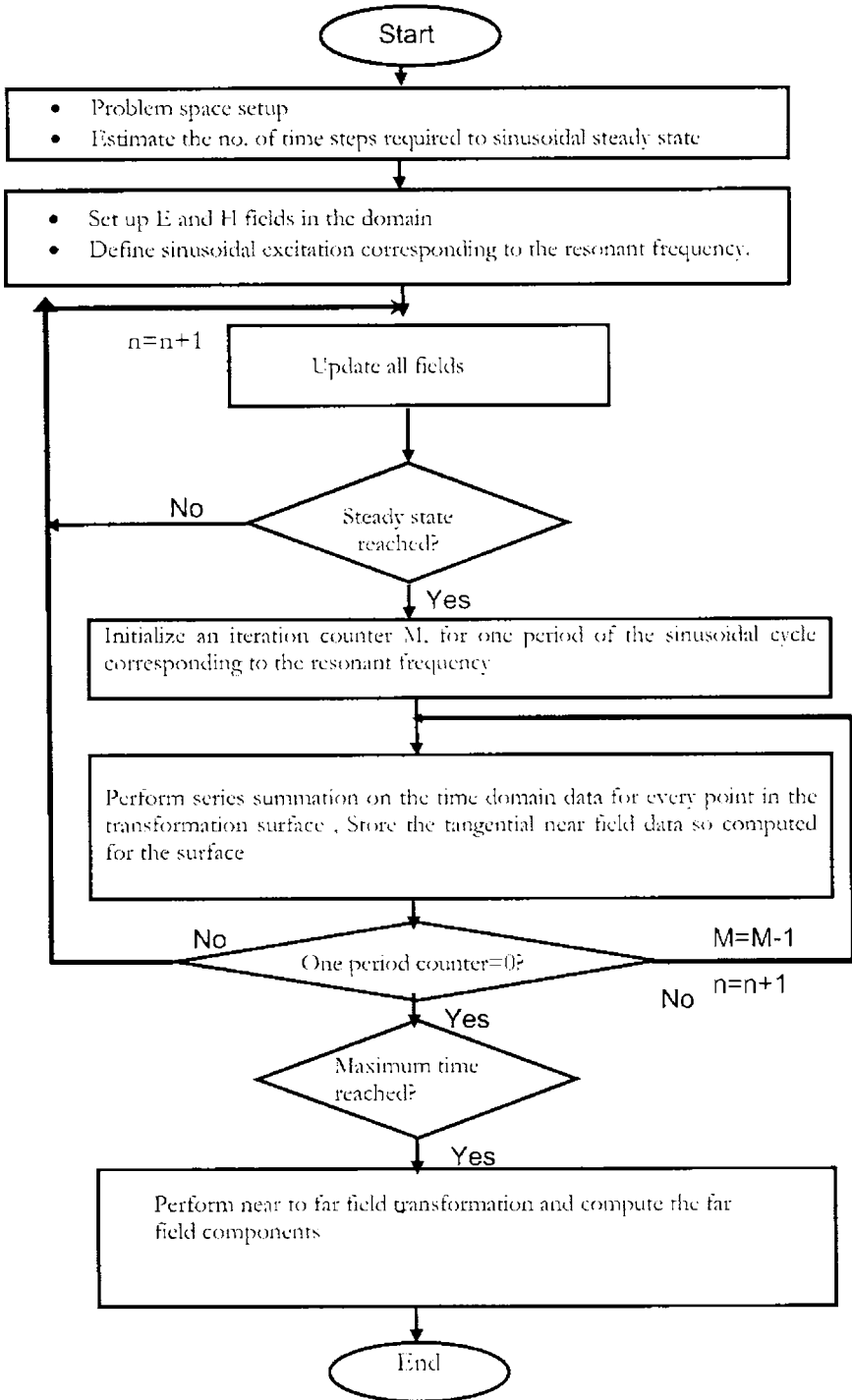


Fig A.10. Flow chart for radiation pattern computation

A.4.2 Antenna gain

For calculating the wide band gain, the input power fed to the antenna is needed. The equivalent steady state input power can be obtained at each frequency from the complex Fourier transforms of source voltage and source current (Equation A.69).

$$P_{in}(\omega) = \text{Re}[V_s(\omega) * I_s^*(\omega)] \dots\dots\dots (A.86)$$

Far zone electric field in the desired direction can be obtained from the equation A.84, and then antenna gain in the θ, ϕ direction relative to an isotropic antenna is given by

$$Gain(\omega, \theta, \phi) = \frac{[E(\omega, \theta, \phi)]^2 / \eta_0}{P_{in}(\omega) / 4\pi}$$

where η_0 is the impedance of the free space.

A.4.3 Efficiency

Antenna efficiency is determined from the input power and dissipated power. Dissipated power can also be computed quite simply [16].

$$Efficiency = \frac{P_{in} - P_{dis}}{P_{in}}$$

A.4.4 References

[1] K. S. Yee, "Numerical solution of initial boundary value problems involving Maxwell's equations in isotropic media," *IEEE Transactions on Antennas and Propagation*, AP-14, 4, pp. 302- 307, 1966.

[2] David.M.Sheen, Sami.M.Ali, Mohamed D.Abouzahra and Jin Au Kong, "Application of the Three-Dimensional Finite- Difference Time-Domain method to the analysis of planar Microstrip circuits," *IEEE Trans. Microwave Theory Tech.*, vol.38, no.7, pp.849-857, July 1990.

- [3] G. Mur, "Absorbing Boundary Conditions for the Finite Difference Approximation of the Time-Domain Electromagnetic Field Equations," *IEEE Trans. Electromagn. Compat.*, Vol. EMC-23, Nov. 1981, pp. 377-382.
- [4] J. P. Berenger, "A Perfectly Matched Layer for the Absorption of Electromagnetic Waves," *J. Computational Phys.*, Vol. 114, 1994, pp. 185-200.
- [5] D. S. Katz, E. T. Thiele, and A. Taflove, "Validation and Extension to Three Dimensions of the Berenger PML Absorbing Boundary Condition for FD-TD Meshes," *IEEE Microwave Guided Wave Lett.*, Vol. 4, No. 8, Aug. 1994, pp. 268- 270.
- [6] X.Zhang,J.Fang,y.Liu and K.K Mei, "Calculation of dispersive characteristics of Microstripes by time domain finite difference method", *IEEE Trans.Mirowave theory and tech.* vol 36,pp.263-267,1988.
- [7] Enquist and Majada, "Absorbing Boundary Conditions for the Numerical simulation of waves", *Mathematics of computation*, Vol. 31, 1977, pp. 629-651.
- [8] D.S. Katz, E.T. Thiele, and A. Taflove, "Validation and extension to three dimensions of the Berenger PML absorbing boundary conditions for FD-TD meshes," *IEEE Micro. Guided Wave Lett.*, vol. 4, no. 6, Aug. 1994, pp. 268– 270.
- [9] J.P. Berenger, "Perfectly matched layer for the FDTD solution of wave structure interaction problems," *IEEE Trans. Ant. Prop.*, vol. 44, no. 1, Jan. 1996, pp. 110–117.
- [10] Sullivan Dennis M, "Electromagnetic simulation using the FDTD method", *IEEE press series on RF and Microwave Technology*, USA.
- [11] Z. S Sacks, D. M. Kingsland, R. Lee, and J.F. Lee, "A perfectly matched anisotropic absorber for use as an absorbing boundary condition", *IEEE Transactions on Antennas and Propagation*, Vol. 43. December 1995, pp. 1460-1463.
- [12] R.J Leubbers and H.S Langdon., "A simple feed Model that reduces Time steps Needed for FDTD Antenna and Microstrip Calculations" *IEEE Trans. Antennas and Propogat.* Vol.44,No.7,July 1996, pp.1000-1005.
- [13] Allen Taflove and Morris E. Brodwin, "Numerical solution of steady – state electromagnetic scattering problems using the time-dependent Maxwell’s equations," *IEEE Trans. Microwave Theory Tech.*, vol.23, pp.623-630, August 1975.

- [14] R.J Leubbers, Karl s Kunz, Micheal Schneider and Forrest Hunsberger, “ A finite difference time Domain near zone to far zone transformation”, IEEE Trans. Antennas and Propagat.vol.39,pp429-433, April 1991.
- [15] Martin L Zimmerman and Richard Q Lee, “Use of FDTD method in the design of microstrip antenna arrays”., Int.Journal of Microwave and Millimeter wave Comp. aided Engg.vol.4,no.1,pp 58-66,1994.
- [16] R.J Leubbers, Karl s Kunz, “ Finite difference time domain method for electromagnetics”., CRC press, New York 1993.

CONFORMAL FDTD MODELLING OF CIRCULAR MICROSTRIP ANTENNA

A new algorithm for Conformal Finite Difference Time Domain FDTD (C-FDTD) modeling and analysis of curve edged Microstrip Patch Antennas (MPAs) by superimposing suitable Rectangular MPAs is presented. It has the advantage of using the simple, well developed and proven FDTD algorithms for Rectangular MPA with simple modifications. It offers wide flexibility in design, modeling, and analysis of arbitrary shaped MPAs. This new technique is applied to an electromagnetically fed Circular MPA. The computed results match with the experimental observations and theoretical data from literature.

B.1 Introduction

FDTD method [1-2] is widely used in the study of MPAs because of its flexibility and versatility, especially in the recent wake of large computational capability and memory availability. By suitable selection of the Yee cells and Courant criterion, Conventional FDTD can be used to give excellent performance in the case of Rectangular MPA. However, the algorithm causes errors while modeling the curved edges, as in Circular MPA. These inaccuracies are mainly due to the stair casing approximation. In order to minimize the error, a fine mesh is needed which can be demanding in terms of CPU time and memory. To overcome these difficulties, several conformal FDTD (C-FDTD) methods have been proposed [3]. However, most of these techniques require complicated mesh generation and often suffer from the instability problems.

This paper proposes a robust FDTD technique, with simple modifications of the Cartesian type of FDTD. A multiple number of rectangular patches of

appropriate sizes are superimposed, to achieve the closest approximation to the geometry under study. Here there is an added advantage of coarse or finer meshing depending upon the geometry. In this paper, Circular patch antenna fabricated on a standard FR4 substrate is studied using the proposed algorithm.

B.2 Antenna Geometry

Figure 1 shows the layout of the Circular MPA under study. The CPA with radius $r=21\text{mm}$, is etched on FR4 substrate of dielectric constant $\epsilon_r=4.28$ and thickness $h=1.6\text{mm}$. A 50 Ohm Microstrip feed line, fabricated on a similar substrate, is used to excite the patch through Electromagnetic coupling. The experimentally optimized feed length and feed offset from the geometrical centre of the patch are $F_l=70\text{mm}$ and $F_p=5.5\text{mm}$ respectively. The substrate dimensions $L*W$ are $75\text{mm}*72.5\text{mm}$ as shown. The experimental observations are taken using HP 8510C network analyzer.

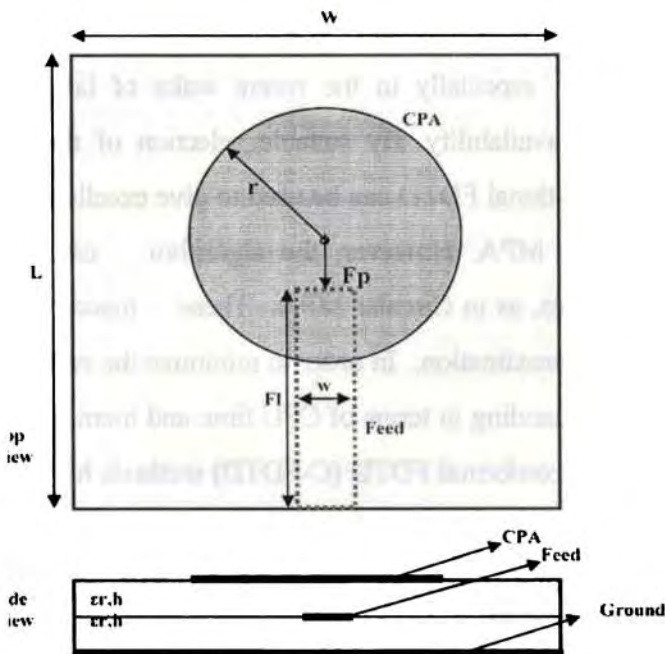


Fig. B.1 Geometry of the proposed antenna

B.3 Theoretical Investigations Based on FDTD

Any arbitrary shaped MPA can be visualized as superimposition of multiple rectangular patches of appropriate dimensions. FDTD run for the simple Rectangular Microstrip Patch Antenna is then performed in the entire computational domain. For the CPA under study, 12 rectangles of suitable dimensions are chosen for moderate accuracy and computation time. The computational domain dimensions are $115 \times 144 \times 20$ with grid dimensions $\Delta x = \Delta y = 1.167 \text{ mm}$ and $\Delta z = 0.4 \text{ mm}$. A Gaussian pulse of half width 15 ps and time delay 45 ps is launched into the computational domain. The Electric (E) and Magnetic (H) fields in the computational domain are updated based on the FDTD algorithm. The iterations are carried out for 10000 time steps. No instability is observed when the time steps are increased to 20000. Figure 2 shows the Voltage and Current variation at the observation point within the domain, over 5000 time steps. The Input impedance of the antenna is computed as ratio of the FFT of voltage derived from E field values at the observation point, over the entire time steps, to the FFT of current at the same point, derived from the H field values. Reflection Coefficient S_{11} (in dB) is then computed.

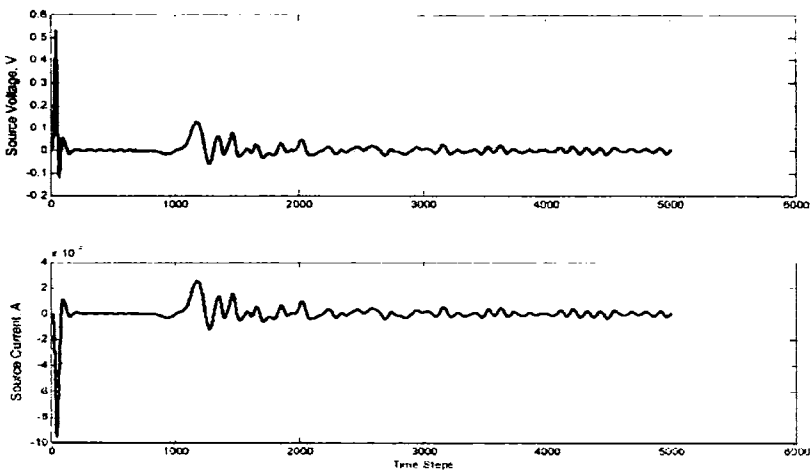


Fig. B.2 Voltage and Current Distribution at observation point ,for 5000 time steps

B.4 Results

The experimental and theoretical Return loss characteristics in the two lower order modes of the CPA is shown in Figure 3. Good agreement is observed between the results as illustrated in Table 1. The antenna resonates at 1.9GHz with a 2:1VSWR band width of 80MHz. The numerically computed resonance is at 1.892GHz with a band width of 123MHz.

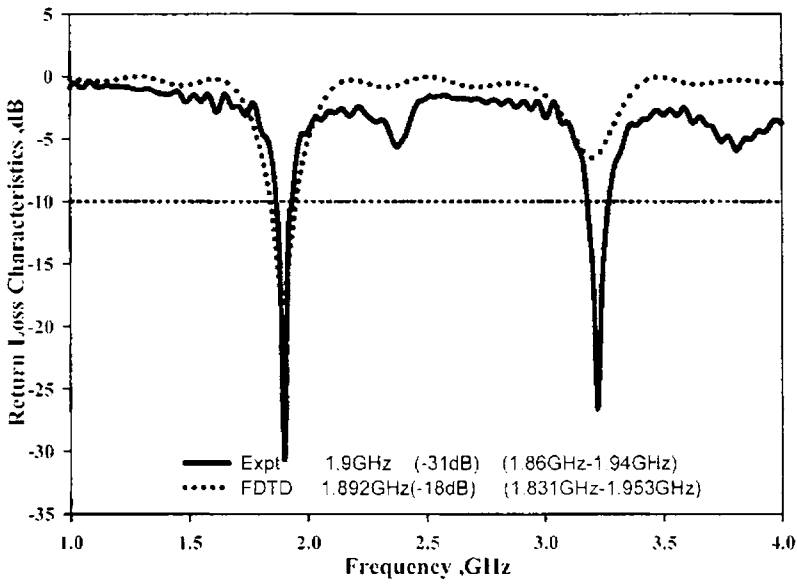


Fig. B.3 Return Loss Characteristics of the CPA

Table B.1 Comparison of Reflection Characteristics

	Expt	FDTD
Resonant Frequency (GHz)	1.9	1.892
% error between FDTD and expt	+0.01%	
2:1VSWR Band (GHz)	1.86-1.94	1.83-1.953
2:1 VSWR Bandwidth (MHz)	80	123
%BW	4.2	6.5

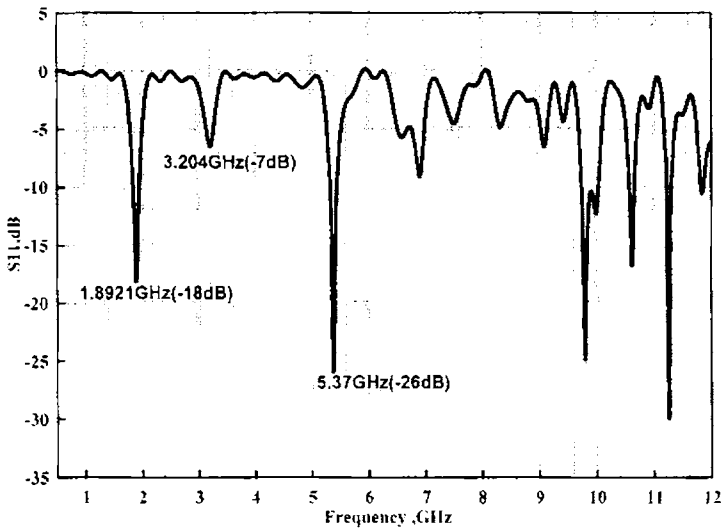


Fig. B.4 Illustrates the computed Reflection characteristics of the CPA illustrating the higher order modes .

B.5 Conclusions

A novel FDTD method suitable for analyzing arbitrary shaped MPA is proposed. Results of computation show good agreement with the experimental observation of the CPA. The algorithm is fast and employs the Cartesian type FDTD with simple modifications.

B.6 References

- [1] David M. Sheen, Sami M .Ali, Mohamed D. Abouzahra and Jin Au Kong , “Application of Three – Dimensional Finite Difference Time Domain Method for the analysis of Planar Microstrip Circuits” ,*IEEE Trans. on Microwave Theory and Techniques*, 1990.**38**(7) pp.849-857.
- [2] Allen Taflove, “Computational Electromagnetics: The Finite Difference Time Domain Method,” Artech House Publishers, 1995, ch.3
- [3] Wenhua Yu , Raj Mittra, “A conformal FDTD algorithm for modeling perfectly conducting objects with curve shaped surfaces and edges,” in *Microwave and Opt. Technol. Lett .* vol. 27, no. 2, October 20, 2000, pp 136-138.

List of Publications of the Author

INTERNATIONAL JOURNALS

- “Wide Band Dumbbell Shaped Patch Antenna” **K. Francis Jacob**, Suma M.N, Manoj Joseph and P.Mohanan, *Microwave and Optical Technology Letters*. Volume 48, Issue 11, Date: November 2006, Pages: 2295-2296.
- “Planar Branched Ultra Wide Band Monopole Antenna” **K. Francis Jacob**, Suma M.N, Rohith K Raj , Manoj Joseph and P.Mohanan, *Microwave and Optical Technology Letters*. Volume 49, Issue 1, January 2007, Pages: 45-47.

CONFERENCES

- “Conformal FDTD Modelling of Circular Microstrip Antenna” **K. Francis Jacob**, C.K. Aanandan, K. Vasudevan and P. Mohanan, *Proc. of the National Symposium on Microwave Antennas and Propagation, APSYM-04*, pp.181-184, Cochin, 2004

Resume of the Author

K. FRANCIS JACOB I.T.S

Dy. General Manager Telecom,
Bharat Sanchar Nigam Limited,
Coimbatore –641 043, Tamil Nadu, India.
Tel: +91-422-2435200, Mob: +91-9443000403
Fax: +91-422-2439999

&

Part –Time Research Scholar,
Centre for Research in Electromagnetics and Antennas (CREMA),
Department of Electronics,
Cochin University of Science and Technology,
Cochin-22, Kerala, India.
Tel: +91-484-2576418, Mob: +91-9443000403
Fax: +91-484-2575800
Email: francisjacob_k@bsnl.co.in and francisjacobk@gmail.com

Objective

To pursue research activities in the field of Printed antennas, Ultra Wide Band (UWB) Antennas, Smart Antennas (SA) for mobile communications, Specific antennas for 3G and 4G Mobile communications.

Education

M.Tech in Electronics and communication Engineering.
Specialization: Microwave and Optical Communication Engineering.
IIT , Kharagpur, India (1990)
Score: CGPA 8.86 with distinction and Topper of the batch.

B. Tech in Electronics and communication Engineering.
College of Engineering, Trivandrum.
University of Kerala (1988)
Score: 82.9% First class with distinction and 2nd Rank holder of the Kerala University.

Awards Obtained

GATE scholarship in 1988.

Senior Fellowship of “Integrated Guided Missile Development Programme (IGMDP)” by Defense Research and Development Organization (DRDO), Ministry of Defense, Govt. of India.

Recipient of “ **Vishisht Sanchar Seva Medal**” of BSNL, Kerala for the year –2005.

Research Experience

Worked as a **Scientist** in the Research Project entitled “Development of Fiber Integrated Optic Gyroscope (FIOG) for Missile applications” in DRDO, Hyderabad, Ministry of Defense, Govt. of India from April 1990 to February 1993.

Working Experience

Joined in “**Indian Telecommunication service (ITS)**” through Indian Engineering Service Examination (1991) of UPSC and worked as Asst. Divisional Engineer Telecom, Divisional Engineer Telecom, Area Manager Telecom and Dy. General Manager Telecom at various places in Department of Telecommunications(DoT) and BSNL, Ministry Of Communication, Govt. of India.

Publications

International Journal	2
National Conference	1

Computer Proficiency

FORTRAN , BASIC, C, C++, MATLAB, Assembly Level Programming, Ansoft HFSS, Designer, Zeland IE3D, Zeland FIDELITY, Microwave Office, and CST Microwave Studio.

Index Words

3G 1

4G 1, 21, 22

A

Absorbing Boundary condition 256

Anechoic Chamber 93

Ansoft – HFSS 96

Antenna Gain 95

Antenna efficiency 95

Aperture coupling 9, 10

Asymmetric strips 154

B

Bandwidth 90, 148

Broadband 1, 20,23,33,108,115,210

C

Cavity model 12

Circular disc 138, 139, 141

Coaxial feed 7

Combo model 184, 197

Compact Antenna 3,36

Compactness 168,183,205

Computed 100, 101, 103, 104

Conformal 259

Coplanar feed 11

Courant 100, 102

Cross polarization 148, 165, 166, 120

Current distribution 123, 160,164,176

D

Defected Ground Structure (DGS) 150,183

Dielectric constant 5,8,10,23

Dipole 1,7,21,29

E

Efficiency 107, 108, 205, 209

Elliptical 125,135,136,148

EM coupling 9

E8362B 88

Excitation techniques 8, 13, 245

F

FDTD 85,97,98,103,104,257

FFT 102,103,104,249

Finite Element method 15, 18

Fourier Transform 99

G

Gain 86,91,94,95

Gaussian 102,103,104

Group delay 206

H

Helical 36,65,72

Hexagonal 145,146,148,208,211

HIPERLAN 5,204

Homogeneous 17,19,15

Horn 91,92

HPBW 120,148

HP8510C 87

I

IE3D 46, 64

Impedance matching 164,174,186

Input impedance 89,95,96,103

Inverted-F 5

ISM band 21, 107

Isotropic 121

L

Leap-frog 222

Leubbers 242 112,132,256,257

M

Magnetic field 218

Method of Moments 14

Microstrip Antenna 3
Microstrip line feed 8
Monopole 110,123, 126

N

Network Analyser 87, 88
Numerical stability 100, 241

O

Octagonal monopole 142
Optimisation 131, 135 ,159
Offset 157, 191

P

Parametric analysis 128,185
Patch antenna 4
Peak gain 133,137,183
Phase linearity 206
PICA 3, 6
PIFA 2, 5
Polarisation 123
Printed monopole 6, 110
Prototype 169,184,205
Proximity coupling 9

R

Radiation pattern 120
Rectangle monopole 126
Reflection characteristics 90,110
Resonant frequency 114, 127
Return Loss 89 ,127

S

Simulation 96
Slots 170,172,184

Smart Antenna 2
Strip monopole 110
Strip loaded 149
Surface current 123, 161,199

T

TLM 18
Transmission line 109
Truncated ground 114
Turn table 91

U

UMTS 5
UWB antenna 22,197,205,208

W

Wearable antenna 216
Wheeler cap 95
Wi Max 1
Wi Fi 1
WLAN 2

Y

Yee cells 218, 248